Molecular Basis of Angiogenesis and Neuroprotection by Angiogenin

By

Trish T. Hoang

A dissertation submitted in partial fulfillment of

the requirements for the degree of

Doctor of Philosophy

(Biochemistry)

at the

UNIVERSITY OF WISCONSIN–MADISON

2016

Date of final oral examination: May 09, 2016

The dissertation is approved by the following members of the Final Oral Committee:

Ronald T. Raines, *Henry Lardy Professor of Biochemistry*, Biochemistry and Chemistry
Jeffrey A. Johnson, Professor, Pharmaceutical Sciences
David J. Pagliarini, Associate Professor, Biochemistry
Samuel E. Butcher, Professor, Biochemistry
Nader Sheibani, Professor, Ophthalmology and Visual Sciences

Molecular Basis of Angiogenesis and Neuroprotection by Angiogenin

Trish Truc Hoang

Under the Supervision of Professor Ronald T. Raines

at the University of Wisconsin–Madison

Cancer and neurodegeneration are disorders with profound impact on human health. Cancer results from uncontrolled cell growth, whereas neurodegeneration is caused by premature neuronal cell death. Although these disease mechanisms seem to be at opposite ends of a spectrum, an increasing number of cellular and molecular studies have linked the two disorders. Activation and deregulation of the cell cycle appear to be core features of both diseases; thus, many genes associated with cell cycle control, DNA repair, and kinase signaling have been studied extensively. Despite continuing efforts to understand the underlying pathophysiology of both diseases, key regulatory factors that modulate balance between cell growth and cell death remain unknown.

In addition to cell cycle regulation, another cellular process implicated in both cancer and neurodegeneration is angiogenesis—the process of establishing new blood vessels from pre-existing vasculature. Angiogenesis is a vital physiological event that supplies cells with oxygen and nutrients. Up-regulation of angiogenesis in cancer promotes progression of the disease while insufficient angiogenic signals contribute to neurodegeneration. There are two angiogenic factors–vascular endothelial growth factor (VEGF) and angiogenin (ANG)–that play roles in

both diseases. While the roles of VEGF have been well-documented, ANG functions and signaling pathway are understood less completely.

ANG is a prevalent protein that acts directly on the proliferation of endothelial cells to promote neovascularization. ANG is up-regulated in cancer cells, but also functions to protect neurons against oxidative stress. Hence, drugs that target this pro-tumorigenic protein could also promote neurological damage, as loss-of-function mutations of the *ANG* gene are associated with amyotrophic lateral sclerosis. My efforts have been focused on understanding the molecular mechanisms of ANG underlying these diseases. The findings could offer novel therapeutic strategies that target one disorder without advancing the other.

ANG belongs to the pancreatic-type ribonuclease superfamily. ANG relies on its ribonucleolytic activity to affect protein translation during cell growth and cell death. To meet the high demand for protein synthesis during cell proliferation, cells increase ribosome biogenesis. ANG promotes rRNA production to satisfy this demand. In contrast, cells that suffer toxic insults will undergo cell death without activation of anti-apoptotic signals. Those cells urge energy conservation to repress global protein translation and focus on production of cytoprotective factors. ANG stalls protein translation by cleaving a subset of tRNAs to generate RNA products that specifically inhibit translation initiation.

Indeed, ANG acts as a double-edged sword; overproduction of this protein is correlated with cancer progression, but deprivation is associated with neurological disorders. Although the molecular roles of ANG are not understood completely in either diseases, a central theme emerging from ANG actions is its re-programming of protein synthesis. The purposes of this thesis are to explore the effect of ANG on protein synthesis in the context of cancer and neurodegeneration, to determine how ANG promotes cell proliferation, to pinpoint the role of

ANG neuroprotection, and ultimately, to lay a foundation for the development of new ANG-based therapeutics for treating these diseases.

In CHAPTER 1, I summarize the large body of evidence indicating the important role of ANG in cancer and neurodegenerative diseases. I discuss the role of ribosome biogenesis in cancer development. I also highlight the importance of stress granule formation in repressing protein translation and its pathological connection to neurodegeneration. Depending on the state of the cell, ANG navigates itself into two distant and distinctive cellular foci: nucleoli during proliferation or stress granules during oxidative stress. My studies report molecular details of ANG actions in these foci. In CHAPTER 2, I report on the unprecedented mechanism of signal transduction by ANG that promotes cell proliferation. This mechanism allows the protein to execute its angiogenic activity. In CHAPTER 3, I discuss another pathway that ANG manifests in astrocytes–brain cells that regulate neuronal function–to employ its neuroprotection.

By elucidating the elegant network of ANG actions, features of ANG required for a particular pathway might be used to design ANG-based therapeutics. CHAPTER 4 outlines several future directions for developing ANG therapeutics that can selectively target one disease without exacerbating the other. Taken together, the results of this thesis offer a deeper understanding of the molecular basis of the divergence of cancer and neurodegeneration and inspire innovative treatment approaches.

Acknowledgments

I would like to express my deepest gratitude towards all the people who have generously provided their support and assistance during my graduate career. First and foremost, I would like to thank my advisor, Professor Ron Raines. I am grateful for the opportunity he has given me to pursue my Ph.D. thesis work in his research group. His enthusiasm and optimism for science, breadth of knowledge, as well as his extraordinary ability with words have been truly inspirational. Ron has cultivated a collaborative environment, where we are encouraged to pursue interesting questions from a number of different angles. As a result, I have had 7 in total of both intra- and inter-collaboration projects. He has taught me much, especially regarding science communication and writing.

I am also grateful to my thesis committee: Professor Jeffrey Johnson, Professor Dave Pagliarini, Professor Nadia Sheibani, Professor Alan Attie and Professor Sam Butcher. Their guidance, patience, constructive criticism, and excellent advice, have all contributed to my development as a scientist. I would like to give special thanks to Professor Jeffrey Johnson and Professor Delinda Johnson for “adopting” me to their lab and have treated me like their graduate student.

Now, I must acknowledge those individuals that initially inspired me to pursue science as a career. Their enthusiasm for their respective fields and passion for teaching were the reason I chose to study biochemistry. First is my undergraduate supervisor, Dr. Mariangela Segre, whom I worked for 3 years as a lab technician. She consistently told me that “Trish! You need to go to graduate school. Research is the right career path for you.” And surely, she was right. Second, I thank my undergraduate mentor, Professor Marie Spies. She has provided great opportunities for me to work independently as an undergrad and often encouraged me to attend graduate school.

Third, I was fortunate to work in Professor Lauren Trepanier's lab at UW-Madison in summer 2008 as a REU student. She introduced me to clinically relevant type of research. It was definitely an eye opening experience for me. Certainly, I felt in love to Madison and decided to come back for graduate school.

It can often be quite easy to overlook all of the individuals in core facilities and biochemistry media lab that make our research possible. I have special thanks to Laura Vanderploeg for her patience and willingness to teach me how to use Illustrator and Photoshop. I thank Dr. Darrel McCaslin for his assistance and insightful discussion in the Biophysics Instrumentation Facility. I also want to thank Dr. Elle Grevstad for her continued service and passion for science.

I could have not made it thus far without the help from many talented individuals in the Raines lab. Thanks to all members of the Raines Laboratory, past and present, who have been invaluable source of advice, support, and friendship to me during those years. Moreover, I also had the privilege to work alongside Greg Jakubczak, Amit Choudhary, Ben Caes, Greg Ellis, Mike Palte, John Lukesh, Nadia Sundlass, Raso Biswas, Ho-Hsuan Chou, Christine Bradford, Brett VanVeller, Caglar Tanrikulu, Kevin Desai, Sean Johnston, Kalie Mix, Wen Chyan, Jesus Dones Monroig, Leland Hyman, Aubrey Ellison, Brian Graham, Brian Gold, Henry Kilgore, Lindsey Orgren, Nimu Sidhu, Sydney Thomas, Cara Jenkins, and many others. Mentoring Stephen Leeb, Quinn Vatland and Trieu Hoang were always fun and rewarding. Next, I would like to thank those lab members that I have had the pleasure of calling my friends including Mike Levine, Joelle Lomax, Chelcie Eller, Robert Presler, Jim Vasta, Kristen Andersen, Ian Windsor, Thom Smith, and Robert Newberry. I cannot imagine the last couple months without the encouragement and support from my TEV (Trish Emily Val) team. Emily Garnett and Val Tripp were there through the best and worst of times and supported me when I needed it the most.

I am grateful to my friends outside of lab who have been a constant source of support and laughter. These include my best buddy, Robert Presler (aka Mr. “Coolawesome”), and my Vietnamese “gang”. Our gang had done all the “fun” activities that we could think of including biking around Madison, jumping in the lake, dumpster diving, taking Taekwondo classes and many more. In addition, I would like to thank many new friends from Madison including Angie Umana, Melanie Preston, Chris Lapointe, Camila Lopez-Anido, Graham Erwin, Shruti Waghray, Daniel Wilinski, Kahlilia Blanco, Rasa Valiauga, Corey Nemec.

I cannot express how grateful I am to my parents, Duc Hoang and Kristina Vo, my sister, Trianna Hoang, my brother, Trieu Hoang, my mother-in-law, Van Ly, and the rest of the Hoang’s and Vo’s family. My parents, my sister and my brother have been a source of unconditional and endless love and support to me. My extended families have been a source of encouragement through these years.

Last, and of course most importantly, I am eternally grateful to my husband and the love of my life, An Nguyen. His love, encouragement, patience, and unfailing support have seen me through every single day in the last five and half years. He has been my best friend and strongest critic, and his ability to see through my smiles and tears, and to offer constructive advice was invaluable. I am looking forward to being his supporter, and I wish him the best success in his MBA program.

Table of Contents

List of Figures

List of Tables

List of Abbreviations

ACN	acetonitrile
Ala, A	alanine
ALS	Amyotrophic Lateral Sclerosis
AD	Alzheimer's disease
ANG	angiogenin
Arg, R	arginine
Asp, D	aspartate
Asn, N	asparagine
ATCC	American Type Culture Collection
ATP	adenosine triphosphate
BCA	bicinchoninic acid
BODIPY	4,4-difluoro-4-bora-3a,4a-diaza-s-indacene
BSA	bovine serum albumin
cDNA	complementary deoxyribonucleic acid
CDK	cyclin-dependent kinase
DEFIA	2',7'-diethylfluorescein-5-iodoacetamide
DMEM	Dulbecco's modified Eagle's medium
DMF	dimethylformamide
DMSO	dimethylsulfoxide
DNA	deoxyribonucleic acid
Dnmt	DNA methyltransferase
DSF	differential scanning fluorimetry

DTT	dithiothreitol
DTNB	5,5’-dithiobis(2-nitrobenzoic acid)
EDTA	ethylenediaminetetraacetic acid
ER	endoplasmic reticulum
ETOH	ethanol
FBS	fetal bovine serum
FPLC	fast performance liquid chromatography
Gln, Q	glutamine
Gly, G	glycine
h	hour
HCl	hydrochloric acid
HDAC	histone deacetylase
HeLa	human epithelial cervical adenocarcinoma
HEPES	2[4-(2-hydroxyethyl)-l-piperazinyl]ethanesulfonic acid
His, H	histidine
HUVEC	human umbilical vein endothelial cells
IC_{50}	half maximal inhibitory concentration
Ile, I	isoleucine
IPTG	isopropyl-β-D-1-thiogalactopyranoside
IRES	internal ribosome entry sites
K_d	equilibrium dissociation constant
kDa	kilodalton
K_i	inhibitor dissociation constant

K_M	Michaelis constant
λ_{em}	emission wavelength
λ_{ex}	excitation wavelength
LB	Luria-Bertani medium
LNA	locked nucleic acid
LRR	leucine-rich repeat
Lys, K	lysine
MALDI-TOF	matrix-assisted laser desorption/ionization time-of-flight
MeOH	methanol
Met, M	methionine
MDM2	mouse double minute 2 homolog
MHz	megahertz
min	minute
mRNA	messenger ribonucleic acid
MW	molecular weight
NaCl	sodium chloride
NaOH	sodium hydroxide
ND	neurodegenerative disease
NLS	nuclear localization signal
NMR	nuclear magnetic resonance
NoRC	nucleolar remodeling complex
Nrf2	nuclear factor erythroid 2-relatted factor 2
OD	optical density

p value	probability value
PCR	polymerase chain reaction
PBS	phosphate-buffered saline
PD	Parkinson's disease
PDB	protein data bank
Phe, F	phenylalanine
pK_a	log of the acid dissociation constant
PKC	protein kinase C
Pol	Polymerase
pRNA	promoter-associated RNA
qPCR	quantitative polymerase chain reaction
rDNA	ribosomal deoxyribonucleic acid
RI	ribonuclease inhibitor
RNA	ribonucleic acid
rRNA	ribosomal ribonucleic acid
RNase	ribonuclease
RNase 1	human pancreatic-type ribonuclease 1
RNase A	bovine pancreatic-type ribonuclease A
ROS	reactive oxygen species
RP	ribosomal protein
s	second
SDS-PAGE	sodium dodecyl sulfate polyacrylamide gel electrophoresis
SG	stress granule

siRNA	small interfering ribonucleic acid
SNF2h	non-fermenting protein 2 homologue
SOD1	Cu/Zn superoxide dismutase 1
SSEA-4	stage-specific embryonic antigen-4
TB	terrific broth medium
Thr, T	threonine
TIP5	transcription termination factor I-interacting protein 5
tiRNA	stress-induced small RNA
T_m	melting point
Tris	2-amno-2-(hydroxymethyl)-1,3-propanediol
tRNA	transfer ribonucleic acid
Trp, W	tryptophan
UV	ultraviolet
UW	University of Wisconsin
VEGF	vascular endothelial growth factor
Vis	visible
v/v	volume per volume
w/v	weight per volume

CHAPTER 1

Angiogenin in Cancer and Neurodegeneration

1.1 Overview

As two of the leading causes of death, cancer and neurodegenerative diseases (NDs) are certainly topics of interest for researchers worldwide. At first glance, cancer and neurodegeneration seem to have little in common. Whereas cancer cells are characterized by an enhanced resistance to cell death, neurodegeneration results in the death of post-mitotic neurons. Multiple mechanistic studies have begun to uncover a connection between these two disorders. In pathological situations, several important biological processes are dysregulated, including cell division, epigenetic modifications, and RNA/protein metabolisms.[1-4] For instance, cell cycle regulators are either abnormally expressed or aberrantly regulated such that malignant cells are capable of bypassing cell cycle checkpoints and growing uncontrollably, whereas degenerating neurons are unable to exit the cell cycle and subsequently undergo programmed cell death.[5-7] Complex and interconnected epigenetic modifications can occur in conjunction with genetic alterations in disease pathogenesis.[8-10] Altered RNA or protein metabolisms can disturb cellular compositions and networks, ultimately leading to devastating outcomes, such as cancer and NDs.[11-13] These cellular processes highlight the link between cancer and NDs and suggest that discovering the underlying cause of one disease could be beneficial for understanding, treating and ultimately curing the other.

Genetic analyses have indicated that the risks of cancer and ND development are correlated inversely. Several case-control and cohort studies have reported a reduced risk of cancer among individuals with Alzheimer’s disease (AD), Parkinson's disease (PD), or amyotrophic lateral sclerosis (ALS).[14-16] Conversely, cancer survivors have a lower incidence of developing neurological disorders.[17,18] The vast majority of cancer or ND incidences are non-hereditary and

sporadic in nature; less than 10% of incidences are inherited in a Mendelian fashion.[19,20] Thus, valuable diagnostic genetic biomarkers have not been identified for these conditions.

Proteins that are implicated in both diseases are particularly interesting. These molecules often serve different purposes in actively dividing cells or post-mitotic neurons. Although the cell responses and signaling pathways might differ, aberrant regulation of protein expression and function in either case would lead to disease.

Angiogenin (ANG) is one of the few proteins that serve specific functions in both diseases. ANG is involved in variety of cellular processes, including promoting cell proliferation, altering cellular RNAs through its ribonucleolytic activity, and modifying histone epigenetic marks to modulate gene expression.[21-23] An excess of ANG is associated with cancer, while a lack of ANG contributes to ALS and PD (Figure 1.1).[24-26] As diseases result from imbalanced ANG function, studying ANG is not only particularly valuable and interesting but also a potential source of insight into the pathogenesis of cancer and NDs. Herein, I review the current knowledge of ANG functions in the context of cancer and NDs. I provide the historical perspectives of the protein, discuss ANG molecular properties in detail, and illustrate how these properties coordinate its roles in both cancer and NDs.

1.2 The basis of angiogenin

1.2.1 Discovery of ANG

ANG was first identified by Vallee and his colleagues at Harvard in 1985.[27] The protein was isolated from conditioned media of the human adenocarcinoma cell line HT-29. Indeed, ANG was the first human tumor-derived protein characterized as a potent inducer of neovascularization. Applying ANG onto the chick chorioallantoic membrane, the rabbit cornea or the rabbit meniscus at femtomolar doses stimulated the growth of new blood vessels.[28] The

discovery of ANG provided the first evidence directly supporting Folkman's hypothesis that angiogenesis contributes to tumor growth.[29,30] The importance of angiogenesis generated hope that manipulating this process could lead to effective cancer therapeutics. All currently approved anti-angiogenic therapies have been developed to starve tumors by destroying their vascular supply.[31] Therefore, ANG has quickly become an attractive target for cancer treatment. Tremendous efforts have been focused on studying the biophysical properties of ANG as well as its molecular action in angiogenesis for the development of ANG inhibitors.

Shortly after ANG was discovered, the same group determined the amino acid and cDNA sequences of ANG.[32,33] The ANG transcript does not contain any intronic sequences, and it is translated as a precursor protein with a signal peptide for secretion. The mature form of the ANG polypeptide is composed of 123 amino acids, yielding a 14.4-kDa protein. The *ANG* gene is highly conserved in nearly all vertebrates, including fish, reptiles, birds, and mammals, but it is not conserved in invertebrates.[34] Interestingly, there is only 1 functional *ANG* gene in the human genome, whereas the mouse genome possesses the largest *Ang* family, consisting of 6 different paralogs.[35] Mouse *Ang 1* (*mAng 1*) has the highest sequence identity (73%) with respect to human *ANG* and is the only member that displays robust angiogenic activity.[36] The gene variability among the 6 mouse paralogs is mainly in the signal localization and nucleotide binding of *mAng*, which supports the possibility of functional divergence among *mAng* copies.[37]

The human and mouse *ANG* loci have a unique gene arrangement.[38] Two distinct exons encoding *ANG* and *RNase 4* are located immediately following two non-coding exons (Figure 1.2). These 2 functional genes are under 2 shared promoters; promoter 1 is active universally, while promoter 2 is active only in hepatic cells. This gene arrangement allows the transcript levels of ANG and RNase 4 to be comparable. Indeed, the tissue distribution and

cellular localization of *ANG* and *RNase 4* are very similar in humans and mice.[39,40] In addition, the organization of these 2 genes is highly conserved in other mammalian species, reflecting selection constraints that maintain the co-regulation of ANG and RNase 4.[41]

1.2.2 Molecular properties of ANG

ANG is a member of the vertebrate secretory ribonucleases (RNases) superfamily.[32] These RNases are composed of a conserved catalytic triad (*i.e.*, H13, K40, and H114) that catalyzes the cleavage of phosphodiester bonds on the 3′ side of cytidine or uridine residues in single-stranded RNA.[42,43] Despite the highly similar protein sequences of ANG and other members of the superfamily, ANG has markedly different enzymatic activity and specificity. For instance, ANG shares 33% sequence identity and 65% sequence similarity with its bovine homolog, RNase A; yet, its ribonucleolytic activity toward conventional substrates is 10^4- to 10^6-fold lower than that of RNase A.[44]

The crystal structure of human ANG was determined to resolve the discrepancy between the catalytic activity of ANG and other RNases.[45] Indeed, ANG crystallization has been instrumental in many molecular and biomedical studies. The structure illustrates the limited accessibility of the pyrimidine binding site of ANG (Figure 1.3). This active site is largely obstructed by residue Q117, the side chain of which forms two hydrogen bonds with T44 and receives support from intramolecular hydrophobic interactions with I119 and F120. Removing the side chain via glycine substitution (Q117G) is not sufficient to endow ANG with catalytic activity comparable to that of RNase A, suggesting that ANG might have evolved to cleave a particular cellular RNA.[46]

The ANG structure resembles a kidney bean and contains 3 disulfide bridges, unlike other RNases, which contain 4 disulfide bonds.[45] The lack of the fourth disulfide bond results in a loop

region, which has been identified as a putative receptor binding site. This receptor loop is a unique feature that distinguishes ANG from other RNases. Whereas the loop serves as a site for ANG to bind its receptor, the region is important for other RNases to bind RNA purines. Another distinctive feature of ANG suggesting that it functions in the nucleus is a nuclear localization signal (NLS) ^{30}MRRRG^{35}.[47,48] Taken together, the Q117 side chain, the receptor-binding site, and the NLS of ANG not only provide a rationale for its low ribonucleolytic activity, but also enable diverse biological functions. Perhaps, ANG evolved away from catalytic efficiency toward intracellular roles. If ANG hydrolyzes RNAs as effectively as do other RNases, intracellular RNAs would be destroyed, leading to cellular toxicity.

1.2.3 Molecular actions of ANG

Receptor

Secreted ANG enters the cell via receptor-mediated endocytosis and ultimately accumulates in the nucleolus. This journey allows ANG to direct its angiogenic activity toward endothelial cells and to exert mitogenic effects on different cell types.[21,49,50] Thus far, two ANG receptors have been identified: a putative 170-kDa protein and syndecan-4.[51,52] The putative receptor was isolated using ANG affinity chromatography, but its identity remains unclear. A more recent study reported that syndecan-4 anchored on the surface of astrocytes is an ANG receptor. Syndecan-4 is a cell surface heparan sulfate proteoglycan that is also expressed by both cancer cells and endothelial cells.[53-55] ANG interacts with the receptor by binding to heparan sulfate. A heparinase treatment to remove heparan sulfate from the receptor prevented ANG from entering the cell.[52] ANG endocytosis was also compromised by the addition of heparin, a carbohydrate very similar to heparan sulfate, to compete for the heparan sulfate binding sites of the receptor.[56] These findings indicate that syndecan-4 is the preferred receptor of ANG.

Ribonuclease inhibitor modulates ANG function

After entering the cell, ANG encounters an endogenous ribonuclease inhibitor (RI) in the cytosol. RI and ANG form one of the tightest biomolecular complexes, having a K_d value in the femtomolar range.[57] RI is a 50-kDa protein composed of 15 leucine-rich repeats and is approximately 3 times larger than ANG.[58-60] The RI•ANG binding interface consists of a large contact surface on both proteins.[61] The most important contacts reside at the C-terminal segment of RI, ranging from the 434th to 460th residues, and at the notable active site of ANG, K40. Thus, binding to RI blocks the active site of ANG and abolishes ribonucleolytic activity.[62,63] The high degree of complementarity observed among the 4 tryptophan residues of RI, *i.e.*, 261, 263, 318, and 375, and the 84–89 loop of ANG is another significant contributor toward the strong interaction. In addition, the 3 arginine residues within the NLS of ANG interact with RI residues to some extent, suggesting that RI binding might apprehend ANG in the cytoplasm.

RI is ubiquitously expressed in the cytosol at concentrations in the high micromolar range.[62] Although direct interactions between RI and ANG in the cytosol have not been demonstrated, several gain- and loss-of-function experiments have elucidated the roles of RI in modulating ANG function *in cellulo*. For example, up-regulating RI suppressed tumor growth and tumor microvessel density through suppression of ANG function.[64] Conversely, RI knockdown promoted tumor growth because the lack of RI increased the number of free ANG molecules available to facilitate cell proliferation and angiogenesis.[65] Furthermore, a rabbit cornea assay demonstrated that an RI-evasive variant of ANG disrupted RI•ANG interaction and enhanced the angiogenic potency of ANG.[63]

ANG drives rDNA transcription in the nucleolus

The NLS brings ANG into the nucleolus, its final destination.[47] This particular NLS peptide has been characterized as a specialized signal peptide for the nucleolar compartment. Appending this peptide onto non-nuclear carrier proteins allows these proteins to migrate into the nucleolus.[48] Within the nucleolus, ANG stimulates ribosomal DNA (rDNA) transcription via binding to the ANG-binding element on the rDNA promoter.[66] ANG further induces promoter activation by modulating epigenetic marks on the promoter.[22] Up-regulated rRNA production is a common cellular response during proliferation. In fact, ANG-activated rDNA transcriptional activity is essential for manifesting its proliferative and angiogenic activities.[47,21]

1.3 Contribution of angiogenin to cancer development and progression

1.3.1 ANG in angiogenesis

ANG was named after its primary function, which is promoting angiogenesis—the development of blood vessels.[67,27] As the vascular network nourishes all tissues, it is not surprising that structural and functional vessel abnormalities contribute to many diseases.[68,69] Excessive vessel growth and function are hallmarks of cancer and expedite progression of the disease. Conversely, inadequate vessel maintenance or growth is associated with NDs.

Angiogenesis is a complex, highly coordinated, well-regulated process that can be summarized by 6 major steps: activation of endothelial cells by angiogenic factors; degradation of the capillary wall by extracellular proteinases; formation of a branch point in the vessel wall; migration of activated endothelial cells toward the angiogenic stimulus; formation of endothelial cells into tubules; and interconnecting the new tubules to form a branched network.[70,71]

ANG participates in multiple steps of angiogenesis. ANG can stimulate endothelial cells to proliferate, migrate, and form tubules.[72,73] ANG supports endothelial cell adhesion and stimulates plasminogen activators to generate plasmin, which activates collagenases to initiate cell

invasion.[74,75] Furthermore, ANG stimulates metalloproteinases to disrupt the basement membrane and extracellular matrix, thereby allowing endothelial cell penetration and migration.[76,77,73] Importantly, the angiogenic stimulation resulting from ANG depends primarily on ANG promoting rRNA production.[47,49] Knockdown of ANG expression or inhibition of ANG activity in endothelial cells resulted in decreased rRNA production and an insensitivity to stimuli from such growth factors as vascular endothelial growth factor (VEGF).[21]

1.3.2 VEGF in angiogenesis

VEGF is renowned as a crucial factor in controlling the growth and permeability of blood vessels, and has become the prime anti-angiogenic drug target.[78] There are several VEGF receptor-based inhibitors that have been approved by the FDA for clinical use.[79,80] In combination with chemotherapy or cytokine therapy, the anti-VEGF antibody (bevacizumab) is approved for treating several types of advanced metastatic cancers.[81] Additionally, four multi-targeted pan-VEGF receptor inhibitors have been approved: sunitinib, pazopanib, sorafenib, and vandetanib.[82] The clinical benefits of VEGF inhibitor treatments are attributed to their abilities to inhibit tumor vessel expansion and induce the regression of pre-existing tumor vessels. Nonetheless, only a fraction of cancer patients benefit from these treatments because tumors evolve resistance mechanisms or are refractory toward VEGF inhibitors.[83] Certain tumors produce pro-angiogenic factors other than VEGF even prior to being treated and are thus relatively insensitive to VEGF inhibition.[84] ANG is potentially one of those pro-angiogenic factors that prime tumor resistance to VEGF inhibitor treatment because ANG induces angiogenesis via a pathway that is mechanistically distinct from that of VEGF.[85,25]

1.3.3 ANG in tumorigenesis

Tumorigenesis is a multistep process involving both genetic and epigenetic changes in tumor cells that support the conditions of the tumor microenvironment.[86] ANG fuels tumorigenesis by promoting malignant cell proliferation, enhancing cell migration and invasion, and inducing angiogenesis.[72,75,76,21] In the tumor microenvironment, ANG is secreted by transformed cells and directly promotes tumor growth. This protein constantly translocates into the nucleoli to produce rRNAs, thereby satisfying the high demand of these highly proliferative cells for ribosome biogenesis. ANG is released from glioblastoma cells and stimulates endothelial cell tubule formation.[87] Hepatocellular carcinoma cells also secrete ANG to induce hepatic stellate cells and remodel the composition of the extracellular matrix.[88] In prostate cancer, ANG stimulates the invasion of normal prostate fibroblasts.[50,89,90] ANG can also induce vasculogenic mimicry in a fibrosarcoma cell line.[91] Overall, the central theme emerging from ANG actions in many different types of cancer is the generation of vascular network to encourage tumor growth.

The contributions of ANG to tumor growth and progression are also reflected by elevated serum protein levels in patients with solid tumors. In some patients, the level of ANG progressively increases as prostatic epithelial cells transform from a benign to an invasive phenotype.[92] Conversely, cancer therapy leads to a reduced ANG level, which increases during tumor recurrence.[89,93] These results suggest that this protein could be a useful clinical biomarker for monitoring responses to tumor treatment and for detecting tumor recurrence. Serum ANG levels vary between cancer types and study cohorts. Thus, different ranges might need to be established for particular tumors, stages and treatments in order to use ANG as a cancer biomarker.

1.4 Impact of ribosome biogenesis in cancer

1.4.1 Basis of ribosome biogenesis

ANG supports tumor growth by promoting the production of rRNA, which is a key component for ribosome assembly.[21,49,93] To gain more insight into the mechanism of ANG-activated rDNA transcription, it is important to understand ribosome biogenesis and its regulation. Ribosomes are the cellular components that are responsible for building proteins. Ribosome biogenesis is a complex process that demands large amounts of energy and involves several hundred factors.[94] Ribosome assembly requires a series of well-coordinated steps to take place in the nucleolus. Within the nucleolus, ribosomal genes are transcribed by RNA polymerase I (Pol I) to produce the 47S rRNA precursor that is further processed to generate the mature 28S, 18S, and 5.8S rRNAs.[95,96] The last rRNA, 5S rRNA, is transcribed by RNA polymerase III (Pol III).[97] These rRNAs are then assembled with numerous ribosomal proteins (RPs), which are brought into the nucleolus from the cytoplasm, to form pre-60S and pre-40S subunits.[98,99] These subunits then migrate back to the cytoplasm and form the final 80S ribosome, which is ready to translate proteins from mRNA transcripts.[100,101]

To maintain their cancer phenotypes, tumor cells are highly dependent on the hyper-activation of ribosome biogenesis.[102-104] A proliferating HeLa cell produces approximately 7,500 ribosomes per minute.[105] This process requires the transcription of 150–200 rRNA genes and the synthesis of ~300,000 RPs, as well as numerous interactions with assembly factors and small nucleolar ribonucleoprotein particles. This assembly line certainly requires the cooperation of thousands of molecules and consumes tremendous amounts of cellular energy. This intensive energy consumption by ribosome production could partially explain why cancer cells consume so much more energy (*e.g.*, glucose) than do normal cells.[106]

1.4.2 Epigenetic modifications regulate rDNA transcriptional activity

Among the multiple process steps of ribosome assembly, rDNA transcription is a rate-limiting step; thus, it is tightly regulated.[107] On average, there are 300–400 copies of rDNA genes in a cell. In a metabolically active cell, approximately 50% of rDNA genes are silenced by epigenetic control mechanisms (Figure 1.4).[108-110] These silent genes exist in heterochromatic architectures—transcriptionally silent chromatin structures. The establishment of heterochromatin at an rDNA promoter is controlled by a nucleolar remodeling complex (NoRC), which contains Snf2h and TIP5.[111] NoRC recruits DNA methyltransferase (DNMT) and histone deacetylase (HDAC) to decorate the histones with repressive marks, thereby condensing the structure of the promoter and inhibiting rDNA transcription.[112]

For NoRC to bind to an rDNA promoter, a non-coding RNA that is complementary to the rDNA promoter is required; this RNA is called promoter-associated RNA (pRNA).[113] pRNA is essential for NoRC nucleolar localization and repressive activity.[114-116] This particular RNA folds into a conserved stem-loop; mutations in this loop attenuate the interaction between pRNA and NoRC. In this case, the complex fails to accumulate in the nucleoli to suppress rDNA transcription. In contrast, ectopically delivering pRNA can trigger *de novo* DNA methylation at the rDNA promoter, thereby inhibiting transcription. These findings revealed a compelling mechanism by which non-coding RNA can target DNMT and HDAC to a specific genomic site, thereby inducing DNA methylation and transcriptional silencing. These findings emphasize further the importance of non-coding RNAs as biological regulators rather than simply by-products of background transcription.

1.4.3 Nucleolar size and number as markers of active, proliferating cells

Nucleoli are nuclear foci that serve as a core facility for manufacturing rRNAs and processing pre-ribosomal subunits.[117] Hence, nucleolar structure and size are parameters that can be used for evaluating the rate of ribosome biogenesis, as a measurement of the rapidity of cell proliferation.[102-104] As expected, cancer cells with high rates of ribosome biogenesis commonly exhibit large nucleoli.[118,119] In fact, this relationship between nucleolar size and cancer was recognized by pathologists over 100 years ago through the common detection of large and abnormal nucleoli in cancer cells. Consequently, nucleolar size has become a diagnostic marker of highly proliferative transformed cells.[120] The rate of ribosome biogenesis is highly variable among different cancer types, resulting in different nucleolar sizes that make this diagnostic tool challenging to use for assessing cancer progression.[121,122]

The upregulation of rRNA synthesis is mandatory for all tumors. Thus, potential strategies for downregulating rRNA synthesis and inducing an anti-proliferative response in cancer cells are of special interest.[123-125] Current chemotherapeutics agents for treating neoplastic diseases target damaged DNA or hinder DNA synthesis, but these drugs have been shown to exert toxic action mainly by inhibiting rRNA production.[126,125]As a result, these treatments lead to the loss of nucleolar integrity, interfere with ribosome biogenesis, and ultimately induce cell-cycle arrest in a p53-dependent manner.[127-129] Disrupted ribosome biogenesis leaves several unused ribosomal proteins remaining, and these become available to bind mouse double minute 2 homolog (MDM2), which is a p53 inhibitor.[130,131] When MDM2 is preoccupied, p53 is free to trigger cell apoptosis.

Aside from MDM2, there are many endogenous p53 inhibitors that are targets for cancer therapy, including ANG. ANG inhibits p53 function by interacting with the protein and

preventing phosphorylation.[132] Thus, p53 remains bound to the E3 ligase MDM2 and is targeted for proteasomal degradation via ubiquitination. Therefore, inhibiting ANG function could provide two prominent benefits: antagonizing the inhibitory effect of ANG on p53 and prohibiting ANG from promoting rRNA synthesis.

Several ANG inhibitors have demonstrated anti-tumor activity. Small-molecule inhibitors, an anti-ANG monoclonal antibody, and *ANG* expression knockdown via siRNA have been shown to markedly reduce the establishment and growth of human tumor cell xenografts in athymic mice.[133-136,50] These inhibitors offer limited utility in humans because of their large size, high cost, and lack of specificity.

1.5 ANG in neurodegeneration

Deficient angiogenesis can have devastating physiological consequences, such as those in the pathological conditions of NDs.[68,137,138] The first line of evidence linking an angiogenic factor to an ND was that VEGF deprivation under hypoxic conditions resulted in cells developing classic features of ALS-like motor neurons.[139] VEGF directly affects the health of motor neurons by acting as a neurotrophic or neuroprotective factor and by regulating the blood supply.[140,141] In this particular study, the hypoxia-response element was removed from the *VEGF* gene, which resulted in mice with normal baseline *VEGF* expression but with a pronounced deficit in the ability to induce VEGF in response to hypoxia.[139] As motor neurons require correctly patterned vascular networks for optimal oxygen delivery, the lack of VEGF-induced blood vessel formation under hypoxic conditions resulted in motor neuron degeneration. In contrast, the addition of VEGF protected motor neurons from degeneration in both *in vitro* and *in vivo* ALS models.[142,143] *VEGF* mutations have not yet been identified in ALS patients.

1.5.1 Amyotrophic lateral sclerosis—Lou Gehrig's disease

ALS is an adult-onset ND and is the most common motor neuron disease. The primary hallmark of ALS is the selective death of motor neurons in the brain and spinal cord.[144,145] ALS patients suffer from progressive paralysis in mid-life that ultimately leads to death within a few years of diagnosis. Initially described in 1869 by the famous French neurobiologist and physician Jean-Martin Charcot, ALS first became known as Charcot's sclerosis.[146,147] ALS is now commonly known in the United States as Lou Gehrig's disease, in honor of the great baseball player who developed the disease in the 1930s, and died two years after diagnosis.[148]

ALS currently afflicts approximately 30,000 Americans and has an overall prevalence of 2 out of 100,000 people.[149,150] In 90–95% of instances, there are no apparent genetic linkages, but in the remaining 5–10% of cases, the disease is inherited in a dominant manner. The most common genetic determinants of ALS are mutations in the Cu/Zn superoxide dismutase 1 (*SOD1*) and the expansion of non-coding GGGGCC repeats in a non-coding region of the chromosome 9 open reading frame 72 (*C9ORF72)* locus.[151-154]

More than 90 mutations in the *SOD1* gene have been found to be causative for ALS.[155,156] Mutations account for 15–20% of familial ALS instances and contribute to 1–2% of ALS cases overall.[157] SOD1 is an antioxidant enzyme that protects the cell from reactive oxygen species (ROS).[158,159] This enzyme is responsible for converting superoxide, which is produced primarily by oxidative phosphorylation errors in mitochondria, into water and hydrogen peroxide.[160,161] SOD1 variants with gain-of-function mutations result in the toxic disruption of many cellular pathways, leading to increased oxidative stress, reduced mitochondrial function, altered subcellular transport and ER stress induction. *SOD1* mutant mice have been used as a model for studying ALS.[162-165]

The GGGGCC hexanucleotide repeat expansion upstream of the *C9ORF72* coding region is the most common genetic determinant associated with familial and sporadic ALS, affecting approximately 10% of all patients.[153,154] The GGGGCC repeat length in healthy individuals ranges from 2–23 hexanucleotide units, whereas the repeat length in ALS patients is approximately 700–1,600 units.[166,167] The extended length of these repeats is present in approximately 40% of familial ALS and 8–10% of sporadic ALS instances.[168] The discovery of the expanded GGGGCC repeat has sparked great interest in investigating its molecular pathogenesis. In 2015, two papers published in *Nature* and one published in *Nature Neuroscience* reported a remarkable convergence of the primary consequence of these toxic repeats.[169-171] These expanded hexanucleotides are transcribed into repetitive RNAs, which are then translated into dipeptide repeats. The accumulation of either repetitive RNAs or dipeptide repeats consistently resulted in a deficit of nucleocytoplasmic transport through the nuclear pores. This obstruction of nucleus–cytoplasm traffic by the GGGGCC expansion-derived, toxic products reveals a novel mechanism involved in neurodegeneration.

1.5.2 Loss of function of ANG contributes to ALS

The search for other gene mutations associated with ALS led to the identification of loss-of-function mutations in the *ANG* gene in 2006.[24,172,173] To date, a total of 29 unique and nonsynonymous variants of the ANG gene have been identified in ALS patients. Many mutations result in impaired ribonucleolytic activity and nuclear translocation capacity, resulting in inhibited angiogenic activity.[174-176] Several ANG mutants also exhibit defects in neuronal pathfinding and are unable to confer neuroprotection.[177,178]

Plasma ANG levels in ALS patients are controversial. One study reported a modest elevation in serum ANG in ALS patients.[179] Later, the results from a larger cohort studied by the same

research group showed that the protein level was significantly *lower* in ALS patients.[180] Other studies have detected variable levels of ANG at different disease stages. The inconsistency in ANG levels that are reportedly associated with ALS highlights the need to develop a method for accurately quantifying ANG in human serum. One might consider a zymogram to be a potential option because it is a highly sensitive gel-based assay that can detect low nanogram levels of ANG.[181,44] This assay only detects enzymatically active ANG, which is the version capable of inducing neuroprotection. Therefore, this assay could provide more qualitative information of ANG levels for ALS diagnosis.

1.5.3 Neuroprotective activity of ANG

The most compelling evidence supporting the utility of ANG for ALS treatment arises from a study in which the administration of human ANG to SOD1 mutant mice not only extended their lifespan but also improved their motor function.[182] Further investigations have determined that ANG exerts neuroprotection by promoting motor neuron survival from a variety of insults, such as excitotoxicity, ER stress-induced cell death and hypoxic conditions.[182-184] Under these adverse conditions, treatment with an inactive ANG variant resulted in no neuroprotection, suggesting that ANG relies on its ribonucleolytic activity to modulate the health of motor neurons.[177,174,185]

To promote neuronal survival against oxidative damage, ANG triggers the cellular stress response program. Specifically, ANG cleaves a subset of mature tRNAs at the anticodon loop to generate 5′ and 3′ stress-induced small RNAs (5′- and 3′-tiRNA, respectively).[186,187] The tiRNAs then recruit YB-1, a translational silencer, to inhibit the formation of the translation initiation complex.[23,188] tiRNAs can suppress global protein translation by inhibiting both cap-dependent and cap-independent translation, including that mediated by weak internal ribosome entry sites (IRESs). Strong IRES-mediated translation—a mechanism often used by genes involved in pro-

survival and anti-apoptosis—is not affected. The formation of tiRNAs might contribute to motor neuron survival via the inhibition of apoptosis and the promotion of SG formation. Synthesized 5′-tiRNA delivered to stressed neurons led to the same anti-apoptotic result.

1.5.4 Stress granule formation to repress protein translation

SGs are cytoplasmic foci at which untranslated RNA packaged into ribonucleoproteins are transiently concentrated.[189] In fixed cells, SGs appear to be well-defined structures; however, they are highly dynamic and are characterized by a constant exchange of RNA and protein in the cytoplasm.[190] SG formation is an important cell survival mechanism under adverse conditions.[191] In response to environmental and genetic stresses, mammalian cells sequester key signaling molecules in SGs. These granules constitute signaling hubs that help to determine the fate of stressed cells: stress recovery or apoptosis. For stress recovery, cells reprogram protein translation by suppressing global protein expression while selectively enhancing the expression of pro-survival and anti-apoptosis genes. Failure of cells to recover from extreme stress triggers programmed cell death.

ANG contributes to stress-induced translation repression by promoting SG assembly. Both ANG and tiRNAs have been found to localize in SGs. The protein did not appear to induce SG assembly on its own, but rather enhanced the assembly of sodium arsenite- and pateamine A-induced SGs.[192] In contrast, the small non-coding RNA, 5′- but not 3′-tiRNA, was found to be capable of triggering SG formation.[186] Later, YB-1 was identified as a partner interacting with tiRNA; together, they act cooperatively to induce SG assembly.[188]

1.5.5 ANG exerts its neuroprotection in paracrine communication

Astrocytes are the largest cell population in the mammalian brain. They have been long recognized as physical and metabolic supporters of neurons.[193-195] They optimize the environment surrounding neurons, control neuro-developmental processes, and regulate synaptic transmission and plasticity. Many of these functions require close contact between astrocytes and neighboring neurons. Despite their supportive role, if astrocytes become pathologic, they can instead harm neurons. These cells can transmit toxic molecules to neighboring neurons and cause neuronal degeneration. In fact, dysfunctions of astrocytes have been implicated in the development and progression of several NDs.

In the case of ALS, mutated SOD1-expressing astrocytes trigger the death of motor neurons by secreting factors that are selectively toxic to motor neurons.[196,197] This toxic transfer from astrocytes to motor neurons has been demonstrated by co-culture and by the application of astrocyte-conditioned medium. Intriguingly, this interaction appears to be cell-type specific: mutant SOD1-expressing primary astrocytes reduced the viability of motor neurons, but not that of interneurons or dorsal root ganglion neurons.

In contrast, astrocytes also promote neuroprotection when their nuclear factor erythroid 2-related factor 2 (Nrf2), a redox-sensitive transcription factor, pathway is activated to neutralize ROS toxicity.[198] Crossbreeding mice in which the *Nrf2* gene is selectively overexpressed in astrocytes with mice of two ALS models produced offspring exhibiting significantly delayed ALS onset.[199-201] The offspring with ALS also survived for longer periods. Activation of the Nrf2 pathway in astrocytes is required for the promotion of neuronal survival. Together, these results not only show that astrocyte functions can be undermined or exacerbated, mediating motor neuron death, but also define paracrine interactions as critical regulators of ALS progression.

ANG confers neuroprotection via paracrine signaling pathways.[52] This protein is a neuronally secreted factor that executes its neuroprotective activity after being endocytosed by astrocytes. In addition, syndecan-4 receptor expression is restricted to astrocytes, which allows the protein to travel from neurons to astrocytes but not in the reverse direction. Furthermore, conditioned medium derived from astrocytes treated with ANG promoted motor neuron survival of stress stimuli. The astrocytic secretome in the medium constituted a set of astrocytic proteins, 60 of which were found to be significantly altered.[202] The secreted proteins included chemokines, cytokines, proteases, and protease inhibitors, as well as proteins involved in extracellular matrix re-organization; many of these proteins are important pro-survival regulators.

1.5.6 ANG mutations found in Parkinson's disease

A new theory of the role of ANG in other NDs began with the observation that a few ALS patients carrying ANG variants showed signs of Parkinson's disease (PD).[203,204] Furthermore, relatives of ALS patients have an increased risk of developing PD, and the prevalence of concomitant motor neuron disease in PD is higher than expected based on chance. ALS and PD are classified as movement disorders; yet, the molecular pathogenesis of each disease is remarkably distinctive, as specific neuron classes are degenerated in each case. Whereas dopaminergic neurons of the substantia nigra degenerate in PD, motor neurons degenerate in ALS.

PD is a progressive movement disorder characterized by the degeneration of midbrain regions that control motor movement.[205] Currently, PD is affecting more than 1 million Americans.[206] Although several single-gene mutations have been shown to result in PD, most forms of PD are sporadic. Lewy bodies are the neuropathological hallmark of PD.[169] One of the primary components of Lewy bodies is aggregated α-synuclein; this small neuronal protein plays

a significant pathogenic role in both familial and sporadic PD.[207,208] Aggregation of this protein is a neuropathological feature predominantly found in the substantia nigra of PD patients.

One microarray study reported an exciting result: mice overexpressing human α-synuclein exhibited modest alterations in the expression of 200 genes, but their *mAng 1* expression was 7.5-fold lower than that of wild-type littermates.[209] The mANG 1 protein level was also dramatically reduced in this transgenic mouse model of PD. Furthermore, treatment with WT ANG significantly reduced dopaminergic cell death in response to such toxic reagents as rotenone or 1-methyl-4-phenylpyridinium.[210,211] This study broadened the neuroprotective impact of ANG to include PD as well as ALS.

1.6 Prospectus

Cancer cells modulate cell-cycle regulation to achieve uncontrollable outgrowth, whereas degenerating neurons are extremely vulnerable to cell death. A growing body of work has reported that multiple cellular processes, when they are regulated aberrantly, can contribute to the development of cancer or NDs. Several of these processes are common to both cancer and NDs, including cell division, angiogenesis, and RNA and protein metabolism. Thus, exploring the cause of one disease is likely to have major benefits for understanding, treating and ultimately curing the other.

As these two diseases are linked, it is not surprising that cancer treatments can advance ND and vice versa.[212] Chemotherapeutic agents can promote neurodegeneration by activating p53 and other mechanisms.[213] Patients who receive chemotherapy can have cognitive complaints that persist long after the course of treatment has ended.[214,215] Adjuvant chemotherapy for breast cancer has been associated with short- and long-term changes in brain structure and function.[216] These reported side effects are controversial. Perhaps, more extensive studies and larger cohorts

are required to determine precisely how cancer treatment modulate the risk of neurodegeneration and how neuroprotective strategies, such as antioxidants, affect the action and efficacy of certain chemotherapeutic agents.

As mentioned above, there are currently several strategies of inhibiting ANG to suppress tumor angiogenesis and cancer progression. These strategies include siRNA that targets ANG mRNA and monoclonal antibodies and soluble binding proteins that sequester ANG protein. Utilizing ANG inhibitors to treat cancer is considered with caution because of the potential for ALS or PD development. Conversely, while ANG delivery is particularly promising for treating ALS and PD, long-term ANG treatment might potentially promote unnecessary blood vessel formation, and trigger cell transformation or tumor metastasis. Therefore, the purpose of this thesis is to explore the molecular role of ANG in cancer and neurodegeneration, to determine how ANG promotes cell proliferation, and to pinpoint the role of ANG in neuroprotection. Understanding the molecular divergence of ANG in cancer and neurodegeneration could lay a foundation for the development of ANG-based drug strategies to treat one disease without advancing the other.

Figure 1.1

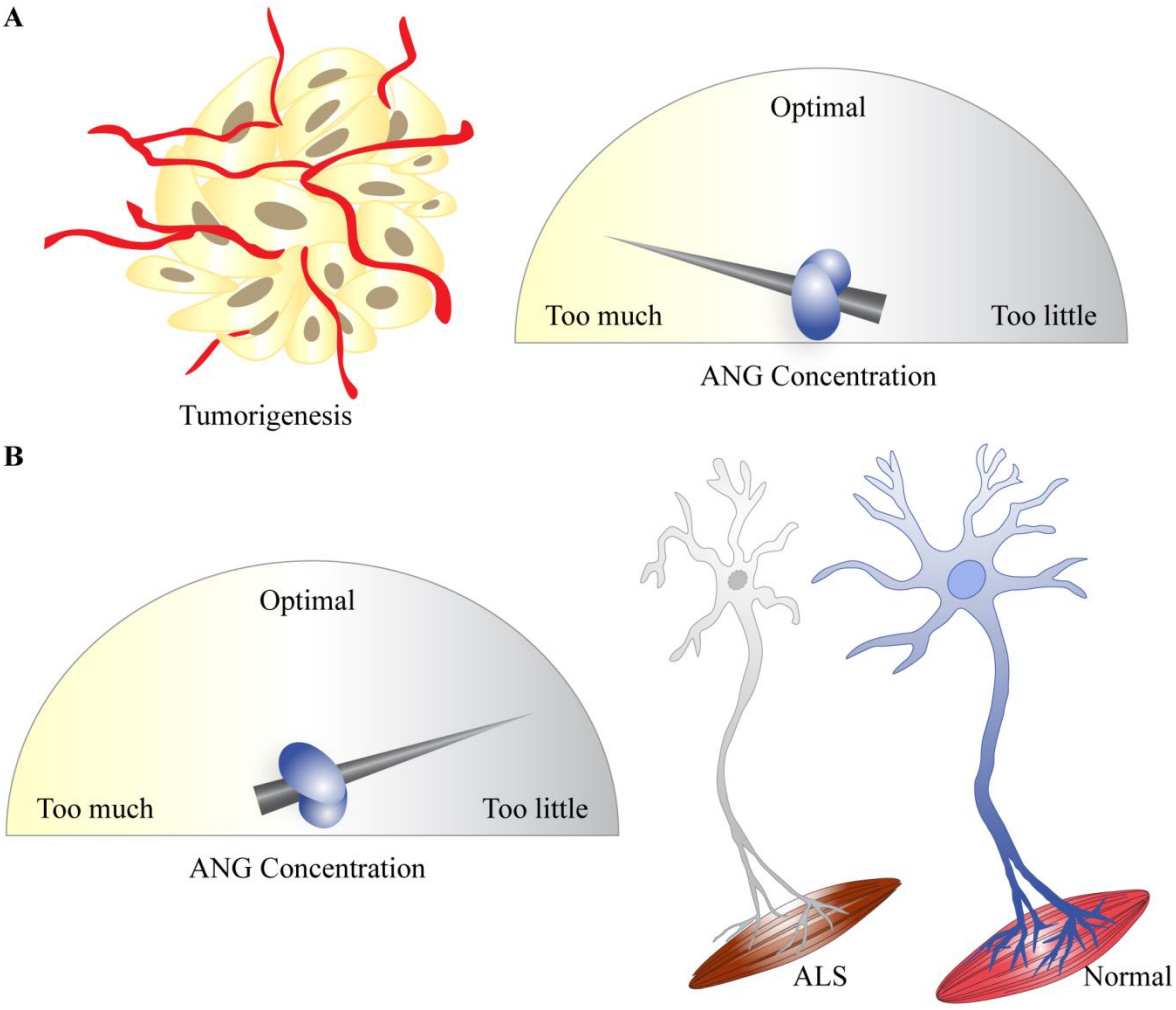
A
Tumorigenesis
Optimal
Too much
Too little
ANG Concentration
B
Optimal
Too much
Too little
ANG Concentration
ALS
Normal

Figure 1.1 Imbalance of ANG associated with pathological consequences

A, B ANG acts as a double-edged sword in that overproduction of this protein is correlated with tumorigenesis, while deprivation is associated with such NDs as ALS.

Figure 1.2

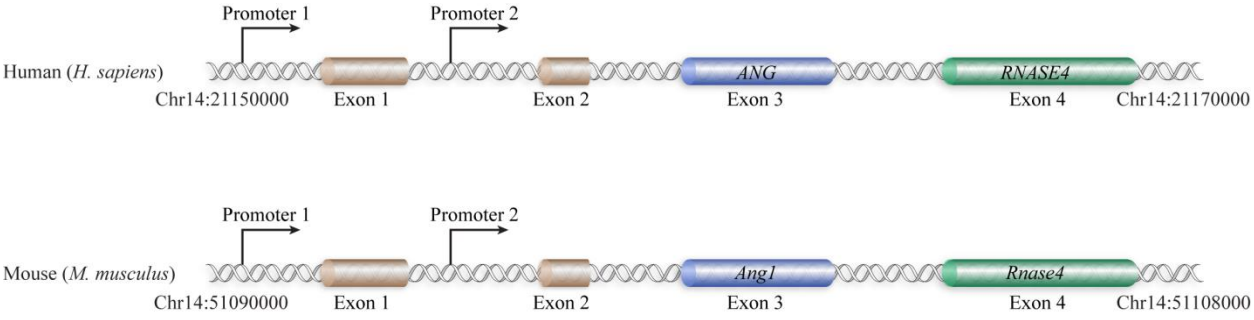
Promoter 1
Promoter 2
Human (H. sapiens)
ANG
RNASE4
Chr14:21150000
Exon 1
Exon 2
Exon 3
Exon 4
Chr14:21170000
Promoter 1
Promoter 2
Mouse (M. musculus)
Ang1
Rnase4
Chr14:51090000
Exon 1
Exon 2
Exon 3
Exon 4
Chr14:51108000

Figure 1.2 Unique gene arrangement of human and mouse ANG and RNase 4

The two exons encoding for ANG and RNase 4 are located downstream of the two non-coding exons. Transcripts of ANG and RNase 4 are controlled by 2 shared promoters. Promoter 1 is universally active, while Promoter 2 is designated for activation by hepatic cells. The organization of ANG and RNase 4 is highly conserved in other mammalian species, reflecting selection constraints maintaining the co-regulation of the two proteins.

Figure 1.3

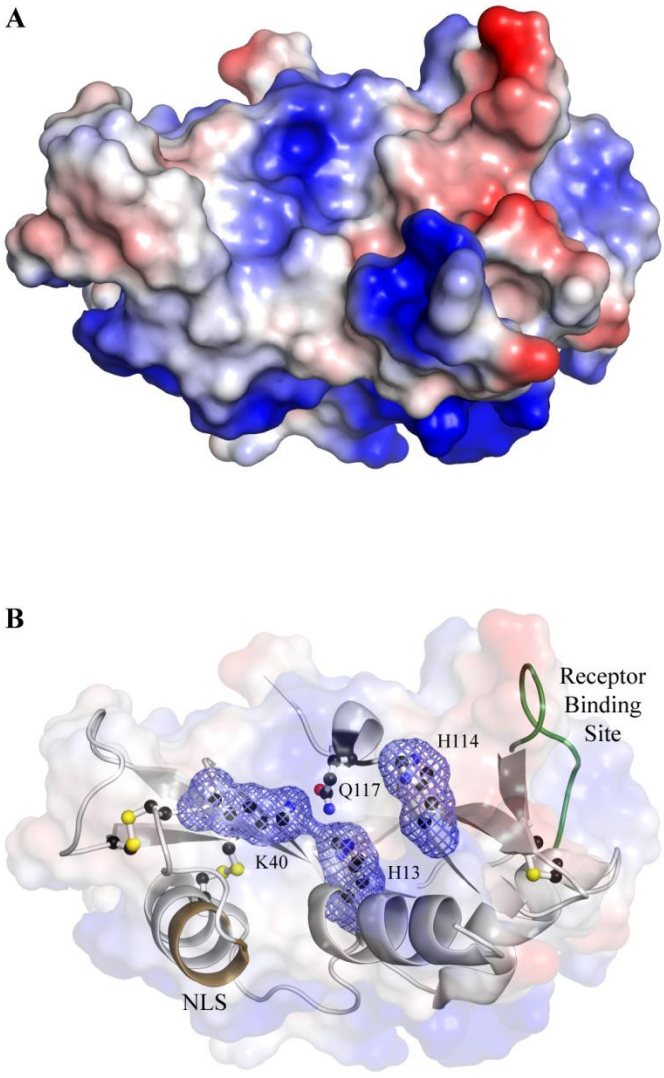

Figure 1.3 Structure of human ANG

A. The Coulombic surface of ANG is depicted with negative and positive indicated by red and blue, respectively (PDP entry 1ang).

B. Three conserved catalytic residues, H13, K40, and H114, and the obstructed site in ANG, Q117 (grey ribbon), are labeled and depicted in ball-and-stick. Three native disulfide bonds are also represented in ball-and-stick. The receptor binding site and NLS of ANG are highlighted in green and brown, respectively.

Figure 1.4

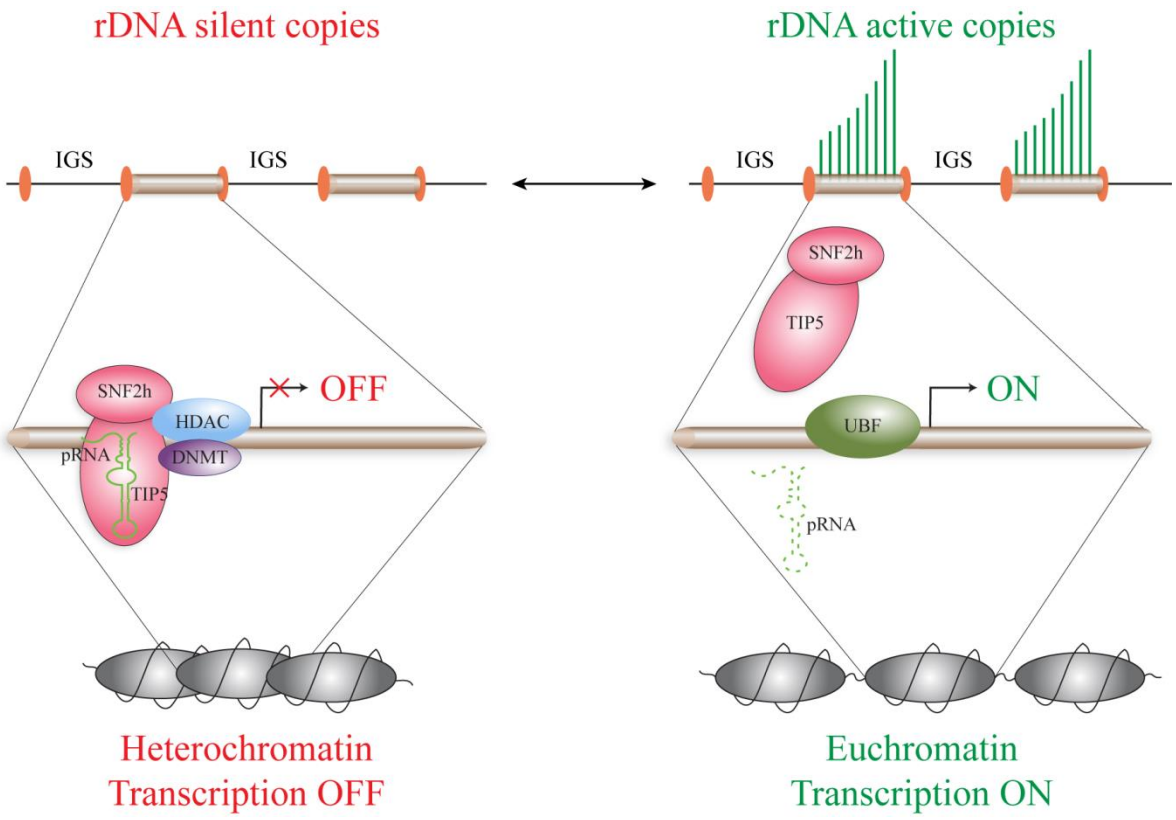
rDNA silent copies
rDNA active copies
IGS
IGS
IGS
IGS
SNF2h
HDAC
DNMT
pRNA
TIP5
OFF
SNF2h
TIP5
UBF
ON
pRNA
Heterochromatin
Transcription OFF
Euchromatin
Transcription ON

Figure 1.4 Transcriptional regulation of rDNA genes

On average, there are 300–400 copies of rDNA genes flanked by intergenic space (IGS) in a cell. In a metabolically active cell, approximately 50% of rDNA genes are silenced by epigenetic regulation. These silent genes exist in heterochromatic architectures, which are transcriptionally silent chromatin structures. The formation of heterochromatin at the rDNA promoter is controlled by NoRC, which contains Snf2h and TIP5. NoRC recruits DNMT and HDAC to decorate histones with repressive marks, thereby condensing the structure of the promoter and inhibiting rDNA transcription. The repressive activity of NoRC requires pRNA binding. Deprivation of this particular RNA diminishes NoRC accumulation at the rDNA promoter, allowing a transcriptional activator, or upstream binding factor (UBF), to bind and initiate rDNA transcription.

CHAPTER 2

Angiogenin Promotes Cell Proliferation by a Novel Signal Transduction Mechanism

Contribution: Prof. Raines and I designed the experiments, analyzed data and wrote the manuscript. I performed experiments.

Prepared for submission as:

Hoang, T.T. and Raines, R.T. (2016) Angiogenin promotes cell proliferation by a novel signal transduction mechanism

2.1 Abstract

Canonical growth factors act indirectly via receptor-mediated signal transduction pathways. Here we report on a novel direct pathway in which a growth factor is internalized, has its localization regulated by phosphorylation, and ultimately uses intrinsic catalytic activity to effect epigenetic change. Angiogenin (ANG), a secreted vertebrate ribonuclease, is known to promote cell proliferation, leading to neovascularization as well as neuroprotection in mammals. Upon entering cells, ANG encounters the cytosolic ribonuclease inhibitor protein, which binds with femtomolar affinity. We find that protein kinase C and cyclin-dependent kinase phosphorylate ANG, enabling ANG to evade its inhibitor and enter the nucleus. After migrating to the nucleolus, ANG cleaves pRNA, which prevents the recruitment of the nucleolar remodeling complex to the rDNA promoter. The ensuing derepression of rDNA transcription promotes cell proliferation. The biochemical basis for this unprecedented mechanism of signal transduction suggests new modalities for the treatment of cancers and neurological disorders.

2.2 Introduction

Angiogenesis, the process of establishing new blood vessels from pre-existing ones, is essential for the growth and development of mammals. Over forty years ago, Judah Folkman postulated that tumors compose new blood vessels to nourish their growth.[29,31] A few years later, his colleague Bert Vallee isolated a small protein from the conditioned medium of HT29 human adenocarcinoma cells and found that this protein, named "angiogenin" (ANG), promotes neovascularization.[27] This discovery was lauded widely as the first of a "substance that initiates the growth of any human organ".[28] Subsequently, ANG levels in the serum of cancer patients were found to correlate with the progression of their tumors.[50,217]

In addition to promoting neovascularization, ANG is neuroprotective.[30,52] *ANG* mutations are common in amyotrophic lateral sclerosis (ALS) patients.[24,176] Moreover, administration of ANG to an ALS mouse model was shown to improve motor functions and extend lifespan.[182]

Despite its biological and historical importance, the cellular mechanism by which ANG promotes cell proliferation is unclear. Remarkably, ANG belongs to the pancreatic-type ribonuclease (RNase) superfamily, beget by RNase A.[32] These secretory proteins catalyze the cleavage of a phosphodiester bond on the 3′ side of cytidine or uridine residues in single-stranded RNA. ANG is the only RNase with angiogenic activity, and the only angiogenic factor with ribonucleolytic activity.[218] Even though ANG shares 33% sequence identity with RNase A, including a conserved active-site triad (His14, Lys40, and His114), its ribonucleolytic activity toward di- and tetraribonucleotide substrates is 10^6-fold less than that of RNase A.[43,44] Still, this low ribonucleolytic activity is essential for the promotion of neovascularization.[219] The crystal structure of ANG revealed that Gln117 blocks the pyrimidine-binding pocket in the active site.[45] A Q117G substitution increases the catalytic activity of ANG toward conventional substrates by

30-fold.[46] Still, the Q117G substitution is not sufficient to endow ANG with catalytic activity comparable to that of RNase A, suggesting that ANG might have evolved to cleave a particular cellular RNA. The identity of that RNA substrate is unknown.

The activity of ANG is modulated by ribonuclease inhibitor (RI), a protein that resides in the cytosol. RI and ANG form one of the tightest biomolecular complexes, having a K_d value in the femtomolar range.[57] Up-regulating RI suppresses tumor growth and tumor microvessel density through suppression of ANG function.[64] Conversely, ANG variants endowed with the ability to evade RI display enhanced angiogenic activity.[63] Inside of cells, ANG exists in two pools: one is bound to RI in the cytosol and the other is unbound in the nucleus[65], where ANG manifests its angiogenic activity.[47,21] How ANG, which is a secretory protein, evades cytosolic RI on its way to the nucleus is unknown.

Here we reveal the cellular basis for the biological activities of ANG. Specifically, we show that ANG catalyzes the cleavage of a particular phosphodiester bond in a nucleolar substrate, promoter-associated RNA (pRNA). That cleavage prevents the silencing of ribosomal DNA (rDNA) transcription by the nucleolar remodeling complex (NoRC). We also show that phosphorylation of key serine residues enables ANG to evade cytosolic RI and translocate to the nucleus. Thus, unlike canonical growth factors that deliver epigenetic information to DNA indirectly via receptor-mediated signal-transduction pathways, ANG is unique in conveying its proliferative signal from outside of the cell directly to a nucleic acid.

2.3 Results

2.3.1 Wild-type ANG degrades pRNA in vitro in a specific manner

Cell proliferation requires continuous ribosome synthesis to support ongoing translation. The rate of ribosome biogenesis is limited by the transcription of DNA encoding rRNA.[121] ANG is known

to stimulate the transcription of rDNA in a manner that leads to endothelial cell proliferation and the induction of neovascularization.[47,22]

The transcription of rDNA is regulated tightly.[123,220] Importantly, rDNA transcription is silenced by NoRC, in which transcription termination factor I-interacting protein 5 (TIP5) is a large subunit and non-fermenting protein 2 homologue (SNF2h) is a small subunit.[111,112] Upon the binding of NoRC to the rDNA promoter, the complex recruits histone deacetylase and DNA methyltransferase activity to remodel or maintain a repressive conformation of heterochromatin.[221,115,222] The binding of NoRC to the rDNA promoter requires pRNA, which is a product of a long, processed non-coding RNA transcribed by RNA polymerase I from the intergenic space of rDNA. pRNA (~200 nt) has a conserved stem-loop structure and a sequence that forms a triple helix with the rDNA promoter.[114,221] TIP5 binds to pRNA via its TAM domain. Removing that domain or knocking-down pRNA abolishes the repression of rDNA transcription by NoRC.[113,116] We hypothesized that pRNA could be the cellular substrate for ANG.

We examined pRNA as a substrate of ANG *in vitro*. To do so, we first incubated an internal ^{32}P-labeled pRNA containing only the stem–loop structure (97 nt) with recombinant ANG and monitored its cleavage over time. Approximately 80% of the pRNA was cleaved after 10 min (Figure 2.1A). Next, we determined if any of the single-stranded RNA loops of pRNA are important for cleavage. Excision of the lower loop led to no change in cleavage (Figure 2.1B). In contrast, deleting a series of 4 uridine residues in pRNA decreased the ability of pRNA to serve as a substrate for ANG. This decrease was even greater upon removal of the upper loop. By examining different loops of pRNA we determined that ANG relies primarily on the U_4 region

and the upper loop for the manifestation of its catalytic activity. Indeed, removing the putative binding region on pRNA obliterates catalysis by ANG (Figure 2.1B).

We found that ANG cleaved pRNA at a specific location to give a product of ~85 bases and, subsequently, smaller fragments. This specificity was unique to ANG, as RNase A cleaved RNA nonspecifically (Figure 2.1C). Importantly, the specificity was resistant to the excision of single-stranded RNA loops on pRNA (Figure 2S.1). To determine the cleavage site on pRNA by ANG, we isolated the ~85-base product and determined its sequence. We found that a C–G phosphodiester bond near the 3′ end of pRNA is cleaved specifically by ANG (Figure 2.1C). This finding is consistent with the known preference of ANG to cleave RNA between a pyrimidine and purine residue.[223,44] ANG and pRNA have co-evolved in mammals with the conservation of this C/T–G phosphodiester bond (Figure 2S.2).

We interrogated the putative C–G cleavage site in pRNA by mutagenesis. Based on the predicted secondary structure of pRNA, the cytidine residue participates in Watson–Crick base-pairs with a guanidine residue from the 5′ end. When we replaced the three G·C base pairs in pRNA with C·G, ANG no longer cleaved the substrate (Figure 2S.3). Further, a single C·G→ G·C substitution at the putative cleavage site impaired ANG from degrading the substrate (Figure 2.1D). In contrast, RNase A degraded pRNA efficiently regardless of these modifications.

2.3.2 ANG degrades pRNA in cellulo

Having shown that pRNA is a substrate for ANG *in vitro*, we asked if ANG can access and degrade nucleolar pRNA in HeLa cells. Using qPCR to quantify the level of pRNA, we found that treatment with ANG reduced pRNA levels by 50%. This lower level is the same as that achieved with locked nucleic acid (LNA)-mediated knockdown of pRNA (Figure 2.2A). We

used variants of ANG, including those found in ALS patients (S28N, C39W, and H114R), to probe enzymatic activity *in cellulo*.[24,174,176] We found that substitutions that affect the nuclear localization (S28N) or thermostability (C39W) of ANG had no effect on its catalytic activity *in vitro* but diminished its catalytic activity *in cellulo* (Figure 2.2B). Replacing a critical active-site residue (H114R) led to no degradation of pRNA either *in vitro* or *in cellulo*. In contrast, a hyperactive variant (Q117G) degraded pRNA robustly.

We next sought evidence for a direct interaction between ANG and pRNA *in cellulo*. We installed a FLAG tag on ANG and used RNA immunoprecipitation to probe for the existence of an ANG·pRNA complex. Because WT ANG degraded pRNA (Figure 2.1), we used the inactive H114R variant. This variant was unable to cut pRNA (Figure 2.2B), but bound to pRNA with nanomolar affinity (Figure 2S.4). Following treatment with the FLAG–H114R ANG variant, cellular RNAs were treated with RNase A to cleave unprotected RNAs. With or even without UV-mediated crosslinking, we were able to detect a fragment of pRNA that was protected by ANG, and confirmed its identity as the conserved stem–loop structure of pRNA by sequence analysis (Figure 2.2C).

2.3.3 ANG promotes dissociation of TIP5 via targeting pRNA

As described above, the silencing of rDNA transcription by NoRC is mediated by the binding of pRNA to TIP5.[113] The depletion of pRNA leads to TIP5 dissociation from the rDNA promoter and thereby activates rDNA transcription via chromatin remodeling. To demonstrate further the involvement of ANG in suppressing NoRC function, we used immunofluorescence microscopy to probe for the accumulation of TIP5 in nucleoli as an indicator of rDNA silencing in the presence and absence of ANG (Figure 2.3A). Punctate staining of TIP5 in the nucleolus was observed in untreated cells but not in cells treated with ANG. The absence of TIP5 in nucleoli is

consistent with its being unable to bind to the rDNA promoter because pRNA had been cleaved by ANG and no longer remained at the rDNA promoter region.

pRNA could exist in a complex with TIP5 prior to interacting with ANG. Thus, angiogenic activity might require ANG to cleave pRNA within a TIP5·pRNA complex. To test for this ability, we reconstituted an *in vitro* model wherein an excess of the TAM domain of TIP5, which is necessary and sufficient to interact with pRNA, was incubated with the RNA substrate and then exposed to wild-type ANG and its Q117G and H114R variants (Figure 2.3B).[113] Over the course of 40 min, pRNA degradation was observed with wild-type ANG but not the H114R variant. Even more degradation was observed with the Q117G variant. Notably, the rate of pRNA cleavage by ANG was slower with pRNA in the bound state than in the unbound state (Figure 2.1A). Still, the data indicate that ANG can access its cleavage site on pRNA within a pRNA·TIP5 complex and that the cleavage leads to dissociation of that complex from the promoter. We note that, *in cellulo*, ANG could target nascent pRNA to prevent NoRC from anchoring to the rDNA promoter.

The assembly of NoRC facilitates heterochromatic histone modification, resulting in a reduction in the methylation of H3K4, which is a euchromatic histone mark. NoRC also promotes H3K9 methylation, which marks repressive transcription.[224] Accordingly, we probed H3K4 and H3K9 methylation upon treating cells with ANG variants of varying enzymatic activity. We found that the enrichments of histone-methylation occupancy at the rDNA promoter correlated with enzymatic activity (Figure 2.3C).

Chromatin immunoprecipitation (ChIP) of H3K4me^3 at the rDNA promoter revealed a 2- and 3-fold increase in methylation upon treatment with ANG and the Q117G variant, respectively, but no change with the H114R variant (Figure 2.3C). Conversely, ChIP to probe methylation of

H3K9, which marks repressive transcription, revealed that that the level of H3K9me^3 at the rDNA promoter decreased upon treatment with either ANG or the Q117G variant, but not the H114R variant.

2.3.4 ANG is phosphorylated by PKC and CDK

The activation of rDNA transcription via the degradation of pRNA and consequent suppression of NoRC function can occur only if ANG gains access to the nucleus. A femtomolar inhibitor of ANG, RI lurks in the cytosol at low micromolar concentrations.[225] We hypothesized that ANG undergoes a post-translational modification to evade RI.

The extraordinary tight binding between RI and ANG is due largely to favorable Coulombic interactions, as RI is highly anionic and ANG is highly cationic.[59] Hence, appending phosphoryl groups on ANG residues can generate Coulombic repulsion and diminish affinity for RI. Among the sixteen serine and threonine residues of ANG, four were of particular interest to us: Ser87, which is at the molecular interface of the RI·ANG complex and is in a known "hotspot" for amino-acid substitutions that engender evasion of RI, and a cluster of three near the nuclear localization signal: Ser28, Thr36, and Ser37 (Figure 2.4A).[61,226,63]

We discovered that ANG is phosphorylated by intracellular kinases. Incubation of wild-type ANG with a whole cell lysate and [γ-^{32}P]ATP led to ^{32}P-labeled ANG (Figure 2.4B). We used variants of ANG to determine the specificity of the phosphorylation reaction. None of these interested residues is essential for the ribonucleolytic activity or conformational stability of ANG.[227] We found that S28N ANG (which is linked to ALS) was phosphorylated *in vitro* approximately as extensively as was the wild-type enzyme (Figure 2.4B). In contrast, the T36A/S37A and S87A variants had a severe reduction in their phosphorylation. Then, we examined phosphorylation *in cellulo*. Wild-type ANG and variants with a FLAG tag were

isolated by immunoprecipitation from HeLa cells after incubation for 4 h. The uniform intensity of the input samples indicated that neither the amino-acid substitutions nor the FLAG tag affected cellular uptake (Figure 2.4C), which occurred via the syndecan-4 receptor (Figure 2S.5). Likewise, the substitutions had inconsequential effects on thermostability (Table 2S.1). To detect phosphorylated species, we used antibodies to phosphoserine or phosphothreonine. No detection was observed with the phosphothreonine antibodies (data not shown). In contrast, immunoblots with phosphoserine antibodies displayed a strong band for wild-type ANG, indicating the existence of phosphorylated ANG *in cellulo* (Figure 2.4C). A weaker band was observed with the S28N variant, consistent with the phosphorylation of Ser28 by cellular kinases. A very weak band was detected for both the T36A/S37A and the S87A variants. These data indict Ser28, Ser37, and Ser87 as sites of phosphorylation *in cellulo*.

We identified kinases that phosphorylate ANG. For guidance, we analyzed the amino-acid sequence of ANG with the program NetPhos 2.0.[228] The computational results indicated that protein kinase C (PKC) and cyclin-dependent kinase (CDK) were likely kinases. We then treated cells with small-molecule inhibitors of PKC and CDK, namely, bisindolylmaleimide I and roscovitine.[229,230] The inhibitors did not influence the cellular uptake of ANG, but did reduce its phosphorylation (Figure 2.4D). We conclude that ANG is a substrate for PKC and CDK.

2.3.5 Phosphorylation of ANG is essential for its nuclear translocation

We probed the effect of phosphorylating residues 28, 36/37, and 87 on the affinity of ANG for RI. To do so, we generated phosphomimetic variants and determined the value of K_d for the ensuing ANG·RI complexes. The femtomolar affinity of RI for WT ANG required month-long assays to detect complex dissociation.[57] In comparison, the dissociation of the ANG variants was rapid and monitored readily by using a fluorescence-based assay described previously.[139] Both

the T36D/S37D and the S87D variants had 10^7-fold lower affinity for RI than did wild-type ANG (Table 2.1). Moreover, the S28D/T36D/S37D/S87D variant exhibited a $>10^9$-fold reduction in affinity. These data are consistent with a mechanism in which phosphorylation of interface residues 37 and 87 enables ANG to evade RI.

Finally, we probed the effect of phosphorylating residues 28, 36/37, and 87 of FLAG-tagged ANG on its nuclear translocation. With immunofluorescence microscopy, we found that alanine substitution at residues 28, 36/37, or 87 (which creates a phosphorylation defect) leads to the retention of ANG in the cytosol (Figure 2.5A). Conversely, aspartate substitution leads to its accumulation in the nucleus. Using pRNA degradation as a marker for the entry of ANG into the nucleus, we found that pRNA remained intact *in cellulo* upon treatment with S28N, T36A/S37A, or S87A ANG (Figure 2.5B), even though these variants cleaved pRNA *in vitro* (data not shown). These data indicate that the phosphorylation of residues Ser28, Ser37, and Ser87 enables internalized ANG to enter the nucleus and degrade pRNA.

2.3.6 ANG promoting angiogenesis requires nuclear translocation and rDNA transcription

We found that ANG is phosphorylated at the same sites by PKCs and CDKs in endothelial cells as in HeLa cells (Figure 2.6A). Moreover, the extent of phosphorylation of the S28N/T36A/S37A/S87A variant (STSS/NAAA ANG) was indistinguishable from that of a variant in which all nine serine residues were replaced with alanine (Ser-Free ANG), indicating that no other serine residues are susceptible to phosphorylation. Phosphorylation governed ANG entry into the nucleus of endothelial cells (Figure 2.6B). Once in the nucleus, ANG reached the nucleolus to activate rDNA transcription via cleaving pRNA (Figure 2.6C). Most importantly, these features—ANG phosphorylation and activation of rDNA transcription—are essential for ANG proliferative and angiogenic activities. HUVE cell-proliferation in basal medium

containing ANG or a variant was stimulated by the wild-type enzyme, but not the inactive H114R or STSS/NAAA variant (Figure 2.6D). Moreover, cells pre-exposed to small-molecule inhibitors of CDKs and PKCs were quiescent, even after treatment with ANG. Using a tube-formation assay,[231] we found that pre-incubating endothelial cells with ANG led to the assembly of capillary-like networks (Figure 2.6E). In contrast, cells pre-incubated with the H114R or STSS/NAAA variant constructed fewer junctions and tubules, and the tubules were of shorter length (Figure 2.6F–H). Likewise, ANG treatment did not revive network formation in cells pre-treated with kinase inhibitors.

2.4 Discussion

Members of the pancreatic-type RNase superfamily have evolved to be efficient non-specific catalysts of RNA degradation.[232] Unlike its homologs, ANG has nearly immeasurable ribonucleolytic activity towards model substrates.[223,44] Moreover, whereas other pancreatic-type RNases function in the extracellular space or cytosol, ANG acts in the nucleus.[47,21] Here we have revealed the cellular mechanism used by ANG to effect cell proliferation by virtue of specific ribonucleolytic activity. That mechanism is depicted in Figure 2.7.

Intracellular kinases enable ANG to manifest its ribonucleolytic activity. Like its homologs, ANG is a highly cationic protein that enters mammalian cells via endocytosis. A fraction of the ANG in endosomes escapes into the cytosol, where it encounters a potent inhibitor, RI. The RI·ANG complex is stabilized largely by favorable Coulombic interactions, as RI is highly anionic. The introduction of anionic phosphoryl groups into ANG generates Coulombic (as well as steric) repulsion with RI, resulting in weaker binding. We note that site-directed mutagenesis has been used to endow other pancreatic-type RNases with the ability to evade RI, and such

variants are cytotoxic at the nanomolar level.[226] In contrast, the ribonucleolytic activity of ANG is so low, that its evasion of RI does not lead to any apparent cytotoxicity.

ANG binds to the same region of pRNA as does TIP5. The reported K_d value of the TIP5·pRNA complex is 0.3 nM,[113] whereas the K_d value of the H114R ANG·pRNA complex is 192 nM (Figure 2S.4). These disparate values indicate that TIP5 competes favorably with ANG for binding to pRNA. We note, moreover, that ANG is an enzyme and that its cleavage of a phosphodiester bond in pRNA is irreversible. Accordingly, only a transient interaction between ANG and pRNA is necessary for ANG to assert its biological activity. Thus, the cleavage of pRNA by ANG is apparent even in the presence of TIP5 (Figure 2.3B).

An angiogenin-binding element (ABE) near the rDNA promoter has been proposed to be responsible for driving the expression of genes encoding rRNA upon stimulus with ANG.[66] We find that the affinity of ANG for pRNA is 3-fold higher than that for ABE (Figure 2S.4). Moreover, as noted above, the binding of ANG to pRNA leads to an irreversible event—phosphodiester bond cleavage. As ribonucleolytic activity is essential for ANG action,[219] the cleavage of pRNA is likely to play a larger role in the action of ANG than does its binding to the ABE.

pRNA is not the only cellular substrate of ANG under all conditions. We have demonstrated that ANG can localize in the nucleolus and cleave a particular phosphodiester bond in pRNA, thereby inducing rDNA gene expression. This up-regulation satisfies the rRNA demands of ongoing translation and promotes angiogenesis. In contrast, in cells that have suffered oxidative damage, ANG localizes in stress granules (Figure 2S.6) and cleaves a subset of tRNAs, thereby generating tRNA-derived, stress-induced small RNAs that stall translation and drive the

production of anti-apoptotic proteins that inhibit cell death.[186-188] The molecular basis for the localization of ANG in stress granules as a consequence of oxidative stress is unclear.

The mechanism of action of ANG is unique. Typical growth factors bind to the extracellular face of membrane-bound receptors and rely upon changes in receptor conformation or valency to transduce a signal to the cytosol, often leading to kinase or phosphatase activity.[233,234] The growth factors themselves do not enter cells. This action-at-a-distance model contrasts markedly with the mechanism of ANG action (Figure 2.7). Instead of conveying signals via other proteins, ANG has evolved to deliver its proliferative signal directly. We speculate that this unique mechanism is conserved in mammals (Figure 2S.2).

The mechanism of ANG action resembles that of clustered, regularly interspaced, short palindromic repeats (CRISPR)–Cas9. CRISPR–Cas9 has been engineered such that its guide RNA acts as both a scaffold to recruit transcriptional regulators and dock them with a double-stranded DNA target, leading to transcription repression or activation (Figure 2S.7).[235,236] Likewise, pRNA recruits NoRC and docks them to a double-stranded DNA target, leading to transcription repression. pRNA also recruits ANG, leading to pRNA cleavage and transcription activation.

The route taken by ANG has other implications. In astrocytes, ANG is internalized after binding to syndecan-4, a transmembrane heparan sulfate proteoglycan.[175,52] This receptor is also displayed by endothelial cells and involved in inflammatory reactions, wound healing, and angiogenesis.[54] We found that this receptor also mediates the uptake of ANG into HeLa cells (Figure 2S.5). Because syndecan-4 is involved in the activation of PKCα,[55] ANG could be phosphorylated immediately by this PKC isoform upon cytosolic entry.

Finally, we note a dichotomy: ANG is upregulated in transformed cells but is necessary to prevent neurodegeneration of nontransformed cells. Hence, drugs that target this pro-tumorigenic protein could also promote neurological damage, as loss-of-function mutations of *ANG* genes are associated with ALS.[24,176] The understanding of ANG action provided in this work suggests new chemotherapeutic strategies. For example, Ser37 and Ser87 of ANG, which are phosphorylated *in cellulo*, make intimate contacts with Ile459 and Trp261/Trp318 of RI, respectively, in the RI·ANG complex (Figure 2.4A).[61] Replacing those large RI residues with smaller ones in endothelial cells could effect a "bump–hole" strategy that leads to an RI variant capable of apprehending ANG even after its phosphorylation. Alternatively, expression of an uncleavable pRNA variant in endothelial cells could elicit a dominant negative phenotype that sequesters ANG and thereby decreases its activity. We believe that modulating kinase activity holds special promise. Antagonizing the activity of PKC or CDK in endothelial cells, but not astrocytes, could benefit ALS patients treated with exogenous ANG. Indeed, known drugs that inhibit these kinases in cancer patients could be acting, in part, by unappreciated mechanism—decreasing the activity of endogenous ANG (Figure 2.7). For example, flavopiridol and enzastaurin are inhibitors of CDK and PCK, respectively, and both antagonize angiogenesis.[237,238] Our data provide a plausible link for these two clinical paradigms.

2.5 Materials and methods

2.5.1 General Procedures

Production and purification of ANG and its variants,[44] and of His_6–$TIP5_{510\text{-}611}$ (TAM), immunofluorescence of TIP5 and knockdown of pRNA,[113] and chromatin immunoprecipitation of the rDNA promoter.[221] RI-binding assays with variants of Q19C ANG were performed as described previously.[239] Briefly, fluorescence spectroscopy was used to monitor the binding of

an RI to a diethylfluorescein (DEFIA)-labeled ANG, availing the decrease in fluorescence upon binding to RI. Data were normalized to unbound DEFIA–ANG and fitted with nonlinear regression analysis to obtain a value of K_d for each complex.

2.5.2 Run-off Transcription

A DNA template encoding the 97 bases of pRNA downstream from a T7 RNA polymerase promoter was obtained from Integrated DNA Technology (IDT). pRNA biosynthesis was accomplished with the AmpliScribe™ T7-*Flash*™ Transcription kit (Epicentre) in the presence of 3 μL of [α-^{32}P]UTP. Transcribed pRNA was purified by excision from a urea polyacrylamide (8% w/v) gel. Modified pRNAs were made in a similar manner.

2.5.3 Gel-based assay of ribonucleolytic activity

In each reaction mixture, pRNA containing [α-^{32}P]UTP (~1000 cpm) was subjected to either wild-type ANG (50 nM) or buffer at 37 °C. At known times, a 10-μL aliquot was removed and quenched with 2 μL of 6× urea gel-loading dye. Samples were heated to 95 °C and resolved electrophoresis through a urea polyacrylamide (8% w/v) gel. The gel was dried and exposed to a phosphor screen for 24 h. Radiography of the screen was performed with a Typhoon LFA9000 phosphorimager (GE Healthcare Life Sciences).

2.5.4 Sequencing of pRNA fragments

Nonradioactive pRNAs were made as described above. In a 40-μL reaction mixture, wild-type ANG (~1 μM) was used to degrade pRNA (1 μg) at 37 °C for 10 min. The reaction was quenched with proteinase K (Qiagen). Degraded pRNAs were resolved in a urea polyacrylamide (8% w/v) gel. The major pRNA fragment was purified as described above. The fragment was then treated with alkaline phosphatase (New England Biolabs) to generate a 3′-hydroxyl

terminus. A poly(A) tail was added to the 3′ end of the fragment by using poly(A) polymerase (New England Biolabs). A reverse transcription (RT) reaction was conducted using the RT primer (Table 2S.2). The ensuing cDNAs were amplified further by PCR and subjected to TOPO-cloning for Sanger sequencing with an M13 forward primer.

2.5.5 Cell culture

HeLa cells were grown in Dulbecco's Modified Eagle's Medium (DMEM) containing fetal bovine serum (10%) and penicillin/streptomycin (1%) (Invitrogen) at 37 °C under 5% v/v CO_2(g). Human umbilical vein endothelial (HUVE) cells were grown in EGM^{TM}-2 at 37 °C under 5% v/v CO_2(g). Cells (5×10^5) were plated in complete medium in 10-cm dishes. After 24 h, cells were washed with DMEM or endothelial basal medium-2 (EBM-2) and then incubated with wild-type ANG or a variant (to 1 μg/mL) for another 24 h [49]. For kinase-inhibitor treatment, cells were pre-incubated with either bisindolylmaleimide I (4 μM) and roscovitine (14 μM) for 30 min prior to treatment with ANG. Cells were then harvested for isolation of either RNA or protein.

2.5.6 Quantification of cellular RNAs by qRT-PCR

Total cellular RNA was isolated by extraction with Trizol (Invitrogen). RNA samples were treated with DNase I (Invitrogen) at 37 °C for 15 min. RNA were purified by phenol:chloroform extraction, followed by ethanol precipitation. RNA concentrations and purities were assessed with a NanoVue instrument (GE Healthcare Life Sciences).

Purified cellular RNA (~1 μg) was used in the reverse transcription reaction along with random hexamers from the SuperScript III Reverse Transcriptase kit (Invitrogen). A 1-μL solution of the ensuing cDNAs were used in qPCR reactions using PerfeCTa SYBR Green

FastMix Reaction Mixes (Quanta Biosciences). Amplified cDNAs were evaluated with an ABI Prism 7200 sequence detector (Perkin Elmer). The sequences of the primers used for qPCR are listed in Table 2S.2.

2.5.7 RNA immunoprecipitation (RIP)

Cells were treated with FLAG–H114R ANG, and then washed with cold PBS. Cells were UV-crosslinked with $\lambda_{254\,nm}$ at 1500 J/cm^2. Cells were lysed in IP buffer (20 mM HEPES–KOH buffer, pH 7.5, containing 250 mM NaCl, 1 mM EDTA, 1% v/v NP-40, 10% v/v glycerol, and a protease-inhibitor cocktail) for 20 min at 4 °C, and then subjected to centrifugation. Clarified lysate was treated with 500 pM RNase A and 2 µL of 2 units/µL DNase I (Invitrogen) for 10 min at 37 °C. Then, the lysate was incubated with α-FLAG magnetic beads (Sigma Chemical). Beads were washed and then eluted 3× with 150 ng/µL 3× FLAG peptides (APExBIO). Eluates were combined and split into two portions: one for an immunoblot and the other for RT-PCR to identify co-precipitated RNAs.

2.5.8 Immunoblots

Per 10-cm dish, cells were lysed with 1 mL M-PER mammalian protein extraction reagent (Pierce) containing a protease-inhibitor cocktail. Protein (~30 µg) was separated by SDS–PAGE (Biorad), and the resulting gel was subjected to immunoblotting. Densitometry of the bands were analyzed using ImageQuant TL software. For immunoprecipitation experiments, cells were lysed with IP buffer containing protease- and phosphatase-inhibitor cocktails. Clarified lysates were incubated with α-FLAG magnetic beads (Sigma Chemical) and washed 3 times. Samples were eluted with 30 µL of SDS loading dye and processed further for immunoblotting.

2.5.9 Immunofluorescence

Prior to immunofluorescence experiments, HeLa and HUVE cells were plated for 24 h at a density of 1 × 10^5 cells in 0.2 mL of medium in an 8-well µ-chamber (Ibidi). Cells were washed with serum-free medium (3 × 0.2 mL). FLAG–WT ANG and its variants (1 µg/mL) were added in serum-free medium, and the resulting medium was incubated for 3 h. All the subsequent steps were performed at room temperature and with PBS washes between steps. Cells were fixed with 4% v/v paraformaldehyde (Thermo) in PBS for 10 min and permeabilized using freshly prepared 0.1% v/v Triton X-100 (Sigma Chemical) in PBS for 10 min. Next, cells were incubated with blocking solution (Thermo) for 1 h. Then, incubation of mouse anti-FLAG monoclonal antibody (Sigma) was performed for 1 h. After extensive washes, goat anti-mouse Alexa Fluor 488 was incubated for 1 h. Cells were counterstainded with the nuclear probe Hoechst 33342 (Invitrogen) at 37 °C during the final 5 min. Cells were imaged with an Eclipse TE2000-U laser scanning confocal microscope (Nikon) equipped with an AxioCam digital camera from Carl Zeiss (Oberkochen, Germany).

2.5.10 Cell proliferation assay

HUVE cells in EGM™-2 were plated at 5,000 cells per well in a 96-well microplate. After 24 h, cells were switched to EBM-2 containing ANG or a variant (1 µg/mL). At known times, growth medium was removed and cells were incubated with fluorescent dye CyQUANT® NF (Invitrogen) binding solution. Fluorescence intensity was recorded on an M1000 fluorimeter (Tecan) with excitation at 485 nm and emission detection at 530 nm. Data were analyzed with Prism 5.0 software (GraphPad).

2.5.11 Tube formation assay

HUVE cells were grown in EGM™-2 at 125,000 cells per well in a 6-well plate. After 24 h, cells were incubated with EBM-2 containing ANG or a variant (1 µg/mL) for another 24 h. On the

same day, Matrigel was coated on a µ-Slide Angiogenesis (Ibidi) for 1 h at 37 °C under 5% v/v CO_2(g). Treated cells (1×10^4) were plated on the Matrigel, and the resulting slide was incubated at 37 °C under 5% v/v CO_2(g). After 2 h, phase-contrast images were acquired with an N-STORM Eclipse Ti-E inverted microscope (Nikon) using 10× magnification. For a *z*-stack series, images were constructed using NIS-Elements software. The mean numbers of junctions and tubules and the total tubule length were counted with ImageJ software (NIH).

2.5.12 Gel-shift assay for protein·nucleic acid complexation

In each reaction mixture, pRNA (0.2 nM) labeled with [γ-^{32}P]ATP was pre-incubated with His_6–$TIP5_{510\text{-}611}$ (5 µM) for 15 min before adding wild-type ANG or a variant (5 µM). At known times, a 7-µL aliquot was removed and quenched on ice with RI (5 µM). The samples were resolved by electrophoresis through a TBE polyacrylamide (4% w/v) gel. Radioactivity was detected as described above. Bound and unbound pRNA was quantified by densitometry with ImageQuant TL software, and values of K_d were determined with the program Prism 5.0 (GraphPad).

2.5.13 In vitro assay of kinase activity

In each reaction mixture, wild-type ANG or a variant (20 µM) was incubated with a HeLa cell lysate containing protease and phosphatase inhibitors and [γ-^{32}P]ATP. Reactions were allowed to proceed for 2 min at 30 °C, and then quenched with SDS gel-loading dye. Samples were subjected to SDS–PAGE, and radioactivity was detected as described above.

2.6 Acknowledgements

We thank Dr. E. Lund, Dr. D. A. Wassarman, R. J. Presler, C. H. Eller, and K. A. Andersen for contributive discussions. T.T.H. was supported by an Advanced Opportunity/Graduate Research

Scholar Fellowship and by Molecular Biosciences Training Grant T32 GM007215 from the National Institutes of Health (NIH). This work supported by grant R01 CA073808 (NIH). We are grateful to T. F. J. Martin for the use of his confocal microscope.

Figure 2.1

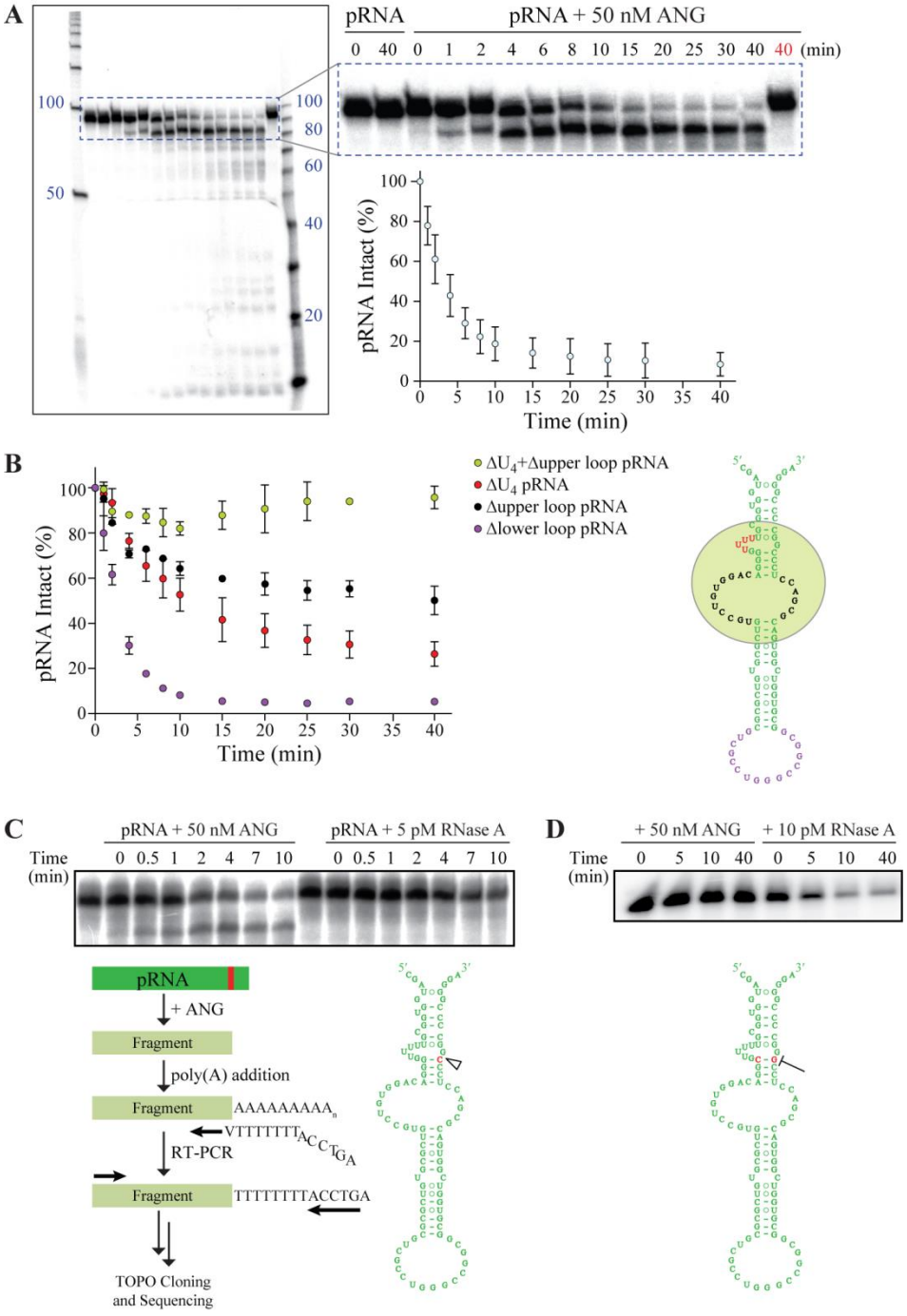
A
pRNA
pRNA + 50 nM ANG
0 40 0 1 2 4 6 8 10 15 20 25 30 40 40 (min)
100
50
100
80
60
40
20
pRNA Intact (%)
Time (min)
B
ΔU4+Δupper loop pRNA
ΔU4 pRNA
Δupper loop pRNA
Δlower loop pRNA
pRNA Intact (%)
Time (min)
C
pRNA + 50 nM ANG
pRNA + 5 pM RNase A
Time (min)
0 0.5 1 2 4 7 10 0 0.5 1 2 4 7 10
pRNA
+ ANG
Fragment
poly(A) addition
Fragment
AAAAAAAAn
VTTTTTTTACCTGA
RT-PCR
Fragment
TTTTTTTACCTGA
TOPO Cloning
and Sequencing
D
+ 50 nM ANG
+ 10 pM RNase A
Time (min)
0 5 10 40 0 5 10 40

Figure 2.1 ANG cleaves pRNA *in vitro* in a specific manner

A. Autoradiogram of a urea–polyacrylamide gel and graph of ensuing densitometry data demonstrating that ANG cleaves ^{32}P-labeled pRNA specifically and completely to generate a product of ~85 nucleotides and, subsequently, smaller fragments. Heat-inactivated ANG was used at 40 min (red).

B. Graph showing that ANG cleavage of pRNA is affected by deletion of the U_4 loop (red), the upper loop (black), and the combined loops (green), but not the lower loop (purple). The green circle highlights the putative ANG-binding region on pRNA. Values represent the mean ± SD (n = 3, technical replicates).

C. Autoradiogram demonstrating that RNase A, unlike ANG, cleaves ^{32}P-labeled pRNA non-specifically. Sequencing reveals that ANG cleaves pRNA specifically after residue C86 (red).

D. Autoradiogram showing that replacement of G18–C86 in ^{32}P-labeled pRNA with C18–G86 eliminates cleavage by ANG but not RNase A.

Figure 2.2

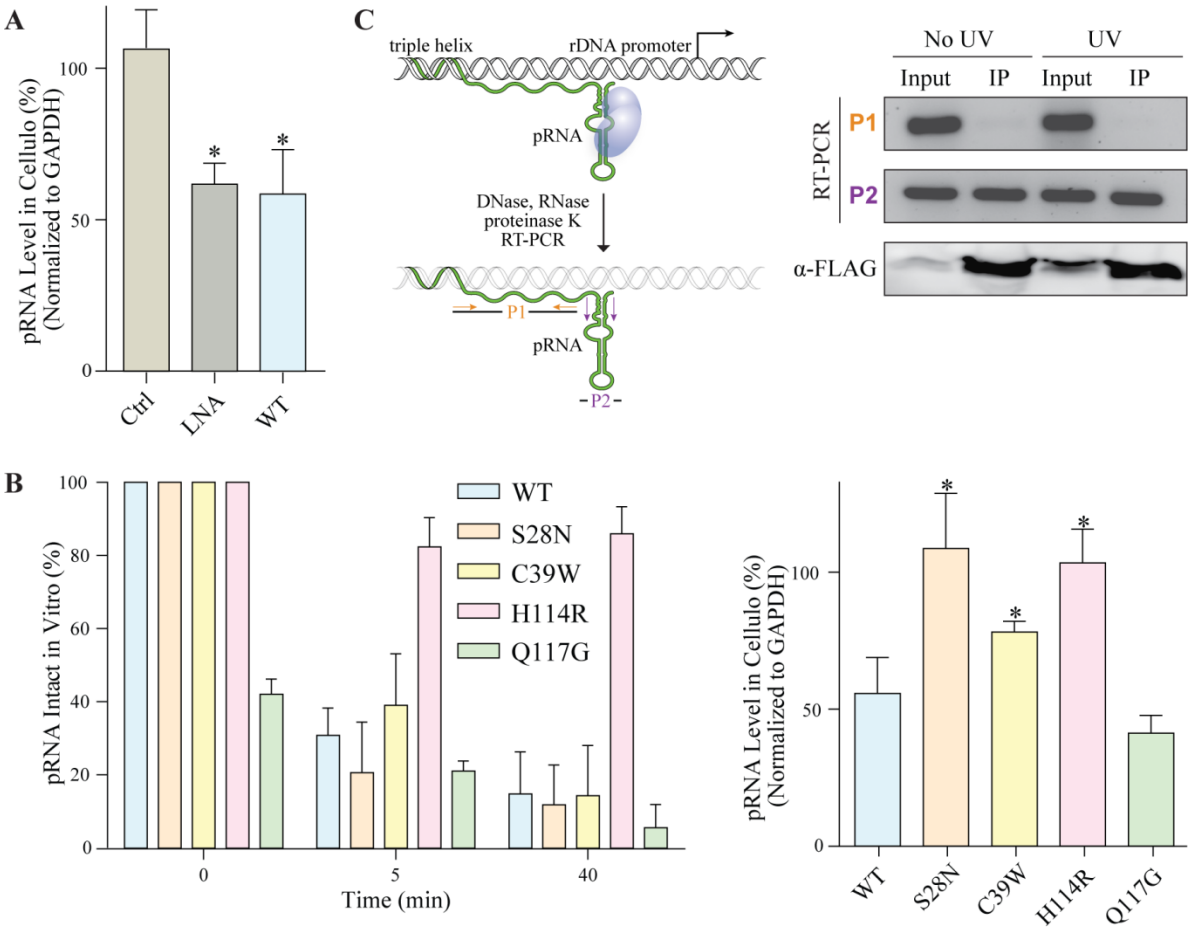
A
pRNA Level in Cellulo (%)
(Normalized to GAPDH)
100
50
0
Ctrl
LNA
WT
C
triple helix
rDNA promoter
pRNA
DNase, RNase
proteinase K
RT-PCR
P1
pRNA
P2
No UV
UV
Input
IP
Input
IP
RT-PCR
P1
P2
α-FLAG
B
pRNA Intact in Vitro (%)
100
80
60
40
20
0
0
5
40
Time (min)
WT
S28N
C39W
H114R
Q117G
pRNA Level in Cellulo (%)
(Normalized to GAPDH)
100
50
0
WT
S28N
C39W
H114R
Q117G

Figure 2.2 ANG cleaves pRNA *in cellulo*

A. Graph of qRT-PCR data indicating that ANG (1 µg/mL) reduces the level of pRNA in HeLa cells by 50%, which is the same level achieved with LNA antisense knockdown done as described previously . Values represent the mean ± SD (n = 3, biological replicates).

B. Graphs showing that ANG variants have differential effects on pRNA levels *in vitro* (left) and *in cellulo* (right). S28N ANG, which is an active enzyme *in vitro* but defective in nuclear localization, leads to no change in pRNA level *in cellulo*. C39W ANG, which is unstable, reduces pRNA level by only 25% *in cellulo*. H114R ANG, which has a deleterious active-site substitution, leads to no change in pRNA levels *in vitro* or *in cellulo*. Q117G ANG, which has an advantageous active-site substitution, leads to highly reduced pRNA levels *in vitro* and *in cellulo*. Values represent the mean ± SD (n = 3, *in vitro*: technical replicates, *in cellulo*: biological replicates). Paired Student's t-test: differences were considered significant at $*p < 0.05$.

C. An RNA co-immunoprecipitation with FLAG–H114R ANG (1 µg/mL) demonstrates a direct interaction between ANG and pRNA *in cellulo*. EtBr-stained agarose gel of PCR products that were amplified from the pRNA region corresponding to primer 1 (P1) and primer 2 (P2). Only the P2-derived pRNA region was detected in the IP samples, indicating that this region was protected by FLAG–H114R ANG. The P1-derived pRNA region as well as other cellular RNAs were vulnerable to degradation by RNase A. The PCR product of P2 was sequenced and its identity was confirmed as the conserved stem-loop structure of pRNA.

Figure 2.3

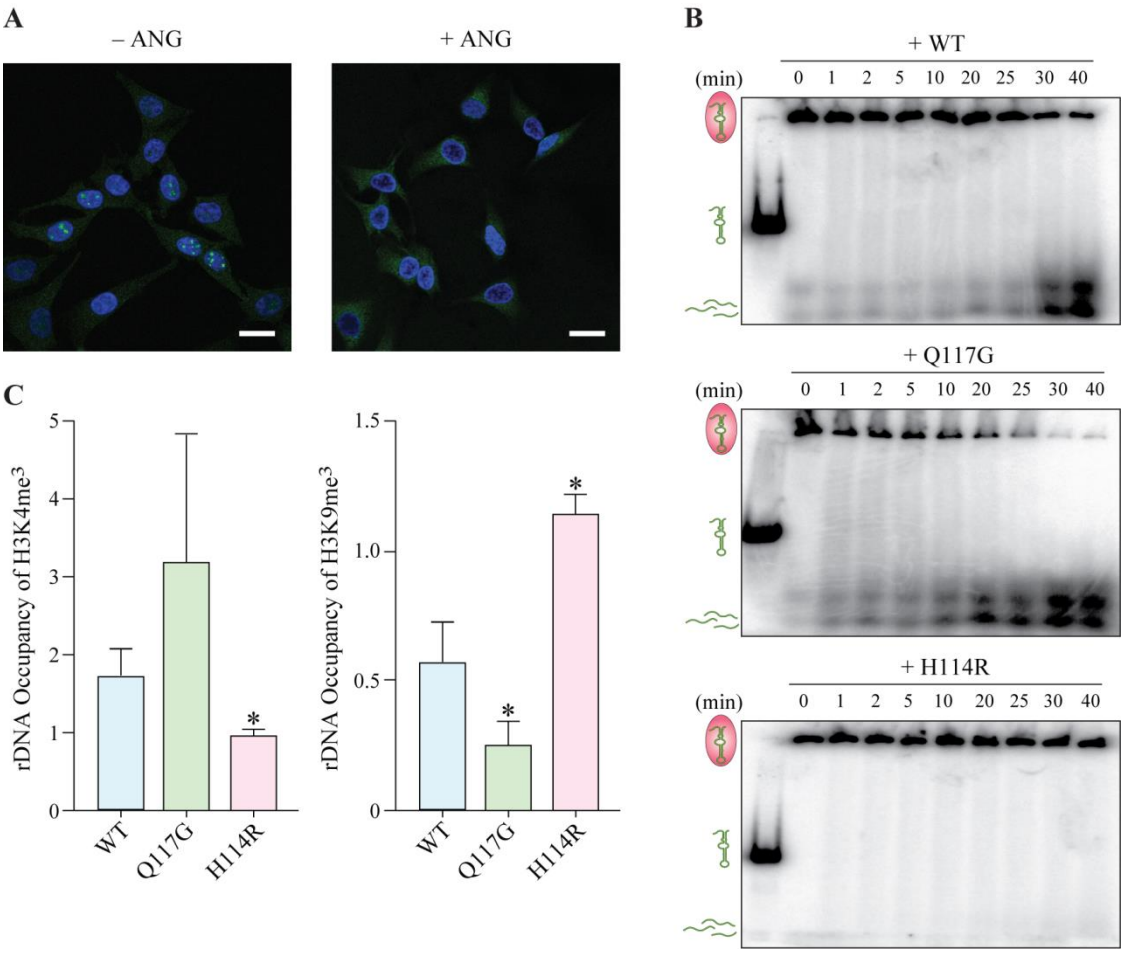
A
– ANG
+ ANG
B
+ WT
(min)
0 1 2 5 10 20 25 30 40
+ Q117G
(min)
0 1 2 5 10 20 25 30 40
+ H114R
(min)
0 1 2 5 10 20 25 30 40
C
rDNA Occupancy of H3K4me3
0
1
2
3
4
5
WT
Q117G
H114R
*
rDNA Occupancy of H3K9me3
0
0.5
1.0
1.5
WT
Q117G
H114R
*

Figure 2.3 Cleavage of pRNA by ANG promotes dissociation of TIP5 *in cellulo*

A. Immunofluorescence images of nucleolar TIP5 (green) in HeLa cells indicating that ANG (1 μg/mL) limits the accumulation of TIP5 in the nucleolus. Blue: Hoechst 33342. Scale bar: 20 μm.

B. Autoradiograms of gel-shift assays indicating that ANG and the hyperactive Q117G variant degrade the pRNA within a TAM·pRNA complex *in vitro*; the inactive H114R variant does not.

C. Chromatin immunoprecipitation at the rDNA promoter revealing that treatment with ANG and the Q117G variant enrich the occupancy of H3K4me^3, which is a marker of active transcription, but decrease the occupancy of H3K9me^3, which is a marker of repressive transcription. The H114R variant does not change H3K4me^3 or H3K9me^3 levels. Values represent the mean ± SD (n = 3, biological replicates). Paired Student's t-test: differences were considered significant at $*p < 0.05$.

Figure 2.4

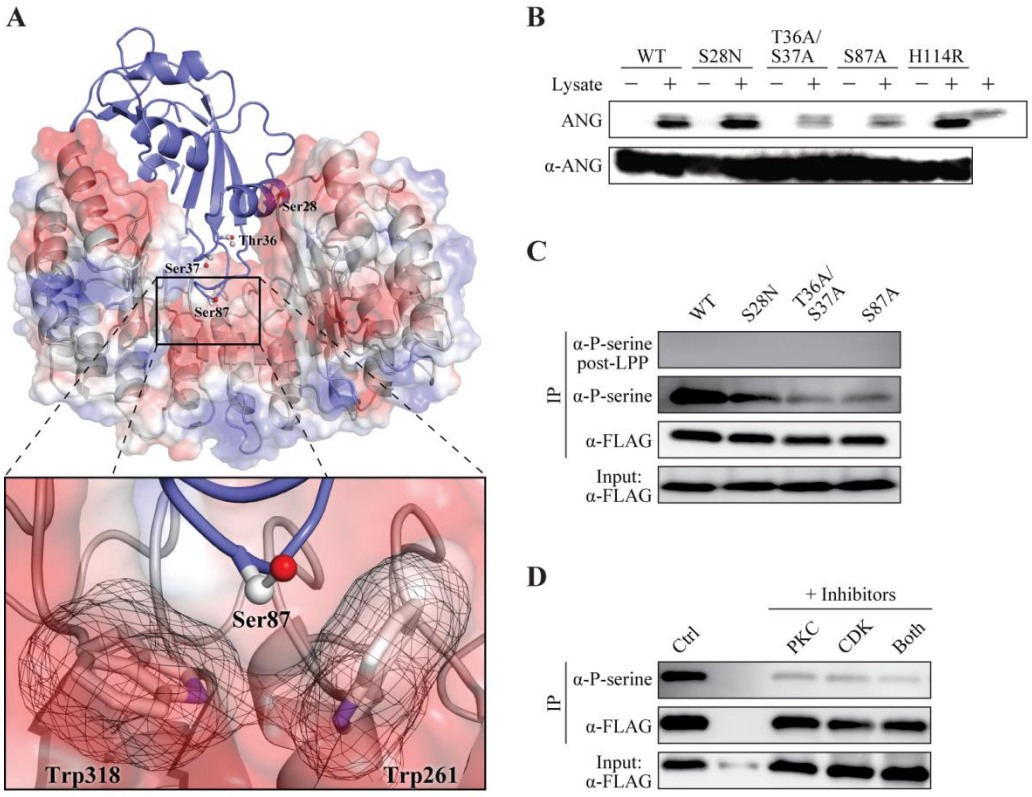
A
Ser28
Thr36
Ser37
Ser87
Ser87
Trp318
Trp261
B
WT
S28N
T36A/
S37A
S87A
H114R
Lysate
ANG
α-ANG
C
WT
S28N
T36A/
S37A
S87A
IP
α-P-serine
post-LPP
α-P-serine
α-FLAG
Input:
α-FLAG
D
+ Inhibitors
Ctrl
PKC
CDK
Both
IP
α-P-serine
α-FLAG
Input:
α-FLAG

Figure 2.4 ANG is phosphorylated by PKC/CDK

A. Structure of the human RI·ANG complex (PDB entry 1a4y). Putative phosphorylation sites in ANG (blue ribbon) are labeled and depicted in ball-and-stick. The Coulombic surface of RI (grey ribbon) is depicted with red = negative and blue = positive. Inset: Close contact between Ser87 of ANG and two tryptophan residues of RI.

B. Autoradiogram of a polyacrylamide gel demonstrating that ANG is phosphorylated upon incubation with a HeLa cell lysate and [γ-^{32}P]ATP. Replacing Thr36/Ser37 or Ser87 with an alanine residue decreases phosphorylation. An immunoblot of the same gel shows consistent loading of ANG and its variants.

C. Immunoblots showing that FLAG–ANG (1 μg/mL) taken up by HeLa cells and isolated by immunoprecipitation (IP) with an anti-FLAG antibody (α-FLAG) is recognized by an anti-phosphoserine antibody (α-P-serine). Recognition is eliminated by treatment with lambda protein phosphatase (LPP). IP of the S28N variant was reduced, and that of the T36A/S37A and S87A variants was even more reduced.

D. Immunoblots showing that small-molecule inhibitors of CDK or PKC reduce the phosphorylation of FLAG–ANG by HeLa cells. For kinase-inhibitor treatment, cells were pre-incubated with either bisindolylmaleimide (4 μM) or roscovitine (14 μM) for 30 min prior to the treatment with ANG.

Figure 2.5

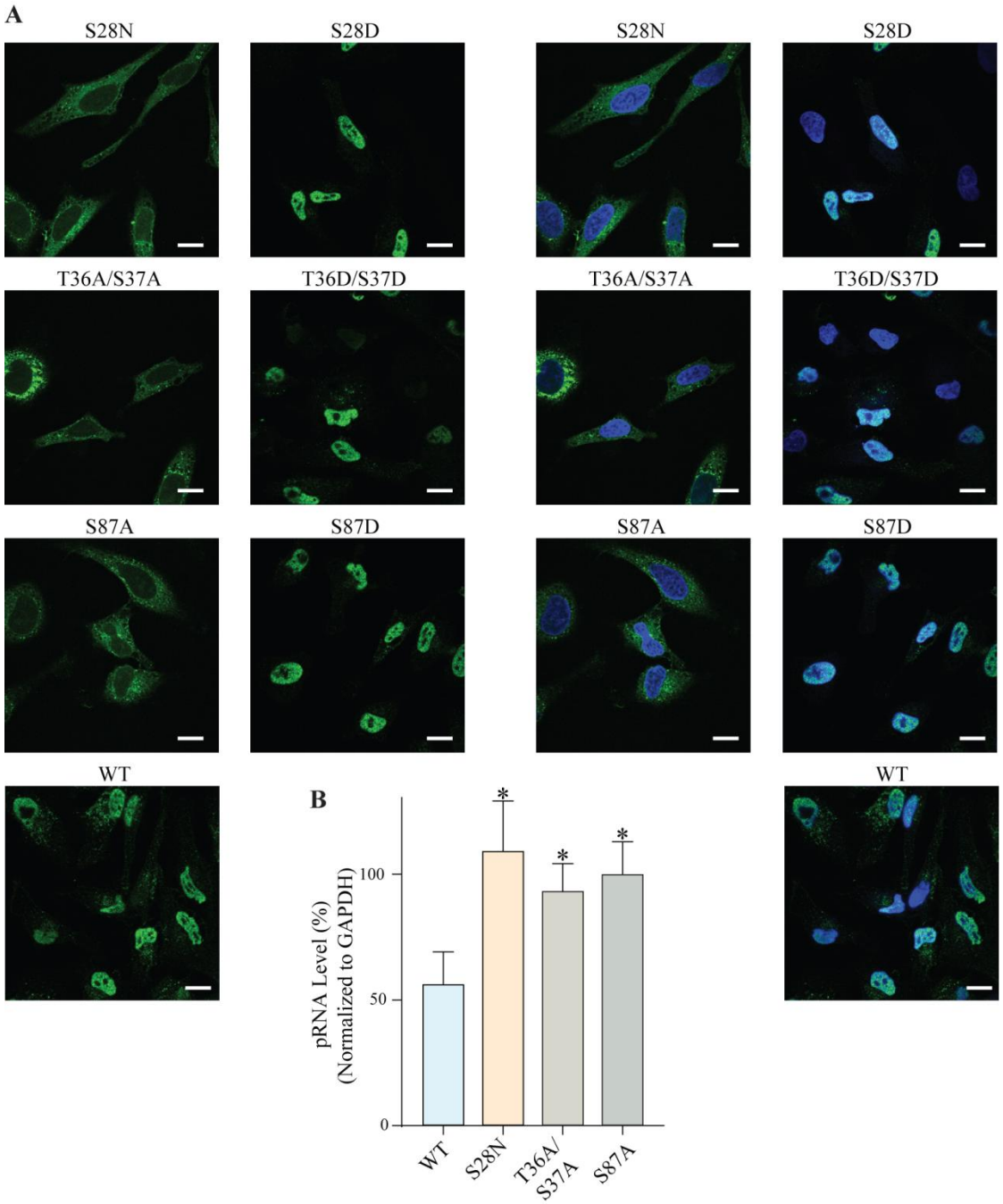
A
S28N
S28D
S28N
S28D
T36A/S37A
T36D/S37D
T36A/S37A
T36D/S37D
S87A
S87D
S87A
S87D
WT
WT
B
pRNA Level (%)
(Normalized to GAPDH)
100
50
0
*
*
*
WT
S28N
T36A/
S37A
S87A

Figure 2.5 Phosphorylation of ANG is essential for its nuclear translocation

A. Immunofluorescence images of FLAG–ANG (1 μg/mL; green) in HeLa cells showing its nuclear localization. Blue: Hoechst 33342. Scale bar: 20 μm. FLAG–ANG variants with a defective phosphorylation site are cytosolic; FLAG–ANG variants with a phosphomimetic substitution are nuclear. Left: green channel only. Right: overlay.

B. Graph of qRT-PCR data indicating that ablating nuclear localization prevents ANG from cleaving pRNA in HeLa cells. Data for wild-type ANG and its S28N variant are from Fig 2A. Values represent the mean ± SD ($n = 3$, biological replicates). Paired Student's *t*-test: differences were considered significant at $*p < 0.05$.

Figure 2.6

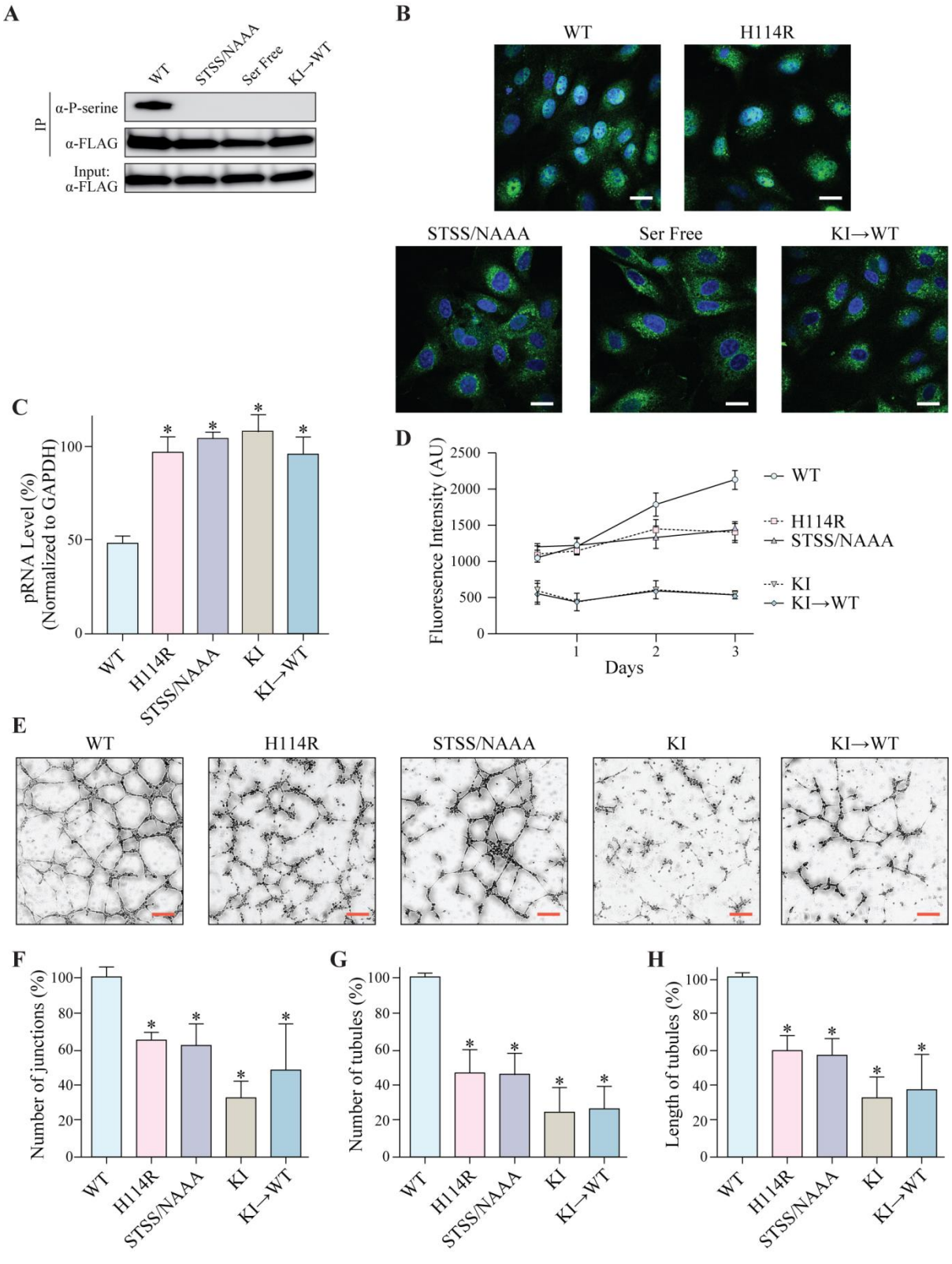
A
WT
STSS/NAAA
Ser Free
KI→WT
IP
α-P-serine
α-FLAG
Input:
α-FLAG
B
WT
H114R
STSS/NAAA
Ser Free
KI→WT
C
pRNA Level (%)
(Normalized to GAPDH)
WT
H114R
STSS/NAAA
KI
KI→WT
D
Fluoresence Intensity (AU)
Days
WT
H114R
STSS/NAAA
KI
KI→WT
E
WT
H114R
STSS/NAAA
KI
KI→WT
F
Number of junctions (%)
G
Number of tubules (%)
H
Length of tubules (%)

Figure 2.6 ANG promoting angiogenesis requires nuclear translocation and rDNA transcription

A. Immunoblots showing that FLAG–ANG taken up and phosphorylated by HUVE cells. Deletion of phosphorylation sites in variants (STSS/NAAA and Ser Free) or treatment of the wild-type enzyme with kinase inhibitors (KI→WT) decreases ANG phosphorylation.

B. Immunofluorescence images of FLAG–ANG (green) in HUVE cells showing its nuclear localization. Deficient phosphorylation (STSS/NAAA, Ser Free, and KI→WT) restricts ANG to the cytosol. Blue: Hoechst 33342. Scale bar: 20 μm.

C. Graph of qRT-PCR data showing that wild-type ANG reduces the level of pRNA in HUVE cells. pRNA level is not altered by the inactive H114R variant or upon deficient phosphorylation (STSS/NAAA, Ser Free, and KI→WT). Values represent the mean ± SD (n = 3, biological replicates). Paired Student's t-test: differences were considered significant at $*p < 0.05$.

D. Graph showing that ANG promotes the growth of HUVE cells. Growth is not affected by the inactive H114R variant or upon deficient phosphorylation (STSS/NAAA). Treating HUVE cells with kinase inhibitors arrests cell division and could not be rescued by treatment with wild-type ANG. Values represent the mean ± SD (n = 3, technical replicates).

E. Images of capillary-like tubules showing that wild-type ANG stimulates angiogenesis *in cellulo*. Potency is less from the inactive H114R variant or upon deficient phosphorylation (STSS/NAAA, KI, and KI→WT). Scale bar: 100 μm.

F, **G**, **H** Graphs of key parameters extracted from tubule images like those in panel **E**. Values represent the mean ± SD (n = 3, biological replicates). Paired Student's t-test: differences were considered significant at $*p < 0.05$.

Figure 2.7

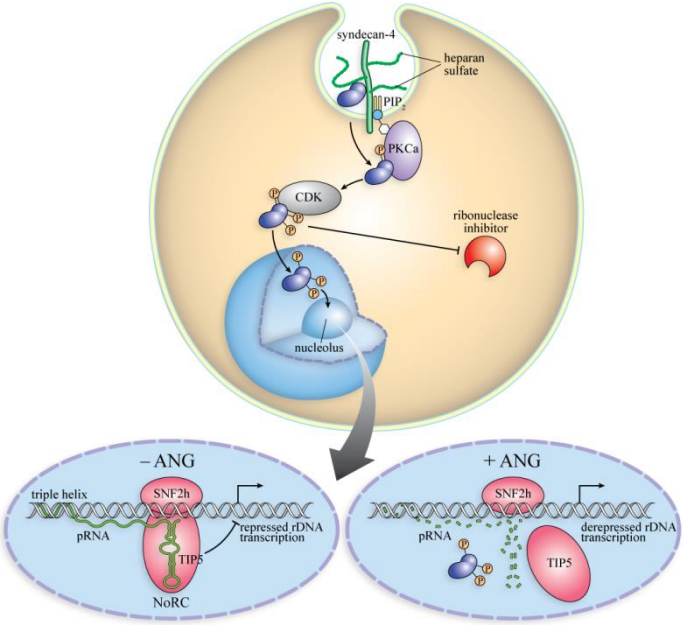
syndecan-4
heparan sulfate
PIP2
PKCa
CDK
ribonuclease inhibitor
nucleolus
– ANG
triple helix
SNF2h
pRNA
repressed rDNA transcription
TIP5
NoRC
+ ANG
SNF2h
pRNA
derepressed rDNA transcription
TIP5

Figure 2.7 Scheme of the cellular action of ANG

Angiogenin binds to syndecan-4 on the cell surface and is internalized by endocytosis. A fraction translocates to the cytosol, where ANG is phosphorylated by PKC and CDK. Phosphorylation endow ANG with the ability to evade the ribonuclease inhibitor protein. Phosphorylated ANG translocates into the nucleus and accumulates in the nucleolus. There, ANG digests pRNA, leading to the dissociation of TIP5 from the rDNA promoter. Ensuing rDNA transcription enables the proliferation of endothelial cells (neovascularization) and tumor cells (cancer progression).

Table 2.1

ANG	K_d (nM)[a]	Fold change
Wild-type[b]	0.7×10^{-6}	1
T36D/S37D	4.2 ± 0.5	6×10^6
S87D	8.7 ± 0.8	1.2×10^7
T36D/S37D/S87D	90 ± 5	1.3×10^9
S28D/T36D/S37D/S87D	150 ± 10	2.1×10^9

[a]Values represent the mean ± SD (n = 3, technical replicates).

[b]Data from Ref 57.

Table 2.1 Values of K_d (± SD) of the complexes of RI with wild-type ANG and its phosphorylation-mimetics

Figure 2S.1

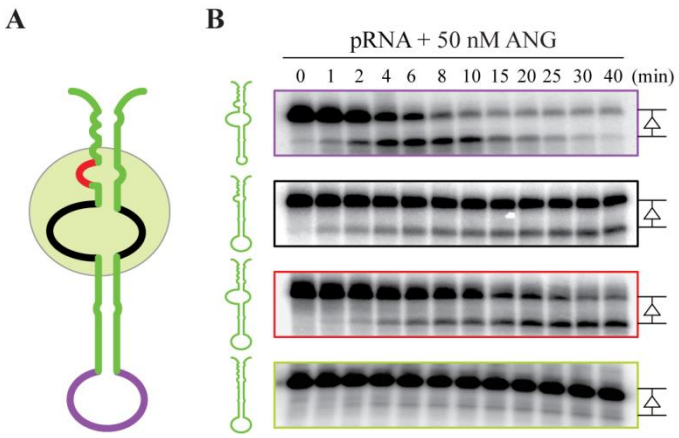

Figure 2S.1 Excision of single-stranded RNA loops does not alter ANG specificity

To identify regions of RNA important for cleavage by ANG, the lower loop (purple), upper loop (black), and series of uridine residues (red) of pRNA were deleted individually. Only deletion of the upper loop and series of uridine residues attenuated catalysis by ANG, and deleting both regions (light green) made pRNA resistant to cleavage by ANG. Notably, the size of the substrate and product is constant (Δ) regardless of the pRNA substrate, indicative of the high specificity of ANG for a particular C–G phosphodiester bond near the 3′ end of pRNA (Figure 2.1C).

Figure 2S.2

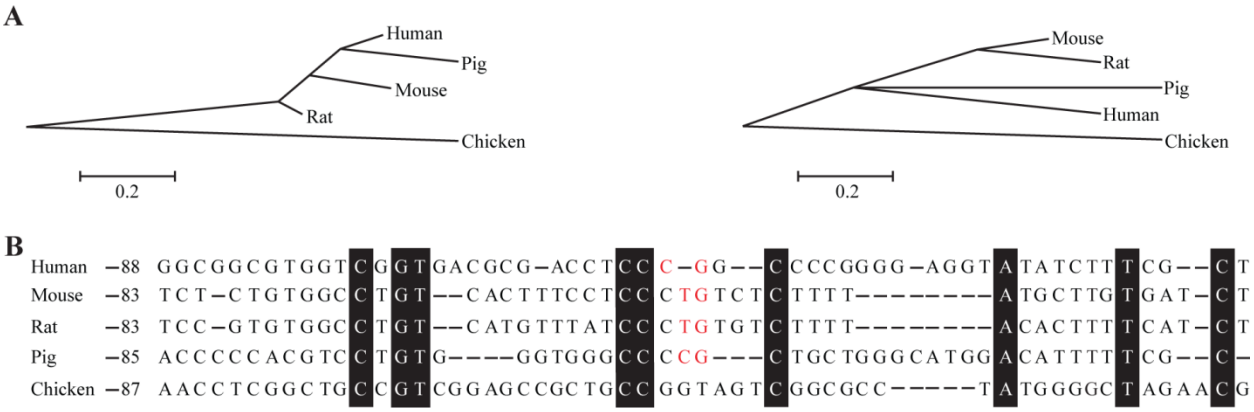
A
Human
Pig
Mouse
Rat
Chicken
0.2
Mouse
Rat
Pig
Human
Chicken
0.2
B
Human −88 GGCGGCGTGGTCGGTGACGCG−ACCTCCC−GG−−CCCCGGGG−AGGTATATCTTTCG−−CT
Mouse −83 TCT−CTGTGGCCTGT−−CACTTTCCTCCCTGTCTCTTTT−−−−−−−−ATGCTTGTGAT−CT
Rat −83 TCC−GTGTGGCCTGT−−CATGTTTATCCCTGTGTCTTTT−−−−−−−−ACACTTTTCAT−CT
Pig −85 ACCCCCACGTCCTGTG−−−−GGTGGGCCCCG−−−CTGCTGGGCATGGACATTTTTCG−−C−
Chicken −87 AACCTCGGCTGCCGTCGGAGCCGCTGCCGGTAGTCGGCGCC−−−−TATGGGGCTAGAACG

Figure 2S.2 Co-evolution of mammalian pRNA and ANG

A. To examine the conservation of pRNA and ANG during evolution, we performed a phylogenetic analysis of ANG (left) and pRNA (right) with MEGA 6 software. We found that ANG and pRNA have co-evolved in mammals, and that the enzyme and its substrate from chicken are outliers.

B. To examine the conservation of the ANG-cleavage site in pRNA, we aligned pRNA sequences with CLUSTALW software. Fully conserved nucleotides are highlighted (black box), and numbers refer to their position with respect to the polymerase I transcription start site. We found that the cleavage sites (red) are conserved in human, mouse, rat, and pig, but not in chicken. Accession numbers: Homo sapiens (X01547), Mus musculus (BK000964), Rattus norvegicus (X00677), Sus scrofa (L31782), Gallus gallus (DQ112354).

Figure 2S.3

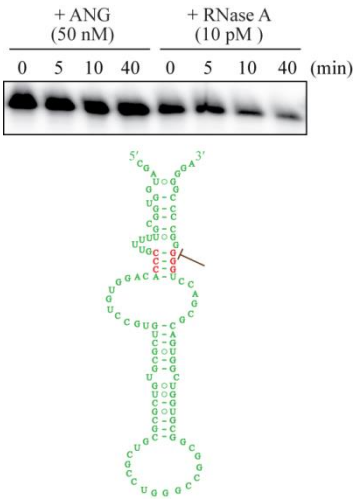

Figure 2S.3 Swapping three G·C base pairs makes pRNA resistant to ANG cleavage

After identifying the cleavage site of pRNA by ANG, the three G·C base pairs (red) were replaced with C·G. The swap prevented hydrolysis by ANG but not by RNase A.

Figure 2S.4

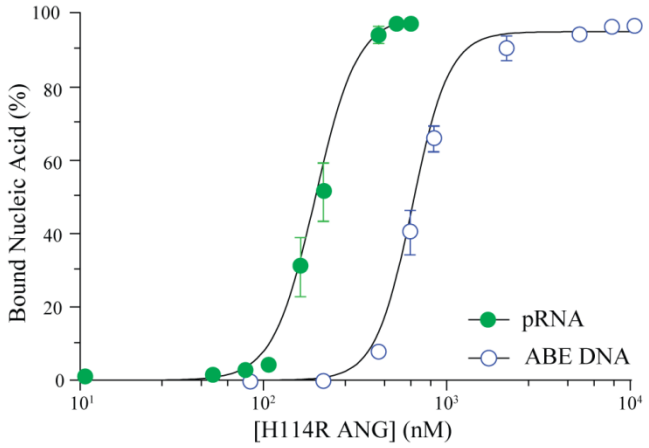
Bound Nucleic Acid (%)
100
80
60
40
20
0
10^1
10^2
10^3
10^4
[H114R ANG] (nM)
pRNA
ABE DNA

Figure 2S.4 ANG has higher affinity for pRNA than for ABE DNA

pRNA and ABE DNA were labeled on their 5′ end with [γ-^{32}P]ATP. pRNA was heated and allowed to refold prior to conducting the assay. Nucleic acid (0.2 nM) was incubated with increasing concentrations of H114R ANG, and binding was assessed with a gel-shift assay. Values of K_d (± SE) were determined to be (192 ± 8) and (651 ± 12) nM for the H114R ANG·pRNA and H114R ANG·ABE DNA complexes, respectively. Values represent the mean ± SD (n = 3, technical replicates).

Figure 2S.5

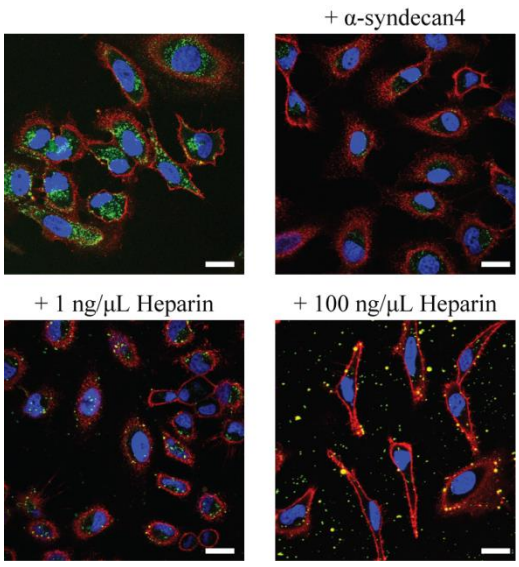

Figure 2S.5 ANG uptake in HeLa cells occurs via the syndecan-4 receptor

BODIPY-labeled ANG was internalized into HeLa cells after a 3-h incubation. Pre-incubating cells with α-syndecan-4, an antibody that binds to syndecan-4, blocked ANG internalization. Internalization was also impaired by adding heparin, which leads to the formation of extracellular heparin·ANG complexes. Green: BODIPY-labeled ANG. Red: Alexa Fluor 594-labeled wheat germ agglutinin, which is a cell-surface stain. Blue: Hoechst 33342, which is a nuclear stain. Scale bar: 20 μm.

Figure 2S.6

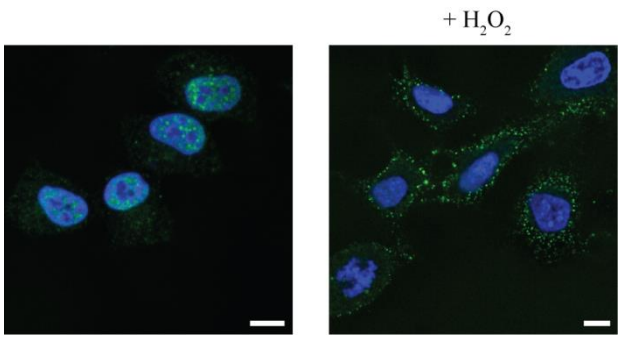

Figure 2S.6 Oxidative stress alters ANG localization

Immunofluorescence images of FLAG–ANG (green) in HUVE cells without or with oxidative stress. Cells were incubated for 3-h with FLAG–ANG (1 μg/mL) in EBM-2 medium or EBM-2 medium containing H_2O_2 (0.1 mM). ANG localizes in the nucleolus, but not in cells suffering oxidative stress. Blue: Hoechst 33342, which is a nuclear stain. Scale bar: 10 μm

Figure 2S.7

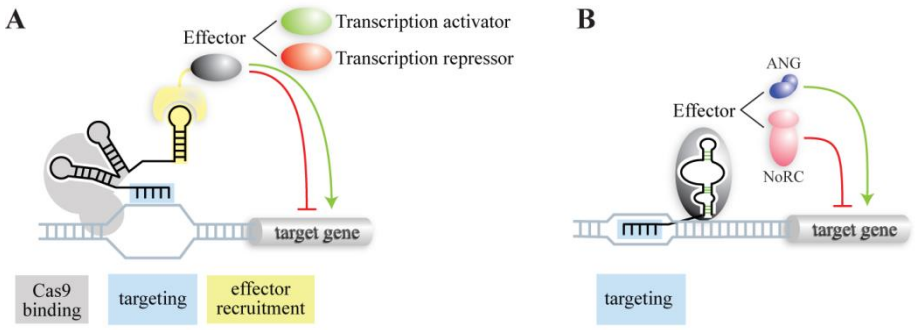
A
Effector
Transcription activator
Transcription repressor
target gene
Cas9 binding
targeting
effector recruitment
B
ANG
Effector
NoRC
target gene
targeting

Figure 2S.7 Similarity of the action of ANG with that of an Engineered CRISPR–Cas9

CRISPR–Cas9 has been engineered such that its guide RNA acts as both a scaffold to recruit transcriptional regulators and dock them with a double-stranded DNA target, leading to transcription repression or activation. Likewise, pRNA recruits NoRC and docks them to a double-stranded DNA target, leading to transcription repression. pRNA also recruits ANG, leading to pRNA cleavage and transcription activation.

Table 2S.1

ANG	T_m (°C)[a]	ANG	T_m (°C)
Wild-type	61.3 ± 0.2	FLAG–wild-type	65.4 ± 0.9
S28N	61.4 ± 0.2	FLAG–S28N	64.5 ± 0.2
T36A/S37A	58.7 ± 0.1	FLAG–S28D	65.5 ± 0.5
C39W	44.4 ± 0.3	FLAG–T36A/S37A	62.1 ± 0.2
S87A	61.4 ± 0.4	FLAG–T36D/S37D	59.6 ± 1.1
H114R	62.5 ± 0.2	FLAG–S87A	63.5 ± 0.6
Q117G	56.0 ± 0.4	FLAG–S87D	61.7 ± 1.1
S28N/T36A/S37A/S87A	56.8 ± 0.1	FLAG–H114R	65.5 ± 1.4
		FLAG–S28N/T36A/S37A/S87A	58.7 ± 0.1
		FLAG–Ser free	51.7 ± 0.1

[a]Values represent the mean ± SD (n = 3, technical replicates).

Table 2S.1 Thermal stability of wild-type ANG, its variants and FLAG fusions as determined by differential scanning fluorimetry

Table 2S.2

Primer	Sequence (5′→3′)	Usage
pRNA-For (P1)	GTGTCCTGGGGTTGACCAG	qPCR & PCR (RIP)
pRNA-Rev (P1)	GGACACCTGTCCCCAAAAAC	qPCR & PCR (RIP)
GAPDH-For	GTGACTAACCCTGCGCTCC	qPCR
GAPDH-Rev	ATCACCCGGAGGAGAAATCG	qPCR
RT	GCCTTGGCACCCGAGAATTCCATTTTTTTTTTTTTTV	RT & PCR (RNA sequencing)
For-P2	GAAATTAATACGACTCACTATACGATGGTGGCG	PCR (RNA sequencing & RIP)
Rev-P2	TCCCCGGGGCCGGGAGGTC	PCR (RIP)

Table 2S.2 Oligonucleotide primers used in this work

CHAPTER 3

Angiogenin Activates the Astrocytic Nrf2-ARE Pathway to Protect Neurons from Oxidative Stress

Contribution: Prof. Johnson and I designed the experiments, analyzed data and wrote the manuscript. I performed experiments.

Prepared for submission as:

Hoang, T.T., Johnson, D.A., Raines, R.T., Valiauga, R., Johnson, J. A. (2016) Angiogenin Activates the Astrocytic Nrf2-ARE Pathway to Protect Neurons from Oxidative Stress

3.1 Abstract

The angiogenin (*ANG*) gene is frequently mutated in patients suffering from amyotrophic lateral sclerosis, a fatal neurodegenerative disease characterized by the progressive loss of motor neurons. While the lack of ANG contributes to neurodegeneration, delivering human ANG to $SOD1^{G93A}$ mice, which display ALS-like symptoms, extends their lifespan and improves motor function. These findings highlight the need to explore the mechanism underlying ANG neuroprotective effects. A growing body of research reports that ANG facilitates neuroprotection by inhibiting protein synthesis. As a secreted vertebrate ribonuclease, ANG cleaves a subset of tRNAs to generate tRNA-derived, stress-induced RNAs, which hinder the initiation of protein translation. Here, we report another ANG neuroprotective pathway through which ANG triggers *trans* activation of the Nrf2 pathway, a major source of cellular defense against oxidative stress, in astrocytes to protect neurons. First, stressed neurons produce elevated levels of ANG. When taken up by astrocytes via the syndecan-4 receptor, the secreted ANG activates PKCα. The activated kinase phosphorylates Nrf2, allowing it to dissociate from its binding partner, Keap1, to enter the nucleus. In the nucleus, Nrf2, which is a redox-sensitive transcription factor, drives the expression of antioxidant enzymes to neutralize the deleterious effects of reactive oxidants. The ANG-mediated activation of the Nrf2 pathway in astrocytes promotes the survival of neurons suffering from oxidative injury. Our findings suggest the utility of ANG as a promising neuroprotective agent to combat oxidative stress-induced cellular toxicity.

3.2 Introduction

Amyotrophic lateral sclerosis (ALS) is a progressive, late-onset and fatal neurodegenerative disease that is characterized by selective motor neuron loss in the spinal cord, brainstem and motor cortex.[144,240,145] Approximately 10% of ALS cases are inherited dominantly. The most common genetic determinants of ALS are the expansion of non-coding GGGGCC repeats in *C9ORF72* and mutations in the Cu/Zn superoxide dismutase 1 (*SOD1*) locus.[169,170,165] The search for other gene mutations that segregate with disease in ALS pedigrees has led to the identification of *loss-of-function* mutations in the human angiogenin (*ANG*) gene.[24,172,173] While the lack of ANG contributes to neurodegeneration, the delivery of human ANG to ALS-like transgenic mice that overexpress human mutant $SOD1^{G93A}$ increases their lifespan and improves their motor function.[182] These findings indicate that ANG plays an important role in neuroprotection.

ANG belongs to the pancreatic-type ribonuclease (RNase) superfamily.[32] These secretory proteins catalyze the cleavage of a phosphodiester bond on the 3′ side of cytidine or uridine residues in single-stranded RNA. ANG exhibits extremely low ribonucleolytic activity but potently induces angiogenesis.[219,218] Because the lack of angiogenic signals has been increasingly recognized as a contributor to neurodegeneration, the angiogenic activity of ANG has been implicated in ANG-mediated neuroprotection.[29,241,242]

Most *ANG* mutations that segregate with ALS do not alter the secondary structure or stability of ANG significantly. Instead, they disrupt its ribonucleolytic activity or subcellular distribution.[174,185,176,178] This observation has stimulated interest in understanding the molecular basis of ANG role in neuroprotection. Mechanistic studies have shown that the neuroprotective impact of ANG depends on its inhibition of protein translation. ANG cleaves the anticodon loops

of mature tRNAs to produce 5′ and 3′ fragments that are designated as tRNA-derived, stress-induced RNAs (tiRNAs).[186,188] Only 5′-tiRNAs, not 3′-tiRNAs, recruit the translational silencer protein YB-1 and sequester the eukaryotic translation initiation factor 4G/A complex to inhibit translation.[187] Specific 5′-tiRNAs also trigger the assembly of stress granules at sites of ANG localization.[23]

Stress-induced translation repression is critical yet insufficient to combat oxidative stress, which is a hallmark of neurological disorders.[243,244] Oxidative stress results from an imbalance in the production and detoxification of free radicals from reactive oxygen species (ROS).[245-247] To neutralize ROS toxicity, cells replenish antioxidants by activating nuclear factor erythroid 2-related factor 2 (Nrf2), a redox-sensitive transcription factor.[198,248] This transcription factor is usually latent inside cells. Under basal conditions, the dimeric multidomain protein Keap1 binds Nrf2 via its Kelch domain and promotes the ubiquitination and proteasome degradation of Nrf2 by functioning as an adaptor for the Cul3-based E3 ligase. Oxidants, which react with sulfhydryl groups, chemically modify key reactive cysteine residues of Keap1, which then loses its ability to target Nrf2 for degradation. Consequently, Nrf2 is able to enter the nucleus, where it forms a heterodimer with Maf. The dimer then binds to antioxidant response elements (AREs) to drive the expression of antioxidant enzymes to compensate for the physiological and pathophysiological outcomes of oxidant exposure.[199,249,250]

Crossing mice in which the *Nrf2* gene is overexpressed selectively in astrocytes with two ALS mouse models produced offspring that showed a significant delay in the onset of ALS. The offspring with ALS also survived for longer periods.[251,200] Activation of the Nrf2 pathway in astrocytes is required for the promotion of neuronal survival.[201] This positive feedback loop between astrocytes and neurons is crucial for combatting oxidative stress and is reminiscent of

the molecular mechanism of ANG-mediated neuroprotection. ANG is enriched in motor neurons and protects them against various ALS-related insults, such as excitotoxicity, hypoxia, and endoplasmic reticulum stress.[182-184] Upon toxic insult, the ANG produced by motor neurons is selectively taken up by astrocytes.[52] That uptake of ANG into astrocytes stimulates pro-survival signals, which are then transmitted to the motor neurons to promote their survival.[202]

Nrf2 is a substrate of PKCα kinase.[252] PKCα phosphorylation has been shown to up-regulate the transcriptional activity of Nrf2.[253] PKCα is known to be activated when ANG binds to the syndecan-4 receptor.[55,175,52] This evidence raises an obvious question: could ANG activate the Nrf2 pathway? Here, we reveal that ANG triggers *trans* Nrf2 activation to promote neuronal survival. Specifically, we show that neurons subjected to H_2O_2-mediated oxidative stress secrete higher levels of ANG, which binds to the syndecan-4 receptor and is internalized into astrocytes. The syndecan-4 receptor activates PKCα, leading to Nrf2 phosphorylation. The phosphorylated Nrf2 then translocates into the nucleus to stimulate antioxidant gene expression. The ANG-induced activation of the Nrf2 pathway in astrocytes transmits survival-promoting signals to neighboring neurons, protecting them from H_2O_2-mediated toxicity.

3.3 Results

3.3.1 ANG activates ARE-dependent gene expression selectively in astrocytes

ARE mediates the transcriptional induction of a battery of genes that comprise the antioxidant response system. First, we examined if ANG activates ARE-dependent gene expression. To do so, we utilized a reporter assay in which the heat-stable human placenta alkaline phosphatase (*hPAP*) reporter gene was under the control of an ARE-containing promoter. Upon induction by an activator, the promoter drives hPAP expression, leading to hPAP protein production. The

phosphatase activity of hPAP was measured as a readout of ARE-dependent promoter activation.[254]

Tert-butylhydroquinone (tBHQ) is a known inducer of ARE-dependent promoter.[255] tBHQ stimulates hPAP activity to various extents, depending on cell type. In astrocytes, tBHQ-treatment led to a 15-fold increase in hPAP activity (Figure 3.1A), but only a 7-fold increase in neurons (Figure 3.1C). In mixed cultures of both astrocytes and neurons, the phosphatase activity was remarkably elevated by 249-fold. (Figure 3.1E), suggesting that cellular crosstalk between neurons and astrocytes is required to amplify activation of the ARE-dependent promoter.

The hPAP activation caused by wild-type (WT) ANG was similar to that observed after tBHQ treatment. Compared to PBS, WT ANG induced the highest hPAP signal in mixed cultures, induced the second-highest signal in astrocytes, and led to no change in neurons (Figure 3.1B, 3.1D, and 3.1F). Notably, the ANG-mediated induction was not as robust as that mediated by tBHQ, yet the effect of ANG was dose-dependent. ANG treatment at 5 μg/mL produced greater hPAP activity than at 1 μg/mL. To demonstrate signal specificity, we evaluated the phosphatase activity produced by ALS-associated ANG variants. H114R ANG has a deleterious active-site substitution, S28N ANG exhibits defective nuclear localization, and C39W ANG is unstable.[219] None of these variants were able to promote hPAP gene expression to produce hPAP activity.

3.3.2 ANG drives the expression of ARE-dependent genes in astrocytes

We next sought to demonstrate the intrinsic activation of ARE-dependent gene expression upon ANG treatment. ARE mediates the transcriptional induction of an array of antioxidant genes, and we selected three genes for analysis. NAD(P)H:quinone acceptor oxidoreductase 1 (NQO1) is involved in the reduction of quinones to hydroquinones to prevent redox cycling, which often

generates free radicals.[256] Glutamate-cysteine ligase modifier subunit (GCLM) is the first rate-limiting enzyme for the synthesis of glutathione—a free radical scavenger.[257] Glutathione S-transferase alpha 4 (GSTα4) catalyzes the conjugation of reduced glutathiones to electrophilic substrates, detoxifying endogenous and xenobiotic alkylating agents.[258]

Using qPCR, we evaluated the expression of the genes that encode these enzymes as a measure of ANG-induced ARE-dependent gene expression. tBHQ again served as a positive control in this experiment. tBHQ treatment significantly up-regulated the expression of NQO1, GCLM, and GSTα4, consistent with the results of the reporter assay. The mixed cultures were most responsive to tBHQ induction, followed by astrocytes ,and then neurons (Figure 3.2A–C).

The addition of WT ANG stimulated the expression of NQO1, GCLM and GSTα4 in astrocytes and mixed cultures but not in neurons. The higher dose of ANG also produced a larger gene expression response (Figure 3.2A–C). Taken together, the results of the reporter assay and antioxidant gene expression indicate that WT ANG activates ARE-dependent gene expression.

3.3.3 ANG-mediated ARE-dependent gene expression depends on Nrf2

Next, we asked if Nrf2 is required for the ANG-mediated induction of ARE-dependent gene expression. In WT astrocytes, we obtained results comparable to those presented in Figures 3.1B and 3.2A regarding the ANG-mediated activation of hPAP and induction of the expression of antioxidant genes (Figure 3.3A and 3.3B). In *Nrf2*-deprived astrocytes ($Nrf2^{-/-}$), the WT ANG-mediated induction of antioxidant gene expression was completely absent (Figure 3.3A and 3.3B). These results suggest that ANG activates the Nrf2 pathway to induce ARE-dependent gene expression.

In astrocytes, ANG is internalized after it binds to syndecan-4, a transmembrane heparan sulfate proteoglycan.[175,52] To compete for the heparan sulfate binding site of the receptor, we

applied a saturating amount of heparin to form complexes with ANG, resulting in the ablation of intracellular ANG.[56] Thus, treating the cells with heparin prior to WT ANG treatment prevented the changes in hPAP activity and the expression of antioxidant genes (Figure 3.3A). These data support the idea that ANG binding to syndecan-4 is essential for activation of the Nrf2 pathway.

3.3.4 ANG protects neurons against oxidative stress via astrocyte communication

As described above, Nrf2 is the master regulator of antioxidant responses.[198] Small-molecule Nrf2 activators often provide cells with powerful protection from oxidative damage.[248] Accordingly, tBHQ treatment protected cells from H_2O_2-mediated toxicity. The degree of protection did vary among cell types; astrocytes were most responsive to tBHQ treatment, followed by mixed cultures and then neurons (Figure 3.4A, 3.4C, and 3.4E).

We noticed that WT ANG treatment activated the Nrf2-ARE pathway less robustly than did tBHQ treatment (Figure 3.1 and Figure 3.2). The robustness of Nrf2-ARE pathway activation appeared to correlate positively with the degree of cellular protection against H_2O_2-mediated toxicity. As expected, WT ANG treatment protected astrocytes and the mixed culture less potently than did tBHQ (Figure 3.4B and 3.4D). Still, the protective effect of WT ANG in these cultures was significant, though no protection was observed in neurons (Figure 3.4F). Once again, the results emphasized the necessity of neuron-astrocyte communication in supporting neuronal survival against the deleterious effects of oxidative stress.

3.3.5 Neurons use ANG as a messenger to signal their need for protection to astrocytes

Previous studies have demonstrated that stressed neurons secrete ANG, which is then taken up by astrocytes.[52] We replicated these findings. Specifically, we detected a high level of secreted ANG in the conditioned medium collected from neurons exposed to H_2O_2. Using zymogram, a

highly sensitive enzyme-based assay, we first established a standard curve between known WT ANG concentrations and the intensity of bands on the gel (Figure 3.5A). Based on the standard curve and intensity of the band obtained from the conditioned medium sample, we estimated that 0.5 µg and 4 µg WT ANG were secreted per mL of normal and stressed neuronal conditioned medium.

We then investigated the capacity of conditioned medium collected from astrocytes that were pre-exposed to WT ANG to protect neurons. First, we treated astrocytes with 5 µg/mL of WT ANG or the inactive H114R variant. After 24 hours, we collected the astrocyte-conditioned medium and treated neurons with it. These neurons were then subjected to H_2O_2 toxicity. Only conditioned medium from astrocytes exposed to WT ANG protected the neurons; conditioned medium from astrocytes exposed to the H114R ANG variant had no such effect (Figure 3.5B). Conditioned medium collected from *Nrf2*$^{-/-}$ astrocytes exposed to ANG did not have a protective effect.

3.4 Discussion

Members of the pancreatic-type RNase superfamily have evolved to be efficient non-specific catalysts of RNA degradation.[232] Unlike its homologs, ANG has nearly immeasurable ribonucleolytic activity towards model substrates.[223,44] Moreover, whereas other pancreatic-type RNases function in the extracellular space, ANG acts inside the cell.[47,21] Previous studies show that ANG cleaves tRNA to mediate its neuroprotective activity.[186-188] Herein, we report that ANG activates the Nrf2 pathway in astrocytes and subsequently protect neurons from oxidative injury via paracrine signaling. The underlying mechanism is depicted in Figure 3.6.

Stressed neurons secrete high levels of ANG, which then binds to syndecan-4 receptors to enter astrocytes via endocytosis. Upon ligand binding, the receptor activates PKCα. The kinase

phosphorylates Nrf2, endowing it with the ability to evade the Keap1 inhibitor.[252] Phosphorylated Nrf2 translocates to the nucleus and forms heterodimers with Maf. These dimers bind to AREs to stimulate the antioxidant gene expression to defend against H_2O_2-mediated toxicity.

A fraction of the ANG in endosomes escapes into the cytosol, where it encounters a potent ribonuclease inhibitor (RI).[63,65] How ANG evades this inhibitor, which is ubiquitously present in the cytosol, to be sequestered in stress granules remains unclear. A growing body of evidence indicates that ANG is localized in the granules through the recruitment of 5'-tiRNAs, which are produced by ANG-mediated cleavage of tRNAs. Furthermore, these tiRNAs interact with the translational silencer protein YB-1 and sequester the eukaryotic translation initiation factor 4G/A complex to suppress protein translation.[186-188]

As noted, the endogenous inhibitors of ANG and Nrf2–RI and Keap1–respectively, contain atypically high numbers of cysteines, which are susceptible to oxidation in the presence of ROS.[228,59,259,60] Small-molecule Nrf2 activators often serve as electrophilic inducers and react with Keap1 cysteine thiols to prevent Keap1•Nrf2 complex formation, releasing Nrf2 to induce the expression of ARE-dependent genes.[260,261] We speculate that RI cysteine thiols might undergo the same oxidation reaction to liberate ANG, which can then be recruited into stress granules.

Another intriguing question is the composition of the conditioned media collected from ANG-treated astrocytes. Oxidative stress irritates neurons, leading to the release of ANG, which acts as a distress signal that is conveyed to astrocytes. Within astrocytes, ANG generates specialized tiRNAs that contain G-quadruplex to arrest protein translation. Delivery of these tiRNA to neurons has been demonstrated to be neuroprotective.[188] In addition, Nrf2 activation in

astrocytes protects neighboring neurons.[200,257] We speculate that ANG-treated astrocytic conditioned media contains tiRNAs and perhaps other RNA molecules that regulate antioxidants and that these molecules can be transported to neurons to induce ROS clearance.

We showed that ANG activates Nrf2 pathway via receptor-induced kinase activation. Unexpectedly, the inactive H114R ANG did not trigger the Nrf2 pathway even though the mutation does not affect astrocyte internalization, which should activate PKCα at least partially. The data support the idea that the ribonucleolytic activity of ANG is essential for Nrf2-dependent protection from H_2O_2-mediated toxicity. Perhaps both effects of ANG—the cleaving of tRNAs and activation of the Nrf2 pathway—must occur in a coordinated manner to generate its highly effective antioxidant functions.

The molecular effects of ANG act together in an orchestrated fashion. ANG activates the intracellular Nrf2 pathway like typical ligands that bind to the extracellular face of membrane-bound receptors and depend on receptor-mediated signal transduction to activate a transcriptional factor, which then leads to changes in gene expression. On the contrary, ANG also enters astrocytes and navigates to stress granules to suppress protein translation. Hence, ANG, in part, directs the translation machinery to temporarily focus on the synthesis of antioxidant enzymes and specifically induces ARE-dependent gene expression through Nrf2. This mechanism of ANG-mediated neuroprotection is distinct from its role in promoting cell proliferation and neovascularization; in this case, ANG is found in the nucleolus and promotes rDNA transcription.[47,65,22] This distinction raises the interesting question of how ANG senses the local cellular environment, which dictates its mode of action.

Nrf2 is the master regulator of the cellular antioxidant system. Nrf2 senses the presence of oxidants and is responsible for the production of a vast array of antioxidants to counterbalance

these reactive oxidants. Many attempts have been made to develop small-molecule activators of the Nrf2 pathway to combat free radicals. Currently, one dietary supplement, Protandim, and one FDA-approved drug, Tecfidera, claim to be Nrf2 activators.[262,263] Here, we report an endogenous protein–ANG–that activates the Nrf2 pathway and counteracts the deleterious effects of ROS. Its activation of Nrf2 further underscores ANG as a preeminent neuroprotective agent to combat oxidative stress-mediated cellular toxicity. This study highlights the therapeutic potential of ANG as a promising treatment for ALS.

3.5 Materials and Methods

ANG and its variants were produced and purified as described previously.[44]

3.5.1 Cell culture

Primary astrocyte cultures were prepared from the cortices of 1-day-old mice as described previously.[200] Astrocytes were plated at a density of 2 x 10^4 cells/cm^2 in 6-well or 96-well collagen-coated plates and maintained in complete media (CEMEM). The CEMEM contained MEM supplemented with 10% v/v fetal bovine serum, 10% v/v horse serum, 0.5 mM L-glutamine, 1% v/v penicillin (100 IU/mL), and streptomycin (100 lg/mL). Neuronal cultures were prepared from E15–E16 embryos as previously described.[254] Neurons were plated at a density of 3 x 10^4 cells/cm^2 in 6-well or 96-well poly-D-Lysine-coated plates and maintained in CEMEM for 45 min before the media was replaced with fresh Neurobasal media (NBM). Every 2–3 days, half of the old NBM was replaced with fresh NBM. The mixed cultures were prepared similarly to the neuronal cultures with the following exceptions. After the cells were plated in CEMEM and incubated for 45 min, the medium was replaced with fresh CEMEM. At day 2, the

media was switched to NBM. Every 2–3 days, half of old the NBM was replaced with fresh NBM.

3.5.2 hPAP reporter assay

Cells were grown in 96-well plates and seeded at the density indicated for the various cell types. Fully differentiated cultures were treated with vehicle, tBHQ or WT ANG and its variants for 24 hours. Whole-cell extracts were prepared by lysing cells in 96-well plates. HPAP levels were quantified by measuring alkaline phosphatase activity. Briefly, cells were lysed in lysis buffer (50 mM Tris–HCl, 5 mM $MgCl_2$, 100 mM NaCl, 1% w/v CHAPS), and the extracts were incubated at 65 °C for 30 min to inactivate endogenous alkaline phosphatase activity. Next, the alkaline phosphatase substrate (CSPD, Tropix) and its enhancer (Emerald, Tropix) were added to the phosphatase reaction. The measurements of hPAP activity were based on the luminescent signal produced by the luminescent product produced by dephosphorylation of the substrate. Paired Student's *t*-tests were used to assess the statistical significance of differences between treatment groups.

3.5.3 Cell survival assay (MTS assay)

Cells were grown in 96-well plates and seeded at the density indicated for the various cell types. Fully differentiated cultures were treated with vehicle, tBHQ or WT ANG and its variants for 24 hours and then treated with increasing concentrations of H_2O_2. After 48 hours, the medium was removed, and the cells were incubated with CellTiter 96 MTS reagent (Promega) for 1–4 hours depending on cell type. Absorbance at 490 nm was recorded using an M1000 fluorimeter (Tecan). The data were analyzed with Prism 5.0 software (GraphPad).

3.5.4 Quantification of cellular RNA by qRT-PCR

Total cellular RNA was isolated by extraction with Trizol (Invitrogen), and the RNA samples were then treated with DNase I (Invitrogen) at 37 °C for 15 min. The RNA was purified through phenol:chloroform extraction followed by ethanol precipitation. RNA concentrations and purities were assessed with a NanoVue instrument (GE Healthcare Life Sciences).

Purified cellular RNA (~1 µg) was used in the reverse transcription reaction along with random hexamers from the SuperScript III Reverse Transcriptase kit (Invitrogen). A 1-µL aliquot of the resultant cDNA solution was used in qPCR reactions in conjunction with PerfeCTa SYBR Green FastMix Reaction Mixes (Quanta Biosciences). Amplified cDNAs were evaluated with an ABI Prism 7200 sequence detector (Perkin Elmer). The primers used for qPCR were designed as described previously.[200]

3.6 Acknowledgments

We thank Dr. K. Blanco and Dr. K. Sankar for their assistance in primary culture preparation. T.T.H. was supported by an Advanced Opportunity/Graduate Research Scholar Fellowship and by Molecular Biosciences Training Grant T32 GM007215 from the National Institutes of Health (NIH). This work supported by grant R01 CA073808 (NIH).

Figure 3.1

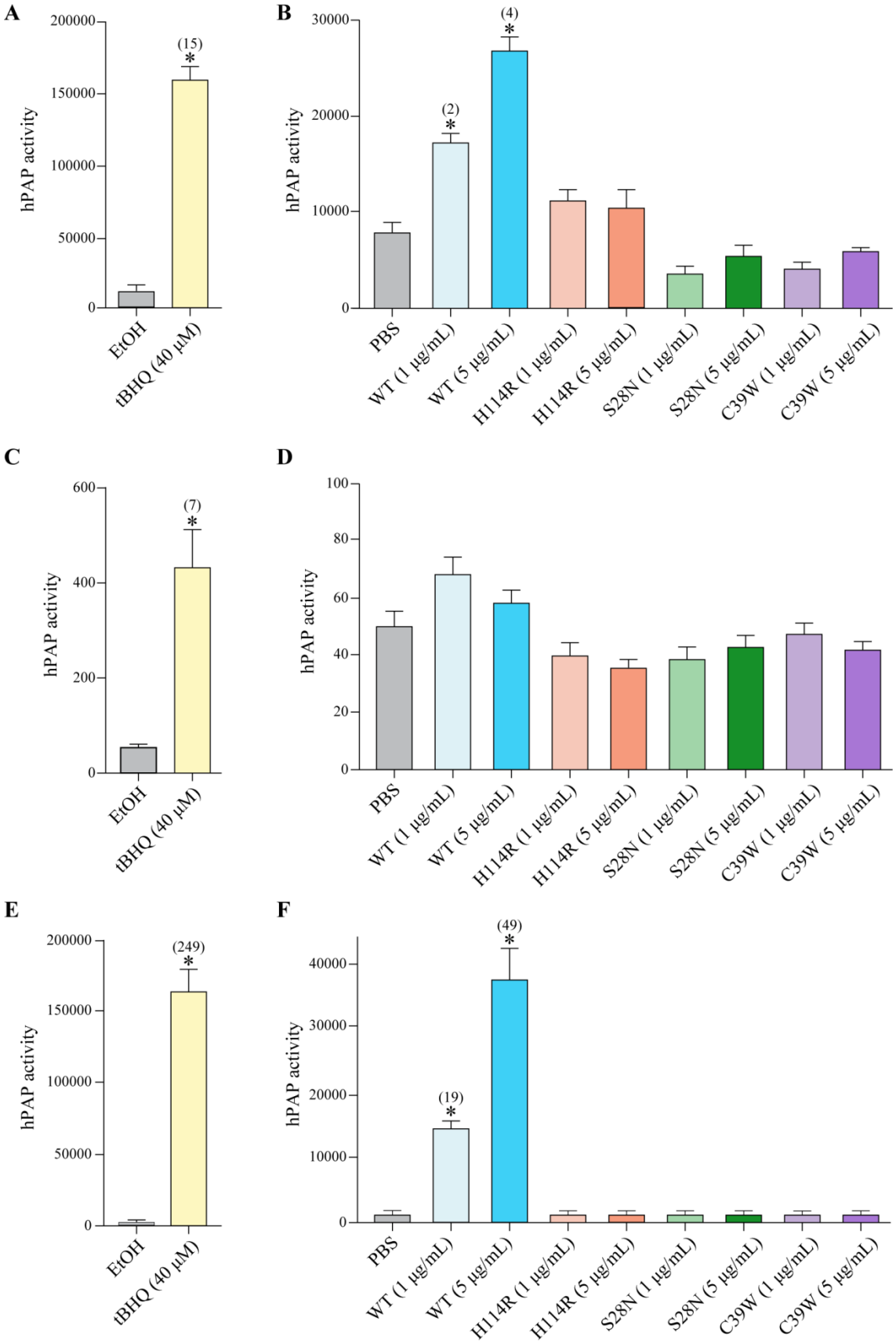
A
hPAP activity
200000
150000
100000
50000
0
(15)
*
EtOH
tBHQ (40 µM)
B
hPAP activity
30000
20000
10000
0
(2)
*
(4)
*
PBS
WT (1 µg/mL)
WT (5 µg/mL)
H114R (1 µg/mL)
H114R (5 µg/mL)
S28N (1 µg/mL)
S28N (5 µg/mL)
C39W (1 µg/mL)
C39W (5 µg/mL)
C
hPAP activity
600
400
200
0
(7)
*
EtOH
tBHQ (40 µM)
D
hPAP activity
100
80
60
40
20
0
PBS
WT (1 µg/mL)
WT (5 µg/mL)
H114R (1 µg/mL)
H114R (5 µg/mL)
S28N (1 µg/mL)
S28N (5 µg/mL)
C39W (1 µg/mL)
C39W (5 µg/mL)
E
hPAP activity
200000
150000
100000
50000
0
(249)
*
EtOH
tBHQ (40 µM)
F
hPAP activity
40000
30000
20000
10000
0
(19)
*
(49)
*
PBS
WT (1 µg/mL)
WT (5 µg/mL)
H114R (1 µg/mL)
H114R (5 µg/mL)
S28N (1 µg/mL)
S28N (5 µg/mL)
C39W (1 µg/mL)
C39W (5 µg/mL)

Figure 3.1 ANG activates ARE-dependent promoters selectively in astrocytes

A,C,E Graphs of hPAP activity indicating that compared to vehicle, tBHQ (40 μM) increased hPAP activity by 15-fold in astrocytes, 7-fold in neurons, and 249-fold in mixed cultures. (B,D,F) WT ANG treatment also increased hPAP activity but not as robustly as did tBHQ treatment. Compared to PBS, WT ANG (5 μg/mL) increased phosphatase activity by 4-fold in astrocytes and 49-fold in mixed cultures but did not change the activity in neurons. **B,D,F** hPAP activity remained unchanged upon treatment with ALS-associated ANG variants. H114R ANG has a deleterious active-site substitution, S28N ANG exhibits defective nuclear localization, and C39W ANG is unstable.

Figure 3.2

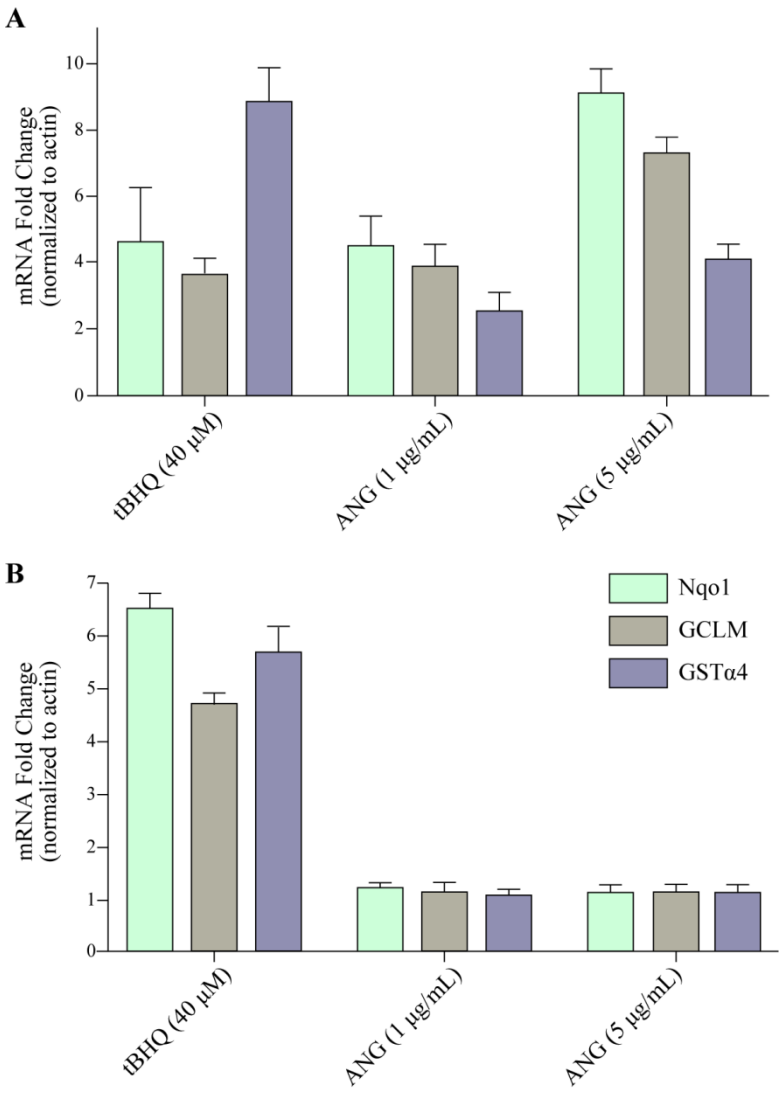
A
mRNA Fold Change
(normalized to actin)
0
2
4
6
8
10
tBHQ (40 μM)
ANG (1 μg/mL)
ANG (5 μg/mL)
B
mRNA Fold Change
(normalized to actin)
0
1
2
3
4
5
6
7
Nqo1
GCLM
GSTα4
tBHQ (40 μM)
ANG (1 μg/mL)
ANG (5 μg/mL)

Figure 3.2 ANG drives the expression of ARE-dependent genes in astrocytes

A. Graphs of qRT-PCR demonstrating that the expression of ARE-dependent genes was up-regulated upon tBHQ and ANG treatment. Treatment with tBHQ (40 μM) increased NQO1, GCLM, and GSTα4 gene expression in both astrocytes and neurons.

B. In contrast, WT ANG exclusively promoted the expression of these genes in astrocytes and not in neurons. The ANG-mediated promotion of gene expression thus appears to be dose-dependent.

Figure 3.3

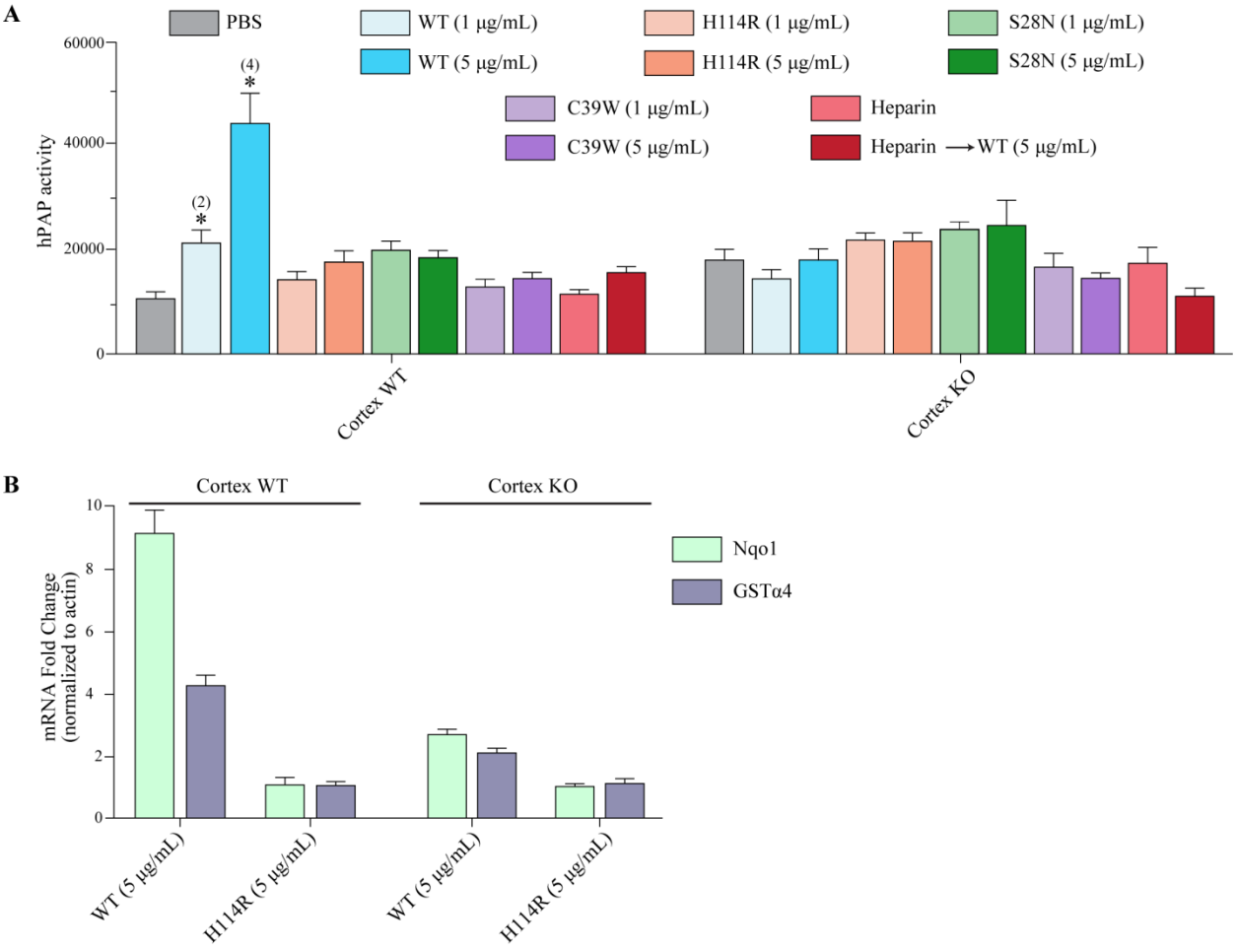
A
PBS
WT (1 µg/mL)
WT (5 µg/mL)
H114R (1 µg/mL)
H114R (5 µg/mL)
S28N (1 µg/mL)
S28N (5 µg/mL)
C39W (1 µg/mL)
C39W (5 µg/mL)
Heparin
Heparin → WT (5 µg/mL)
hPAP activity
60000
40000
20000
0
(2)
*
(4)
*
Cortex WT
Cortex KO
B
Cortex WT
Cortex KO
Nqo1
GSTα4
mRNA Fold Change
(normalized to actin)
10
8
6
4
2
0
WT (5 µg/mL)
H114R (5 µg/mL)
WT (5 µg/mL)
H114R (5 µg/mL)

Figure 3.3 ANG depends on Nrf2 to induce ARE-dependent gene expression

A,B In WT astrocytes, ANG-mediated hPAP activation and induction of the expression of antioxidant genes were similar to those presented in Figures 3.1B and 3.2A. In *Nrf2*-deprived astrocytes (*Nrf2*$^{-/-}$), the WT ANG-mediated ARE-dependent gene expression was diminished completely. In addition, using heparin to sequester extracellular ANG caused intracellular depletion of the protein. Hence, treating the cells with heparin prior to ANG stimulation prevented the ANG-induced changes in hPAP activity and antioxidant gene expression.

Figure 3.4

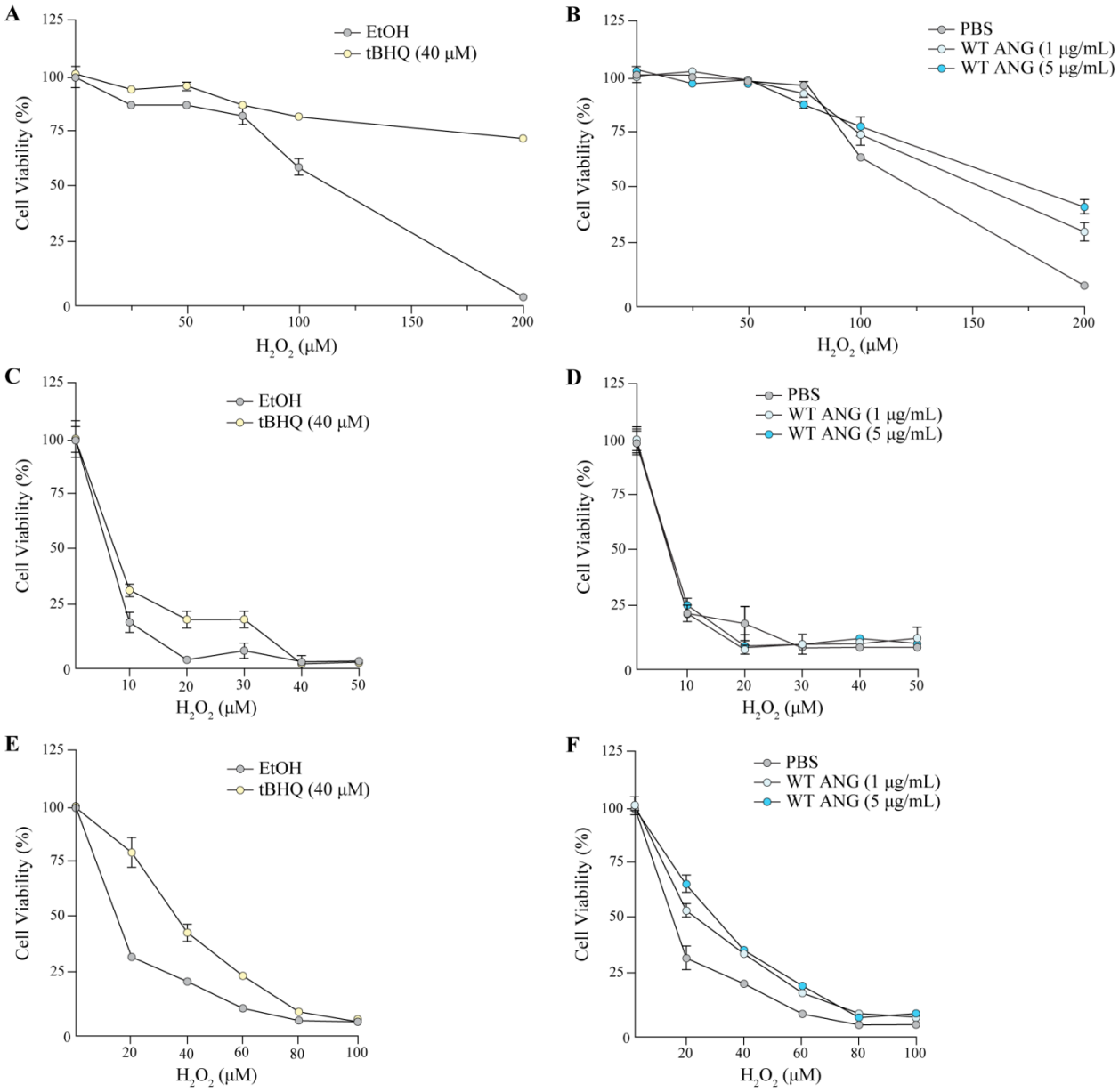
A
EtOH
tBHQ (40 µM)
Cell Viability (%)
H_2O_2 (µM)
B
PBS
WT ANG (1 µg/mL)
WT ANG (5 µg/mL)
Cell Viability (%)
H_2O_2 (µM)
C
EtOH
tBHQ (40 µM)
Cell Viability (%)
H_2O_2 (µM)
D
PBS
WT ANG (1 µg/mL)
WT ANG (5 µg/mL)
Cell Viability (%)
H_2O_2 (µM)
E
EtOH
tBHQ (40 µM)
Cell Viability (%)
H_2O_2 (µM)
F
PBS
WT ANG (1 µg/mL)
WT ANG (5 µg/mL)
Cell Viability (%)
H_2O_2 (µM)

Figure 3.4 ANG protects neurons from oxidative stress via astrocyte communication

A,C,E tBHQ treatment (40 μM) protected the cells from H_2O_2-mediated toxicity. The degree of protection varied among cell types. Astrocytes were the most responsive to the treatment, followed by the mixed cultures and then neurons.

B,D,F In contrast, treating the cells with WT ANG, at two doses, protected only astrocytes and mixed cultures, not neurons.

Figure 3.5

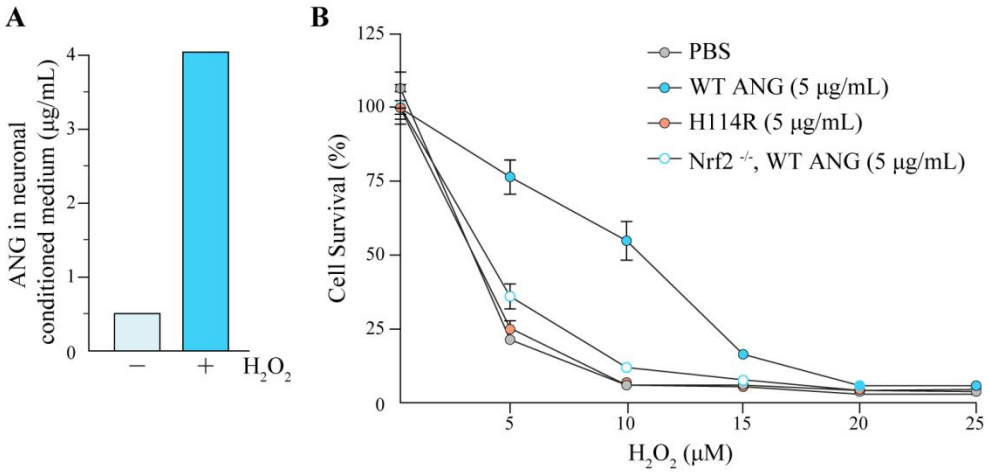
A
ANG in neuronal conditioned medium (µg/mL)
0
1
2
3
4
−
+
H2O2
B
Cell Survival (%)
0
25
50
75
100
125
5
10
15
20
25
H2O2 (µM)
PBS
WT ANG (5 µg/mL)
H114R (5 µg/mL)
Nrf2 -/-, WT ANG (5 µg/mL)

Figure 3.5 Neurons use ANG to signal their need for protection to astrocytes

A. Pre-exposing neurons to H_2O_2 (1 μM) caused the release of ANG into the conditioned medium. A zymogram gel of conditioned medium collected from stressed neurons demonstrating a high level of 4 μg/mL active ANG, in comparison to healthy neurons sample of 0.5 μg/mL. **B.** Conditioned medium collected from astrocytes that were pre-exposed to WT ANG (5 μg/mL) displays robust neuronal protection. The protection depended on Nrf2 and the ribonucleolytic activity of ANG. Conditioned medium collected from *Nrf2*$^{-/-}$ astrocytes failed to protect neurons from H_2O_2-mediated toxicity, and conditioned medium collected from astrocytes exposed to the inactive H114R ANG variant did not have a protective effect.

Figure 3.6

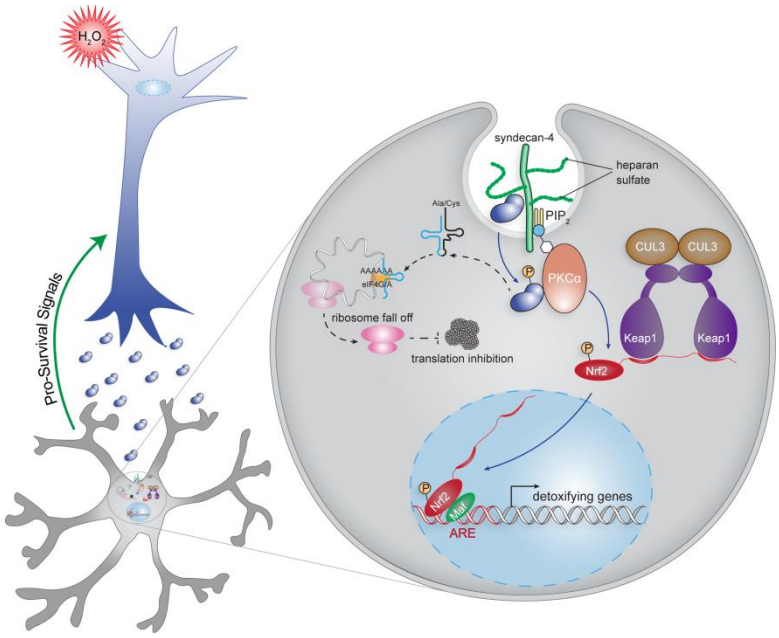
H_2O_2
Pro-Survival Signals
syndecan-4
heparan sulfate
Ala/Cys
PIP_2
AAAAAA
eIF4G/A
PKCα
ribosome fall off
translation inhibition
CUL3
CUL3
Keap1
Keap1
Nrf2
Nrf2
MafF
ARE
detoxifying genes

Figure 3.6 The ANG neuroprotective pathway

ANG binds to syndecan-4 on the cell surface and is internalized through endocytosis. Upon ligand binding, syndecan-4 activates PKCα to phosphorylate Nrf2. Phosphorylation enables Nrf2 to evade its binding partner, Keap1. Phosphorylated Nrf2 translocates into the nucleus and forms a heterodimer with Maf. The dimer binds to ARE, driving the expression of antioxidant genes to counteract cellular oxidative injury. In addition, ANG participates in stress-induced protein translation repression by generating tiRNAs. ANG must execute both actions—cleaving tRNAs and activating the Nrf2 pathway—in a coordinated manner to achieve its highly effective antioxidant effects.

CHAPTER 4

Future Directions

Contribution: I am currently pursuing the idea of delivering an ROS-activatable ANG into glial cells for targeted ALS therapy. The synthesis of BBVC and BVC was performed by Thom Smith. I appended these molecules on K40C ANG variant and its FLAG fusion.

4.1 Delivery of ROS-activatable ANG into glial cells for targeted ALS therapy

ALS affects approximately two in every 100,000 people, and ALS patients typically survive only two to five years after diagnosis.[149,150] Treating ALS has been challenging due to an insufficient understanding of its underlying cause and pathogenesis.[264,265] Current treatment strategies include lowering microglial activation, introducing muscle hypertrophy agents, and increasing motor neuron trophic factor levels.[266-268] These strategies have, however, only achieved marginal success. The more successful *in vivo* treatments involve gene or stem cell therapy, either to replace damaged motor neurons or to encourage the production of new motor neurons.[269-271] Unfortunately, these therapies do not yet address the full landscape of ALS symptoms. The only approved chemotherapeutic agent for ALS is Riluzole®, which extends survival by only 2–3 months and does not improve motor function.[272,273] Hence, developing enhanced ALS treatments is a primary focus of many research laboratories.

Oxidative stress is a hallmark of neurodegenerative diseases (NDs), including ALS, and is caused by an imbalance between ROS formation and cellular antioxidant capacity.[274,275] Potential therapeutic approaches for NDs that involve elevating the cellular antioxidant response have demonstrated promise in clinical studies.[276-278] Many studies have focused on developing small-molecule activators to trigger the Nrf2 pathway, which is a key stimulator of the cellular antioxidant response.[257,279,280] In CHAPTER 4, I demonstrate that ANG activates the Nrf2 pathway in astrocytes to exert its neuroprotective activity. My findings suggest that ANG is a promising neuroprotective agent for treating ALS.

As ANG is a potent inducer of cell proliferation and angiogenesis, ANG treatment could potentially have side effects associated with neovascularization promotion, including

hemorrhage and tumor growth.[27,30,85,49] Therefore, an ideal ANG-based drug would utilize a pro-ANG variant that is only functional in target cells.

A well-characterized feature of ALS pathology is an enhanced ROS generation in neurons and glial cells.[281,282] Thus, I propose masking the catalytic residue of ANG with a protecting group that is removed by ROS. This masked ANG will be inert to normal cells due to the lack of enzymatic activity. But inside cells with high ROS levels, the ROS will unmask ANG, restoring its biological function. In this way, my pro-ANG drug strategy could be beneficial for treating ALS with a low risk of cancer development.

A recent study by Xu and coworkers demonstrated a chemical approach to reversibly modulate RNase A function in response to ROS.[283] The conjugation of RNase A with 4-nitrophenyl 4-(4,4,5,5-tetramethyl-1,3,2-dioxaborolan-2-yl)benzyl carbonate (NBC) blocked Lys residues and temporarily deactivated the protein. The RNase A–NBC was re-activated by high levels of intracellular ROS inside of tumor cells. This work demonstrated the feasibility of reversibly controlling enzyme function using ROS. Still, this method has some notable disadvantages. First, NBC was not appended to a specific Lys residue, such as the one at the catalytic site; instead, all 10 Lys residues were likely masked, with an average of 7 residues labeled per molecule. Whereas RNase A activity can be re-activated by an H_2O_2 trigger, the total number of NBC molecules conjugated to each RNase A molecule is detrimental to protein internalization. The innate ability of the protein to enter cells is significantly compromised when positive charges are masked. To compensate for this defect, RNase A–NBC needed to be encapsulated into cationic lipid nanoparticles for intracellular protein delivery.

To improve upon this technology, I have designed an NBC derivative with an alkene handle, called boronated benzyl vinyl carbamate (BBVC), which can undergo thiol-ene addition to thiol

groups on Cys residues. In addition, as ANG lacks surface-exposed Cys residues, I can use site-directed mutagenesis to replace any residue of interest with a Cys residue, thereby enabling site-specific labeling. For example, an ROS-inducible ANG can be produced by replacing the active-site residue Lys40 with a Cys residue (K40C) and labeling it with BBVC. Upon entering an oxidatively stressed cellular environment, ROS will induce a self-immolative reaction at K40C–BBVC that unmasks a thioether mimic of the native catalytic residue, K40*S*-(aminoethyl) cysteine, thus restoring biological activity to ANG. Although not the native residue, this thioether analog of Lys has been shown to have a minimal effect on the catalytic activity of RNase A.[284] This thioether substitution will be considered when assessing ANG neuroprotective activity. Once the K40C–BBVC cage is released in oxidatively stressed cells, functional ANG will be replenished, activating antioxidant responses to provide additional ROS clearance.

To illustrate the necessity of the aryl boronic acid in designing an ROS-responsive protein, a parent BVC molecule that lacks the boronic acid moiety should also be appended to ANG as a control. Then, these modified ANG variants will be characterized *in vitro* for ribonucleolytic activity and *in cellulo* for neuroprotective capacity. Specifically, FRET-based enzymatic assay will be used to validate the deficient ribonucleolytic activity of ANG–BBVC and demonstrate the recovery of activity upon exposure to H_2O_2.[285] Then, the neuroprotective potency of ANG–BBVC shall be evaluated by changes in ARE-dependent gene expression in response to a variety of ALS-associated stressors.

Precise intracellular control of spatiotemporal protein function is an appealing tool for therapeutic applications. My proposed ROS-activatable ANG design will create a stimulus-responsive protein precisely controlled to activate under oxidative stress conditions. Moreover, my strategy has the potential to overcome hurdles that have hindered the development of

effective therapies for ALS. Unlike components of current therapies, *e.g.*, gene- or stem cell-based approaches, ANG has an innate ability to enter cells, thus circumventing the need for an elaborate delivery system. Furthermore, ROS-activatable ANG could have broad therapeutic efficacy for ALS as it is only effective in cells with high ROS accumulation, which limits the likelihood of unintended side effects. Thus, I put forth ANG as a model drug to demonstrate the potential advantages of ROS-responsive chemical modifications of proteins for targeted ALS therapy.

Figure 4.1

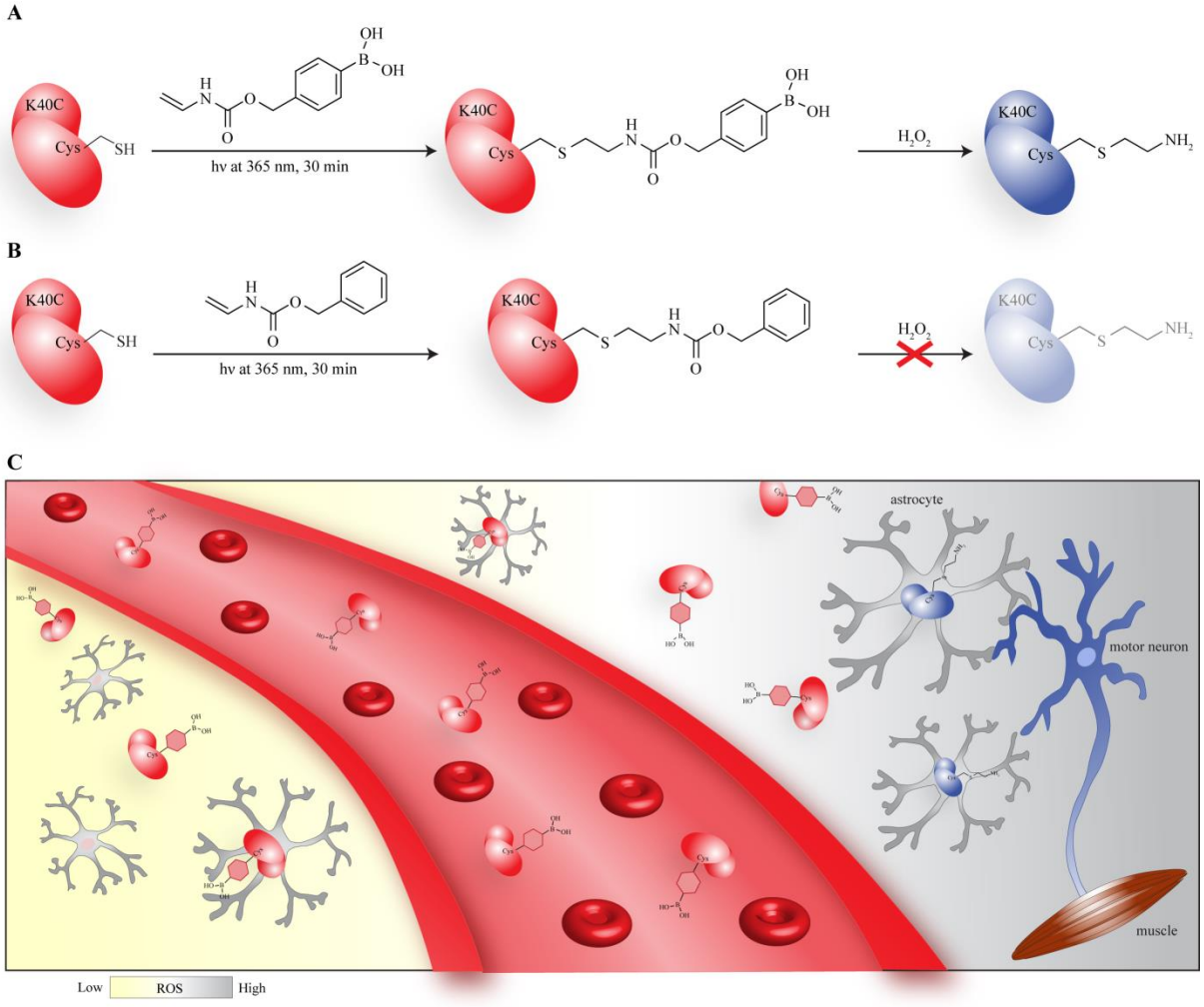
A
K40C
Cys
SH
hv at 365 nm, 30 min
H_2O_2
NH_2
B
C
astrocyte
motor neuron
muscle
Low
ROS
High

Figure 4.1 Scheme of ROS-activatable ANG-BBVC delivery

A,B ANG K40C variant with the free cysteine modification with BBVC for ROS-responsive and with BVC for nonresponsive engineered proteins.

C. Intravenous administration of ANG–BBVC into the blood stream. In healthy environments, ANG–BBVC taken up by cells will be latent. In environments with high ROS levels, ANG–BBVC undergoes a self-immolative reaction, unmasking Lys and restoring ANG neuroprotective activity. Replenishment of functional ANG in astrocytes triggers Nrf2 pathway activation, thereby elevating the cellular antioxidant response. Consequently, the activated astrocytes protect neighboring motor neurons from oxidative damage.

4.2 Delivery of heterobifunctional RNases for targeted cancer therapy

A strong correlation between nucleolar morphology and cancer was recognized by pathologists over 100 years ago, when large and abnormal nucleoli were first observed to be common in cancer cells. Today, the nucleolar contribution to cancer is well established with respect to its role in producing ribosomal RNA (rRNA), which is critical for ribosome biogenesis and thus for proliferative capacity.[118,286,287] Tumor cells are highly dependent on the hyper-activation of ribosome biogenesis to maintain their cancerous phenotypes.[102-104] This dependency suggests that modulating the activity of ribosome biogenesis could be a therapeutic strategy for cancer.[123,288]

In fact, 20 out of 36 chemotherapeutic drugs in clinical use for cancer treatment already inhibit ribosome biogenesis.[126,289] Most of these drugs were designed to target highly proliferating cells by damaging DNA or by interfering with DNA synthesis or mitosis. The degree to which ribosome biogenesis disruption contributes to the efficacy of these drugs is difficult to distinguish from toxicity that is mediated by other means. For example, actinomycin D (AMD), which is a DNA intercalator, functions primarily to inhibit DNA synthesis.[290,291] This drug has a preference for GC-rich DNA sequences; as rDNA regions have above-average GC-richness, low concentrations of AMD preferentially inhibit RNA polymerase I (Pol I) transcription.[292,293] Other examples of anticancer drugs that are also known to interfere with Pol I activity include alkylating drugs, such as cisplatin and oxaliplatin, or topoisomerase poisons, such as camptothecin.[294-297]

Recently, two new anticancer agents, CX-5461 and BMH-21, were specifically designed to suppress ribosome biogenesis by blocking Pol I transcriptional activity.[128] CX-5461 was designed to inhibit Pol I transcription by disrupting pre-initiation complex formation at the

rDNA promoter.[124,127] BMH-21, like AMD, is a DNA intercalator with a preference for GC-rich sequences.[298,299] BMH-21 is a potent and specific inhibitor of rDNA transcription; BMH-21 causes nucleolar stress, resulting in decreased proliferation and cell death.[300,301] This new class of drugs highlights the growing potential of targeting rRNA synthesis through Pol I modulation for use in cancer therapy.

Nevertheless, the targeting modalities of these drugs also cause toxicity in normal tissues with high proliferation rates. Therapeutics that selectively kill tumor cells *in vivo* while sparing normal cells are of special interest. Herein, I propose a novel protein-based therapy for selectively targeting ribosome biogenesis in cancer cells. Specifically, I plan to generate an ANG–RNase 1 heterodimer using heterobifunctional crosslinkers. Individually, both ANG and RNase 1 are preferentially internalized by cancer cells.[302,49,303,304] Furthermore, this heterodimer would inherit two advantageous features from its parent monomers. First, ANG would allow the ANG–RNase 1 molecule to access the nucleolus.[47,48] Second, RNase 1 would confer potent RNA hydrolytic activity.[232,305] By combining these features, I plan to create a cancer-targeting heterodimer that can effectively degrade rRNA in the nucleolus, which leads to dysregulated ribosome assembly and subsequently results in cell death.

ANG and RNase 1 are members of the pancreatic-type ribonuclease superfamily; they both are small, extremely stable, easily produced, and tolerant of chemical modifications.[284,232] For many of these reasons, RNases have a strong precedent as effective protein scaffolds for therapeutic modulation.[306-308] As noted, RNase 1 is incapable of killing cells due to the presence of its cytosolic inhibitor, RI, which is ubiquitous intracellularly.[57,62,59] Hence, I shall use a clinically relevant RNase 1 variant, QBI-139, which is engineered to resist RI binding.[309,310] In addition, in CHAPTER 2, I describe the molecular action of ANG promoting rDNA

transcription, which is an unfavorable event associated with this particular drug design. To address this off-target activity, an inactive H114N ANG variant will be used instead. In summary, I propose to synthesize a more effective RNase-based anticancer drug, H114N-ANG–QBI-139.

I will take advantage of heterobifunctional crosslinkers that possess different reactive groups at their ends in order to connect the two proteins. The most widely used heterobifunctional crosslinkers are those having an amine-reactive succinimidyl ester at one end and a sulfhydryl-reactive group at the other. *N*-Succinimidyl[4-iodoacetyl]aminobenzoate (SIAB) is an ideal candidate. This crosslinker contains an amine-reactive *N*-Hydroxysuccinimide (NHS) ester and a sulfhydryl-reactive iodoacetyl group. NHS esters will react with primary amino groups present on Lys residue side chains as well as the N-terminus of the H114N ANG variant. The iodoacetyl group will react with the free sulfhydryls via nucleophilic substitution of iodine with the thiol group of QBI-139 Cys, resulting in a stable thioether linkage.

Certain cell-surface glycans are known to be up-regulated during cancer transformation. The H114N ANG variant and QBI-139 both have strong interactions with those cancer-specific glycans, resulting in cellular uptake.[302,49,303,304] Upon entering the cytoplasm, both proteins evade RI interaction in mechanistically distinct manners.[311-313] The NLS signal from ANG brings the heterodimer to the nucleolus, where QBI-139 will deplete the pool of nascent rRNA and disrupt ribosome biogenesis. The disruption of this vital cellular process would trigger cell apoptosis.

To elucidate the requirements of both monomers (H114N ANG and QBI-139) for mediating cell death, each will also be examined for cytotoxicity. I speculate that treatment with the inactive H114N ANG variant will not result in any cytotoxicity. Furthermore, though treatment with QBI-139 has been reported to kill cancer cells effectively, I anticipate that my heterodimer

will produce more impressive results. The QBI-139 monomer only degrades cytosolic RNAs, which constitute only a small portion of the total RNAs. H114N ANG will provide a "piggyback ride" to QBI-139, carrying the protein into the nucleolus. There, QBI-139 could prey upon nascent rRNAs, which account for more than 80% of all RNAs in rapidly growing mammalian cells.[314] In addition, as the dimer is twice as large as the monomer, the dimer will have slower passive renal clearance, thus extending its persistence in circulation.[315] Overall, this new RNase-based therapy that selectively targets ribosome biogenesis and extends the circulation time of the therapeutic moieties could benefit the treatment of cancer.

Figure 4.2

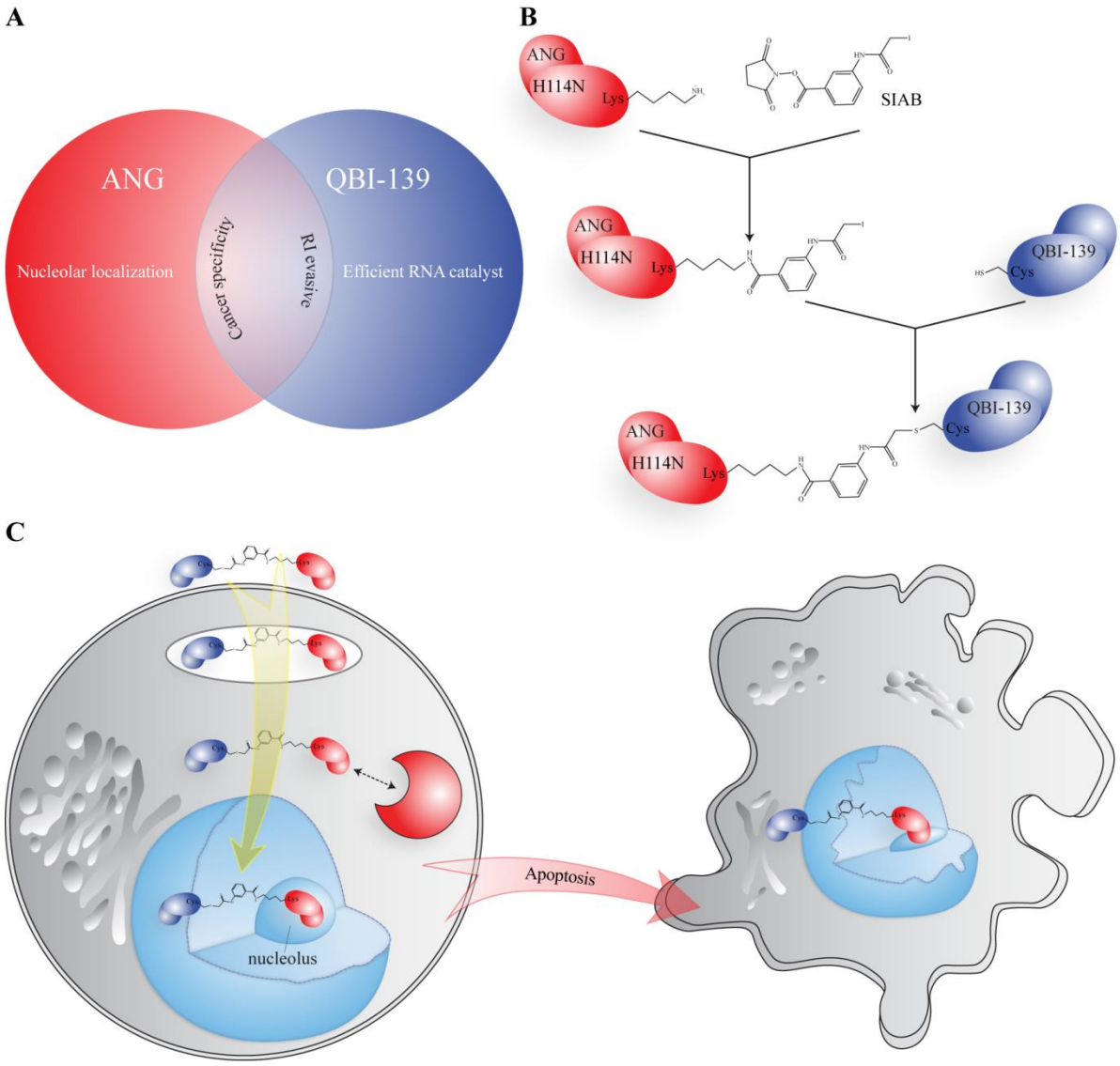
A
ANG
QBI-139
Nucleolar localization
Cancer specificity
RI evasive
Efficient RNA catalyst
B
ANG
H114N
Lys
SIAB
QBI-139
Cys
C
nucleolus
Apoptosis

Figure 4.2 Scheme of H114N-ANG–QBI-139 delivery

A. The shared and distinctive features of ANG (red) and QBI-139 (blue) are depicted in a Venn diagram.

B. A heterobifunctional linker, *N*-Succinimidyl[4-iodoacetyl]aminobenzoate (SIAB), will be used to connect H114N ANG and QBI-139.

C. The heterodimer is taken up preferentially by cancer cells. Upon entering the cytoplasm, both proteins evade RI interaction in mechanistically distinct manners. The NLS of ANG allows the dimer to navigate to the nucleolus. There, the QBI-139 portion of the dimer manifests its ribonucleolytic activity by degrading nascent rRNA transcripts, which leads to ribosome biogenesis disruption and ultimately triggers cell death.

4.3 RtcB reverses the biological consequences of tiRNAs

Dysregulated tRNA metabolism has been implicated in the pathogenesis of a variety of human diseases.[23,316,317] Under adverse conditions, such as hypoxia and oxidative stress, cytoplasmic, mature tRNAs are cleaved by ANG in the anticodon loop to produce 5′- and 3′-tRNA fragments, which are designated as 5′-tiRNAs and 3′-tiRNAs, respectively.[186,187] tiRNAs function to inhibit stress-induced apoptosis, thereby promoting cell survival.[318,188] Still, tiRNA overproduction has been reported to have detrimental consequences on cell physiology.

In neurons, excessive accumulation of 5′-tiRNAs derived from a specific subset of tRNAs (*i.e.*, Asp, Glu, Gly, His, Val, and Lys) triggers a sustained stress response that leads to neuronal loss.[319] This process links aberrant tRNA metabolism to the development of certain forms of intellectual disability. In epithelial cells infected with respiratory syncytial virus (RSV), ANG activation results in abundant production of tRNA fragments that resemble classic 5′-tiRNAs.[320] A certain type of 5′-tiRNA is required for RSV replication. Currently, no vaccine exists for RSV. Therapies that interfere with tiRNA function or inhibit ANG could potentially disrupt RSV infection.

The biogenesis of 5′-tiRNA is controlled by ANG.[186,23] This enzyme catalyzes tRNA cleavage to yield 5′-tiRNA with a 2′,3′-cyclic phosphate end and 3′-tiRNA with a 5′-OH end. The mechanisms modulating the production of these tiRNAs need to be elucidated, as the continuous accumulation of tiRNAs negatively impacts cell physiology. A recently discovered noncanonical RNA ligase, RtcB, might provide insight into the regulation of tiRNA abundance. RtcB mediates the joining of the 2′,3′-cyclic phosphate and 5′-OH ends of RNAs.[321-323] Hence, an obvious question emerges as to whether RtcB can ligate the two halves of tRNAs produced by ANG.

RtcB activity has only two known functions: tRNA ligation after intron removal, and XBP1 mRNA ligation during activation of the unfolded protein response (UPR).[324-326] The UPR is a well-known adaptive mechanism for cells to maintain endoplasmic reticulum (ER) homeostasis. The most conserved UPR branch is defined by IRE1, an ER transmembrane kinase/endoribonuclease.[327] Upon sensing unfolded proteins, IRE1 undergoes a conformational change during activation. Activated IRE1 removes a 26-nt intron from the unspliced XBP1u mRNA to generate a mature mRNA for the production of XBP1, a stress sensor. The maturation of the mRNA is governed by RtcB ligase, supporting the ligase role in ER stress.[328,329]

RtcB function has been linked to stress response. Coincidently, the ANG-induced tRNA cleavage is highly dependent on stressor stimuli. Under those adverse conditions, adequately produced tiRNAs mediate anti-apoptotic effects. Yet, continued tiRNA production leads to cellular toxicity. RtcB could mitigate this toxicity by ligating these tRNA halves and replenishing functional tRNAs within cells. This new potential function of RtcB further suggests a broader impact of RtcB in stress response. Moreover, RtcB could counteract RSV infection by depleting tiRNAs, which are activators of RSV replication.

Further, RtcB might be a regulator during early stages of cellular development. The recent discovery that the abundance of 5′-tRNA halves found in sperm and oocytes decreases rapidly upon fertilization suggests that this class of molecules can be regulated physiologically.[330] Nonetheless, what controls the levels of these tiRNA pools remains unclear. RtcB could potentially ligate these RNAs, thus reducing the abundance of 5′-tRNA halves.

Biochemical studies can be used to test the hypothesis that tiRNAs are RtcB substrates. First, tRNA can be exposed to ANG to produce 5′-tRNA halves. Then, RtcB ligase can be introduced to the reaction and monitored for substrate tRNA recovery. Based on the *in vitro* results, an *in*

cellulo quantification of tiRNAs would evaluate the effect of ANG treatment in either WT or *RtcB* knock-down cells. The amount of tiRNA generated by ANG is likely to be much higher in WT cells than in *RtcB* knock-down cells. This study will increase the understanding of RtcB roles in stress response, viral infection and cell development.

Figure 4.3

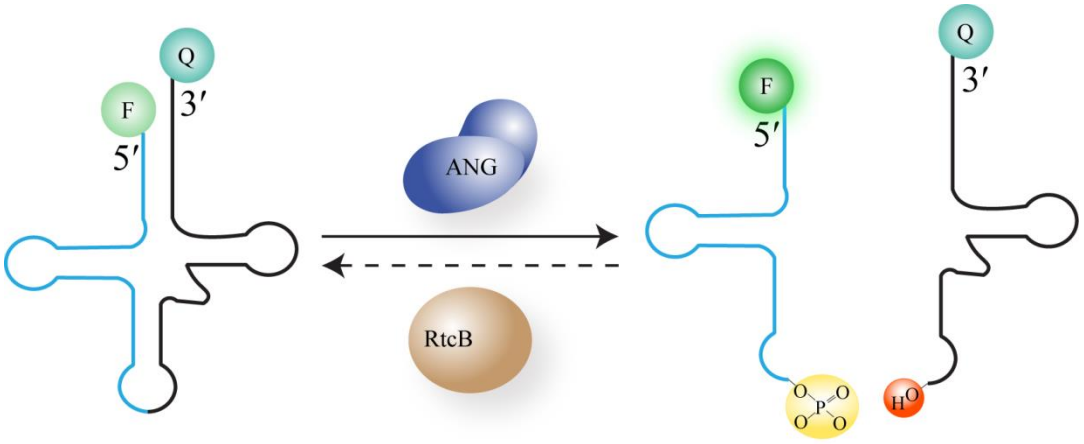

Figure 4.3 RtcB, a potential ligase of tRNA halves

A fluorogenic tRNA shall be used as a substrate for ANG and RtcB. A fluorophore and a quencher will be installed to each end of the tRNA. Upon ANG cleavage, an increase in fluorescence signal will be detected, indicating the production of tRNA halves. After using RI to quench ANG activity, the addition of RtcB will re-generate the full-length tRNA, decreasing the intensity of the fluorescence signal.

APPENDIX I

Fluorogenic Probe for Constitutive Cellular Endocytosis

Contribution: Dr. Levine and Prof. Raines designed the experiments, analyzed data and wrote the manuscript. I provided assistance in culturing human cell lines, and preparing samples for microscopy and flow cytometry.

Manuscript accepted as:

Levine, M.N, Hoang, T.T., Raines, R.T. (2013) Fluorogenic probe for constitutive cellular endocytosis. *Chemistry & Biology 20*, 614-618.

A1.1 Abstract

Endocytosis is a fundamental process of eukaryotic cells that is critical for nutrient uptake, signal transduction, and growth. We have developed a molecular probe to quantify endocytosis. The probe is a lipid conjugated to a fluorophore that is masked with an enzyme-activatable moiety known as the trimethyl lock. The probe is not fluorescent when incorporated into the plasma membrane of human cells but becomes fluorescent upon internalization into endosomes, where cellular esterases activate the trimethyl lock. Using this probe, we found that human breast cancer cells undergo constitutive endocytosis more rapidly than do matched noncancerous cells. These data reveal a possible phenotypic distinction of cancer cells that could be the basis for chemotherapeutic intervention.

A1.2 Introduction

Endocytosis is the key regulator of macromolecular internalization into eukaryotic cells.[331] In this intricate process, proteins mediate the invagination of the plasma membrane and then its fusion to pinch off a lipid bilayer-encased vesicle within a cell.[332] Many endocytic pathways operate in parallel. The most studied pathway, clathrin-mediated endocytosis, occurs constitutively in all cell types and generally involves the binding of a ligand to a receptor prior to internalization.[333] Another pathway, caveolae-mediated endocytosis, is characterized by vesicles enriched in glycosphingolipids, cholesterol, and the integral membrane protein, caveolin.[334] These endocytic pathways are the portals for delivery of essential nutrients, such as iron via transferrin and cholesterol via lipoprotein particles. Deleteriously, these pathways can facilitate the transit of pathogens.[335,336]

Endocytosis regulates the concentration of cell-surface receptors by transporting them to and from the plasma membrane.[337] Accordingly, endocytosis has a direct influence on signal transduction pathways that can malfunction in cancer patients.[338] Conversely, differences in endocytosis between cancerous and noncancerous cells could lead to new treatment options. For example, pancreatic-type ribonucleases (RNases) have emerged as putative cancer chemotherapeutic agents.[339-342] These cationic enzymes are internalized by receptor-independent endocytosis, and then escape from endosomes to the cytosol where they catalyze the degradation of cellular RNA. The basis for their cancer cell-specific toxicity is not clear, but could entail differential rates of endocytosis.

Two types of assays have been used to monitor constitutive endocytosis.[343] In one, endocytosis has been quantified by assaying the uptake of soluble enzymes, such as horseradish peroxidase.[344] Data are acquired by fixing cells, and then staining them with a colorimetric

substrate. This assay is discontinuous and vulnerable to the artifacts that can accompany the use of fixed cells.[345] Alternatively, the fate of a fluorescent lipid has been monitored continuously by microscopy.[346-350] These assays require extensive washing to remove unincorporated lipid and are not amenable to automated cell counting and sorting techniques.

We sought to develop a facile means to assess endocytosis continuously in live cells. An ideal molecular probe would have no background fluorescence, and would be able to distinguish the lumen of endosomes from the plasma membrane. We reasoned that a lipid with a headgroup that is responsive to an endosomal enzyme could serve as the basis as such a probe, as fluorescence generated over time would reflect the rate of endocytosis. Here we report on the efficacy of our strategy.

A1.3 Results and Discussion

To test our strategy, we designed lipid **1**. Lipid **1** contains a "trimethyl lock" moiety in which an acetyl ester acts as a molecular trigger.[351] This ester linkage is known to be stable to hydrolysis at physiological pH.[352-355] Although the ester linkage in lipid **1** is insulated from the fluorophore, its hydrolysis is coupled to the cleavage of its otherwise recalcitrant amide bond. Analogous probes have been used to quantify the endocytosis of soluble molecules, but not membrane-associated ones.[356-358,303,359] Our expectation here was that upon endocytosis, the headgroup of lipid **1** would encounter endosomal esterases.[360] The ensuing hydrolysis of the acetyl ester would unmask the rhodamine moiety and label the lumen with fluorescence (Figure A1.1). The modularity of lipid **1** facilitated its synthesis by a route ending with the conjugate addition of 1,2-dihexadecanoyl-*sn*-glycero-3-phosphothioethanol to a trimethyl lock–rhodamine–maleimide fragment.

The phosphatidylglycerol moiety of lipid **1** is endogenous to humans and incorporates spontaneously into cellular membranes.[361] Most importantly for us, incorporated lipid **1** paints

HeLa cells incubated at 37 °C with a punctate staining pattern, as shown in Figure A1.2A. This pattern is indicative of vesicular localization, and demonstrates that lipid **1** does indeed report on constitutive endocytosis. Notably, no fluorescence was observed in cells incubated at 4 °C (Figure A1.2B), a temperature that does not allow for endocytosis.[362]

Endocytic pathways are complex.[350] What then is the fate of lipid **1** after endocytosis? As shown in Figure A1.3A, we found that lipid **1** does not colocalize with fluorescently labeled transferrin, which is a marker of recycling endosomes.[363] Consistent with this finding, lipid **1** that had been unmasked by a cellular esterase does not reappear on the plasma membrane (Figure A1.3B). These data indicate that lipid **1** does not recycle to the plasma membrane, but instead enters endosomes and traffics to other destinations. This attribute is desirable because fluorescence from lipid **1** reports only on *new* endocytic events (and not repetitious entry). As shown in Figure A1.3C, we found that lipid **1** does colocalize partially with LysoTracker® Red, a marker of late endosomes or lysosomes, evincing its joining the canonical endosome-to-lysosome pathway along with trafficking to other subcellular compartments.[364]

Lipid **1** can report on the rate of endocytosis. HeLa cells were labeled at 4 °C with lipid **1** and then incubated for various times at 37 °C. Fluorescence was quantified by flow cytometry. As shown in Figure A1.4, the mean fluorescence per cell increases over time until ~2 h. This time course is consistent with morphological observations of mouse fibroblasts, which were seen to engulf their cell surface every 125 min.[365]

Finally, lipid **1** can reveal differences in endocytic rates between similar cells. HTB-125 and HTB-126 are noncancerous and cancerous breast cell lines that were derived from the same patient.[366] We used lipid **1** to assess endocytosis by cells in these matched lines, quantifying the results by flow cytometry. As shown in Figure A1.5, the increase in fluorescence over 3 h of

incubation at 37 °C was 2.5-fold for HTB-125 cells. This increase was less than half that for HTB-126, which was 6.0-fold. Thus, in these cell lines, endocytosis is significantly more rapid in the cancerous than in the noncancerous cells. These differential rates could reflect more rapid turnover of cell-surface receptors in cancer cells, promoting a cancerous phenotype.[367,337] We note that such an intrinsic difference in endocytic rate could provide an opportunity for therapeutic intervention by increasing the relative uptake of ptRNases or other macromolecular drugs.[368-370]

A1.4 Materials and Methods

A1.4.1 General

All reagents, unless noted, were from Aldrich Chemical (Milwaukee, WI) or Fisher Scientific (Hanover Park, IL), and were used without further purification. Thin-layer chromatography was performed by using aluminum-backed plates coated with silica gel containing F_{254} phosphor, and was visualized by UV illumination or developed with ceric ammonium molybdate stain. Flash chromatography was performed on open columns with silica gel-60 (230–400 mesh).

NMR spectra were obtained with a Bruker DMX-400 Avance spectrometer at the National Magnetic Resonance Facility at Madison (NMRFAM). Mass spectrometry was performed with an Applied Biosystems MDS SCIEX 4800 matrix-assisted laser desorption/ionization time-of-flight (MALDI–TOF) mass spectrometer at the Mass Spectrometry Facility in the Biotechnology Center, University of Wisconsin–Madison.

The term “concentrated under reduced pressure” refers to the removal of solvents and other volatile materials using a rotary evaporator at water aspirator pressure (<20 torr) while maintaining the water-bath temperature below 50 °C. The term “high vacuum” refers to vacuum (<0.1 torr) achieved by a mechanical belt-drive oil pump.

A1.4.2 Synthesis of Lipid 1

Maleimidourea–Rh_{110} trimethyl lock (20 mg, 0.026 mmol) was synthesized as described previously [353], and dissolved in anhydrous chloroform (5 mL). The resulting solution was added to a flame-dried 10-mL round-bottom flask that had been flushed with Ar(g). Anhydrous triethylamine (20 µL, 0.14 mmol) was added, followed by 1,2-dihexadecanoyl-*sn*-glycero-3-phosphothioethanol, sodium salt (Avanti Polar Lipids, Alabaster, AL; 20 mg, 0.027 mmol). The flask was covered in foil, and the reaction mixture was stirred for 3 h under Ar(g). Reaction progress was monitored by thin-layer chromatography (10% v/v methanol in DCM). Once the reaction was complete, the solvent was evaporated under reduced pressure and the residue was placed under high vacuum overnight. The crude product was purified by silica gel chromatography (10–15% v/v methanol in DCM) to yield **1** as a white powder (26 mg, 66%). ^{1}H NMR (400 MHz, $CDCl_3$) δ: 8.52 (bs, 1H), 7.94 (d, J = 6.3 Hz, 1H), 7.79 (s, 1H), 7.64–7.50 (m, 2H), 7.39 (s, 2H), 7.05 (d, J = 6.9 Hz, 1H), 6.97 (bs, 1H), 6.76 (s, 1H), 6.64–6.56 (m, 2H), 6.51 (t, J = 7.2 Hz, 2H), 6.13 (s, 1H), 5.20 (s, 1H), 4.35 (d, J = 10.8 Hz, 1H), 4.15–3.86 (m, 6H), 3.52–3.40 (m, 2H), 3.24–2.92 (m, 7H), 2.87–2.75 (m, 1H), 2.63–2.57 (m, 2H), 2.41 (s, 3H), 2.34 (s, 3H), 2.28–2.15 (m, 7H), 1.64 (s, 6H), 1.56–1.46 (m, 4H), 1.33–1.14 (m, 48H), 0.87 (t, J = 6.2 Hz, 6H) ppm. ^{13}C NMR (100 MHz, $CDCl_3$) δ: 178.5, 175.4, 174.0, 173.7, 172.1, 170.4, 170.0, 156.0, 153.0, 151.8, 151.7, 150.1, 142.5, 140.1, 139.0, 137.3, 135.4, 133.2, 133.1, 129.9, 128.3, 126.5, 125.0, 124.2, 123.5, 115.4, 114.7, 114.0, 111.6, 107.6, 106.0, 83.6, 70.6, 65.3, 63.9, 62.9, 50.9, 40.3, 39.6, 37.0, 36.5, 34.4, 34.2, 32.1, 30.2–29.2, 27.1, 26.7, 25.7, 25.1, 25.0, 22.8, 22.0, 20.3, 14.3 ppm. ^{31}P NMR (162 MHz, $CDCl_3$) δ: –1.7 ppm. MS (MALDI): m/z 1487.75 $[M+H]^+$ ($[C_{80}H_{113}O_{17}N_4NaPS]^+$ = 1487.75).

A1.4.3 Mammalian Cell Culture

HeLa, HTB-125, and HTB-126 cells were from the American Type Culture Collection (ATCC) (Manassas, VA). HeLa cells were grown in Dulbecco's Modified Eagle's Medium (DMEM) containing fetal bovine serum (FBS; 10% v/v), penicillin (100 units/mL), and streptomycin (100 µg/mL). HTB-125 cells were grown in Hybri-Care Medium supplemented with sodium bicarbonate (1.5 g/L), mouse epidermal growth factor (30 ng/mL), FBS (10% v/v), penicillin (100 units/mL), and streptomycin (100 µg/mL). HTB-126 cells were cultured in DMEM supplemented with bovine insulin (10 µg/mL), FBS (10% v/v), penicillin (100 units/mL), and streptomycin (100 µg/mL). Media and supplements were from Invitrogen (Carlsbad, CA), Sigma–Aldrich (Milwaukee, WI), or ATCC. Cells were cultured at 37 °C in a humidified incubator containing CO_2(g) (5% v/v).

A1.4.4 Microscopy

Imaging was performed with a Eclipse TE2000-U laser scanning confocal microscope from Nikon (Tokyo, Japan) equipped with a AxioCam digital camera from Carl Zeiss (Oberkochen, Germany). A blue-diode laser was used to provide excitation at 408 nm, and emission light was passed through a 35-nm band-pass filtered centered at 450 nm. An argon-ion laser was used to provide excitation at 488 nm, and emission light was passed through a 40-nm band-pass filter centered at 515 nm. A HeNe laser was used to provide excitation at 543 nm, and emission light was passed through a 75-nm band-pass filter centered at 605 nm.

HeLa cells were plated 24 h prior to experiments at a density of 1×10^5 cells in 1-cm diameter glass-bottom dishes from Electron Microscopy Sciences (Hatfield, PA) in 1 mL of medium. On the day of an experiment, all cells, media, and pipette tips were pre-cooled to 4 °C for 2 h. Next, cells were washed with serum-free DMEM (3 × 1 mL). Stock solutions of lipid **1**

(50 mM in DMSO) were diluted to 10 mM with absolute ethanol. From this stock, 1 µL was added to 500 µL of serum-free DMEM, which was then vortexed vigorously, and applied to the HeLa cells. Vehicle-treated cells were treated with 500 µL of serum-free DMEM containing 1 µL of ethanol. The labeling reaction was allowed to proceed for 3 h at 4 °C, after which, the cells were washed with serum-free DMEM (3 × 1 mL). Cells were incubated for the given amount of time at 37 °C. LysoTracker® Red (50 nM) from Invitrogen was used to stain acidic vesicles for the final 20 min of incubation at 37 °C. Endocytic marker Alexa Fluor® 594–transferrin (1 µM) from Invitrogen was used to stain recycling endosomes for the final 1 h of incubation at 37 °C. Nuclear counterstaining was performed with Hoechst 33342 (2 µg/mL) from Invitrogen for the final 5 min at 37 °C. Cells were washed with serum-free DMEM prior to imaging.

A1.4.5 Flow Cytometry

Flow cytometry was performed at the University of Wisconsin Carbone Cancer Center with a FACSCalibur instrument equipped with a 488 argon-ion air-cooled laser from Becton Dickinson (Franklin Lakes, NJ). Fluorescence emission light was passed through a 30-nm band pass filter centered at 530 nm. Cell lines were plated 24 h prior to experiments at a density of 3×10^5 HeLa cells and 3.7×10^4 cells HTB-125 or HTB-126 cells in 6 mL of medium (*vide supra*) in T-25 tissue culture flasks from BD Biosciences (San Jose, CA). On the day of an experiment, all cells, media, and pipette tips were pre-cooled to 4 °C for 2 h. Next, the cells were washed with serum-free DMEM (3 × 1 mL). Stock solutions of lipid **1** (50 mM in DMSO) were diluted with absolute ethanol to 10 mM. This stock solution in ethanol was added to serum-free DMEM to a final concentration of 20 µM, and was mixed vigorously by vortexing. The medium was removed from the cells and was replaced with 1 mL of the labeling solution. Vehicle treated cells were treated with 1 mL of serum-free DMEM containing 2 µL of ethanol. The labeling reaction was

allowed to proceed for 3 h at 4 °C, after which, the cells were washed with serum-free DMEM (3 × 1 mL). Cells were incubated for a known time at 37 °C. Cells were then washed with DPBS (1 mL; Invitrogen) and treated with trypsin/EDTA (0.25% w/v; 750 µL) for 5 min at 37 °C. The trypsin was neutralized with DMEM containing FBS (10% v/v; 750 µL), and the cells were collected by centrifugation (5 min at 400*g*). The supernatant was decanted, and the cell pellet was resuspended in 1 mL of DPBS. The cells were collected again by centrifugation (5 min at 400*g*). The supernatant was decanted, and the pellet was resuspended and fixed with 100 µL of aqueous formaldehyde (2% v/v) for 30 min in a vial covered with aluminum foil. This solution was diluted by adding DPBS to 1 mL, and the cells were collected by centrifugation (5 min at 400*g*). The supernatant was decanted, and the cell pellet was resuspended in 1 mL of DPBS. The suspension was strained through a 35-µm filter into a polystyrene flow cytometry test tube from BD Biosciences. The fixed cells were stored on ice until analyzed (~1–4 h). The mean fluorescence per cell was determined in triplicate for 10,000 HeLa cells, 2000 HTB-125 cells, and 2000 HTB-126 cells, and the data were analyzed with FlowJo software from Tree Star (Ashland, OR).

A1.5 Acknowledgments

We are grateful to M. T. Walker for assistance in assay optimization and T. F. J. Martin for the use of his confocal microscope and contributive discussions. T.T.H. was supported by a Graduate Research Scholars Advance Opportunity Fellowship and Molecular Biosciences Training Grant T32 GM07215 (NIH). This work was supported by Grants R01 CA073808 and R01 GM044783 (NIH), and made use of the National Magnetic Resonance Facility at Madison, which is supported by Grants P41 RR002301 and P41 GM066326 (NIH), and the Mass

Spectrometry Facility, which is supported by Grants P50 GM064598 and R33 DK007297 (NIH), and Grants DBI-0520825 and DBI-9977525 (NSF).

Figure A1.1

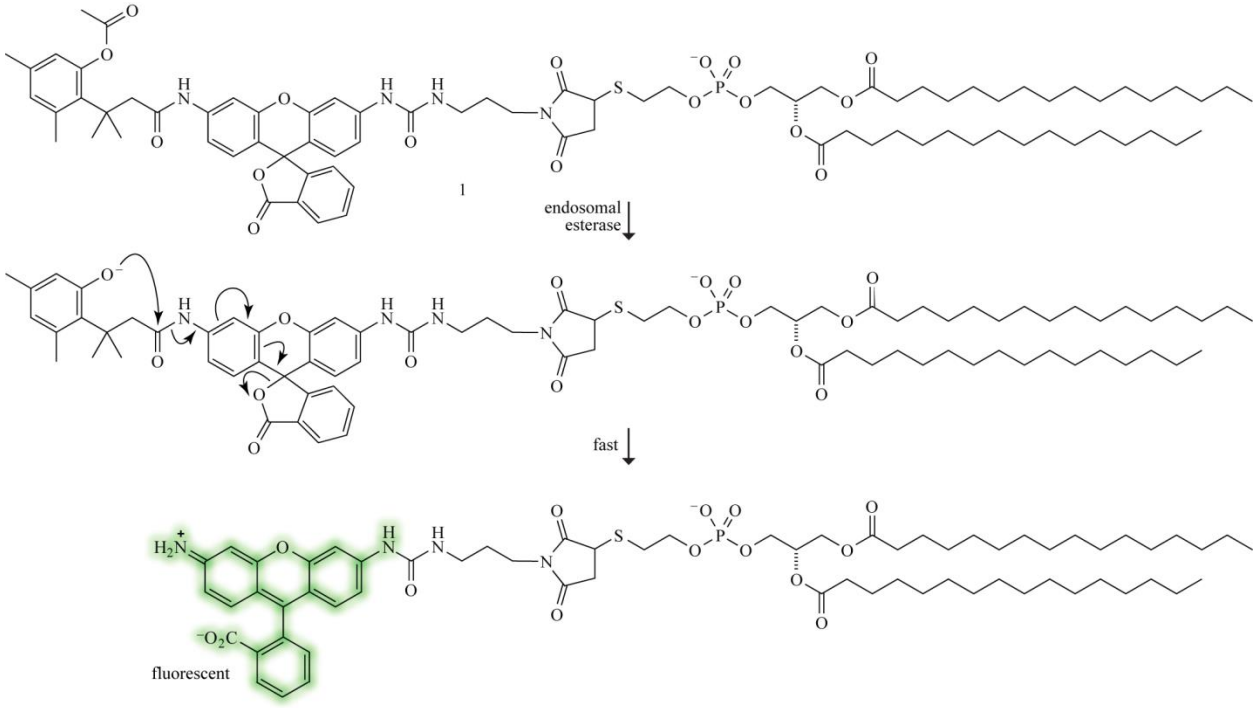

Figure A1.1 Structure and function of lipid **1**

Fluorescence is unmasked by an esterase encountered upon endocytosis.

Figure A1.2

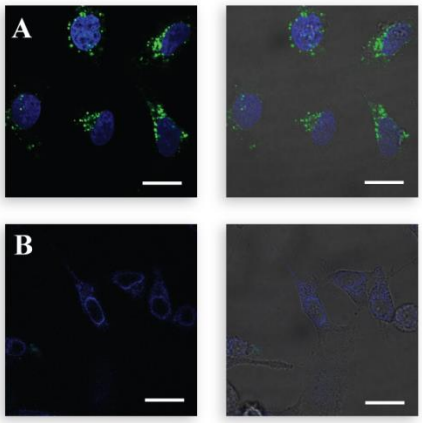

Figure A1.2 Lipid 1 reports on endocytosis

A,B HeLa cells in Dulbecco's modified Eagle's medium (DMEM) containing fetal bovine serum (FBS) were labeled for 3 h at 4 °C with lipid **1** (20 μM), washed with serum-free medium, and then incubated for 3 h at (A) 37 °C, or (B) 4 °C. Left panels, confocal images; right panels, overlay of confocal and bright-field images; blue dye, Hoechst 33342; scale bars, 20 μm.

Figure A1.3

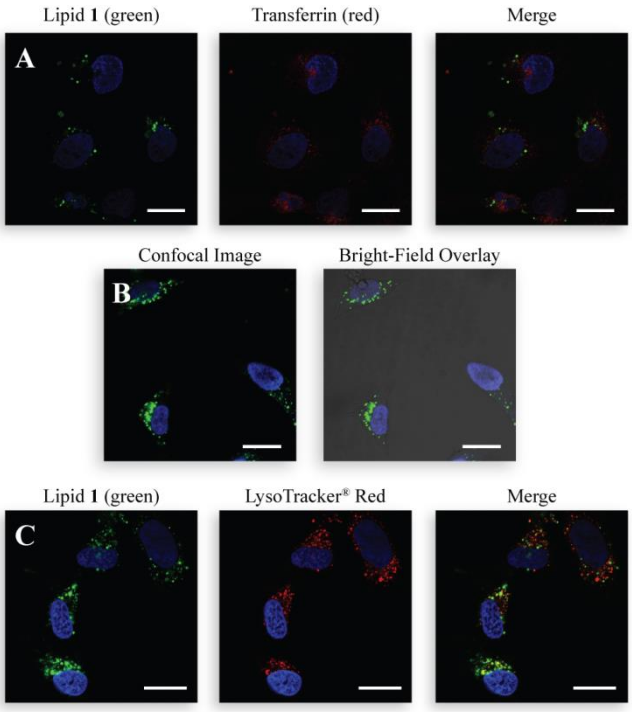
Lipid 1 (green)
Transferrin (red)
Merge
A
Confocal Image
Bright-Field Overlay
B
Lipid 1 (green)
LysoTracker® Red
Merge
C

Figure A1.3 Lipid **1** does not recycle to the cell surface

HeLa cells in DMEM containing FBS were labeled for 3 h at 4 °C with lipid **1** (20 μM), washed with serum-free medium, and then incubated for 3 h at 37 °C.

A. Image after an Alexa Fluor® 549–transferrin conjugate was added for the final 1 h of a 3-h incubation.

B. Image after a 24-h incubation.

C. Image after LysoTracker® Red (50 nM) was added for the final 20 min of a 3-h incubation. Blue, Hoechst 33342; scale bars, 20 μm.

Figure A1.4

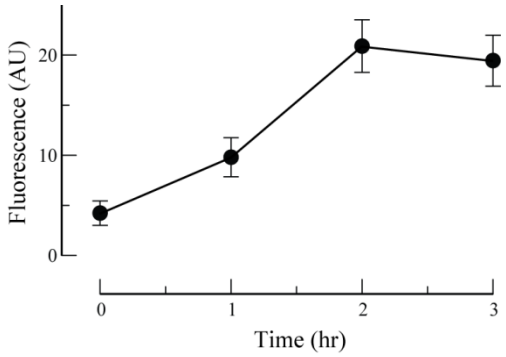

Figure A1.4 Time course of endocytosis by HeLa cells

HeLa cells in DMEM containing FBS were labeled for 3 h at 4 °C with lipid **1** (20 μM), washed with serum-free medium, and incubated for various times at 37 °C. Fluorescence was quantified by flow cytometry. Values in arbitrary units (AU) are the mean ± SD from assays of 10,000 cells.

Figure A1.5

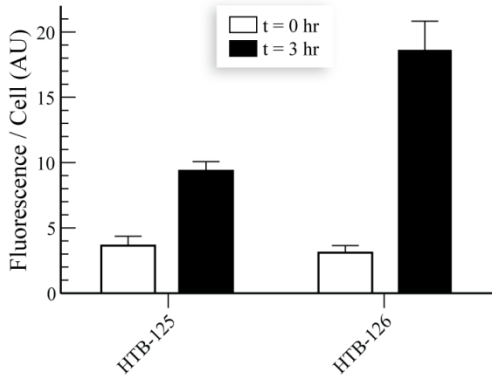

Figure A1.5 Rate of endocytosis is greater in cancerous cells

Matched breast cell lines HTB-125 (noncancerous) and HTB-126 (cancerous) in DMEM containing FBS were labeled for 3 h at 4 °C with lipid **1** (20 μM), washed with serum-free medium, and incubated for 0 or 3 h at 37 °C. Fluorescence was quantified by flow cytometry. Values are the mean ± SD from triplicate assays of 2000 cells. HTB-125 cells: 3.7 ± 0.7 and 9.4 ± 0.7 AU; HTB-126: 3.1 ± 0.6 and 18.6 ± 2.2 AU.

Figure A1.S1

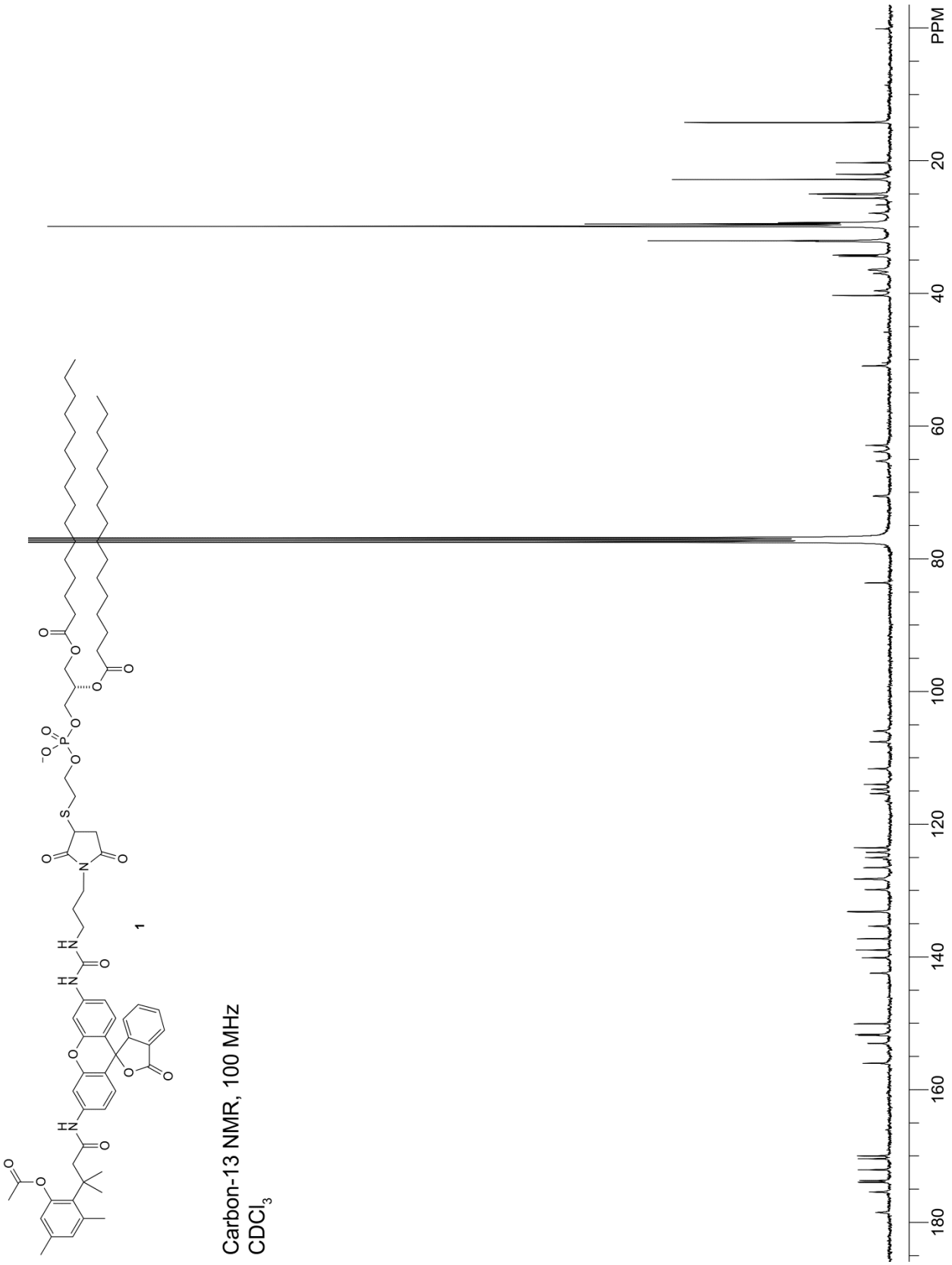

Figure A1.S1 ^{13}C NMR of lipid **1**

Figure A1.S2

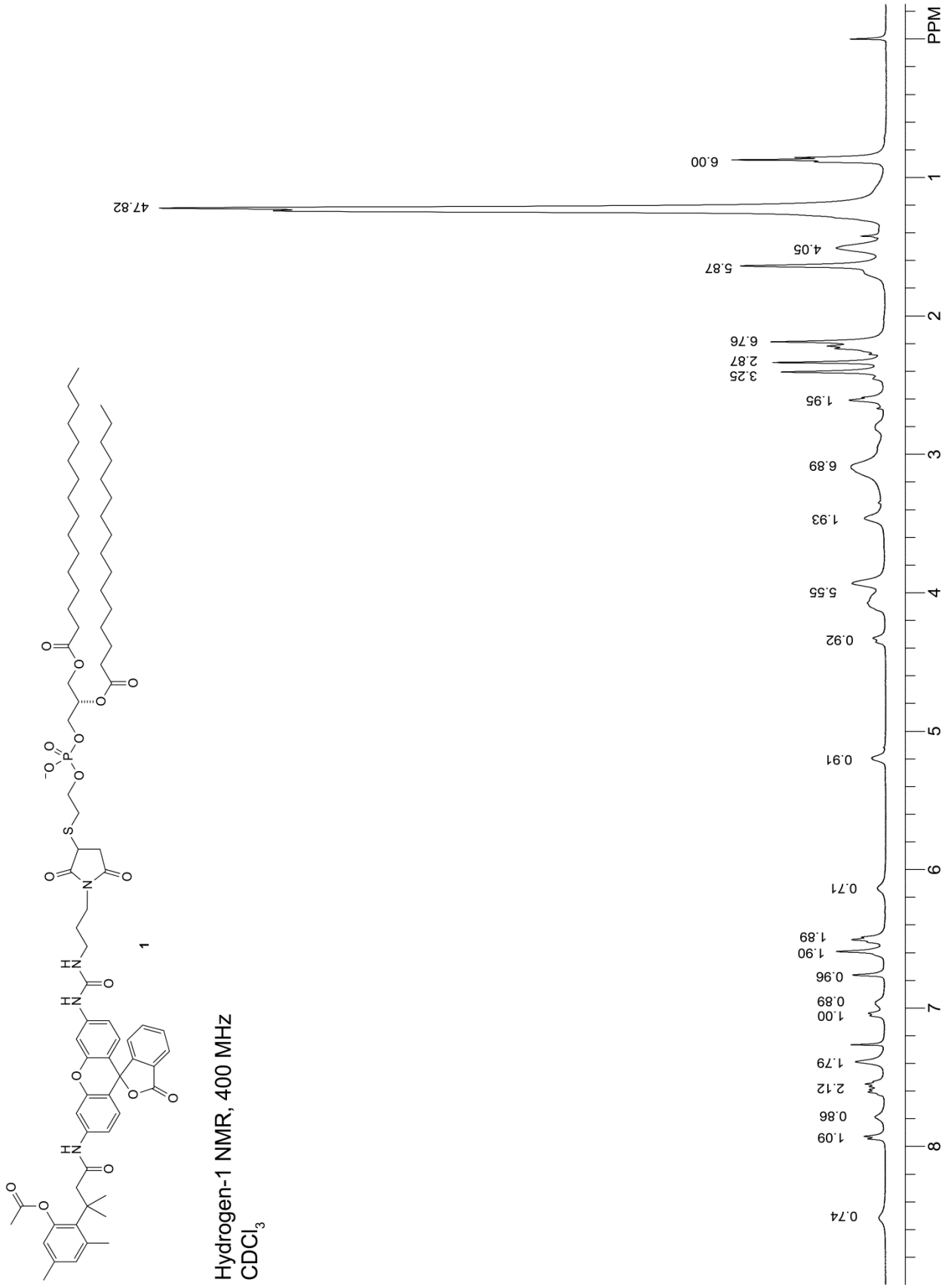
Hydrogen-1 NMR, 400 MHz
$CDCl_3$
1
PPM
0.74
1.09
0.86
2.12
1.79
1.00
0.89
0.96
1.90
1.89
0.71
0.91
5.55
0.92
1.93
6.89
1.95
3.25
2.87
6.76
5.87
4.05
47.82
6.00

Figure A1.S2 ^{1}H NMR of lipid **1**

Figure A1.S3

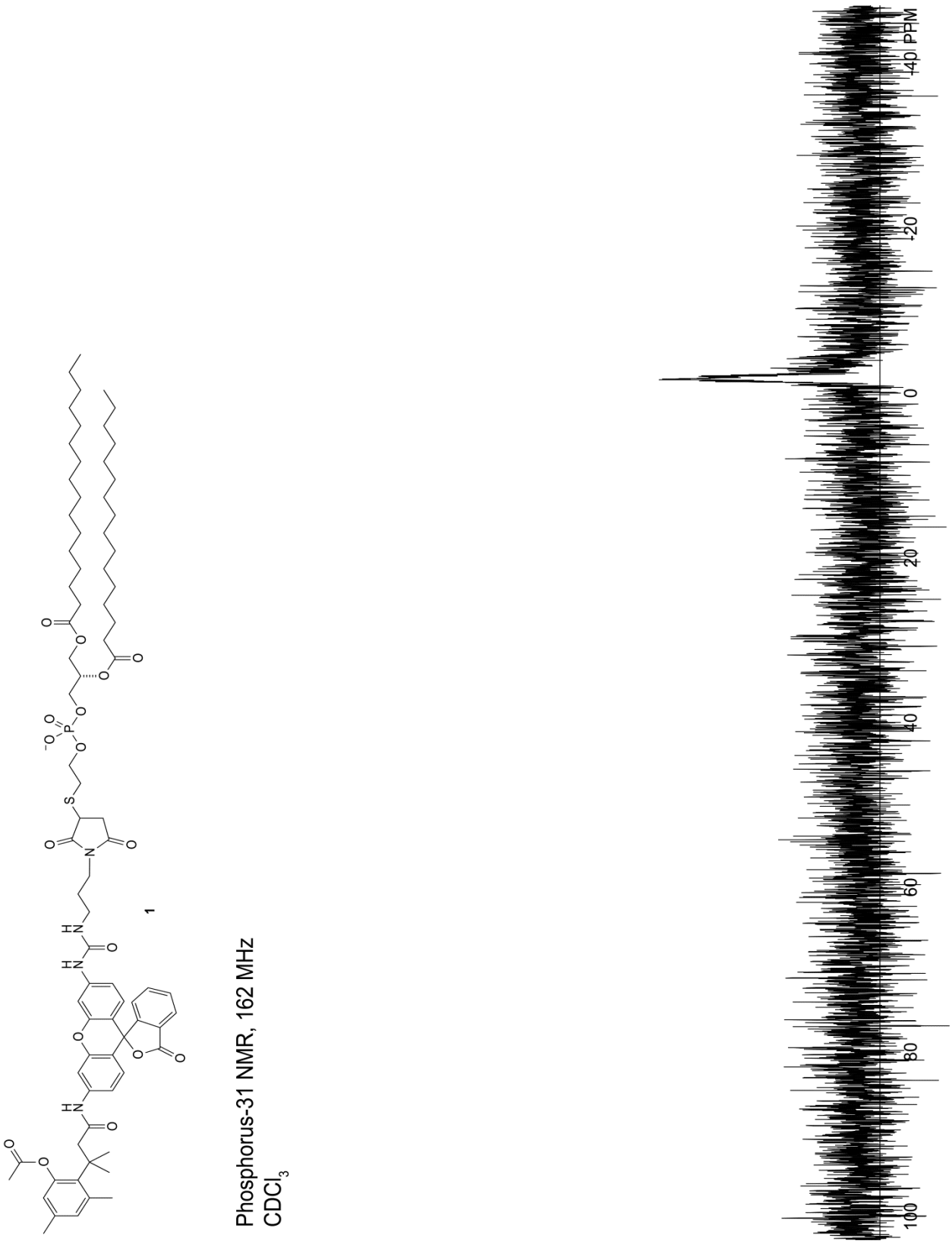

Figure A1.S3 ^{31}P NMR of lipid **1**

APPENDIX II

Phosphorylation Modulates Ribonuclease Inhibitor Sensitivity to Oxidation

Contribution: Prof. Raines and I designed the experiments and analyzed data. Quinn Vatland and Trieu Hoang performed the experiments.

Manuscript will be prepared and submitted as:

Hoang, T.T., Vatland, Q.A., Hoang, T.M., Raines, R.T. Phosphorylation Modulates Ribonuclease Inhibitor Sensitivity to Oxidation.

A2.1 Abstract

Human ribonuclease inhibitor (RI) possesses 32 Cys residues, and oxidation of these residues results in the formation of disulfide bonds that inactivate RI in a rapid and cooperative fashion. We were interested in exploring RI sensitivity to oxidation in human cells. When we overexpressed and purified biotinylated RI from HEK293T cells, the protein was highly resistant to oxidation. The level of resistance was approximately 20-fold higher than the *E.coli*-produced RI. This remarkable enhancement in RI sensitivity to oxidation inspired the idea that RI might undergo post-translational modifications in human cells. These processes are absent in *E.coli*. A particular interest in RI phosphorylation is provoked by the fact that thiol groups of Cys residues are favorably oxidized in basic condition. Appending phosphate groups on Ser, Thr, or Tyr residues neighboring to the Cys would attenuate the basicity, making the Cys less prone to oxidation. Current experiments are attempting to validate the potential of RI phosphorylation in human cells. Following validation, the phosphorylation sites of RI will be determined by mass spectrometry. These sites will be targeted to generate a phosphomimetic RI, aiming to improve the protein resistance to oxidation.

A2.2 Introduction

Ribonuclease inhibitor (RI) is a 50 kDa cytosolic protein found in all mammalian cells.[60] RI is composed of 15 leucine-rich repeats (LLRs), which form α/β horseshoe fold with an interior parallel beta sheet and an exterior array of helices.[371] RI is also rich in Cys residues that are necessarily in the reduced state to maintain the protein structure. Twenty-seven of the 32 Cys residues of human RI are conserved across mouse, porcine, and rat, which signifies that Cys residues play a role in RI functionality.[372,373] Each mammalian species carries a single *RI* gene; however, each tissue within that species has alternate splicing sites resulting formation of different RI isoforms. These alternate isoforms suggest the diverse role of RI within a single organism.

Despite tremendous effort in understanding the biological role of RI, its function is not completely understood. It has been speculative that RI acts as a "cellular sentry" by protecting the mammalian cells from the pancreatic-type ribonucleases (RNases).[62] These secretory RNases catalyze the cleavage of a phosphodiester bond on the 3' side of cytidine or uridine residues in single-stranded RNA.[232] When these enzymes enter the cell via endocytosis, a fraction of the proteins in endosome escapes into the cytosol, where it encounters a potent inhibitor, RI. The RI•RNase complex is stabilized largely by favorable Coulombic interactions, as RI is highly anionic and RNase is highly cationic.[59] The RI•RNase binding interface depicts a large contact surface from both proteins. The most important contacts reside at the C-terminal segment of RI and the active site of RNases.[374,60] Both Coulombic interactions and contacts between RI and RNase produce an exceedingly tight 1:1 complex with a femtomolar binding affinity.

RI is ubiquitously expressed in the cytosol at high micromolar concentration. Binding to RI abolishes ribonucleolytic activity of RNases.[57,59] Engineering RNases to evade RI binding

imbues them with latent cytotoxicity for human cells.[375] These RI-evasive RNase variants have been studied as possible cancer treatments. Another important function of RI is the inhibition of angiogenin (ANG), another member of the RNase superfamily. ANG is a potent inducer of angiogenesis—the process of establishing new blood vessels from pre-existing vasculature.[27] ANG is also a growth factor to promote cell proliferation and up-regulation of ANG has been associated with cancer development.[88,86,87] Several gain- and loss-of-function experiments have elucidated the roles of RI in modulating ANG function *in cellulo*. RI knockdown promotes tumor growth because the lack of RI increased the number of free ANG molecules available to facilitate cell proliferation and angiogenesis.[376,377] In contrast, an RI-evasive ANG variant that disrupts RI•ANG interaction enhanced angiogenic potency posed by ANG.[63] In addition to its biological roles and clinical relevance, RI is also a common reagent used in RNA research. To prevent degradation of RNAs *in vitro*, RI is added to guard RNAs against environmental contaminant RNases.

The efficacy of RI inhibiting RNase is affected by the stability of RI, which is primarily controlled by the state of Cys residues. All Cys residues must be in a reduced form for RI to maintain functionality.[372,373] Once these residues are oxidized to form disulfide bonds, they trigger conformational changes in the RI structure to further promote oxidation.[378] Thus, the cooperative oxidation of RI is detrimental to the protein stability and ultimately lead to proteolysis.

Several studies have attempted to generate a more stable RI by reducing its susceptibility to oxidation. A study postulated that adjacent Cys residues are responsible for initiating the cooperative oxidation of RI because these residues are more prone to form *cis*-disulfide bonds once oxidized. Substitutions of Cys328 and Cys329 with alanine residues by site-directed

mutagenesis generated an RI variant that significantly resisted oxidation while maintaining RNase affinity.[373]

While this study demonstrated a feasible approach to improve RI sensitivity to oxidation, these substitutions do not occur natively in human cells. To explore the oxidative response of RI in human cells, we overexpressed the protein with a biotin tag in HEK293T cells. After purifying the protein from streptavidin beads, the protein was then exposed to H_2O_2. Strikingly, the biotinylated RI appeared to be extremely resistant to oxidation, up to 2 M of H_2O_2. The same protein that was produced in *E.coli* could only withstand up to 100 mM of H_2O_2. This finding engenders the possibility of RI undergoing post-translational modifications in human cells. These modifications are otherwise missing in *E.coli*.

The thiol group of Cys is nucleophilic and easily oxidized. The thiol group reactivity is enhanced when the thiol is ionized, particularly in basic environment due to its pK_a of 8.37.[379] Shifting the pK_a of thiol by an introduction of anionic phosphoryl groups on neighboring Ser, Thr or Tyr residues might mitigate thiol ionization.[380] As a consequence, thiol that is proximal to negatively phosphorylated residues become less reactive to biological oxidants such as hydrogen peroxide (H_2O_2), which reacts exclusively with the thiolate anion.[381] Herein, we hypothesize that RI might undergo phosphorylation to enhance their resistance to oxidation in human cells. We were particularly interested in cysteines that localize near positively charged residues and also neighboring with potential phosphorylating residues (Figure A2.1).

My current goal is to validate the potential of RI phosphorylation in human cells using variety of biochemical methods. Once the validation is successful, phosphorylation sites of RI will be determined by mass spectrometry. These sites will be substituted with aspartate to mimic

phosphorylation state of RI. This phosphomimetic RI variant will inherit an oxidative resistant characteristics and will be overexpressed in *E.coli*.

The successful generation of a RI variant that is extremely resistant to oxidation would have industrial and biological impacts. The RI variant will hold a longer shelf life than the wild-type, which will be beneficial as a biological reagent for RNA research. Furthermore, it is very intriguing to identify kinases that are responsible to phosphorylate RI, thereby providing more insight into the regulation of RI phosphorylation in biology.

A2.3 Results

A2.3.1 Overexpression of biotinylated RI in HEK293T cells

Biotinylated RI was overexpressed in HEK293T cells. BAP-RI and BirA plasmids were co-transfected into the cells. To optimize the expression system, different ratios of Lipofectamine 3000 to DNA (BAP-RI and BirA plasmids) were tested, and the 1:1 ratio yielded the most biotinylated RI (Figure A2.2A). Next, variation in post-transfection time was examined, and all the time points-24, 48 and 72 h-produced similar RI protein level (Figure A2.2B-C). Thus, a 24 h time point was chosen for convenience.

A2.3.2 Oxidation sensitivity of biotinylated RI in cellulo and in vitro

We then interrogated the oxidation sensitivity of biotinylated RI *in cellulo*. Transfected cells were treated with increasing H_2O_2 concentration and RI protein level was evaluated by Western blot. RI appeared to be resistant to oxidation up to 1 mM of H_2O_2 (Figure A2.3A). We noted that treatment of H_2O_2 higher than 1 mM triggered cell toxicity, making the interpretation of RI level to be complicated. It was difficult to segregate if the reduction of RI level was due to oxidation or cell death.

To overcome this issue, we switched to an *in vitro* system to determine the oxidative resistance of RI in a more quantitative manner. Purified RI from streptavidin beads were challenged with increasing H_2O_2 concentrations for 30 min. It was surprising that the amount of RI was mostly unchanged up to 100 mM of H_2O_2 (Figure A2.3B). Taking a step further, we heightened the dose of H_2O_2 up to 4M and observed a significant amount of RI remained at 2 M (Figure A2.3C). The RI that was produced from *E.coli* resisted to oxidation at 100 mM H_2O_2, and rapidly degraded at concentrations of 250 mM and higher (Figure A2.3D). This phenomenon was unique to RI being produced from mammalian cells.

A2.3.3 The first generation of phosphomimetic RI responded to oxidation similarly to E.coli-derived RI

It was striking that the two expression systems produced the same RI protein, yet the protein from human cells responded to H_2O_2 at much higher tolerance. Perhaps, RI might undergo post-translational modification, a major cellular process that is distinguishable between bacteria and mammalian cells. This potential modification must weaken the reactivity of the Cys thiol group. Cys residues that are in vicinity of basic regions are particularly vulnerable to oxidation. Making these regions less basic would discourage the localized Cys residues from being oxidized. Herein, we proposed that RI might undergo phosphorylation-an introduction of anionic phosphoryl groups on Ser, Thr or Tyr residues–to perturb the local charge of nearby Cys residues. Raising the acidity in the proximal reactive thiol groups would enhance their resistance to oxidation in human cells.

We discovered that RI is phosphorylated by intracellular kinases. Incubation of RI produced from *E.coli* with a HEK293T cell lysate and [γ-^{32}P]ATP led to ^{32}P-labeled RI (Figure A2.4A). The phosphorylation sites of RI: S7, T82, S84, S91, T98, S178, S225 and S456 were reported

from mass spectrometry data from PhosphoSitePlus®(Figure A2.4B). We then generated a phosphomimetic RI (pRI) by substituting these Ser and Thr phosphorylation sites to Asp. The protein was overexpressed in *E.coli*, and its expression level was comparable to the WT (Figure A2.4C). Using RNase A affinity column to purify RI, the WT was typically eluted with 3 M of NaCl whereas the pRI variant required 3.5 M of NaCl to dissociate from the column (Figure A2.4D). This higher salt elution suggested that pRI variant interacts more tightly to RNase A than the WT.

We then asked if the pRI variant could tolerate H_2O_2 as much as the HEK293T-derived RI. The pRI was vulnerable to oxidation at 100 mM of H_2O_2, and the response was similar to *E.coli*-derived RI (Figure A2.5). This result suggested that phosphomimetic substitution is not sufficient to recapitulate the oxidative resistance of RI that was observed from mammalian cells. Perhaps, these reported phosphorylation sites require further validation.

A2.3.4 Design the second generation of phosphomimetic RI

To identify the phosphorylation sites, we attempted to isolation phosphorylated RI from the non-phosphorylated species. First, the protein was overexpressed in HEK293T cells, and the whole cell extract was exposed to H_2O_2 to promote RI phosphorylation. Next, biotinylated RI was purified using biotin-streptavidin system. We found that the treatment of H_2O_2 induced RI phosphorylation. This oxidizer caused a mobility shift of RI (lane 4), which did not occur in the untreated sample (lane 2) (Figure A2.6). The shift was reversible in the addition of phosphatase (lane 6). The mobility shift of RI was observed in both a regular SDS-PAGE and a Phos-tag™ gel (Figure A2.6). These findings suggest phosphorylation of RI under mild oxidative condition modulate RI sensitivity to oxidation. Current efforts are trying to identify phosphorylation sites of RI using mass spectrometry.

A2.4 Discussion

RI contains atypical high numbers of Cys; all of which are required to be in reduced form to maintain the protein structure and stability.[378,373] These Cys residues are natively sensitive to oxidation; thus, our initial interest was to investigate oxidation state of these Cys upon exposure to H_2O_2 *in cellulo*. To differentiate from endogenous RI, we successfully installed a biotin tag on RI and overexpressed it in HEK293T cells. We then probed the level of biotinylated RI in response to increasing doses of H_2O_2. The result was difficult to interpret because the decrease of RI level could be derived from oxidation consequence or H_2O_2-mediated cell toxicity. This prompted us to switch to an *in vitro* system at which the amount of biotinylated RI that are susceptible to H_2O_2 can be properly quantified.

Using the *in vitro* assay, we found an astonishing result that the HEK293T-derived RI was greatly resistant to oxidation, up to 2 M of H_2O_2 (Figure A2.3). The level of resistance is approximately 20-fold higher than the *E.coli*-derived RI. Given that the major difference between an eukaryotic expression system and a prokaryotic expression system is post-translational modification, we postulated that the enhanced oxidative resistance of HEK293T-derived RI is mediated by protein phosphorylation. Therefore, we attempted to make the pRI that would markedly resist to oxidation to the same level as those produced in human cells. The production of pRI was accomplished in *E.coli*, and the protein exhibited higher affinity to RNase A than the WT (Figure A2.4). When exposing the proteins to H_2O_2, pRI yielded the same response as the RI being produced from bacteria (Figure A2.5).

Nevertheless, this discouraging result could be explained by the two following reasons. First, the generation of pRI was based on phosphorylation sites reported from PhosphoSitePlus®.[382] The website provides comprehensive coverage of protein phosphorylation that is integrated from

both low- and high-throughput data sources. Yet, these reported phosphorylation sites often require experimental validations tailored to a particular protein of interest. Second, aspartate substitution to mimic phosphorylation might not achieve the same negative charges and steric hindrance imposed by actual phosphorylation of these residues.

We found that RI is phosphorylated *in vitro* using HeLa cell extract (Figure A2.4A). We further observed the mobility shift of RI that is reversible in the phosphatase treatment (Figure A2.6). Together, these findings strongly suggest that RI undergoes phosphorylation to enhance its susceptibility to oxidation. We are currently trying to identify phosphorylation sites by mass spectrometry. Furthermore, we are also interested in identifying kinases that are responsible to phosphorylate RI, thereby providing more insight into the regulation of RI phosphorylation in biology. Taken together, our results hold special promise toward development of oxidative resistant RI variant. This variant could have vast utility as a commercial anti-RNase agent, as well as aid in understanding the fundamental biological roles of RI in human cells.

A2.5 Materials and Methods

A2.5.1 Cloning of WT RI and BirA into pNeo3 vector and pRI into pET22b

An open reading frame for the full-length cDNA of wild-type RI (WT) was a generous gift from Promega Corp. DNA encoding for a biotin-acceptor-peptide (BAP) with a linker was designed to install into the N-terminus of WT RI. The PCR amplified BAP-WT gene was subsequently cloned into pNeo3 vector via Gibson Assembly. Briefly, 50 ng of the insert and 50 ng of the linearized vector were added into 2X Gibson Assembly Mastermix. The reaction was incubated at 50°C for 1 hour. A 3µL Gibson reaction was transformed into 50 µL of XL10 competent cells. Eight colonies were chosen for DNA isolation and sequencing. The DNA sequencing was performed by DNA sequencing facility at UW-Madison. Correct BAP-RI plasmid was

transformed into DH5α for large scale production of DNA using *GenCatch* Endotoxin-Free Maxiprep kit.

An open reading frame of the full-length cDNA of biotin ligase (BirA) was a generous gift from Prof. Marv Wickens (UW-Madison). A gene fragment containing phosphomimetic mutations of RI (pRI) where Ser and Thr residues (S7, T82, S84, S91, T98, S178, S225, S456) were mutated to Asp was obtained from IDT. The cloning of BirA to pNeo3 and pRI to pET22b were performed as described previously.

A2.5.2 HEK293T transfection

HEK293T cells were grown in Dulbecco's Modified Eagle's Medium (DMEM) containing fetal bovine serum (FBS) (10%) and penicillin/streptomycin (Pen/Strep) (1%) (Invitrogen) at 37˚C under 5% (v/v) CO_2 (g). Cells were plated in complete medium in 6-well or 10-cm dishes at a density of 200 cells/μL. After 24h, cells were transfected with BirA and BAP-RI plasmids using Lipofectamine 3000 (Invitrogen). One hour later, biotin (1μM) was added to transfected cells, and then cells were further incubated for another 24 hours prior to harvest.

A2.5.3 Biotinylated RI purification from HEK293T

HEK293T cells were lysed in lysis buffer (M-PER Mammalian Extraction Protein Reagent (Thermo) containing 1 mM DTT and 1X protease inhibitor cocktail (Thermo)). The cell lysis carried at 4˚C for 20 min. Clarified lysate was collected after centrifugation at max speed for 30 min at 4˚C. The lysate was then incubated with prepared streptavidin beads overnight at 4˚C with rotation. The beads were washed twice with lysis buffer. Biotinylated proteins were eluted from the beads using 1X SDS loading dye with the addition of β-ME and boiling at 95˚C for 5 min. The purified proteins were subjected to SDS-PAGE to evaluate the protein purity.

A2.5.4 Phosphomimetic RI expression and purification from E.coli

WT RI or pRI in pET22b was transformed into KRX strain (Promega) for protein expression. The overnight culture of *E. coli* KRX strain harboring the plasmids for expression of WT or pRI was inoculated into 6 L of Terrific Broth containing ampicillin (100 µg/mL). The cultures were grown at 37˚C with shaking until cells reached an OD of 1.7. Protein expression was then induced with 1 mM IPTG and 0.1% L-Rhamnose and shaken at 18˚C for at least 16 h.

Cell pellets from every 2 L culture were resuspended in 30 mL lysis buffer (100 mM Tris, 100 mM NaCl, 0.5 mM EDTA, 0.1 mM PMSF, 10 mM DTT, pH 7.5). The cells were lysed using a TS Cell Disruptor (Constant System) at 22 kPsi. The lysate was clarified by centrifugation at 18,000 rpm for 60 minutes. The clarified lysate was collected and filtered through 5 µm PVDF filter. The filtered lysate was applied to 5 mL RNase A affinity column which was pre-equilibrated with buffer A (50 mM KH_2PO_4, 10 mM DTT, 1 mM EDTA, pH 6.4). The column was washed with buffer A until $A_{280\ nm}$ reached 0. Then, weakly bound proteins were removed by washing the column with buffer B (50 mM KH_2PO_4, 10 mM DTT, 1 mM EDTA, 1 M NaCl, pH 6.4). Tightly bound proteins were eluted with buffer C (100 mM NaOAc pH 5.0, 10 mM DTT, 1 mM EDTA, 3 M NaCl, pH 6.4).

Protein fractions from buffer C elution were pooled together and then dialyzed overnight at 4˚C in HiTrap Q buffer A. Next day, the dialyzed protein was applied to a 5 mL HiTrap Q HP column which was pre-equilibrated with HiTrap Q buffer A (20 mM Tris HCl, 1 mM EDTA, 10 mM DTT, pH 7.5). The column was washed with buffer A until $A_{280\ nm}$ reached 0. Bound RI was eluted with HiTrap Q buffer B (20 mM Tris HCl, 1 mM EDTA, 10 mM DTT, 1 M NaCl pH 7.5).

A2.5.5 H_2O_2 Treatment in cellulo and in vitro

Twenty four hours post-transfection, cells were replaced with fresh complete media. Next, they were treated with increasing concentrations of H_2O_2 for 3 h. Cell were then washed with PBS and further lyzed to collect proteins for Western Blot analysis.

During the purification of biotinylated RI, prior to protein elution, the proteins were incubated with increasing H_2O_2 concentration for 30 min at room temperature. The beads were washed with lysis buffer. Protein elution was performed using 1X SDS loading dye with the addition of β-ME and boiling at 95˚C for 5 min. The eluted proteins were subjected to SDS-PAGE and further analyzed by Western blot using α-biotin (Cell Signaling) or α-RI (Santa Cruz) antibodies. The intensity of RI band was analyzed using ImageQuant software.

Figure A2.1

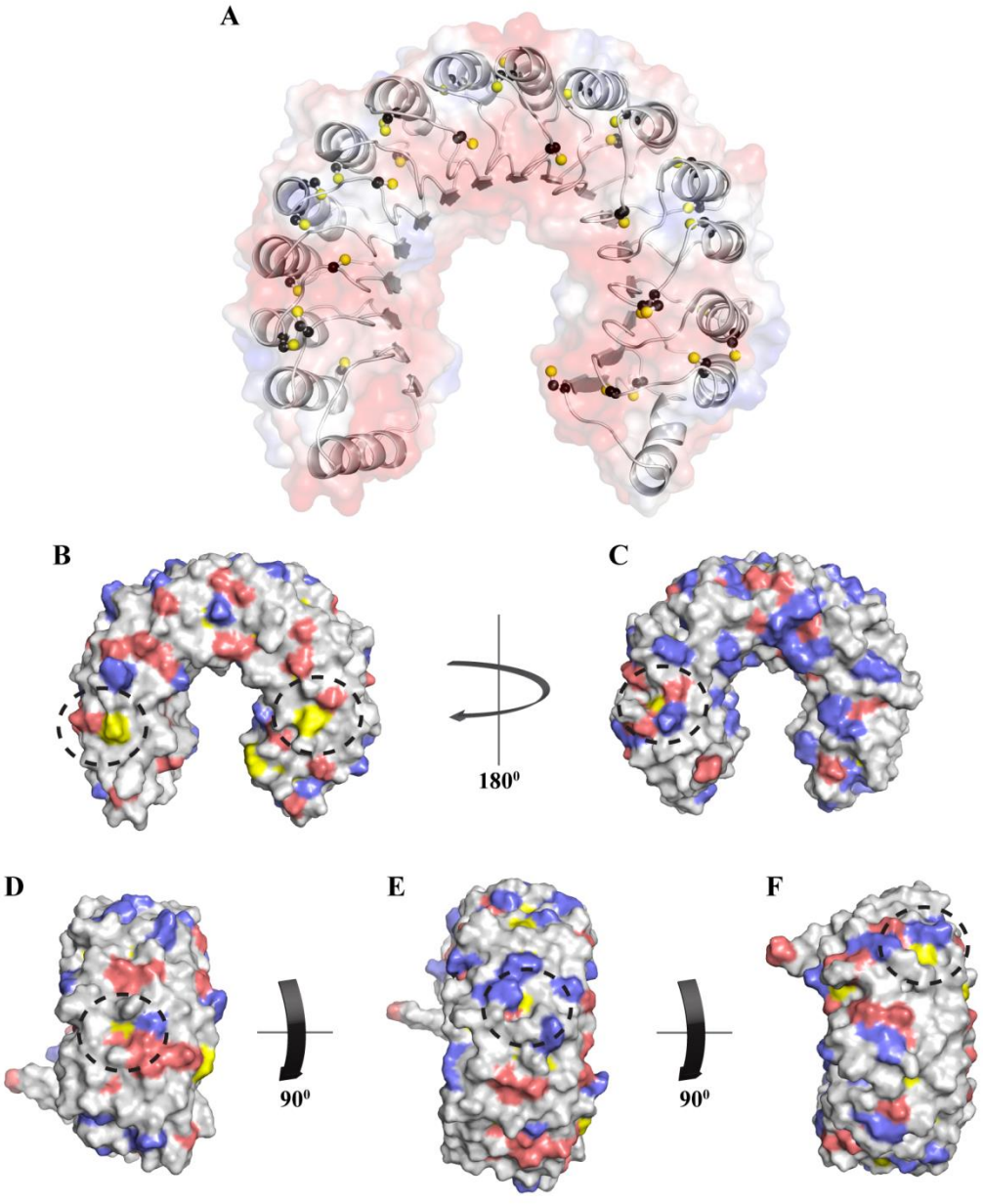

Figure A2.1 Structure of human RI

A. The Coulombic surface of RI is depicted with negative and positive indicated by red and blue, respectively (PDP entry 1a4y). RI is in grey ribbon and 32 Cys residues are depicted in ball-and stick.

B-F RI represents in grey surface. Positive charged residues (Lys and Arg) are in blue, Cys residues are in yellow, and potential phosphorylation sites (Ser and Thr) are in red. We circled clusters of Cys residues of our interest. These Cys residues locate in basic regions with Ser or Thr in vicinity.

Figure A2.2

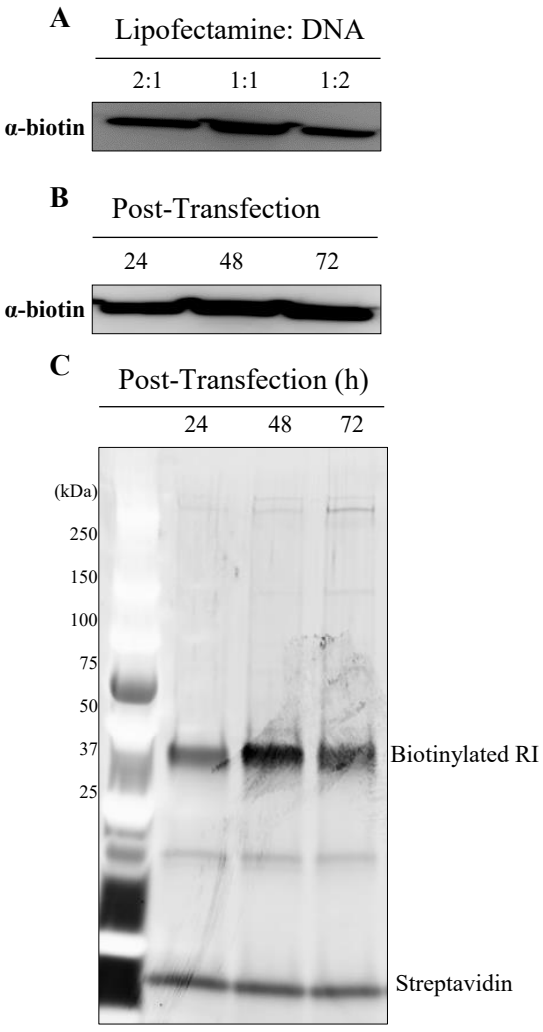
A
Lipofectamine: DNA
2:1
1:1
1:2
α-biotin
B
Post-Transfection
24
48
72
α-biotin
C
Post-Transfection (h)
24
48
72
(kDa)
250
150
100
75
50
37
25
Biotinylated RI
Streptavidin

Figure A2.2 Expression and purification of biotinylated RI in HEK293T cells

A,B Optimization of biotinylated RI expression in HEK293T cells

C. Biotinylated RI was successfully purified using streptavidin affinity beads.

Figure A2.3

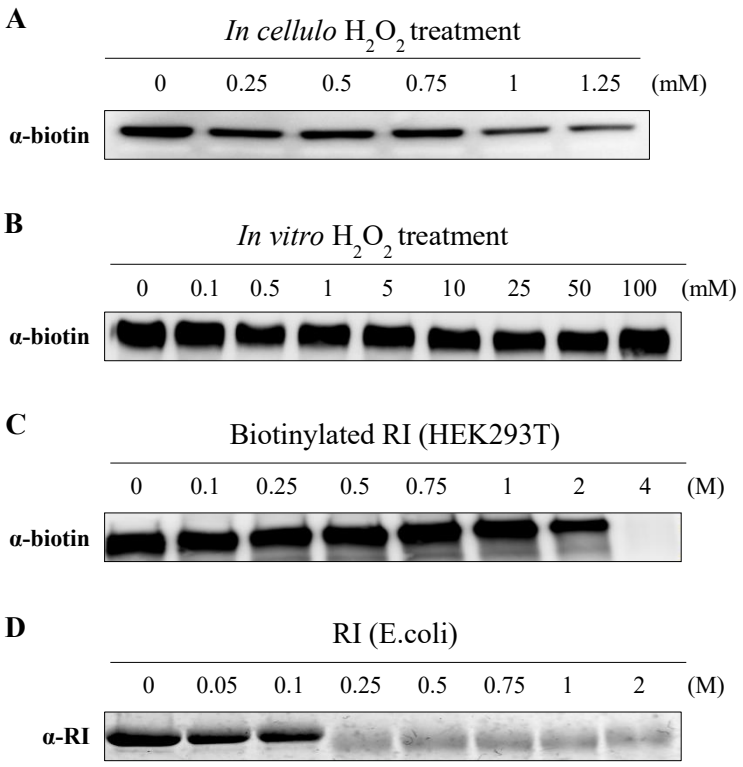
A
In cellulo H_2O_2 treatment
0 0.25 0.5 0.75 1 1.25 (mM)
α-biotin
B
In vitro H_2O_2 treatment
0 0.1 0.5 1 5 10 25 50 100 (mM)
α-biotin
C
Biotinylated RI (HEK293T)
0 0.1 0.25 0.5 0.75 1 2 4 (M)
α-biotin
D
RI (E.coli)
0 0.05 0.1 0.25 0.5 0.75 1 2 (M)
α-RI

Figure A2.3 Susceptibility of RI to oxidation *in cellulo* and *in vitro*

A. HEK293T cells were transfected with DNA encoding for BAP-RI and BirA and incubated for 24 h at 37 °C. Next, cells were treated with increasing concentration of H_2O_2 for 3 h and then lyzed for total proteins collection. The proteins are subjected for SDS-PAGE followed by Western blot. Biotinylated RI was detected using α-biotin antibody, and its level began to degrade at 1 mM of H_2O_2.

B,C After expressing and purifying biotinylated RI from HEK293T cells, the protein was exposed to H_2O_2 varied from 0 to 4 M. Interestingly, HEK293T-derived RI extremely resisted to oxidation, up to 2 M of H_2O_2.

D. *E.coli*-produced RI was vulnerable to oxidation starting at 100 mM of H_2O_2.

Figure A2.4

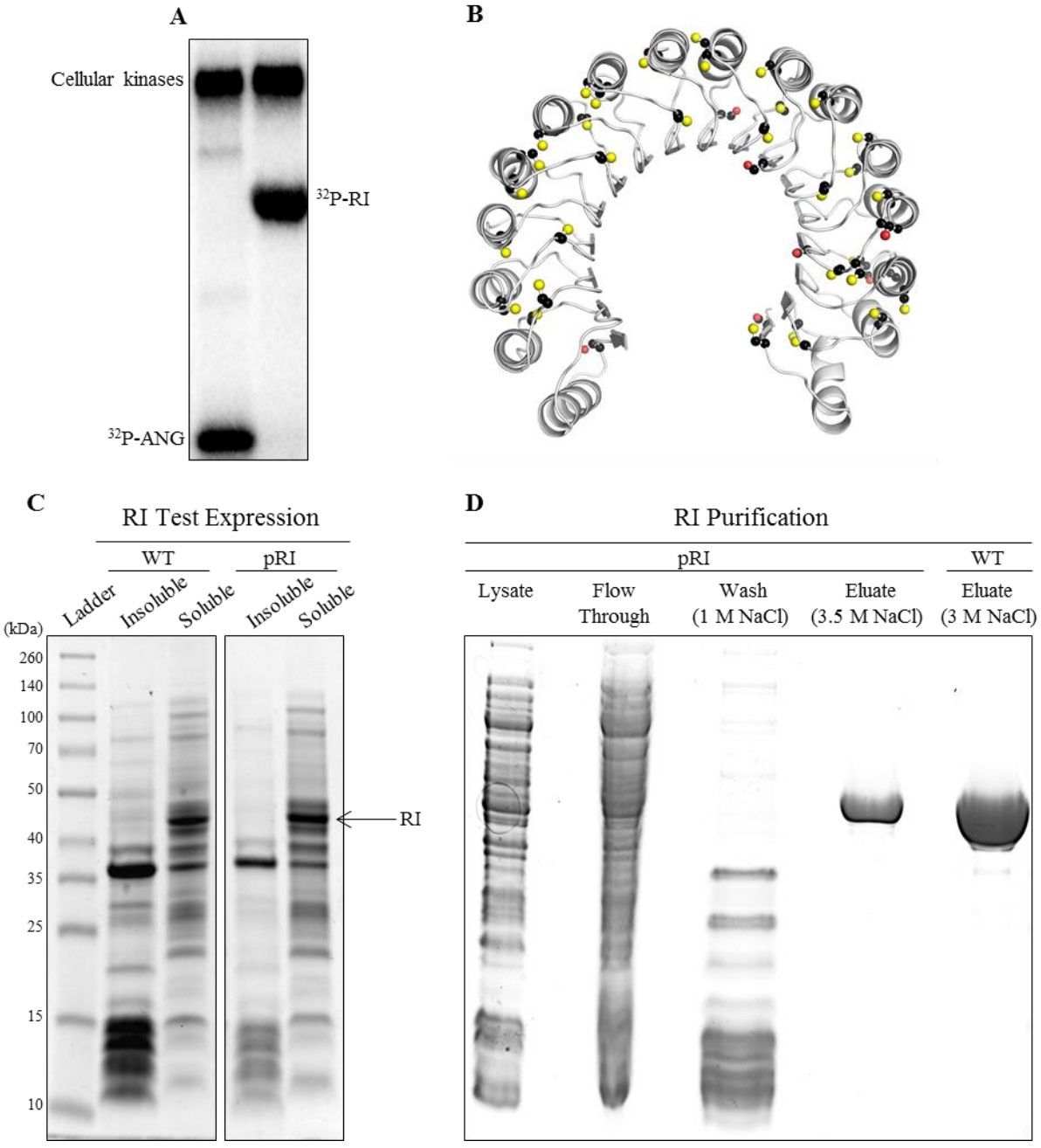
A
Cellular kinases
32P-RI
32P-ANG
B
C
RI Test Expression
WT
pRI
Ladder
Insoluble
Soluble
Insoluble
Soluble
(kDa)
260
140
100
70
50
40
35
25
15
10
RI
D
RI Purification
pRI
WT
Lysate
Flow Through
Wash (1 M NaCl)
Eluate (3.5 M NaCl)
Eluate (3 M NaCl)

Figure A2.4 Rationale and design of the first generation of pRI

A. Autoradiogram of a polyacrylamide gel demonstrating that RI is phosphorylated upon incubation with a HeLa cell lysate and [γ-^{32}P]ATP. ANG serves as a positive control.

B. Structure of the human RI (PDB entry 1a4y). Putative phosphorylation sites and cysteine residues in RI (grey ribbon) are labeled in red and yellow respectively and depicted in ball-and-stick.

C. Serine and threonine of RI were substituted with aspartate to mimic phosphorylation. DNA encoding for phosphomimetic RI (pRI) was overexpressed in *E.coli*. The expression level of pRI was comparable to that of the WT.

D. pRI was purified using RNase A affinity chromatography. We found that pRI requires 3.5 M NaCl to elute from RNase A column while the WT only needs 3 M of salt.

Figure A2.5

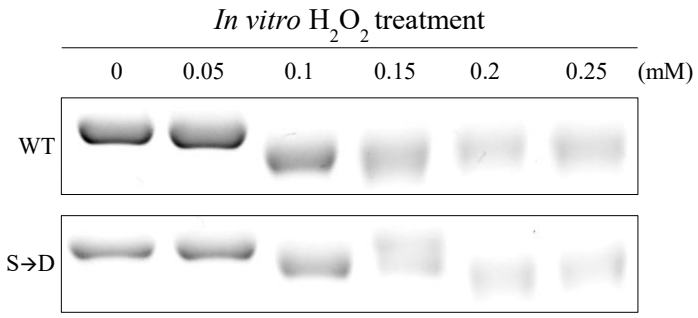

Figure A2.5 pRI resisted to oxidation similarly to *E.coli*-produced RI

Wild-type RI and pRI were produced from *E.coli*. Pure proteins were subjected to H_2O_2 in increasing concentrations. Both proteins responded to the oxidant at comparable levels.

Figure A2.6

Lane #	1	2	3	4	5	6
Protease Inhibitors	+	+	+	+	+	+
Phosphatase Inhibitors	−	+	−	+	−	−
H_2O_2	−	−	+	+	−	+
Phosphatase	−	−	−	−	+	+

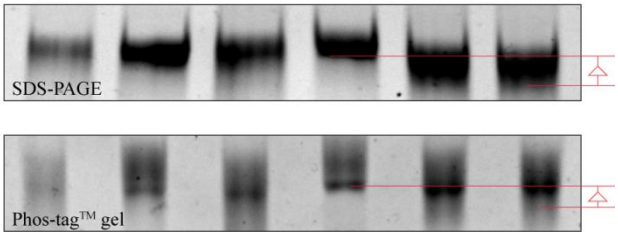

Figure A2.6 Isolation of phosphorylated RI that are produced from HEK293T cells

DNA encoding for biotinylated RI was transfected to HEK293T cells. The transfected cells were lyzed and treated as indicated. Treatment of H_2O_2 (100 mM) was carried at room temperature for 30 min. Next, addition of lambda protein phosphatase (400 U) was performed at room temperature with 15-min incubation. The lysates were further subjected to streptavidin magnetic beads for purification. Pure and biotinylated RI was resolved on a regular SDS-PAGE and a Phos-tag^{TM} gel. We observed a mobility shift of RI that was treated with H_2O_2, and the shift was reversible in the addition of phosphatase (lane 4 versus lane 6). The finding suggests RI undergoes phosphorylation under mild oxidative condition.

APPENDIX III

Globo H and SSEA-4 as Biomarkers for a Ribonuclease Drug

Contribution: Prof. Raines and I designed the experiments and analyzed data. Qiao Li assisted with flow cytometry experiment. Valerie Ressler provided RNase 1.

A manuscript will be prepared and published as:

Hoang, T.T., Li, Q., Ressler, V., Kiessling, L.L., Raines, R.T. Globo H and SSEA-4 as Biomarkers for a Ribonuclease Drug.

A3.1 Rationale

Pancreatic-type ribonucleases (RNases) are a highly conserved family of small, cationic, secretory enzymes that catalyze the cleavage of RNA.[232,342] Interestingly, the human RNase 1 and the bovine RNase A have their innate ability to kill cancer cells selectively.[383,384,375,385] The putative pathway of RNase-mediated cytotoxicity involves cellular entry via endocytosis, endosomal translocation into the cytosol, and cleavage of cellular RNAs, which leads to apoptosis. A variant of RNase 1, QBI-139, is undergoing Phase I clinical trials as a cancer chemotherapeutic agent.[309,310]

Tremendous efforts have elucidated the underlying mechanism of which RNases selectively internalize to cancer cells. Cancer cells often up-regulate glycosaminoglycan profile, phospholipid composition, or glycosphingolipid exposure, making their surface more anionic than those of corresponding normal cells.[386] The anionic cell surface moieties attract cationic RNases for binding, and the protein subsequent internalization.[385,387] In fact, cellular entry of RNase A has been demonstrated to be in a nonsaturable, non-receptor mediated manner.[388] It occurs through both clathrin-coated vesicles and macro-pinocytosis. Further, reducing the negative charge on a cell surface by depriving the biosynthesis of heparan sulfate and chondroitin sulfate decreases a net internalization of RNase A.[387] Together, these data emphasize the importance of favorable Coulombic interactions between cell surface glycans and RNases for the protein preferential entry to cancer cell.

In addition to charges, RNases also interact with a neutral cell surface glycan, Globo H. Our recent work has reported that the interaction of RNase 1 and Globo H mediates the protein internalization and contributes to the efficacy of RNase 1 to kill cancer cells.[304] Globo H is a neutral hexosaccharide glycosphingolipid. It belongs to Globo-series glycans. Two notable

hexasaccharide members of this family are stage-specific embryonic antigen-4 (SSEA-4) and Globo H. These glycans share a common precursor, SSEA-3 (Galβ3GalNAcβ3Galα4Galβ4Glc), but vary in the terminal monosaccharide: β3-linked N-acetylneuraminic acid for SSEA-4 and α2-linked L-fucose for Globo H.[389] Typically, these glycans are retained on the plasma membrane and cluster into lipid rafts. Importantly, expression changes in these glycans are observed throughout differentiation and during tumorigenesis.[390,391] High expression of Globo H has been reportedly associated with variety of cancer types, e.g. non-small cell lung, breast, prostate, lung, pancreas, gastric, ovarian, and endometrial tissues.[392] The up-regulation of Globo H on surface of cancer cells majorly contributes to selectivity of RNases entry to those cells.[304] To pinpoint the contributions of charges and Globo H interaction in RNases-mediated toxicity, we explored the correlation of these two factors to cellular toxicity mediated by the ribonuclease drug, QBI-139.

A3.2 Results

As cell-surface Globo-series glycans have been implicated as cancer-cell antigens, we first sought to determine if these glycans are differentially expressed on cancer cells compared to normal cells. We used 4 different lung cell lines and measured the abundance of both SSEA-4 and Globo H expressed on the surface of each cell line. We compared the non-small cell lung cancer (NSCLC) lines H460, H1299, and H520 to the normal fibroblast cell line WI-38. We fluorescently labeled the glycans using their specific antibodies and quantified the fluorescence intensity by flow cytometry. We found that the overall expression level of these glycans on the cancer cells was higher than that of the non-cancerous fibroblast line WI-38 (Figure A3.1). Notably, these glycans were significantly elevated on the cancerous H1299 and H460 cells, with

3-fold to 4-fold increases of SSEA-4 and Globo H, respectively, relative to that of the WI-38 cells.

To evaluate the toxicity of chemotherapeutic reagent–cisplatin and ribonuclease drug–QBI-139, we measured the effect of each drug on viability of these lung cells. Similar trends in cytotoxicity of the two drugs were observed: H520 cells were the most resistant while H460 cells were the most vulnerable to the drugs (Figure A3.2). Cisplatin treatment was 3-fold more cytotoxic to H1299 cells compared to WI-38 cells (Table A3.1). The potency toward the two cell lines was further enhanced by QBI-139 treatment with 11-fold more cytotoxic to H1299 cells (Table A3.1). These results suggest that the mechanism of cytotoxicity mediated by QBI-139 is more selective than that of cisplatin.

Cancer cells frequently have more anionic surfaces than do their non-cancerous counterparts. To characterize further the relationship between the anionicity of the cell surface and tumorigenicity, we determined the relative cell-surface charge of the normal and NSCLC cells from their electrophoretic mobility (μ). All measured mobility values were converted into the zeta potential (ζ) using the Smoluchowski formula, which is correlated with the surface charge density by a form of the Gouy-Chapman equation.[393] The ζ values for each cell line were provided in Table A3.2. As anticipated, the non-transformed WI-38 cells displayed the lowest surface charge density (the least negative ζ value), followed by H520, H1299 and then H460 cells.

Thus far, we reported the significant elevations in cancer-associated carbohydrate levels and anionicity on cell surface of NSCLC cells. Next, we sought to determine if these elevations are responsible for the toxicity mediated by the ribonuclease drug. We found that the abundance of the biomarkers, Globo H and SSEA-4, and the cell surface anionicity were correlated with

cytotoxicity of QBI-139 (Figure A3.3). The cell lines that owned more of these biomarkers and more negatively charge on the cell surface were more sensitive to treatment with QBI-139. Similar to QBI-139, cytotoxicity of cisplatin displayed correlation to the zeta potential and amount of glycan biomarkers. The slopes of correlation lines associated with QBI-139 treatment appeared to be shallower than that of cisplatin treatment. The trends suggest QBI-139 treatment offers larger therapeutic window than cisplatin treatment, allowing a broader range of the ribonuclease drug dosages which can treat NSCLS effectively without having toxic effects.

Figure A3.1

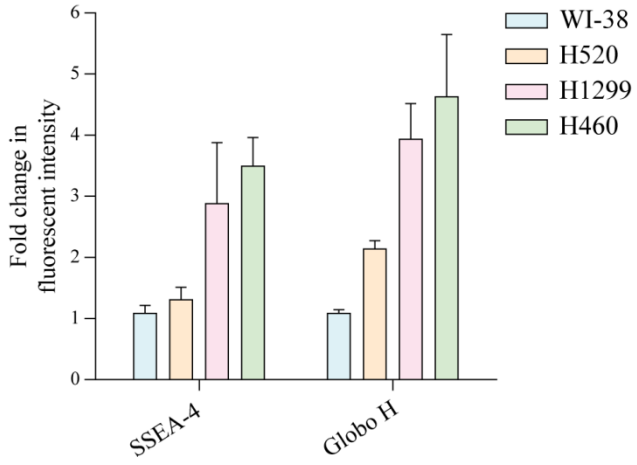
Fold change in fluorescent intensity
0
1
2
3
4
5
6
SSEA-4
Globo H
WI-38
H520
H1299
H460

Figure A3.1 Up-regulation of SSEA-4 and Globo H expressions on non-small cell lung cancer (NSCLC) surfaces

Graph showing that NSCLC cells have higher expression levels of Globo H and SSEA-4 than WI-38 cells. Among the NSCLC cells, H1299 and H460 cells remarkably increased these glycan quantities by 3-fold of SSEA-4 and 4-fold of Globo H comparing to WI-38 cells.

Figure A3.2

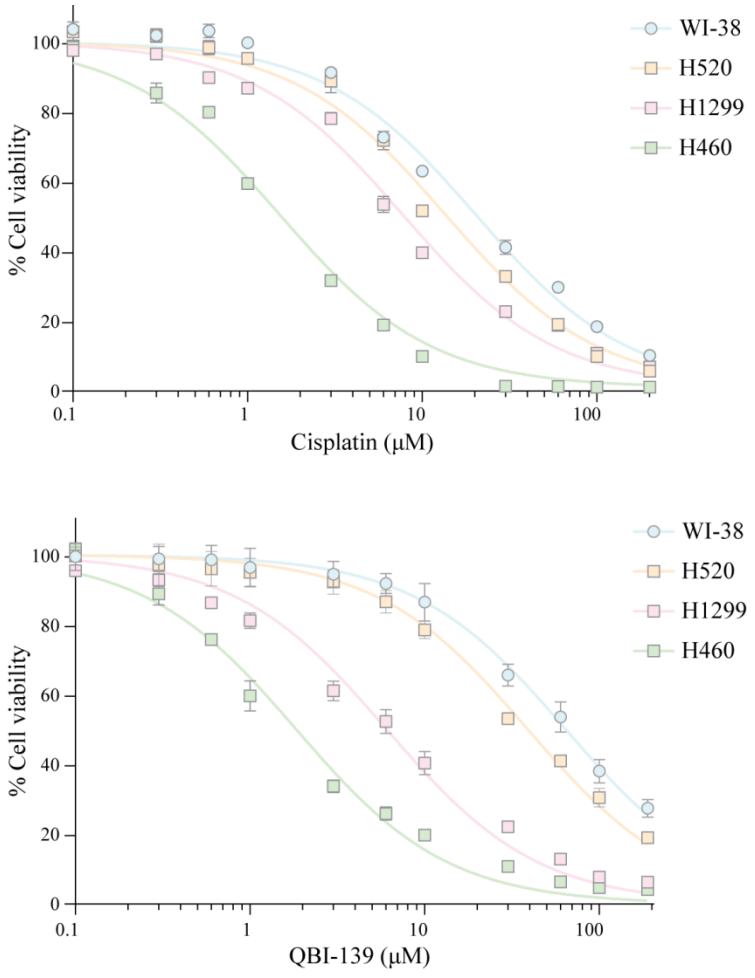

Figure A3.2 Cytotoxicity of cisplatin and QBI-139 toward lung cells

Lung cells were treated with chemotherapeutic agent–cisplatin and ribonuclease drug–QBI-139 at increasing concentrations for 48 hours, after which the cytotoxicity of these agents was evaluated on the basis of proliferation. H460 cells were the most vulnerable to treatment with both agents, while A549 cells were the least vulnerable. Yet, other cells displayed variable susceptibility to these treatments. Cisplatin displayed 3-fold more potency to H1299 cells compared to WI-38 cells. In contrast, QBI-139 exhibited 11-fold more potency towards H1299 cells compared to WI-38 cells.

Figure A3.3

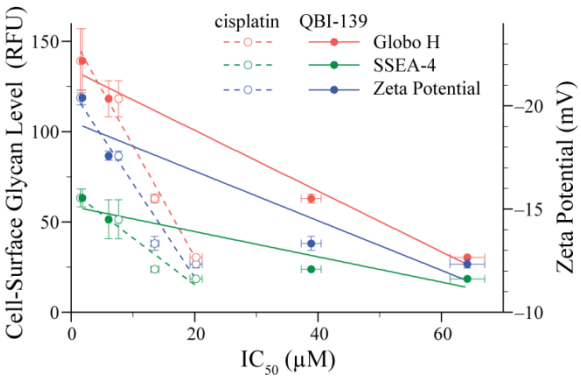
cisplatin
QBI-139
Globo H
SSEA-4
Zeta Potential
Cell-Surface Glycan Level (RFU)
Zeta Potential (mV)
IC50 (μM)
150
100
50
0
−20
−15
−10
0
20
40
60

Figure A3.3 Correlation of cytotoxicity of cisplatin and QBI-139 to zeta-potential and cell surface markers

Although both drugs displayed similar trend in toxicity toward these lung cells, the larger discrepancy in IC_{50} values of QBI-139 cytotoxicity suggested that QBI-139 treatment offers a larger therapeutic window than cisplatin treatment does. Cytotoxicity of both drugs appears to be correlated with the abundance of cell surface biomarkers Globo H and SSEA-4 as well as zeta-potential.

Table A3.1

Cell line	IC_{50} (μM)			
	Cisplatin	Fold change	QBI-139	Fold change
WI-38	20.2	1	64.2	1
H520	13.6	1.5	38.9	1.7
H1299	7.7	2.6	6.1	10.5
H460	1.5	13.5	1.8	35.7

Table A3.1 Values of IC_{50} (μM) for cell viability in the presence of drugs

Table A3.2

Cell line	Zeta-potential (ζ) (mV)
WI-38	-12.3 ± 0.3
H520	-13.3 ± 0.6
H1299	-17.6 ± 0.4
H460	-20.4 ± 0.6

Table A3.2 Zeta-potential measurement of lung cells in PBS at pH 7.4

APPENDIX IV

Detecting the Ribonuclease Inhibitor•RNase 1 Complex in Living Cells with NanoBiT Technology

Contribution: Prof. Raines and I designed the experiments and analyzed data. Valerie Ressler is currently working on experiments to visualize RI•RNase 1 complex in live cells. NanoBiT technology was developed by Promega Corporation.

A manuscript will be prepared and published as:

Hoang, T.T.[*], Ressler, V.[*], Schwinn, M.K., Wood, K.V., Raines, R.T. Detecting the Ribonuclease Inhibitor•RNase 1 Complex in Living Cells with NanoBiT Technology
([*]denotes equal contribution)

A4.1 Rationale

Despite the extensive biochemical studies on the incredible binding affinity between RNases and RI, the interaction of these proteins has never been directly observed *in cellulo*. A major challenge in visualizing the RI•RNases complexes in live cells is a low signal to background ratio. While RNases enter cell readily, majority of the protein localize in the endosomes. About 10% of them translocate to the cytosol to interact with RI.[394] In fact, fluorescently labeled RNase produces punctate staining in live cells, indicating the protein resides mainly in the endosomes.[305]

To improve signal to background ratio, labeled RNase needs to be latent in the endosomes and produces signal once encountering the cytosolic RI. I sought to utilize the technology of a complementation reporter based on NanoLuciferase (NanoLuc), namely NanoLuc Binary Technology (NanoBiT), which involves the reconstitution of luminescence upon association of two subunits of the NanoLuc.[395] The enzyme is small (19 kDa), stable and produces bright and sustained luminescence. Taking advantage of these attributes, a binary reporter system was designed with a large 18 kDa component (11S) and a small 1 kDa component (114). By design, these two components achieve low intrinsic affinity; thus, minimizing their influence on the interaction characteristics of the target proteins.

A4.2 Results

Based on the protein size and spatial organization of the RI•RNase 1 complex, the 114 peptide was appended to the N-terminus of RNase 1 (114-RNase 1), and the 11S subunit was fused to the N-terminus of RI (11S-RI).[374] DNA encoding for each fusion protein was transfected into HeLa cells. The secreted 114-RNase 1 was collected and applied to cells expressing 11S-RI (Figure A4.1). After 24-h incubation, the cell permeable Nano-Glo luciferase assay reagent was added,

and luminescence was measured. In consistence with our previous finding, approximately 10% of 114-RNase 1 in the cytosol participates in RI binding (Figure A4.2).

This NanoBiT technology provides a quantitative measurement of RNase 1 that forms complexes with RI in the cytosol. The complex formation only yielded signal to background ratio of 2 based on calculation of the relative luminescent units of 11S-RI•114-RNase 1 over 11S-RI alone, making the visualization of the complex challenging. To solve this puzzle, I designed to install a fluorophore near the N-terminus of RNase 1 and rely on the bioluminescence resonance energy transfer (BRET) for imaging the complex (Figure A4.3). The advantage of this design is the binary complementation of donor signal, NanoBiT, dependent on the interaction of RNase 1 to its inhibitor. Once the donor signal being excited, the fluorophore acceptor, by design, is in proximity to accept the energy transfer, and fluorescence will be detected. By integrating the two technologies, NanoBiT and BRET, this new strategy will allow us to visualize RI•RNase complex in live cells.

Figure A4.1

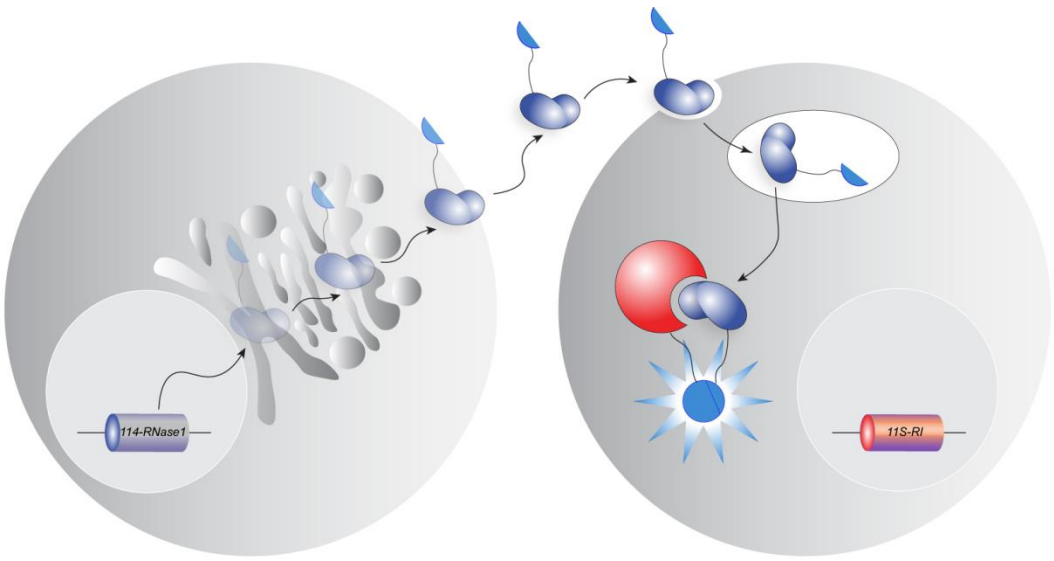

Figure A4.1 Strategy for measuring the formation of RI•RNase 1 complex in living cells with NanoBiT technology

NanoBiT is composed of 2 subunits: a 1.3 kDa peptide named 114 and a 18 kDa polypeptide named 11S. Each of the subunits is appended on RI and RNase 1 accordingly. DNA encoding for 114-RNase 1 and 11S-RI were independently transfected into HeLa cells. Secreted 114-RNase 1 (a blue kidney bean) was collected from conditioned media. Known amount of 114-RNase 1 was added to cells expressing 11S-RI (a horseshoe red). A fraction of 114-RNase 1 in endosomes escapes into the cytosol, where it encounters 11S-RI. The formation of RI•RNase 1 complex will produce luminescent signal because the NanoBiT subunits, by design, weakly associate, so that their assembly into a luminescent complex is dictated by the interaction RI•RNase 1 complex.

Figure A4.2

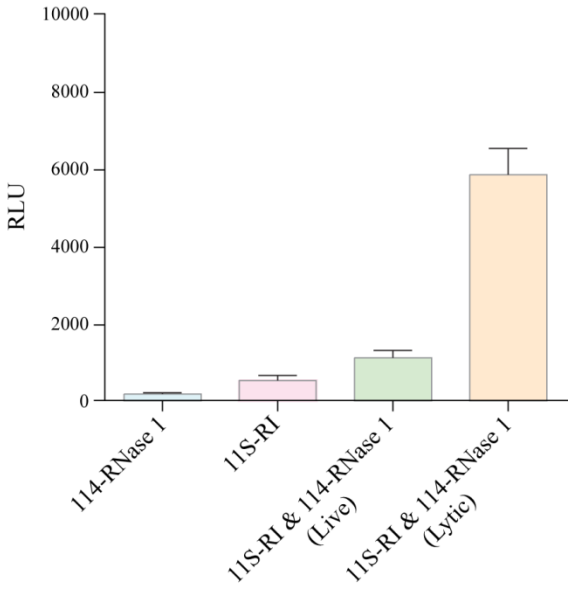
10000
8000
6000
4000
2000
0
RLU
114-RNase 1
11S-RI
11S-RI & 114-RNase 1 (Live)
11S-RI & 114-RNase 1 (Lytic)

Figure A4.2 Cytosolic entry of RNase 1

The fusion 114-RNase 1 (10 μM) was incubated with unmodified HeLa cells and overexpressed 11S-RI cells for 24 hours at 37 °C. The cell permeable Nano-Glo Luciferase Assay Reagent was added, and luminescence was measured. Both 114-RNase 1 and 11S-RI alone produced low background signal. In cells that contain both fusion proteins, the formation of 114-RNase 1•11S-RI complex yielded luminescent signal twice as intense as the 11S-RI did. The result suggests that only a small fraction of 114-RNase 1 in endosomes enters the cytosol. A lytic assay allowed us to detect all 114-RNase 1 that interact with RI, accounting for 100% signal derived from the complex formation. Together, the measurements from both live and lytic assay provide an estimation of amount of cytosolic RNase 1 is approximately 10%.

Figure A4.3

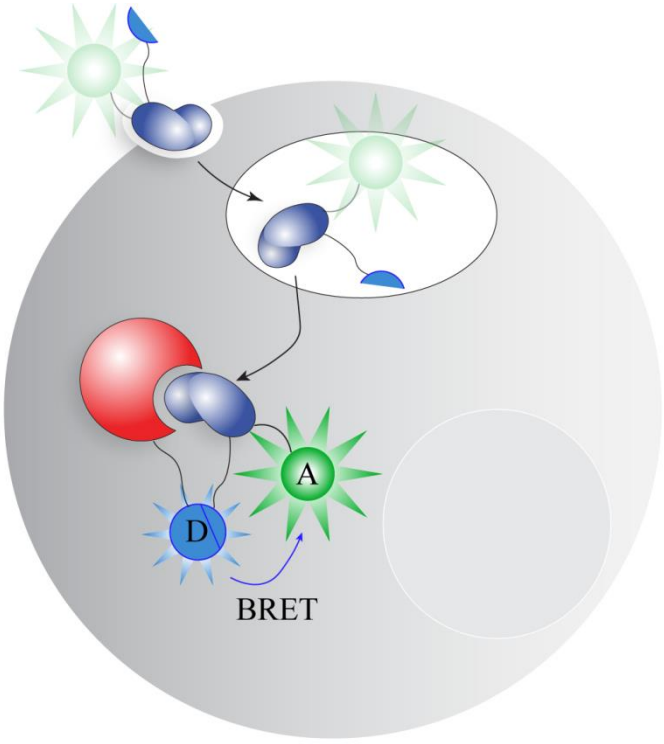

Figure A4.3 Strategy for visualizing RI•RNase 1 interaction in living cells

The 114-RNase 1 with a pendant fluorogenic probe is internalized by endocytosis. The conjugate will be fluorescent via energy transfer from a bioluminescent donor, NanoBiT. Generation of the donor signal relies on the interaction of cytosolic RNase 1 and RI. Once the complex forms, NanoBiT will be proximal to its fluorophore acceptor, allowing favorable energy transfer from the donor to the acceptor to produce fluorescent signal. Therefore, this strategy will offer high signal to background ratio, and make it feasible to visualize RI•RNase 1 complex in the cytosol.

APPENDIX V

Developing Antibodies against Ribonucleases with Phage Display

Contribution: This work is in collaboration with Prof. Jim Wells' lab at University of California at San Francisco. I developed the expression and purification for MBP-BirA. I also optimized a biotinylation reaction for the RNases. Emily and I created DNA constructs for biotinylated human and mouse RNase 1 and ANG. We worked together in purification and characterization of biotinylated mouse RNase 1.

A5.1 Rationale

Antibodies are important reagents for biological research and therapeutics. Since the development of the hybridoma technology by Kohler and Milstein, the production of murine monoclonal antibodies against foreign antigens has become a routine technique.[396] It is generally accepted that the greater the phylogenetic distance between foreign antigens and their recipient immunized animal, the more pronounced the immune response. Highly conserved mammalian proteins usually evoke a weak immune response. Therefore, the immunological system will not be able to recognize an epitope that is highly homologous in the foreign protein and in the corresponding protein of the immunized species.

The hybridoma technology has raised issues of reproducibility for antibody reagents as well as recognition of antibodies to their cognate folded proteins. To address these issues, a recombinant antibody generation by phage display has been developed.[397-400] A target antigen is immobilized on a surface and exposed to a phage-display synthetic antibodies library. After several rounds of repeating affinity selection, clones showing the highest specificity and selectivity to the antigen will be collected. The cloned antibodies can be renewable from the same source, producing reproducible and reliable quality of the antibodies. In addition, this new technology does not rely on animal immunizations and thereby eliminates auto-antigen anti-selection in an animal setting. This *in vitro* method offers a wide range of selection conditions such as buffer, pH, temperature and competitor proteins; thus maintaining the protein antigen in the native and folded state. Given the rapid selection framework and significantly improved antibodies library, this antibody phage display technology has been successfully transformed into an industrialized platform for generating high affinity antibodies at large scale with reduced processing time and cut cost.[401] As a powerful tool for antibody development, we asked if the

antibody phage-display can be utilized to produce antibodies against highly conserved proteins, which has been an unsolved problem with the hybridoma technology.

A5.2 Results

To test this theory, we chose a set of model proteins from members of pancreatic-type ribonucleases (RNases) superfamily. These RNases are highly conserved, small, cationic, secretory enzymes that catalyze the cleavage of RNA.[232] The set of model proteins contained two of human RNases, RNase 1 and ANG, and two of the corresponding proteins from mice. These 4 proteins offer a good range of identity and similarity in protein sequence and structure (Table A5.1). Red highlighted regions on protein that depicted for the most difference in sequence might become great epitopes for antibody recognition (Figure A5.1). To anchor these RNases on a platform, a biotin tag was installed to C-termini of the proteins, flanked by a TEV cleavage site and a linker. We were successful to acquire pure and biotinylated mouse RNase 1, and the protein was susceptible for TEV protease cleavage to remove the biotin tag (Figure A5.2). We are currently working on production of the other 3 proteins to complete the set.

Next, these proteins will be exposed to a phage-display synthetic antibodies library. Repeating affinity selection and anti-selection will be performed, aiming to raise antibodies that distinguishably bind to RNase 1 but not its related antigen, ANG. It will be more incredible if this method can generate mono-specific antibody to one antigen with no cross-species reactivity.

Figure A5.1

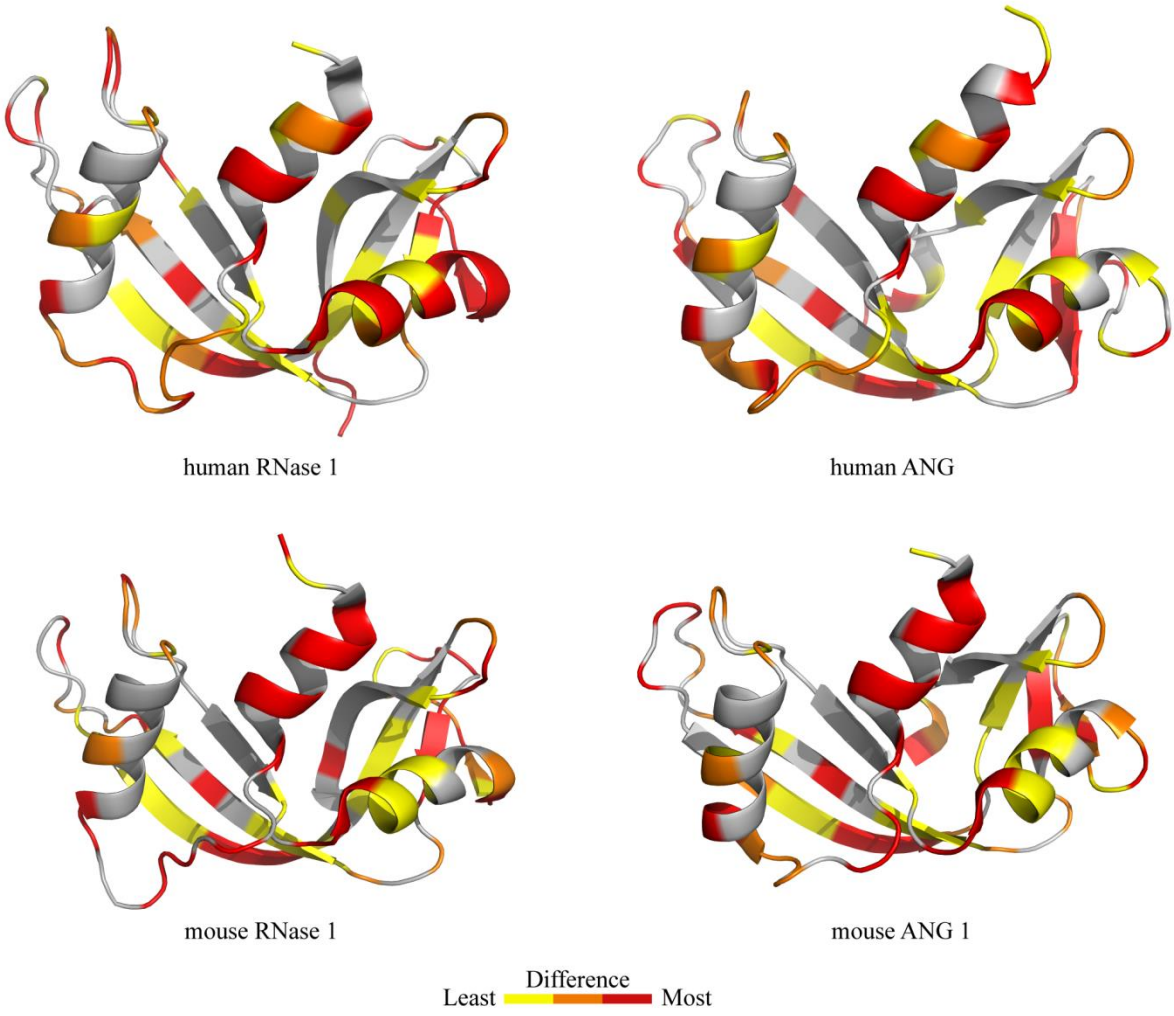
human RNase 1
human ANG
mouse RNase 1
mouse ANG 1
Difference
Least
Most

Figure A5.1 Protein sequence comparison between RNase 1 and ANG in human and in mice

Protein sequences of human and mouse RNase 1 and ANG were aligned using MUSCLE alignment. The degree of difference in sequences among these proteins was color coded, from yellow to red which indicated the least to the most difference. Human RNase 1 (PDB entry 1z7x), human ANG (PDB entry 1ang), mouse RNase 1 (PDB entry 3tsr), mouse ANG 1 (PDB entry 2bwk).

Figure A5.2

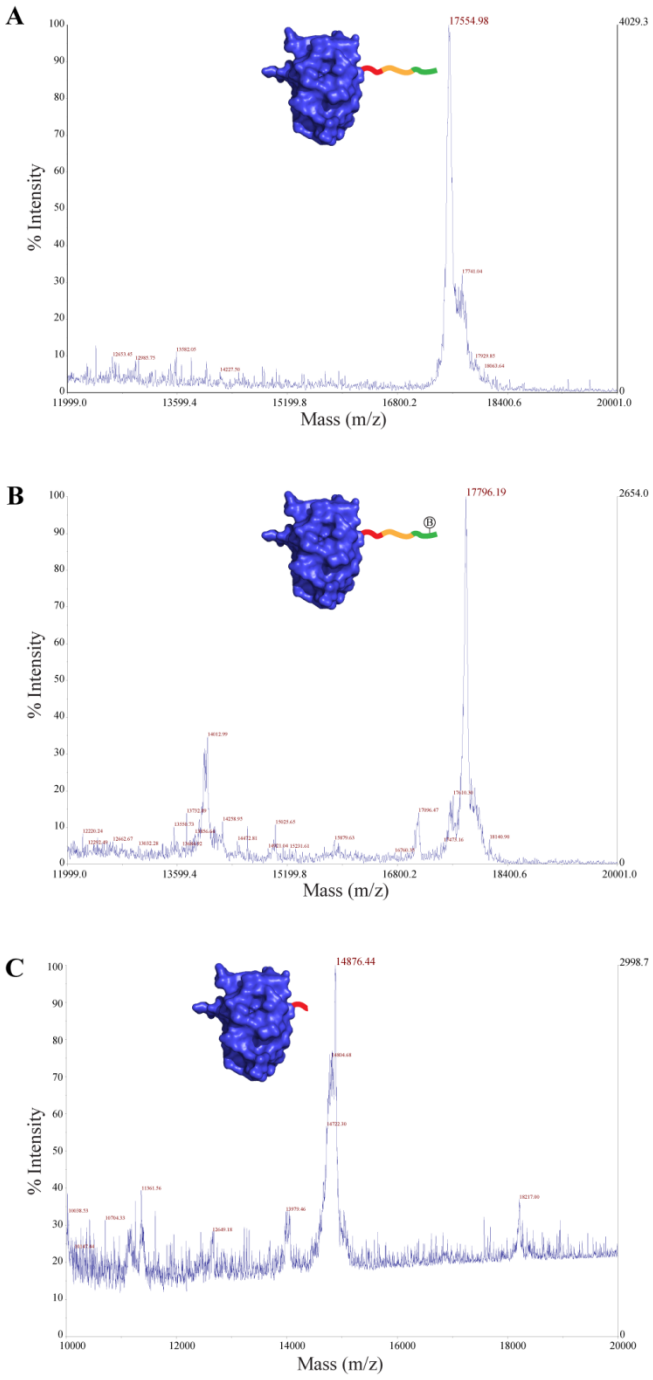
A
17554.98
4029.3
% Intensity
Mass (m/z)
11999.0
13599.4
15199.8
16800.2
18400.6
20001.0
B
17796.19
2654.0
% Intensity
Mass (m/z)
C
14876.44
2998.7
% Intensity
Mass (m/z)
10000
12000
14000
16000
18000
20000

Figure A5.2 Biotinylated human RNase 1 with TEV-cleavage site

The fusion human RNase 1 (blue) with a C-terminal TEV-cleavage site (red), a GS linker (yellow) and a biotin acceptor peptide (green) was over-expressed in *E.coli*.

A. The purity of tagged RNase 1 was determined by mass spectrometry. Expected mass is 17,577 Da and observed mass is 17,555 Da.

B. The biotinylation of tagged RNase 1 was confirmed by mass spectrometry. Expected mass is 17,803 Da and observed mass is 17,796 Da.

C. The biotinylated RNase 1 was accessible for TEV protease cleavage. Expected mass is 14,944 Da and observed mass is 14,876 Da.

Table A5.1

% Identity and Similarity	Human RNase 1	Human ANG	Mouse RNase 1	Mouse ANG 1
Human RNase 1	100	36	70	35
Human ANG	49	100	34	73
Mouse RNase 1	79	50	100	35
Mouse ANG 1	51	84	50	100

Table A5.1 Protein sequence comparisons among human and mouse RNase 1 and ANG

Appendix VI

ANG Thiophosphorylation

Contribution: This work is in collaboration with Prof. Christian Hackenberger's lab at Leibniz-Institut für Molekulare Pharmakologie. I provided S87C ANG variant and its FLAG fusion. Dr. Bertran is responsible for chemical synthesis and optimization of phosphothiolate reaction on ANG variants.

A6.1 Introduction

Protein phosphorylation is one of the major post-translational modifications that plays prominent role in a wide range of cellular processes.[402] The reversible addition of phosphate groups at serine, threonine or tyrosine residues could alter structure, function, and localization of modified proteins.[403-405] Aberrant regulation of phosphorylation on proteins has resulted in numerous diseases including cancer and neurological disorders.[406-408]

A current genetic strategy to mimic phosphorylated state of proteins is to substitute phosphorylated residues with either aspartate or glutamate.[409] The substitution can be easily done by site-direct mutagenesis, making this method widely applicable. A carboxylic acid group of these acidic residues only offers singly negative charge, whereas a phosphate group provides doubly charged at physiological pH. Therefore, there are examples where two acidic residues are needed to mimic one phosphorylation event.[410] Other studies report the activity of the Asp or Glu mutant is more like that of the non-phosphorylated form than the phosphorylated form.[411]

In an attempt to mimic nature of phosphorylation, chemists have developed technologies that can selectively install the phosphorylation modification on proteins at pre-determined sites. The introduction of phosphorylated Tyr analogues has been achieved through the Staudinger-phosphite reaction of azides.[412] This method requires an incorporation of non-natural amino acid, *p*-azidophenylalanine, at a phosphorylation site, making this technology less generalized. Another method developed by Davis and co-workers relies on the reactivity of thiol group on cysteine.[413] A phosphorylation site is genetically engineered to cysteine, which is first converted to dehydroalanine via a bis-alkylation elimination procedure with α,α'-di-bromo-adipyl(bis)amide and subsequently modified via Michael addition with sodium thiophosphate to

generate a thiophosphate group at the site of interest. The potential for nonspecific alkylation might limit the scope of applications of this method.

The Hackenberger's group has recently developed a chemoselective phosphorylation strategy that enables the incorporation of phosphorylated Cys residues on peptides in a stereochemically defined, site-selective manner (Bertran-Vicente *et al*. in review). Intrigued by the success of this novel technology on peptides, they further examined the feasibility of this technology on proteins, and they chose angiogenin (ANG) as a model protein in the study.

ANG is a member of the pancreatic-type ribonuclease superfamily; it is small, extremely stable, easily produced, and tolerant of chemical modifications.[284,232] For many of these reasons, ANG has a strong precedent as an effective protein scaffold for therapeutic modulation. ANG promotes angiogenesis via its activation of rDNA transcription. To manifest this angiogenic activity, it requires ANG to evade its cytosolic ribonuclease inhibitor (RI) to translocate to the nucleus. In CHAPTER 2, I reported that phosphorylation of key serine residues controls nuclear translocation activity of ANG. Among the 3 putative phosphorylation sites on ANG, Ser87 which is at the molecular interface of the RI•ANG complex, has the most profound impact on RI evasion (Figure 2.4A and Table 2.1). In fact, aspartate substitution at Ser87 to mimic phosphorylation bound RI with affinity 10^7-fold lower than did wild-type ANG. The carboxylic acid of the aspartate substitution does not fulfill the net gain of negative charges and stereochemistry of a phosphate group. Perhaps, the innate phosphorylated S87 ANG would result in more Coulombic (as well as steric) repulsion with RI, resulting in weaker binding than the S87D ANG variant.

By utilizing the new technology developed by the Hackenberger's group, we want to generate a thiophosphorylated S87 ANG variant that closely resembles the biologically relevant

phosphorylated serine residue. Studying this variant will further elucidate the impact of phosphorylation on ANG-induced angiogenesis. Most importantly, the success of chemically phosphorylate ANG at site specific manner will emphasize the ease and utility of this novel technology; thus, enabling generality of this technology to widely applicable for site-selective chemical phosphorylation of proteins.

A6.2 Results and Discussion

Our initial experiments with the Ellman´s disulfide S87C ANG protein **1** were carried out using phosphite triesters that had previously been synthesized by our laboratory (**2a-c**) (Figure A6.1).[414,415] We first probed the reactivity with *o*-nitrobenzyl based phosphites **2a** and **2b** in order to provide a UV-cleavable system to form finally the pCys protein. Unfortunately, neither product formation **3a** or **3b** nor consumption of the starting material **1** was observed. We argued that the steric bulk of the o-nitrobenzyl phosphites **2a** and **2b** might hinder the accessibility toward the electrophilic disulfide in S87C ANG. It is well known that bulky phosphines such as TCEP are less efficient than DTT in reducing disulfide bonds in protein.[416] Thereby, we decided to use the tris(2-cyanoethyl) phosphite **2c**, which was shown previously to form in good conversions phosphorothiolate esters on peptide level (Bertran-Vicente *et al*. in review). Protein **1** was dissolved in 50 mM Tris-HCl buffer (pH 7.5) and an excess of phosphite **2c** in MeCN was added. After 2h at room temperature, the reaction was monitored by LC-MS, showing as major product the phosphorothiolate ester protein **3c** together with protein **1** and hydrolyzed S87C protein (Figure A6.2 A,B). Deconvolution of the MS spectra showed an atomic mass of 14459 Da (calculated 14460 Da). Due to the similarity of the molecular mass of protein **1** and **3**, an external addition of protein **1** was added to the reaction crude confirming the identity of the phosphorothiolate ester protein **3c** (Figure A6.2C).

Despite the successful formation of protein **3c** using phosphite **2c**, the need to use basic conditions to deprotect the phosphorothiolate ester and deliver the pCys protein, limits the application of this phosphite for further experiments. pCys as well as pSer is known to undergo beta-elimination to dehydroalanine under basic conditions. Currently, we are evaluating the synthesis of new phosphites to overcome the steric hindrance limitation of the *o*-nitrobenzyl phosphites as well as to find suitable deprotection conditions to deliver finally the pCys target.

A6.3 Methods

Production and purification of S87C ANG variant and its FLAG fusion was performed as previously described.[44]

A6.3.1 Formation of O,O-bis(2-cyanoethyl) phosphorothiolate ester S87C ANG protein

A solution of Ellman´s modified S87C ANG protein **1** (8.3 mg/mL) in 50 mM Tris-HCl buffer (pH 7.5) (10 µL) was prepared. A solution of phosphite **2c** (0.14 mg, 0.58 µmol, 100 eq) in MeCN (10 µL) was added. Final protein concentration was 4.15 mg/mL. The reaction mixture was incubated at room temperature for 2 h and measured afterwards by LC-MS.

A6.3.2 Protein analysis

Proteins samples were dissolved in water (0.28 mg/mL) and analyzed by a reversed-phase capillary liquid chromatography system, Acquity UPLC System (Waters), coupled to an ESI-TOF unit LCT Premier (Waters Micromass Technologies). LC separations were performed on BEH300 C4 column (1.7 µm x 2.1 x 150 mm) at an eluent flow rate of 0.3 mL/min using a gradient of 2–50% B in 10 min. Mobile phase A contained 0.1% formic acid in water, and mobile phase B contained 0.1% formic acid in MeCN.

Figure A6.1

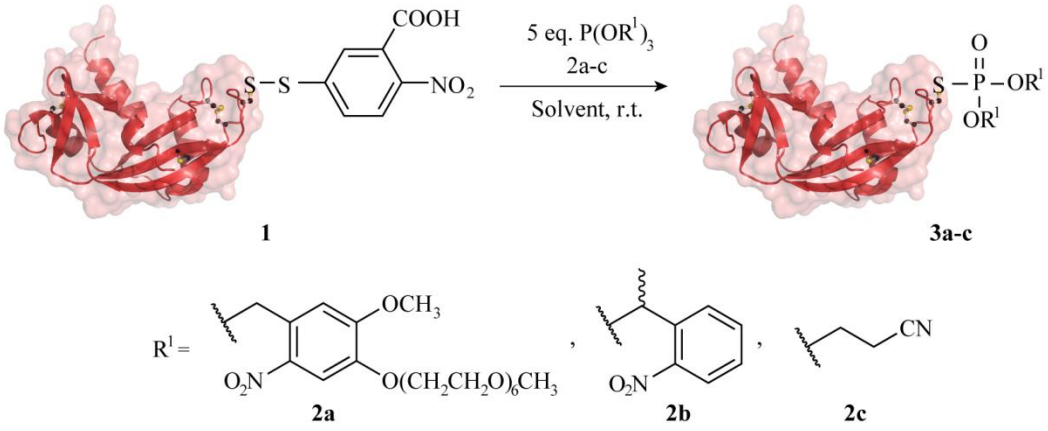
COOH
S–S
NO2
5 eq. P(OR1)3
2a-c
Solvent, r.t.
O
P–OR1
OR1
1
3a-c
R1 =
OCH3
O2N
O(CH2CH2O)6CH3
O2N
CN
2a
2b
2c

Figure A6.1 Site-selective synthesis of phosphothiolate ester ANG protein

The Ellman's disulfide S87C ANG protein (red ribbon) was reacted with phosphite triesters (**2a-c**) to produce a phosphorothiolate ester ANG.

Figure A6.2

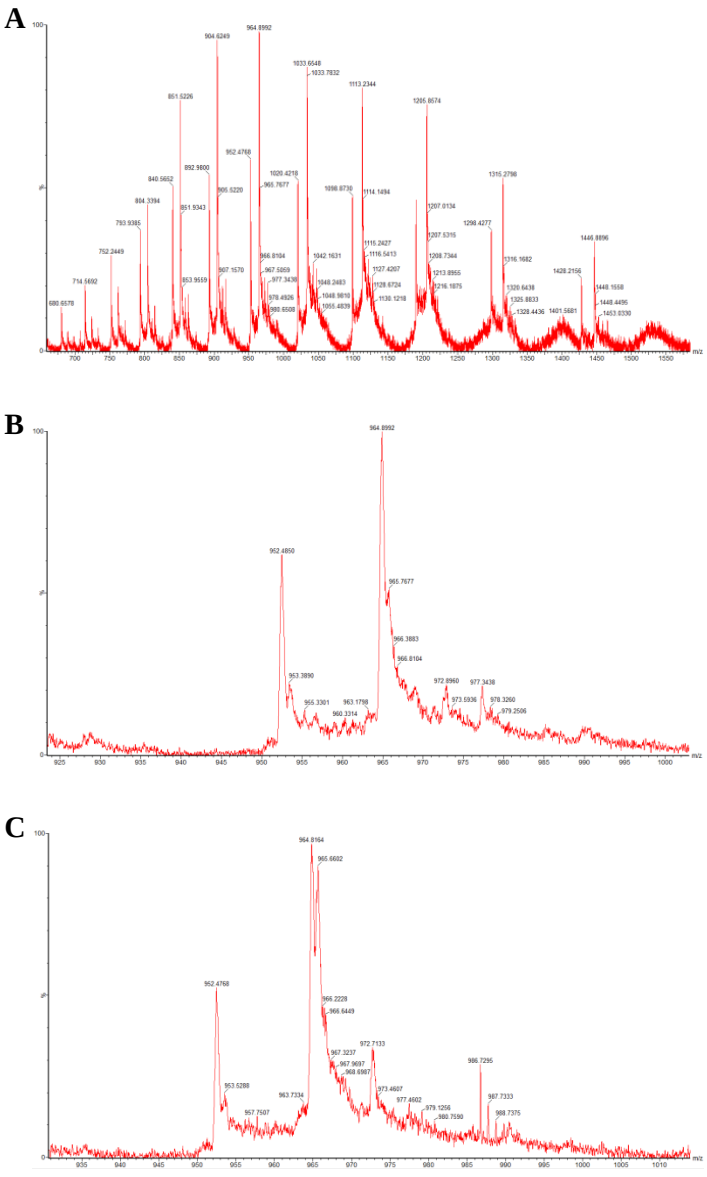

Figure A6.2 Spectra of the reaction crude of protein **1** and phosphite **2c**

A. ESI-spectra

B. Zoom in of the $[M + 15H^+]^{15+}$ ESI-spectra

C. Same spectrum as B with the external addition of protein **1**

Reference

(1) Cancer and neurodegeneration meet. de Strooper, B. *EMBO Mol. Med.* **2010**, *2*, 245-246.

(2) Cancer and neurodegeneration: Between the devil and the deep blue sea. Plun-Favreau, H.; Lewis, P. A.; Hardy, J.; Martins, L. M.; Wood, N. W. *PLoS Genet.* **2010**, *6*, e1001257.

(3) Understanding the link between cancer and neurodegeneration. Driver, J. A. *J. Geriatr. Oncol.* **2012**, *3*, 58-67.

(4) Neurodegeneration and cancer: Where the disorder prevails. Klus, P.; Cirillo, D.; Botta Orfila, T.; Gaetano Tartaglia, G. *Sci. Rep.* **2015**, *5*, 15390.

(5) Cyclin-dependent kinase inhibitors: Cancer killers to neuronal guardians. Monaco, E. A., 3rd; Vallano, M. L. *Curr. Med. Chem.* **2003**, *10*, 367-379.

(6) Cell cycle checkpoints: The role and evaluation for early diagnosis of senescence, cardiovascular, cancer, and neurodegenerative diseases. Golubnitschaja, O. *Amino Acids* **2007**, *32*, 359-371.

(7) Tumorigenesis and neurodegeneration: Two sides of the same coin? Staropoli, J. F. *Bioessays* **2008**, *30*, 719-727.

(8) Epigenetic modifications and human disease. Portela, A.; Esteller, M. *Nat. Biotechnol.* **2010**, *28*, 1057-1068.

(9) DNA methylation in neurodegenerative disorders: A missing link between genome and environment? Iraola-Guzman, S.; Estivill, X.; Rabionet, R. *Clin. Genet.* **2011**, *80*, 1-14.

(10) Epigenetics in neurodegeneration: A new layer of complexity. Marques, S. C.; Oliveira, C. R.; Pereira, C. M.; Outeiro, T. F. *Prog. Neuropsychopharmacol. Biol. Psychiatry* **2011**, *35*, 348-355.

(11) Genetic determinants at the interface of cancer and neurodegenerative disease. Morris, L. G.; Veeriah, S.; Chan, T. A. *Oncogene* **2010**, *29*, 3453-3464.

(12) RNA-binding proteins as molecular links between cancer and neurodegeneration. Campos-Melo, D.; Droppelmann, C. A.; Volkening, K.; Strong, M. J. *Biogerontology* **2014**, *15*, 587-610.

(13) RNA-binding proteins in neurodegeneration: Seq and you shall receive. Nussbacher, J. K.; Batra, R.; Lagier-Tourenne, C.; Yeo, G. W. *Trends Neurosci.* **2015**, *38*, 226-236.

(14) A prospective cohort study of cancer incidence following the diagnosis of Parkinson's disease. Driver, J. A.; Logroscino, G.; Buring, J. E.; Gaziano, J. M.; Kurth, T. *Cancer Epidemiol. Biomarkers Prev.* **2007**, *16*, 1260-1265.

(15) The particular relationship between Parkinson's disease and malignancy: A focus on skin cancers. Inzelberg, R.; Israeli-Korn, S. D. *J Neural. Transm.* **2009**, *116*, 1503-1507.

(16) Cancer in patients with motor neuron disease, multiple sclerosis and Parkinson's disease: Record linkage studies. Fois, A. F.; Wotton, C. J.; Yeates, D.; Turner, M. R.; Goldacre, M. J. *J Neurol. Neurosurg. Psychiatry* **2010**, *81*, 215-221.

(17) Amyotrophic lateral sclerosis mortality in 1.9 million US cancer survivors. Freedman, D. M.; Travis, L. B.; Gridley, G.; Kuncl, R. W. *Neuroepidemiology* **2005**, *25*, 176-180.

(18) Mortality due to amyotrophic lateral sclerosis and Parkinson's disease among melanoma patients. Baade, P. D.; Fritschi, L.; Freedman, D. M. *Neuroepidemiology* **2007**, *28*, 16-20.

(19) The genetic epidemiology of neurodegenerative disease. Bertram, L.; Tanzi, R. E. *J. Clin. Invest.* **2005**, *115*, 1449-1457.

(20) The epigenomics of cancer. Jones, P. A.; Baylin, S. B. *Cell* **2007**, *128*, 683-692.

(21) Endogenous angiogenin in endothelial cells is a general requirement for cell proliferation and angiogenesis. Kishimoto, K.; Liu, S.; Tsuji, T.; Olson, K. A.; Hu, G.-f. *Oncogene* **2005**, *24*, 445-456.

(22) Angiogenin stimulates ribosomal rna transcription by epigenetic activation of the ribosomal DNA promoter. Sheng, J.; Yu, W.; Gao, X.; Xu, Z.; Hu, G.-f. *J. Cell Physiol.* **2014**, *229*, 521-529.

(23) tRNA fragments in human health and disease. Anderson, P.; Ivanov, P. *FEBS Lett.* **2014**, *588*, 4297-4304.

(24) ANG mutations segregate with familial and 'sporadic' amyotrophic lateral sclerosis. Greenway, M. J.; Andersen, P. M.; Russ, C.; Ennis, S.; Cashman, S.; Donaghy, C.; Patterson, V.; Swingler, R.; Kieran, D.; Prehn, J.; Morrison, K. E.; Green, A.; Acharya, K. R.; Brown, R. H., Jr.; Hardiman, O. *Nat. Genet.* **2006**, *38*, 411-413.

(25) Hypoxia-induced up-regulation of angiogenin, besides VEGF, is related to progression of oral cancer. Kishimoto, K.; Yoshida, S.; Ibaragi, S.; Yoshioka, N.; Okui, T.; Hu, G. F.; Sasaki, A. *Oral. Oncol.* **2012**, *48*, 1120-1127.

(26) Three decades of research on angiogenin: A review and perspective. Sheng, J.; Xu, Z. *Acta Biochim. Biophys. Sin.* **2015**, *35*, 131-141.

(27) Isolation and characterization of angiogenin, an angiogenic protein from human carcinoma cells. Fett, J. W.; Strydom, D. J.; Lobb, R. R.; Alderman, E. M.; Bethune, J. L.; Riordan, J. F.; Vallee, B. L. *Biochemistry* **1985**, *24*, 5480-5486.

(28) Protein that sets off growth of a human organ is found. Schmeck, H. M., Jr. In *The New York Times* New York, NY, **1985**, p A1, B11.

(29) Tumor angiogenesis: Therapeutic implications. Folkman, J. *N. Engl. J. Med.* **1971**, *285*, 1182-1186.

(30) Angiogenic factors. Folkman, J.; Klagsbrun, M. *Science* **1987**, *235*, 442-447.

(31) *Dr. Folkman's War: Angiogenesis and the Struggle to Defeat Cancer*. Cooke, R.; Random House: New York, NY, **2001**.

(32) Amino acid sequence of human tumor derived angiogenin. Strydom, D. J.; Fett, J. W.; Lobb, R. R.; Alderman, E. M.; Bethune, J. L.; Riordan, J. F.; Vallee, B. L. *Biochemistry* **1985**, *24*, 5486-5494.

(33) Sequence of the cDNA and gene for angiogenin, a human angiogenesis factor. Kurachi, K.; Davie, E. W.; Strydom, D. J.; Riordan, J. F.; Vallee, B. L. *Biochemistry* **1985**, *24*, 5494-5499.

(34) Structural and functional implications of positive selection at the primate angiogenin gene. Osorio, D. S.; Antunes, A.; Ramos, M. J. *BMC Evol. Biol.* **2007**, *7*, 167.

(35) The mouse angiogenin gene family: Structures of an angiogenin-related protein gene and two pseudogenes. Brown, W. E.; Nobile, V.; Subramanian, V.; Shapiro, R. *Genomics* **1995**, *29*, 200-206.

(36) Characterization of mouse angiogenin-related protein: Implications for functional studies on angiogenin. Nobile, V.; Vallee, B. L.; Shapiro, R. *Proc. Natl. Acad. Sci. USA* **1996**, *93*, 4331-4335.

(37) Mutational dynamics of murine angiogenin duplicates. Codoner, F. M.; Alfonso-Loeches, S.; Fares, M. A. *BMC Evol. Biol.* **2010**, *10*, 310.

(38) The mouse RNase 4 and RNase 5/ang 1 locus utilizes dual promoters for tissue-specific expression. Dyer, K. D.; Rosenberg, H. F. *Nucleic Acids Res.* **2005**, *33*, 1077-1086.

(39) Tissue-specific expression of pancreatic-type RNases and RNase inhibitor in humans. Futami, J.; Tsushima, Y.; Murato, Y.; Tada, H.; Sasaki, J.; Seno, M.; Yamada, H. *DNA Cell Biol.* **1997**, *16*, 413-419.

(40) Ribonuclease 4 protects neuron degeneration by promoting angiogenesis, neurogenesis, and neuronal survival under stress. Li, S.; Sheng, J.; Hu, J. K.; Yu, W.; Kishikawa, H.; Hu, M. G.; Shima, K.; Wu, D.; Xu, Z.; Xin, W.; Sims, K. B.; Landers, J. E.; Brown, R. H., Jr.; Hu, G. F. *Angiogenesis* **2013**, *16*, 387-404.

(41) The expansion and functional diversification of the mammalian ribonuclease a superfamily epitomizes the efficiency of multigene families at generating biological novelty. Goo, S. M.; Cho, S. *Genome Biol. Evol.* **2013**, *5*, 2124-2140.

(42) Characteristic ribonucleolytic activity of human angiogenin. Shapiro, R.; Riordan, J. F.; Vallee, B. L. *Biochemistry* **1986**, *25*, 3527-3532.

(43) Isolation and characterization of a human colon carcinoma-secreted enzyme with pancreatic ribonuclease-like activity. Shapiro, R.; Fett, J. W.; Strydom, D. J.; Vallee, B. L. *Biochemistry* **1986**, *25*, 7255-7264.

(44) The ribonucleolytic activity of angiogenin. Leland, P. A.; Staniszewski, K. E.; Park, C.; Kelemen, B. R.; Raines, R. T. *Biochemistry* **2002**, *41*, 1343-1350.

(45) Crystal structure of human angiogenin reveals the structural basis for its functional divergence from ribonuclease. Acharya, K. R.; Shapiro, R.; Allen, S. C.; Riordan, J. F.; Vallee, B. L. *Proc. Natl. Acad. Sci. USA* **1994**, *91*, 2915-2919.

(46) Role of glutamine-117 in the ribonucleolytic activity of human angiogenin. Russo, N.; Shapiro, R.; Acharya, K. R.; Riordan, J. F.; Vallee, B. L. *Proc. Natl. Acad. Sci. USA* **1994**, *91*, 2920-2924.

(47) Nuclear translocation of angiogenin in proliferating endothelial cells is essential to its angiogenic activity. Moroianu, J.; Riordan, J. F. *Proc. Natl. Acad. Sci. USA* **1994**, *91*, 1677-1681.

(48) Identification of the nucleolar targeting signal of human angiogenin. Moroianu, J.; Riordan, J. F. *Biochem. Biophys. Res. Commun.* **1994**, *203*, 1765-1772.

(49) Angiogenin is translocated to the nucleus of HeLa cells and is involved in ribosomal RNA transcription and cell proliferation. Tsuji, T.; Sun, Y.; Kishimoto, K.; Olson, K. A.; Liu, S.; Hirukawa, S.; Hu, G.-f. *Cancer Res.* **2005**, *65*, 1352-1360.

(50) A therapeutic target for prostate cancer based on angiogenin-stimulated angiogenesis and cancer cell proliferation. Yoshioka, N.; Wang, L.; Kishimoto, K.; Tsuji, T.; Hu, G. F. *Proc. Natl. Acad. Sci. USA* **2006**, *103*, 14519-14524.

(51) A putative angiogenin receptor in angiogenin-responsive human endothelial cells. Hu, G. F.; Riordan, J. F.; Vallee, B. L. *Proc. Natl. Acad. Sci. USA* **1997**, *94*, 2204-2209.

(52) Motoneurons secrete angiogenin to induce RNA cleavage in astroglia. Skorupa, A.; King, M. A.; Aparicio, I. M.; Dussmann, H.; Coughlan, K.; Breen, B.; Kieran, D.; Concannon, C. G.; Marin, P.; Prehn, J. H. *J. Neurosci.* **2012**, *32*, 5024-5038.

(53) Syndecan-4-mediated signalling. Simons, M.; Horowitz, A. *Cell. Signal.* **2001**, *13*, 855-862.

(54) Delayed wound repair and impaired angiogenesis in mice lacking syndecan-4. Echtermeyer, F.; Streit, M.; Wilcox-Adelman, S.; Saoncella, S.; Denhez, F.; Detmar, M.; Goetinck, P. *J. Clin. Invest.* **2001**, *107*, R9-R14.

(55) Syndecans: Proteoglycan regulators of cell-surface microdomains? Couchman, J. R. *Nat. Rev. Mol. Cell Biol.* **2003**, *4*, 926-937.

(56) The dual binding site of angiogenin and its inhibition mechanism: The crystal structure of the rat angiogenin-heparin complex. Yeo, K. J.; Hwang, E.; Min, K. M.; Jee, J. G.; Lee, C. K.; Hwang, K. Y.; Jeon, Y. H.; Chang, S. I.; Cheong, H. K. *Chem. Commun.* **2014**, *50*, 12966-12969.

(57) Tight-binding inhibition of angiogenin and ribonuclease A by placental ribonuclease inhibitor. Lee, F. S.; Shapiro, R.; Vallee, B. L. *Biochemistry* **1989**, *28*, 225-230.

(58) Amino acid sequence of the ribonuclease inhibitor from porcine liver reveals the presence of leucine-rich repeats. Hofsteenge, J.; Kieffer, B.; Matthies, R.; Hemmings, B. A.; Stone, S. R. *Biochemistry* **1988**, *27*, 8537-8544.

(59) Ribonuclease inhibitor: Structure and function. Dickson, K. A.; Haigis, M. C.; Raines, R. T. *Prog. Nucleic Acid Res. Mol. Biol.* **2005**, *80*, 349-374.

(60) Functional evolution of ribonuclease inhibitor: Insights from birds and reptiles. Lomax, J. E.; Bianchetti, C. M.; Chang, A.; Phillips, G. N., Jr.; Fox, B. G.; Raines, R. T. *J. Mol. Biol.* **2014**, *426*, 3041-3056.

(61) Molecular recognition of human angiogenin by placental ribonuclease inhibitor—an X-ray crystallographic study at 2.0 Å resolution. Papageorgiou, A.; Shapiro, R.; Acharya, K. *EMBO J.* **1997**, *16*, 5162-5177.

(62) Ribonuclease inhibitor as an intracellular sentry. Haigis, M. C.; Kurten, E. L.; Raines, R. T. *Nucleic Acids Res.* **2003**, *31*, 1024-1032.

(63) Ribonuclease inhibitor regulates neovascularization by human angiogenin. Dickson, K. A.; Kang, D. K.; Kwon, Y. S.; Kim, J. C.; Leland, P. A.; Kim, B. M.; Chang, S. I.; Raines, R. T. *Biochemistry* **2009**, *48*, 3804-3806.

(64) Ribonuclease inhibitor up-regulation inhibits the growth and induces apoptosis in murine melanoma cells through repression of angiogenin and ILK/PI3K/AKT signaling pathway. Li, L.; Pan, X.-Y.; Shu, J.; Jiang, R.; Zhou, Y.-J.; Chen, J.-X. *Biochimie* **2014**, *103*, 89-100.

(65) Ribonuclease/angiogenin inhibitor 1 regulates stress-induced subcellular localization of angiogenin to control growth and survival. Pizzo, E.; Sarcinelli, C.; Sheng, J.; Fusco, S.; Formiggini, F.; Netti, P.; Yu, W.; D'Alessio, G.; Hu, G. F. *J. Cell Sci.* **2013**, *126*, 4308-4319.

(66) Identification and characterization of an angiogenin-binding DNA sequence that stimulates luciferase reporter gene expression. Xu, Z. P.; Tsuji, T.; Riordan, J. F.; Hu, G. F. *Biochemistry* **2003**, *42*, 121-128.

(67) The 23-million-dollar quest pays off. Marx, J. L. *Science* **1985**, *230*, 161.

(68) Angiogenesis in health and disease. Carmeliet, P. *Nat. Med.* **2003**, *9*, 653-660.

(69) Basic and therapeutic aspects of angiogenesis. Potente, M.; Gerhardt, H.; Carmeliet, P. *Cell* **2011**, *146*, 873-887.

(70) Molecular regulation of vessel maturation. Jain, R. K. *Nat. Med.* **2003**, *9*, 685-693.

(71) Endothelial-mural cell signaling in vascular development and angiogenesis. Gaengel, K.; Genove, G.; Armulik, A.; Betsholtz, C. *Arterioscler. Thromb. Vasc. Biol.* **2009**, *29*, 630-638.

(72) Angiogenin and endothelial cells. Badet, J.; Soncin, F.; Barritault, D. *Exs.* **1992**, *61*, 235-238.

(73) Angiogenin promotes tumoral growth and angiogenesis by regulating matrix metallopeptidase-2 expression via the ERK1/2 pathway. Miyake, M.; Goodison, S.; Lawton, A.; Gomes-Giacoia, E.; Rosser, C. J. *Oncogene* **2015**, *34*, 890-901.

(74) Angiogenin supports endothelial and fibroblast cell adhesion. Soncin, F. *Proc. Natl. Acad. Sci. USA* **1992**, *89*, 2232-2236.

(75) Angiogenin enhances actin acceleration of plasminogen activation. Hu, G. F.; Riordan, J. F. *Biochem. Biophys. Res. Commun.* **1993**, *197*, 682-687.

(76) Angiogenin promotes invasiveness of cultured endothelial cells by stimulation of cell-associated proteolytic activities. Hu, G.; Riordan, J. F.; Vallee, B. L. *Proc. Natl. Acad. Sci. USA* **1994**, *91*, 12096-12100.

(77) Interaction of human angiogenin with copper modulates angiogenin binding to endothelial cells. Soncin, F.; Guitton, J. D.; Cartwright, T.; Badet, J. *Biochem. Biophys. Res. Commun.* **1997**, *236*, 604-610.

(78) Role of the vascular endothelial growth factor pathway in tumor growth and angiogenesis. Hicklin, D. J.; Ellis, L. M. *J. Clin. Oncol.* **2005**, *23*, 1011-1027.

(79) VEGF-targeted therapy: Mechanisms of anti-tumour activity. Ellis, L. M.; Hicklin, D. J. *Nat. Rev. Cancer.* **2008**, *8*, 579-591.

(80) VEGF inhibition: Insights from preclinical and clinical studies. Crawford, Y.; Ferrara, N. *Cell Tissue Res.* **2009**, *335*, 261-269.

(81) Anti-angiogenic treatments in metastatic colorectal cancer: Does a continuous angiogenic blockade make sense? Jary, M.; Borg, C.; Bouche, O.; Kim, S.; Andre, T.; Bennouna, J. *Bull. Cancer* **2015**, *102*, 758-771.

(82) Use of anti-VEGF adjuvant therapy in cancer: Challenges and rationale. Bagri, A.; Kouros-Mehr, H.; Leong, K. G.; Plowman, G. D. *Trends Mol. Med.* **2010**, *16*, 122-132.

(83) Modes of resistance to anti-angiogenic therapy. Bergers, G.; Hanahan, D. *Nat. Rev. Cancer* **2008**, *8*, 592-603.

(84) Pathways mediating VEGF-independent tumor angiogenesis. Ferrara, N. *Cytokine Growth Factor Rev.* **2010**, *21*, 21-26.

(85) Induction of angiogenesis by mixtures of two angiogenic proteins, angiogenin and acidic fibroblast growth factor, in the chick chorioallantoic membrane. Fett, J. W.; Bethune, J. L.; Vallee, B. L. *Biochem. Biophys. Res. Commun.* **1987**, *146*, 1122-1131.

(86) Multistep tumorigenesis and the microenvironment. Schedin, P.; Elias, A. *Breast Cancer Res.* **2004**, *6*, 93-101.

(87) Suppression of uPA and uPAR attenuates angiogenin mediated angiogenesis in endothelial and glioblastoma cell lines. Raghu, H.; Lakka, S. S.; Gondi, C. S.; Mohanam, S.; Dinh, D. H.; Gujrati, M.; Rao, J. S. *PLoS One* **2010**, *5*, e12458.

(88) Increased expression of angiogenin in hepatocellular carcinoma in correlation with tumor vascularity. Hisai, H.; Kato, J.; Kobune, M.; Murakami, T.; Miyanishi, K.; Takahashi, M.; Yoshizaki, N.; Takimoto, R.; Terui, T.; Niitsu, Y. *Clin. Cancer Res.* **2003**, *9*, 4852-4859.

(89) Angiogenin as a molecular target for the treatment of prostate cancer. Li, S.; Ibaragi, S.; Hu, G. F. *Curr. Cancer Ther. Rev.* **2011**, *7*, 83-90.

(90) Prostate cancer-derived angiogenin stimulates the invasion of prostate fibroblasts. Jones, M. L.; Ewing, C. M.; Isaacsa, W. B.; Getzenberg, R. H. *J. Cell Mol. Med.* **2012**, *16*, 193-201.

(91) mir-409-3p inhibits HT1080 cell proliferation, vascularization and metastasis by targeting angiogenin. Weng, C.; Dong, H.; Chen, G.; Zhai, Y.; Bai, R.; Hu, H.; Lu, L.; Xu, Z. *Cancer Lett.* **2012**, *323*, 171-179.

(92) Elevated expression of angiogenin in prostate cancer and its precursors. Katona, T. M.; Neubauer, B. L.; Iversen, P. W.; Zhang, S.; Baldridge, L. A.; Cheng, L. *Clin. Cancer Res.* **2005**, *11*, 8358-8363.

(93) Angiogenin mediates androgen-stimulated prostate cancer growth and enables castration resistance. Li, S.; Hu, M. G.; Sun, Y.; Yoshioka, N.; Ibaragi, S.; Sheng, J.; Sun, G.; Kishimoto, K.; Hu, G. F. *Mol. Cancer Res.* **2013**, *11*, 1203-1214.

(94) Eukaryotic ribosome biogenesis at a glance. Thomson, E.; Ferreira-Cerca, S.; Hurt, E. *J Cell Sci.* **2013**, *126*, 4815-4821.

(95) Pre-ribosomal RNA synthesis in isolated rat-liver nucleoli. Grummt, I.; Lindigkeit, R. *Eur. J. Biochem.* **1973**, *36*, 244-249.

(96) Multiple ribosomal RNA cleavage pathways in mammalian cells. Bowman, L. H.; Rabin, B.; Schlessinger, D. *Nucleic Acids Res.* **1981**, *9*, 4951-4966.

(97) Assembly and isolation of intermediate steps of transcription complexes formed on the human 5S rRNA gene. Weser, S.; Riemann, J.; Seifart, K. H.; Meissner, W. *Nucleic Acids Res.* **2003**, *31*, 2408-2416.

(98) 60s pre-ribosome formation viewed from assembly in the nucleolus until export to the cytoplasm. Nissan, T. A.; Bassler, J.; Petfalski, E.; Tollervey, D.; Hurt, E. *EMBO J.* **2002**, *21*, 5539-5547.

(99) Ribosome assembly in eukaryotes. Fromont-Racine, M.; Senger, B.; Saveanu, C.; Fasiolo, F. *Gene* **2003**, *313*, 17-42.

(100) Nascent ribosomes. Warner, J. R. *Cell* **2001**, *107*, 133-136.

(101) Pre-ribosomes on the road from the nucleolus to the cytoplasm. Tschochner, H.; Hurt, E. *Trends Cell Biol.* **2003**, *13*, 255-263.

(102) An encore for ribosome biogenesis in the control of cell proliferation. Thomas, G. *Nat. Cell Biol.* **2000**, *2*, E71-72.

(103) Ribosome biogenesis and cell growth: mTOR coordinates transcription by all three classes of nuclear RNA polymerases. Mayer, C.; Grummt, I. *Oncogene* **2006**, *25*, 6384-6391.

(104) Dysregulation of the basal RNA polymerase transcription apparatus in cancer. Bywater, M. J.; Pearson, R. B.; McArthur, G. A.; Hannan, R. D. *Nat. Rev. Cancer* **2013**, *13*, 299-314.

(105) Like attracts like: Getting RNA processing together in the nucleus. Lewis, J. D.; Tollervey, D. *Science* **2000**, *288*, 1385-1389.

(106) Cancer cell metabolism: Implications for therapeutic targets. Jang, M.; Kim, S. S.; Lee, J. *Exp. Mol. Med.* **2013**, *45*, e45.

(107) A step subsequent to preinitiation complex assembly at the ribosomal RNA gene promoter is rate limiting for human RNA polymerase I-dependent transcription. Panov, K. I.; Friedrich, J. K.; Zomerdijk, J. C. *Mol. Cell Biol.* **2001**, *21*, 2641-2649.

(108) Regulation of mammalian ribosomal gene transcription by RNA polymerase I. Grummt, I. *Prog. Nucleic Acid Res. Mol. Biol.* **1999**, *62*, 109-154.

(109) Epigenetic silencing of RNA polymerase I transcription. Grummt, I.; Pikaard, C. S. *Nat. Rev. Mol. Cell Biol.* **2003**, *4*, 641-649.

(110) Epigenetic control of RNA polymerase I transcription in mammalian cells. Grummt, I.; Langst, G. *Biochim. Biophys. Acta* **2013**, *1829*, 393-404.

(111) NORC—a novel member of mammalian IWSI-containing chromatin remodeling machines. Strohner, R.; Nemeth, A.; Jansa, P.; Hofmann-Rohrer, U.; Santoro, R.; Langst, G.; Grummt, I. *EMBO J.* **2001**, *20*, 4892-4900.

(112) The nucleolar remodeling complex norc mediates heterochromatin formation and silencing of ribosomal gene transcription. Santoro, R.; Li, J.; Grummt, I. *Nat. Genet.* **2002**, *32*, 393-396.

(113) Intergenic transcripts regulate the epigenetic state of rRNA genes. Mayer, C.; Schmitz, K. M.; Li, J.; Grummt, I.; Santoro, R. *Mol. Cell* **2006**, *22*, 351-361.

(114) The structure of NORC-associated RNA is crucial for targeting the chromatin remodelling complex NORC to the nucleolus. Mayer, C.; Neubert, M.; Grummt, I. *EMBO Rep.* **2008**, *9*, 774-780.

(115) Inheritance of silent rDNA chromatin is mediated by PARP1 via noncoding RNA. Guetg, C.; Scheifele, F.; Rosenthal, F.; Hottiger, M. O.; Santoro, R. *Mol. Cell* **2012**, *45*, 790-800.

(116) pRNA: NORC-associated RNA of rRNA operons. Wehner, S.; Dorrich, A. K.; Ciba, P.; Wilde, A.; Marz, M. *RNA Biol.* **2014**, *11*, 3-9.

(117) The multifunctional nucleolus. Boisvert, F. M.; van Koningsbruggen, S.; Navascues, J.; Lamond, A. I. *Nat. Rev. Mol. Cell Biol.* **2007**, *8*, 574-585.

(118) Nucleolar function and size in cancer cells. Derenzini, M.; Trere, D.; Pession, A.; Montanaro, L.; Sirri, V.; Ochs, R. L. *Am. J. Pathol.* **1998**, *152*, 1291-1297.

(119) Nucleolar size indicates the rapidity of cell proliferation in cancer tissues. Derenzini, M.; Trere, D.; Pession, A.; Govoni, M.; Sirri, V.; Chieco, P. *J. Pathol.* **2000**, *191*, 181-186.

(120) Nucleolus, ribosomes, and cancer. Montanaro, L.; Trere, D.; Derenzini, M. *Am. J. Pathol.* **2008**, *173*, 301-310.

(121) Does the ribosome translate cancer? Ruggero, D.; Pandolfi, P. P. *Nat. Rev. Cancer* **2003**, *3*, 179-192.

(122) What the nucleolus says to a tumour pathologist. Derenzini, M.; Montanaro, L.; Trere, D. *Histopathology* **2009**, *54*, 753-762.

(123) The RNA polymerase I transcription machinery: An emerging target for the treatment of cancer. Drygin, D.; Rice, W. G.; Grummt, I. *Annu. Rev. Pharmacol. Toxicol.* **2010**, *50*, 131-156.

(124) Targeting RNA polymerase I with an oral small molecule CX-5461 inhibits ribosomal rna synthesis and solid tumor growth. Drygin, D.; Lin, A.; Bliesath, J.; Ho, C. B.; O'Brien, S. E.; Proffitt, C.; Omori, M.; Haddach, M.; Schwaebe, M. K.; Siddiqui-Jain, A.; Streiner, N.; Quin, J. E.; Sanij, E.; Bywater, M. J.; Hannan, R. D.; Ryckman, D.; Anderes, K.; Rice, W. G. *Cancer Res.* **2011**, *71*, 1418-1430.

(125) Targeting RNA polymerase I transcription and the nucleolus for cancer therapy. Hannan, R. D.; Drygin, D.; Pearson, R. B. *Expert Opin. Ther. Targets* **2013**, *17*, 873-878.

(126) Chemotherapeutic drugs inhibit ribosome biogenesis at various levels. Burger, K.; Muhl, B.; Harasim, T.; Rohrmoser, M.; Malamoussi, A.; Orban, M.; Kellner, M.; Gruber-Eber, A.; Kremmer, E.; Holzel, M.; Eick, D. *J. Biol. Chem.* **2010**, *285*, 12416-12425.

(127) Inhibition of RNA polymerase I as a therapeutic strategy to promote cancer-specific activation of p53. Bywater, M. J.; Poortinga, G.; Sanij, E.; Hein, N.; Peck, A.; Cullinane, C.; Wall, M.; Cluse, L.; Drygin, D.; Anderes, K.; Huser, N.; Proffitt, C.; Bliesath, J.; Haddach, M.; Schwaebe, M. K.; Ryckman, D. M.; Rice, W. G.; Schmitt, C.; Lowe, S.

W.; Johnstone, R. W.; Pearson, R. B.; McArthur, G. A.; Hannan, R. D. *Cancer Cell* **2012**, *22*, 51-65.

(128) Discovery of CX-5461, the first direct and selective inhibitor of RNA polymerase I, for cancer therapeutics. Haddach, M.; Schwaebe, M. K.; Michaux, J.; Nagasawa, J.; O'Brien, S. E.; Whitten, J. P.; Pierre, F.; Kerdoncuff, P.; Darjania, L.; Stansfield, R.; Drygin, D.; Anderes, K.; Proffitt, C.; Bliesath, J.; Siddiqui-Jain, A.; Omori, M.; Huser, N.; Rice, W. G.; Ryckman, D. M. *ACS Med. Chem. Lett.* **2012**, *3*, 602-606.

(129) The nucleolus as a fundamental regulator of the p53 response and a new target for cancer therapy. Woods, S. J.; Hannan, K. M.; Pearson, R. B.; Hannan, R. D. *Biochim. Biophys. Acta* **2015**, *1849*, 821-829.

(130) Disruption of the nucleolus mediates stabilization of p53 in response to DNA damage and other stresses. Rubbi, C. P.; Milner, J. *EMBO J.* **2003**, *22*, 6068-6077.

(131) Activation of the tumor suppressor p53 upon impairment of ribosome biogenesis. Bursac, S.; Brdovcak, M. C.; Donati, G.; Volarevic, S. *Biochim. Biophys. Acta* **2014**, *1842*, 817-830.

(132) Angiogenin functionally interacts with p53 and regulates p53-mediated apoptosis and cell survival. Sadagopan, S.; Veettil, M. V.; Chakraborty, S.; Sharma-Walia, N.; Paudel, N.; Bottero, V.; Chandran, B. *Oncogene* **2012**, *31*, 4835-4847.

(133) Chimeric anti-angiogenin antibody cAb 26-2F inhibits the formation of human breast cancer xenografts in athymic mice. Piccoli, R.; Olson, K. A.; Vallee, B. L.; Fett, J. W. *Proc. Natl. Acad. Sci. USA* **1998**, *95*, 4579-4583.

(134) Prevention of human prostate tumor metastasis in athymic mice by antisense targeting of human angiogenin. Olson, K. A.; Byers, H. R.; Key, M. E.; Fett, J. W. *Clin. Cancer Res.* **2001**, *7*, 3598-3605.

(135) Inhibition of prostate carcinoma establishment and metastatic growth in mice by an antiangiogenin monoclonal antibody. Olson, K. A.; Byers, H. R.; Key, M. E.; Fett, J. W. *Int. J. Cancer* **2002**, *98*, 923-929.

(136) A small-molecule inhibitor of the ribonucleolytic activity of human angiogenin that possesses antitumor activity. Kao, R. Y.; Jenkins, J. L.; Olson, K. A.; Key, M. E.; Fett, J. W.; Shapiro, R. *Proc. Natl. Acad. Sci. USA* **2002**, *99*, 10066-10071.

(137) Neurovascular signalling defects in neurodegeneration. Zacchigna, S.; Lambrechts, D.; Carmeliet, P. *Nat. Rev. Neurosci.* **2008**, *9*, 169-181.

(138) Are anti-angiogenic drugs useful in neurodegenerative disorders? De Filippis, D.; Cipriano, M.; Esposito, G.; Scuderi, C.; Steardo, L.; Iuvone, T. *CNS Neurol. Disord. Drug Targets* **2010**, *9*, 807-812.

(139) Deletion of the hypoxia-response element in the vascular endothelial growth factor promoter causes motor neuron degeneration. Oosthuyse, B.; Moons, L.; Storkebaum, E.; Beck, H.; Nuyens, D.; Brusselmans, K.; Van Dorpe, J.; Hellings, P.; Gorselink, M.; Heymans, S.; Theilmeier, G.; Dewerchin, M.; Laudenbach, V.; Vermylen, P.; Raat, H.; Acker, T.; Vleminckx, V.; Van Den Bosch, L.; Cashman, N.; Fujisawa, H.; Drost, M. R.; Sciot, R.; Bruyninckx, F.; Hicklin, D. J.; Ince, C.; Gressens, P.; Lupu, F.; Plate, K. H.; Robberecht, W.; Herbert, J. M.; Collen, D.; Carmeliet, P. *Nat. Genet.* **2001**, *28*, 131-138.

(140) A new piece of the ALS puzzle. Cleveland, J. L. *Nat. Genet.* **2003**, *34*, 357-358.

(141) VEGF is a modifier of amyotrophic lateral sclerosis in mice and humans and protects motoneurons against ischemic death. Lambrechts, D.; Storkebaum, E.; Morimoto, M.; Del-Favero, J.; Desmet, F.; Marklund, S. L.; Wyns, S.; Thijs, V.; Andersson, J.; van Marion, I.; Al-Chalabi, A.; Bornes, S.; Musson, R.; Hansen, V.; Beckman, L.; Adolfsson, R.; Pall, H. S.; Prats, H.; Vermeire, S.; Rutgeerts, P.; Katayama, S.; Awata, T.; Leigh, N.; Lang-Lazdunski, L.; Dewerchin, M.; Shaw, C.; Moons, L.; Vlietinck, R.; Morrison, K. E.; Robberecht, W.; Van Broeckhoven, C.; Collen, D.; Andersen, P. M.; Carmeliet, P. *Nat. Genet.* **2003**, *34*, 383-394.

(142) VEGF delivery with retrogradely transported lentivector prolongs survival in a mouse ALS model. Azzouz, M.; Ralph, G. S.; Storkebaum, E.; Walmsley, L. E.; Mitrophanous, K. A.; Kingsman, S. M.; Carmeliet, P.; Mazarakis, N. D. *Nature* **2004**, *429*, 413-417.

(143) Gene and protein therapies utilizing VEGF for ALS. Keifer, O. P., Jr.; O'Connor, D. M.; Boulis, N. M. *Pharmacol. Ther.* **2014**, *141*, 261-271.

(144) [Amyotrophic lateral sclerosis]. Bonduelle, M. *Rev. Prat.* **1965**, *15*, 3911-3924.

(145) The 'omics' of amyotrophic lateral sclerosis. Caballero-Hernandez, D.; Toscano, M. G.; Cejudo-Guillen, M.; Garcia-Martin, M. L.; Lopez, S.; Franco, J. M.; Quintana, F. J.; Roodveldt, C.; Pozo, D. *Trends Mol. Med.* **2016**, *22*, 53-67.

(146) Jean Martin Charcot, 1825-1893. An appreciation. Thorburn, A. L. *Br. J. Vener. Dis.* **1967**, *43*, 77-80.

(147) Jean Martin Charcot (1825-1893): Pathologist who shaped modern neurology. Tan, S. Y.; Shigaki, D. *Singapore Med. J.* **2007**, *48*, 383-384.

(148) Lou Gehrig: The iron man. Brady, G. M. *Manuscripts (NY)* **1980**, *32*, 84-89.

(149) Incidence of amyotrophic lateral sclerosis in three counties in western Washington state. McGuire, V.; Longstreth, W. T., Jr.; Koepsell, T. D.; van Belle, G. *Neurology* **1996**, *47*, 571-573.

(150) The changing scene of amyotrophic lateral sclerosis. Robberecht, W.; Philips, T. *Nat. Rev. Neurosci.* **2013**, *14*, 248-264.

(151) Familial amyotrophic lateral sclerosis. Siddique, T.; Hentati, A. *Clin. Neurosci.* **1995**, *3*, 338-347.

(152) Significantly lower incidence of cancer among patients with Huntington disease: An apoptotic effect of an expanded polyglutamine tract? Sorensen, S. A.; Fenger, K.; Olsen, J. H. *Cancer* **1999**, *86*, 1342-1346.

(153) Expanded GGGGCC hexanucleotide repeat in noncoding region of C9ORF72 causes chromosome 9p-linked FTD and ALS. DeJesus-Hernandez, M.; Mackenzie, I. R.; Boeve, B. F.; Boxer, A. L.; Baker, M.; Rutherford, N. J.; Nicholson, A. M.; Finch, N. A.; Flynn, H.; Adamson, J.; Kouri, N.; Wojtas, A.; Sengdy, P.; Hsiung, G. Y.; Karydas, A.; Seeley, W. W.; Josephs, K. A.; Coppola, G.; Geschwind, D. H.; Wszolek, Z. K.; Feldman, H.; Knopman, D. S.; Petersen, R. C.; Miller, B. L.; Dickson, D. W.; Boylan, K. B.; Graff-Radford, N. R.; Rademakers, R. *Neuron* **2011**, *72*, 245-256.

(154) A hexanucleotide repeat expansion in C9ORF72 is the cause of chromosome 9p21-linked ALS-FTD. Renton, A. E.; Majounie, E.; Waite, A.; Simon-Sanchez, J.; Rollinson, S.; Gibbs, J. R.; Schymick, J. C.; Laaksovirta, H.; van Swieten, J. C.; Myllykangas, L.; Kalimo, H.; Paetau, A.; Abramzon, Y.; Remes, A. M.; Kaganovich, A.; Scholz, S. W.; Duckworth, J.; Ding, J.; Harmer, D. W.; Hernandez, D. G.; Johnson, J. O.; Mok, K.; Ryten, M.; Trabzuni, D.; Guerreiro, R. J.; Orrell, R. W.; Neal, J.; Murray, A.; Pearson, J.;

Jansen, I. E.; Sondervan, D.; Seelaar, H.; Blake, D.; Young, K.; Halliwell, N.; Callister, J. B.; Toulson, G.; Richardson, A.; Gerhard, A.; Snowden, J.; Mann, D.; Neary, D.; Nalls, M. A.; Peuralinna, T.; Jansson, L.; Isoviita, V. M.; Kaivorinne, A. L.; Holtta-Vuori, M.; Ikonen, E.; Sulkava, R.; Benatar, M.; Wuu, J.; Chio, A.; Restagno, G.; Borghero, G.; Sabatelli, M.; Heckerman, D.; Rogaeva, E.; Zinman, L.; Rothstein, J. D.; Sendtner, M.; Drepper, C.; Eichler, E. E.; Alkan, C.; Abdullaev, Z.; Pack, S. D.; Dutra, A.; Pak, E.; Hardy, J.; Singleton, A.; Williams, N. M.; Heutink, P.; Pickering-Brown, S.; Morris, H. R.; Tienari, P. J.; Traynor, B. J. *Neuron* **2011**, *72*, 257-268.

(155) Amyotrophic lateral sclerosis and structural defects in Cu,Zn superoxide dismutase. Deng, H. X.; Hentati, A.; Tainer, J. A.; Iqbal, Z.; Cayabyab, A.; Hung, W. Y.; Getzoff, E. D.; Hu, P.; Herzfeldt, B.; Roos, R. P.; et al. *Science* **1993**, *261*, 1047-1051.

(156) Genetic determinants of amyotrophic lateral sclerosis as therapeutic targets. Bosco, D. A.; Landers, J. E. *CNS Neurol. Disord. Drug Targets* **2010**, *9*, 779-790.

(157) Neuropathology of amyotrophic lateral sclerosis and its variants. Saberi, S.; Stauffer, J. E.; Schulte, D. J.; Ravits, J. *Neurol. Clin.* **2015**, *33*, 855-876.

(158) The utility of superoxide dismutase in studying free radical reactions. I. Radicals generated by the interaction of sulfite, dimethyl sulfoxide, and oxygen. McCord, J. M.; Fridovich, I. *J. Biol. Chem.* **1969**, *244*, 6056-6063.

(159) Superoxide dismutase: The first twenty years (1968-1988). McCord, J. M.; Fridovich, I. *Free Radic. Biol. Med.* **1988**, *5*, 363-369.

(160) Structure and mechanism of copper, zinc superoxide dismutase. Tainer, J. A.; Getzoff, E. D.; Richardson, J. S.; Richardson, D. C. *Nature* **1983**, *306*, 284-287.

(161) SOD1 function and its implications for amyotrophic lateral sclerosis pathology: New and renascent themes. Bunton-Stasyshyn, R. K.; Saccon, R. A.; Fratta, P.; Fisher, E. M. *Neuroscientist* **2015**, *21*, 519-529.

(162) An emerging role for misfolded wild-type SOD1 in sporadic als pathogenesis. Rotunno, M. S.; Bosco, D. A. *Front. Cell Neurosci.* **2013**, *7*, 253.

(163) Mechanisms of mutant SOD1 induced mitochondrial toxicity in amyotrophic lateral sclerosis. Vehvilainen, P.; Koistinaho, J.; Gundars, G. *Front. Cell Neurosci.* **2014**, *8*, 126.

(164) SOD1 misplacing and mitochondrial dysfunction in amyotrophic lateral sclerosis pathogenesis. Tafuri, F.; Ronchi, D.; Magri, F.; Comi, G. P.; Corti, S. *Front. Cell Neurosci.* **2015**, *9*, 336.

(165) Mutant SOD1 mediated pathogenesis of amyotrophic lateral sclerosis. Kaur, S. J.; McKeown, S. R.; Rashid, S. *Gene* **2016**, *577*, 109-118.

(166) C9ORF72 amyotrophic lateral sclerosis and frontotemporal dementia: Gain or loss of function? Mizielinska, S.; Isaacs, A. M. *Curr. Opin. Neurol.* **2014**, *27*, 515-523.

(167) Biomarker development for C9ORF72 repeat expansion in ALS. Mendez, E. F.; Sattler, R. *Brain Res.* **2015**, *1607*, 26-35.

(168) Large-scale screening in sporadic amyotrophic lateral sclerosis identifies genetic modifiers in C9ORF72 repeat carriers. Dekker, A. M.; Seelen, M.; van Doormaal, P. T.; van Rheenen, W.; Bothof, R. J.; van Riessen, T.; Brands, W. J.; van der Kooi, A. J.; de Visser, M.; Voermans, N. C.; Pasterkamp, R. J.; Veldink, J. H.; van den Berg, L. H.; van Es, M. A. *Neurobiol. Aging* **2016**, *39*, 220.e229-220.e215.

(169) The C9ORF72 repeat expansion disrupts nucleocytoplasmic transport. Zhang, K.; Donnelly, C. J.; Haeusler, A. R.; Grima, J. C.; Machamer, J. B.; Steinwald, P.; Daley, E.

L.; Miller, S. J.; Cunningham, K. M.; Vidensky, S.; Gupta, S.; Thomas, M. A.; Hong, I.; Chiu, S. L.; Huganir, R. L.; Ostrow, L. W.; Matunis, M. J.; Wang, J.; Sattler, R.; Lloyd, T. E.; Rothstein, J. D. *Nature* **2015**, *525*, 56-61.

(170) GGGGCC repeat expansion in C9ORF72 compromises nucleocytoplasmic transport. Freibaum, B. D.; Lu, Y.; Lopez-Gonzalez, R.; Kim, N. C.; Almeida, S.; Lee, K. H.; Badders, N.; Valentine, M.; Miller, B. L.; Wong, P. C.; Petrucelli, L.; Kim, H. J.; Gao, F. B.; Taylor, J. P. *Nature* **2015**, *525*, 129-133.

(171) Modifiers of C9ORF72 dipeptide repeat toxicity connect nucleocytoplasmic transport defects to FTD/ALS. Jovicic, A.; Mertens, J.; Boeynaems, S.; Bogaert, E.; Chai, N.; Yamada, S. B.; Paul, J. W., 3rd; Sun, S.; Herdy, J. R.; Bieri, G.; Kramer, N. J.; Gage, F. H.; Van Den Bosch, L.; Robberecht, W.; Gitler, A. D. *Nat. Neurosci.* **2015**, *18*, 1226-1229.

(172) Angiogenin loss-of-function mutations in amyotrophic lateral sclerosis. Wu, D.; Yu, W.; Kishikawa, H.; Folkerth, R. D.; Iafrate, A. J.; Shen, Y.; Xin, W.; Sims, K.; Hu, G. F. *Ann. Neurol.* **2007**, *62*, 609-617.

(173) Identification of new ANG gene mutations in a large cohort of Italian patients with amyotrophic lateral sclerosis. Gellera, C.; Colombrita, C.; Ticozzi, N.; Castellotti, B.; Bragato, C.; Ratti, A.; Taroni, F.; Silani, V. *Neurogenetics* **2008**, *9*, 33-40.

(174) Characterization of human angiogenin variants implicated in amyotrophic lateral sclerosis. Crabtree, B.; Thiyagarajan, N.; Prior, S. H.; Wilson, P.; Iyer, S.; Ferns, T.; Shapiro, R.; Brew, K.; Subramanian, V.; Acharya, K. R. *Biochemistry* **2007**, *46*, 11810-11818.

(175) Molecular mechanisms in amyotrophic lateral sclerosis: The role of angiogenin, a secreted rnase. Aparicio-Erriu, I. M.; Prehn, J. *Front. Neurosci.* **2012**, *6*, 167.

(176) Prediction of functional loss of human angiogenin mutants associated with ALS by molecular dynamics simulations. Padhi, A. K.; Jayaram, B.; Gomes, J. *Sci. Rep.* **2013**, *3*, 1225.

(177) A new role for angiogenin in neurite growth and pathfinding: Implications for amyotrophic lateral sclerosis. Subramanian, V.; Feng, Y. *Hum. Mol. Genet.* **2007**, *16*, 1445-1453.

(178) Computational and functional characterization of angiogenin mutations, and correlation with amyotrophic lateral sclerosis. Padhi, A. K.; Banerjee, K.; Gomes, J.; Banerjee, M. *PLoS One* **2014**, *9*, e111963.

(179) Elevated serum angiogenin levels in ALS. Cronin, S.; Greenway, M. J.; Ennis, S.; Kieran, D.; Green, A.; Prehn, J. H.; Hardiman, O. *Neurology* **2006**, *67*, 1833-1836.

(180) Angiogenin levels and ANG genotypes: Dysregulation in amyotrophic lateral sclerosis. McLaughlin, R. L.; Phukan, J.; McCormack, W.; Lynch, D. S.; Greenway, M.; Cronin, S.; Saunders, J.; Slowik, A.; Tomik, B.; Andersen, P. M.; Bradley, D. G.; Jakeman, P.; Hardiman, O. *PLoS One* **2010**, *5*, e15402.

(181) Zymography: A single-step staining method for quantitation of proteolytic activity on substrate gels. Leber, T. M.; Balkwill, F. R. *Anal. Biochem.* **1997**, *249*, 24-28.

(182) Control of motoneuron survival by angiogenin. Kieran, D.; Sebastia, J.; Greenway, M. J.; King, M. A.; Connaughton, D.; Concannon, C. G.; Fenner, B.; Hardiman, O.; Prehn, J. H. *J. Neurosci.* **2008**, *28*, 14056-14061.

(183) Angiogenin protects motoneurons against hypoxic injury. Sebastia, J.; Kieran, D.; Breen, B.; King, M. A.; Netteland, D. F.; Joyce, D.; Fitzpatrick, S. F.; Taylor, C. T.; Prehn, J. H. *Cell Death Differ.* **2009**, *16*, 1238-1247.

(184) Human angiogenin presents neuroprotective and migration effects in neuroblastoma cells. Cho, G. W.; Kang, B. Y.; Kim, S. H. *Mol. Cell Biochem.* **2010**, *340*, 133-141.

(185) Structural and molecular insights into the mechanism of action of human angiogenin-ALS variants in neurons. Thiyagarajan, N.; Ferguson, R.; Subramanian, V.; Acharya, K. R. *Nat. Commun.* **2012**, *3*, 1121.

(186) Angiogenin cleaves tRNA and promotes stress-induced translational repression. Yamasaki, S.; Ivanov, P.; Hu, G. F.; Anderson, P. *J. Cell Biol.* **2009**, *185*, 35-42.

(187) Angiogenin-induced tRNA fragments inhibit translation initiation. Ivanov, P.; Emara, M. M.; Villen, J.; Gygi, S. P.; Anderson, P. *Mol. Cell* **2011**, *43*, 613-623.

(188) G-quadruplex structures contribute to the neuroprotective effects of angiogenin-induced trna fragments. Ivanov, P.; O'Day, E.; Emara, M. M.; Wagner, G.; Lieberman, J.; Anderson, P. *Proc. Natl. Acad. Sci. USA* **2014**, *111*, 18201-18206.

(189) Stress granules: The tao of RNA triage. Anderson, P.; Kedersha, N. *Trends Biochem. Sci.* **2008**, *33*, 141-150.

(190) Eukaryotic stress granules: The ins and outs of translation. Buchan, J. R.; Parker, R. *Mol. Cell* **2009**, *36*, 932-941.

(191) Stress granules and cell signaling: More than just a passing phase? Kedersha, N.; Ivanov, P.; Anderson, P. *Trends Biochem. Sci.* **2013**, *38*, 494-506.

(192) Angiogenin-induced tRNA-derived stress-induced RNAs promote stress-induced stress granule assembly. Emara, M. M.; Ivanov, P.; Hickman, T.; Dawra, N.; Tisdale, S.; Kedersha, N.; Hu, G. F.; Anderson, P. *J. Biol. Chem.* **2010**, *285*, 10959-10968.

(193) Astrocytes: Biology and pathology. Sofroniew, M. V.; Vinters, H. V. *Acta Neuropathol.* **2010**, *119*, 7-35.

(194) Heterogeneity of reactive astrocytes. Anderson, M. A.; Ao, Y.; Sofroniew, M. V. *Neurosci. Lett.* **2014**, *565*, 23-29.

(195) Astrogliosis. Sofroniew, M. V. *Cold Spring Harb. Perspect. Biol.* **2015**, *7*, a020420.

(196) Astrocytes expressing ALS-linked mutated SOD1 release factors selectively toxic to motor neurons. Nagai, M.; Re, D. B.; Nagata, T.; Chalazonitis, A.; Jessell, T. M.; Wichterle, H.; Przedborski, S. *Nat. Neurosci.* **2007**, *10*, 615-622.

(197) Mutant SOD1-expressing astrocytes release toxic factors that trigger motoneuron death by inducing hyperexcitability. Fritz, E.; Izaurieta, P.; Weiss, A.; Mir, F. R.; Rojas, P.; Gonzalez, D.; Rojas, F.; Brown, R. H., Jr.; Madrid, R.; van Zundert, B. *J. Neurophysiol.* **2013**, *109*, 2803-2814.

(198) Nrf2—a therapeutic target for the treatment of neurodegenerative diseases. Johnson, D. A.; Johnson, J. A. *Free Radic. Biol. Med.* **2015**, *88*, 253-267.

(199) Role of Nrf2-dependent ARE-driven antioxidant pathway in neuroprotection. Li, J.; Calkins, M. J.; Johnson, D. A.; Johnson, J. A. *Methods Mol. Biol.* **2007**, *399*, 67-78.

(200) Nrf2 activation in astrocytes protects against neurodegeneration in mouse models of familial amyotrophic lateral sclerosis. Vargas, M. R.; Johnson, D. A.; Sirkis, D. W.; Messing, A.; Johnson, J. A. *J. Neurosci.* **2008**, *28*, 13574-13581.

(201) Astrogliosis in amyotrophic lateral sclerosis: Role and therapeutic potential of astrocytes. Vargas, M. R.; Johnson, J. A. *Neurotherapeutics* **2010**, *7*, 471-481.

(202) Angiogenin induces modifications in the astrocyte secretome: Relevance to amyotrophic lateral sclerosis. Skorupa, A.; Urbach, S.; Vigy, O.; King, M. A.; Chaumont-Dubel, S.; Prehn, J. H.; Marin, P. *J. Proteomics* **2013**, *91*, 274-285.

(203) Angiogenin variants in Parkinson disease and amyotrophic lateral sclerosis. van Es, M. A.; Schelhaas, H. J.; van Vught, P. W.; Ticozzi, N.; Andersen, P. M.; Groen, E. J.; Schulte, C.; Blauw, H. M.; Koppers, M.; Diekstra, F. P.; Fumoto, K.; LeClerc, A. L.; Keagle, P.; Bloem, B. R.; Scheffer, H.; van Nuenen, B. F.; van Blitterswijk, M.; van Rheenen, W.; Wills, A. M.; Lowe, P. P.; Hu, G. F.; Yu, W.; Kishikawa, H.; Wu, D.; Folkerth, R. D.; Mariani, C.; Goldwurm, S.; Pezzoli, G.; Van Damme, P.; Lemmens, R.; Dahlberg, C.; Birve, A.; Fernandez-Santiago, R.; Waibel, S.; Klein, C.; Weber, M.; van der Kooi, A. J.; de Visser, M.; Verbaan, D.; van Hilten, J. J.; Heutink, P.; Hennekam, E. A.; Cuppen, E.; Berg, D.; Brown, R. H., Jr.; Silani, V.; Gasser, T.; Ludolph, A. C.; Robberecht, W.; Ophoff, R. A.; Veldink, J. H.; Pasterkamp, R. J.; de Bakker, P. I.; Landers, J. E.; van de Warrenburg, B. P.; van den Berg, L. H. *Ann. Neurol.* **2011**, *70*, 964-973.

(204) Angiogenin variation and Parkinson disease. Rayaprolu, S.; Soto-Ortolaza, A.; Rademakers, R.; Uitti, R. J.; Wszolek, Z. K.; Ross, O. A. *Ann. Neurol.* **2012**, *71*, 725-727; author reply 727-728.

(205) Progress in clinical neurosciences: Parkinson's disease with dementia and dementia with Lewy bodies. Camicioli, R.; Fisher, N. *Can. J. Neurol. Sci.* **2004**, *31*, 7-21.

(206) The prevalence of Parkinson's disease: A systematic review and meta-analysis. Pringsheim, T.; Jette, N.; Frolkis, A.; Steeves, T. D. *Mov. Disord.* **2014**, *29*, 1583-1590.

(207) Astrocyte-specific overexpression of Nrf2 delays motor pathology and synuclein aggregation throughout the CNS in the alpha-synuclein mutant (A53T) mouse model. Gan, L.; Vargas, M. R.; Johnson, D. A.; Johnson, J. A. *J. Neurosci.* **2012**, *32*, 17775-17787.

(208) Targeting alpha-synuclein: Therapeutic options. Dehay, B.; Decressac, M.; Bourdenx, M.; Guadagnino, I.; Fernagut, P. O.; Tamburrino, A.; Bassil, F.; Meissner, W. G.; Bezard, E. *Mov. Disord.* **2016**, *1*, 1-7.

(209) Microarray expression analysis of human dopaminergic neuroblastoma cells after RNA interference of SNCA—a key player in the pathogenesis of parkinson's disease. Habig, K.; Walter, M.; Stappert, H.; Riess, O.; Bonin, M. *Brain Res.* **2009**, *1256*, 19-33.

(210) A neuroprotective role for angiogenin in models of Parkinson's disease. Steidinger, T. U.; Standaert, D. G.; Yacoubian, T. A. *J. Neurochem.* **2011**, *116*, 334-341.

(211) Angiogenin in Parkinson disease models: Role of Akt phosphorylation and evaluation of AAV-mediated angiogenin expression in MPTP treated mice. Steidinger, T. U.; Slone, S. R.; Ding, H.; Standaert, D. G.; Yacoubian, T. A. *PLoS One* **2013**, *8*, e56092.

(212) Neurotoxicity of cancer chemotherapy. Yang, M.; Moon, C. *Neural. Regen. Res.* **2013**, *8*, 1606-1614.

(213) p53 and disease: When the guardian angel fails. Royds, J. A.; Iacopetta, B. *Cell Death Differ.* **2006**, *13*, 1017-1026.

(214) Clinical patterns and biological correlates of cognitive dysfunction associated with cancer therapy. Dietrich, J.; Monje, M.; Wefel, J.; Meyers, C. *Oncologist* **2008**, *13*, 1285-1295.

(215) Chemotherapy, cognitive impairment and hippocampal toxicity. Dietrich, J.; Prust, M.; Kaiser, J. *Neuroscience* **2015**, *309*, 224-232.

(216) Chemotherapy-related cognitive dysfunction. Wefel, J. S.; Schagen, S. B. *Curr. Neurol. Neurosci. Rep.* **2012**, *12*, 267-275.

(217) Can serum angiogenin be used to improve the diagnostic performance in prostate cancer screening? Pina, F.; Botelho, F.; Lopes, T.; Lopes, I.; Figueiredo, G.; Portugal, R.; Ferro, A.; Cruz, F.; Barros, H.; Lunet, N. *Eur. J. Cancer Prev.* **2014**, *23*, 166-172.

(218) Angiogenin. Riordan, J. F. *Methods Enzymol.* **2001**, *341*, 263-273.

(219) Site-directed mutagenesis of histidine-13 and histidine-114 of human angiogenin. Alanine derivatives inhibit angiogen-induced angiogenesis. Shapiro, R.; Vallee, B. L. *Biochemistry* **1989**, *28*, 7401-7408.

(220) Epigenetic control of RNA polymerase I transcription in mammalian cells. Grummt, I.; Längst, G. *Biochim. Biophys. Acta* **2013**, *1829*, 393-404.

(221) Interaction of noncoding RNA with the rDNA promoter mediates recruitment of DNMT3b and silencing of rRNA genes. Schmitz, K.-M.; Mayer, C.; Postepska, A.; Grummt, I. *Genes Develop.* **2010**, *24*, 2264-2269.

(222) Large-scale organization of ribosomal DNA chromatin is regulated by TIP5. Zillner, K.; Filarsky, M.; Rachow, K.; Weinberger, M.; Langst, G.; Nemeth, A. *Nucleic Acids Res.* **2013**, *41*, 5251-5262.

(223) Alteration of the enzymatic specificity of human angiogenin by site-directed mutagenesis. Curran, T. P.; Shapiro, R.; Riordan, J. F. *Biochemistry* **1993**, *32*, 2307-2313.

(224) Interaction of nucleolin with ribosomal RNA genes and its role in RNA polymerase I transcription. Cong, R.; Das, S.; Ugrinova, I.; Kumar, S.; Mongelard, F.; Wong, J.; Bouvet, P. *Nucleic Acids Res.* **2012**, *40*, 9441-9454.

(225) Ribonuclease inhibitor as an intracellular sentry. Haigis, M. C.; Kurten, E. L.; Raines, R. T. *Nucleic Acids Res.* **2003**, *31*, 1024-1032.

(226) Evasion of ribonuclease inhibitor as a determinant of ribonuclease cytotoxicity. Rutkoski, T. J.; Raines, R. T. *Curr. Pharm. Biotechnol.* **2008**, *9*, 185-189.

(227) Genetic selection for critical residues in ribonucleases. Smith, B. D.; Raines, R. T. *J. Mol. Biol.* **2006**, *362*, 459-478.

(228) Sequence- and structure-based prediction of eukaryotic protein phosphorylation sites. Blom, N.; Gammeltoft, S.; Brunak, S. *J. Mol. Biol.* **1999**, *294*, 1351-1362.

(229) The bisindoylmaleimide GF 109203X is a potent and selective inhibitor of protein kinase C. Toullec, D.; Pianetti, P.; Coste, H.; Bellevergue, P.; Grand-Perret, T.; Ajakane, M.; Baudet, V.; Boissin, P.; Boursier, E.; Loriolle, F.; Duhamel, L.; Charon, D.; Kirilovsky, J. *J. Biol. Chem.* **1991**, *266*, 15771-15781.

(230) Inhibition of cyclin-dependent kinases by purine analogues. Crystal structure of human CDK2 complexed with roscovitine. De Azevedo, W. F.; Leclerc, S.; Miejer, L.; Havlicek, L.; Strnad, M.; Kim, S.-H. *Eur. J. Biochem.* **1997**, *2443*, 518-526.

(231) *In vitro* angiogenesis: Endothelial cell tube formation on gelled basement membrane extract. Arnaoutova, I.; Kleinman, H. K. *Nat. Protoc.* **2010**, *5*, 628-635.

(232) Ribonuclease A. Raines, R. T. *Chem. Rev.* **1998**, *98*, 1045-1065.

(233) *Signal transduction: Principles, pathways, and processes*; Cantley, L. C.; Hunter, T.; Sever, R.; Thorner, J., Eds.; Cold Spring Harbor Laboratory Press: Cold Spring Harbor, NY, **2014**.

(234) *Cell signaling*. Lim, W.; Mayer, B.; Pawson, T.; Garland Science: New York, NY, 2014.

(235) CRISPR-mediated modular RNA-guided regulation of transcription in eukaryotes. Gilbert, L. A.; Larson, M. H.; Morsut, L.; Liu, Z.; Brar, G. A.; Torres, S. E.; Stern-Ginossar, N.; Brandman, O.; Whitehead, E. H.; Doudna, J. A.; Lim, W. A.; Weissman, J. S.; Qi, L. S. *Cell* **2013**, *154*, 442-451.

(236) Engineering complex synthetic transcriptional programs with CRISPR RNA scaffolds. Zalatan, J. G.; Lee, M. E.; Almeida, R.; Gilbert, L. A.; Whitehead, E. H.; La Russa, M.; Tsai, J. C.; Weissman, J. S.; Dueber, J. E.; Qi, L. S.; Lim, W. A. *Cell* **2015**, *160*, 339-350.

(237) Flavopiridol: Pleiotropic biological effects enhance its anti-cancer activity. Newcomb, E. W. *Anticancer Drugs* **2004**, *15*, 411-419.

(238) Enzastaurin. Chen, Y. B.; LaCasce, A. S. *Expert Opin. Investig. Drugs* **2008**, *17*, 939-944.

(239) Tuning the pK_a of fluorescein to optimize binding assays. Lavis, L. D.; Rutkoski, T. J.; Raines, R. T. *Anal. Chem.* **2007**, *79*, 6775-6782.

(240) Emerging molecular biomarker targets for amyotrophic lateral sclerosis. Costa, J.; de Carvalho, M. *Clin. Chim. Acta* **2016**, *455*, 7-14.

(241) VEGF and ALS. Sathasivam, S. *Neurosci. Res.* **2008**, *62*, 71-77.

(242) Neuro-vascular link: From genetic insights to therapeutic perspectives. Carmeliet, P. *Bull. Mem. Acad. R. Med. Belg.* **2008**, *163*, 445-451.

(243) The role of oxidative stress in neurodegenerative diseases. Kim, G. H.; Kim, J. E.; Rhie, S. J.; Yoon, S. *Exp. Neurobiol.* **2015**, *24*, 325-340.

(244) Emerging mechanisms of molecular pathology in ALS. Peters, O. M.; Ghasemi, M.; Brown, R. H., Jr. *J. Clin. Invest.* **2015**, *125*, 1767-1779.

(245) Free radicals and antioxidants in normal physiological functions and human disease. Valko, M.; Leibfritz, D.; Moncol, J.; Cronin, M. T.; Mazur, M.; Telser, J. *Int. J. Biochem. Cell Biol.* **2007**, *39*, 44-84.

(246) Clinical perspective on oxidative stress in sporadic amyotrophic lateral sclerosis. D'Amico, E.; Factor-Litvak, P.; Santella, R. M.; Mitsumoto, H. *Free Radic. Biol. Med.* **2013**, *65*, 509-527.

(247) Paradoxical roles of antioxidant enzymes: Basic mechanisms and health implications. Lei, X. G.; Zhu, J. H.; Cheng, W. H.; Bao, Y.; Ho, Y. S.; Reddi, A. R.; Holmgren, A.; Arner, E. S. *Physiol. Rev.* **2016**, *96*, 307-364.

(248) Applications of the Keap1-Nrf2 system for gene and cell therapy. Kanninen, K. M.; Pomeshchik, Y.; Leinonen, H.; Malm, T.; Koistinaho, J.; Levonen, A. L. *Free Radic. Biol. Med.* **2015**, *88*, 350-361.

(249) The Nrf2-ARE pathway: An indicator and modulator of oxidative stress in neurodegeneration. Johnson, J. A.; Johnson, D. A.; Kraft, A. D.; Calkins, M. J.; Jakel, R. J.; Vargas, M. R.; Chen, P. C. *Ann. NY Acad. Sci.* **2008**, *1147*, 61-69.

(250) The Nrf2/ARE pathway as a potential therapeutic target in neurodegenerative disease. Calkins, M. J.; Johnson, D. A.; Townsend, J. A.; Vargas, M. R.; Dowell, J. A.; Williamson, T. P.; Kraft, A. D.; Lee, J. M.; Li, J.; Johnson, J. A. *Antioxid. Redox Signal* **2009**, *11*, 497-508.

(251) Activation of the Nrf2-are pathway in muscle and spinal cord during ALS-like pathology in mice expressing mutant SOD1. Kraft, A. D.; Resch, J. M.; Johnson, D. A.; Johnson, J. A. *Exp. Neurol.* **2007**, *207*, 107-117.

(252) Phosphorylation of Nrf2 at Ser-40 by protein kinase C regulates antioxidant response element-mediated transcription. Huang, H. C.; Nguyen, T.; Pickett, C. B. *J. Biol. Chem.* **2002**, *277*, 42769-42774.

(253) Phosphorylation of Nrf2 at Ser40 by protein kinase C in response to antioxidants leads to the release of Nrf2 from INrf2, but is not required for Nrf2 stabilization/accumulation in the nucleus and transcriptional activation of antioxidant response element-mediated NAD(P)H:quinone oxidoreductase-1 gene expression. Bloom, D. A.; Jaiswal, A. K. *J. Biol. Chem.* **2003**, *278*, 44675-44682.

(254) Activation of the antioxidant response element in primary cortical neuronal cultures derived from transgenic reporter mice. Johnson, D. A.; Andrews, G. K.; Xu, W.; Johnson, J. A. *J. Neurochem.* **2002**, *81*, 1233-1241.

(255) Nuclear factor E2-related factor 2-dependent antioxidant response element activation by tert-butylhydroquinone and sulforaphane occurring preferentially in astrocytes conditions neurons against oxidative insult. Kraft, A. D.; Johnson, D. A.; Johnson, J. A. *J. Neurosci.* **2004**, *24*, 1101-1112.

(256) The modest impact of transcription factor Nrf2 on the course of disease in an ALS animal model. Guo, Y.; Zhang, Y.; Wen, D.; Duan, W.; An, T.; Shi, P.; Wang, J.; Li, Z.; Chen, X.; Li, C. *Lab Invest.* **2013**, *93*, 825-833.

(257) A novel small molecule, *N*-(4-(2-pyridyl)(1,3-thiazol-2-yl))-2-(2,4,6-trimethylphenoxy) acetamide, selectively protects against oxidative stress-induced cell death by activating

the Nrf2-ARE pathway: Therapeutic implications for ALS. Kanno, T.; Tanaka, K.; Yanagisawa, Y.; Yasutake, K.; Hadano, S.; Yoshii, F.; Hirayama, N.; Ikeda, J. E. *Free Radic. Biol. Med.* **2012**, *53*, 2028-2042.

(258) The peroxisome proliferator-activated receptor γ (PPARγ) controls natural protective mechanisms against lipid peroxidation in amyotrophic lateral sclerosis. Benedusi, V.; Martorana, F.; Brambilla, L.; Maggi, A.; Rossi, D. *J. Biol. Chem.* **2012**, *287*, 35899-35911.

(259) Modification of Keap1 cysteine residues by sulforaphane. Hu, C.; Eggler, A. L.; Mesecar, A. D.; van Breemen, R. B. *Chem. Res. Toxicol.* **2011**, *24*, 515-521.

(260) Critical cysteine residues of Kelch-like ECH-associated protein 1 in arsenic sensing and suppression of nuclear factor erythroid 2-related factor 2. He, X.; Ma, Q. *J. Pharmacol. Exp. Ther.* **2010**, *332*, 66-75.

(261) Updated research and applications of small molecule inhibitors of Keap1-Nrf2 protein-protein interaction: A review. Zhuang, C.; Miao, Z.; Sheng, C.; Zhang, W. *Curr. Med. Chem.* **2014**, *21*, 1861-1870.

(262) ALSUntangled No. 31: Protandim. *Amyotroph. Lateral. Scler. Frontotemporal. Degener.* **2015**, *17*, 154-156.

(263) Role of dimethyl fumarate in oxidative stress of multiple sclerosis: A review. Suneetha, A.; Rajeswari, R. K. *J. Chromatogr. B. Analyt. Technol. Biomed. Life Sci.* **2016**, *1019*, 15-20.

(264) From Charcot to Lou Gehrig: Deciphering selective motor neuron death in ALS. Cleveland, D. W.; Rothstein, J. D. *Nat. Rev. Neurosci.* **2001**, *2*, 806-819.

(265) Molecular biology of amyotrophic lateral sclerosis: Insights from genetics. Pasinelli, P.; Brown, R. H. *Nat. Rev. Neurosci.* **2006**, *7*, 710-723.

(266) Motor neuron trophic factors: Therapeutic use in ALS? Gould, T. W.; Oppenheim, R. W. *Brain Res. Rev.* **2011**, *67*, 1-39.

(267) Mechanisms regulating skeletal muscle growth and atrophy. Schiaffino, S.; Dyar, K. A.; Ciciliot, S.; Blaauw, B.; Sandri, M. *FEBS J.* **2013**, *280*, 4294-4314.

(268) Microglia centered pathogenesis in ALS: Insights in cell interconnectivity. Brites, D.; Vaz, A. R. *Front. Cell Neurosci.* **2014**, *8*, 117.

(269) Gene therapy for ALS: Progress and prospects. Azzouz, M. *Biochim. Biophys. Acta* **2006**, *1762*, 1122-1127.

(270) Stem cell-based cell therapy in neurological diseases: A review. Kim, S. U.; de Vellis, J. *J. Neurosci. Res.* **2009**, *87*, 2183-2200.

(271) Efficacy of stem cell therapy in amyotrophic lateral sclerosis: A systematic review and meta-analysis. Moura, M. C.; Novaes, M. R.; Zago, Y. S.; Eduardo, E. J.; Casulari, L. A. *J. Clin. Med. Res.* **2016**, *8*, 317-324.

(272) Riluzole for amyotrophic lateral sclerosis (ALS)/motor neuron disease (MND). Miller, R. G.; Mitchell, J. D.; Lyon, M.; Moore, D. H. *Amyotroph. Lateral Scler. Other Motor. Neuron Disord.* **2003**, *4*, 191-206.

(273) Amyotrophic lateral sclerosis: Progress and prospects for treatment. Dib, M. *Drugs* **2003**, *63*, 289-310.

(274) Oxidative stress in ALS: Key role in motor neuron injury and therapeutic target. Barber, S. C.; Shaw, P. J. *Free Radic. Biol. Med.* **2010**, *48*, 629-641.

(275) Impaired autophagy and defective mitochondrial function: Converging paths on the road to motor neuron degeneration. Edens, B. M.; Miller, N.; Ma, Y. C. *Front. Cell Neurosci.* **2016**, *10*, 44.

(276) Antioxidant therapy in ALS. Pioro, E. P. *Amyotroph. Lateral Scler. Other Motor Neuron Disord.* **2000**, *1 Suppl 4*, 5-12; discussion 13-15.

(277) A systematic review of antioxidant treatment for amyotrophic lateral sclerosis/motor neuron disease. Orrell, R. W.; Lane, R. J.; Ross, M. *Amyotroph. Lateral Scler.* **2008**, *9*, 195-211.

(278) [Development of motor neuron restorative therapy in amyotrophic lateral sclerosis using hepatocyte growth factor]. Aoki, M.; Warita, H.; Suzuki, N.; Itoyama, Y. *Rinsho Shinkeigaku* **2009**, *49*, 814-817.

(279) *S*[+]apomorphine is a CNS penetrating activator of the Nrf2-are pathway with activity in mouse and patient fibroblast models of amyotrophic lateral sclerosis. Mead, R. J.; Higginbottom, A.; Allen, S. P.; Kirby, J.; Bennett, E.; Barber, S. C.; Heath, P. R.; Coluccia, A.; Patel, N.; Gardner, I.; Brancale, A.; Grierson, A. J.; Shaw, P. J. *Free Radic. Biol. Med.* **2013**, *61*, 438-452.

(280) Modulation of mitochondrial dysfunction in neurodegenerative diseases via activation of nuclear factor erythroid-2-related factor 2 by food-derived compounds. Denzer, I.; Munch, G.; Friedland, K. *Pharmacol. Res.* **2016**, *103*, 80-94.

(281) Relevance of oxidative injury in the pathogenesis of motor neuron diseases. Agar, J.; Durham, H. *Amyotroph. Lateral Scler. Other Motor Neuron Disord.* **2003**, *4*, 232-242.

(282) ALS: A disease of motor neurons and their nonneuronal neighbors. Boillee, S.; Vande Velde, C.; Cleveland, D. W. *Neuron* **2006**, *52*, 39-59.

(283) Reactive oxygen species-responsive protein modification and its intracellular delivery for targeted cancer therapy. Wang, M.; Sun, S.; Neufeld, C. I.; Perez-Ramirez, B.; Xu, Q. *Angew. Chem. Int. Ed. Engl.* **2014**, *53*, 13444-13448.

(284) Ribonuclease A: Revealing structure-function relationships with semisynthesis. Messmore, J. M.; Fuchs, D. N.; Raines, R. T. *J. Am. Chem. Soc.* **1995**, *117*, 8057-8060.

(285) Hypersensitive substrate for ribonucleases. Kelemen, B. R.; Klink, T. A.; Behlke, M. A.; Eubanks, S. R.; Leland, P. A.; Raines, R. T. *Nucleic Acids Res.* **1999**, *27*, 3696-3701.

(286) Life on a planet of its own: Regulation of RNA polymerase I transcription in the nucleolus. Grummt, I. *Genes Dev.* **2003**, *17*, 1691-1702.

(287) Wisely chosen paths—regulation of rRNA synthesis. Grummt, I. *FEBS J.* **2010**, *277*, 4626-4639.

(288) Targeted cancer therapy with ribosome biogenesis inhibitors: A real possibility? Brighenti, E.; Trere, D.; Derenzini, M. *Oncotarget* **2015**, *6*, 38617-38627.

(289) Functional ribosome biogenesis is a prerequisite for p53 destabilization: Impact of chemotherapy on nucleolar functions and RNA metabolism. Burger, K.; Eick, D. *Biol. Chem.* **2013**, *394*, 1133-1143.

(290) Actinomycin. Dalgliesh, C. E.; Todd, A. R. *Nature* **1949**, *164*, 820.

(291) p53-based cyclotherapy: Exploiting the 'guardian of the genome' to protect normal cells from cytotoxic therapy. Rao, B.; Lain, S.; Thompson, A. M. *Br. J. Cancer* **2013**, *109*, 2954-2958.

(292) Actinomycin D stimulates the transcription of rRNA minigenes transfected into mouse cells. Implications for the in vivo hypersensitivity of rRNA gene transcription.

Hadjiolova, K. V.; Hadjiolov, A. A.; Bachellerie, J. P. *Eur. J. Biochem.* **1995**, *228*, 605-615.

(293) Effect of low doses of actinomycin D on neuroblastoma cell lines. Cortes, C. L.; Veiga, S. R.; Almacellas, E.; Hernandez-Losa, J.; Ferreres, J. C.; Kozma, S. C.; Ambrosio, S.; Thomas, G.; Tauler, A. *Mol. Cancer* **2016**, *15*, 1.

(294) Distinct effects of topoisomerase I and RNA polymerase I inhibitors suggest a dual mechanism of nucleolar/nucleoplasmic partitioning of topoisomerase I. Christensen, M. O.; Krokowski, R. M.; Barthelmes, H. U.; Hock, R.; Boege, F.; Mielke, C. *J. Biol. Chem.* **2004**, *279*, 21873-21882.

(295) Oxaliplatin: A review in the era of molecularly targeted therapy. Alcindor, T.; Beauger, N. *Curr. Oncol.* **2011**, *18*, 18-25.

(296) Coilin participates in the suppression of RNA polymerase I in response to cisplatin-induced DNA damage. Gilder, A. S.; Do, P. M.; Carrero, Z. I.; Cosman, A. M.; Broome, H. J.; Velma, V.; Martinez, L. A.; Hebert, M. D. *Mol. Biol. Cell* **2011**, *22*, 1070-1079.

(297) Depletion of the cisplatin targeted HMGB-box factor UBF selectively induces p53-independent apoptotic death in transformed cells. Hamdane, N.; Herdman, C.; Mars, J. C.; Stefanovsky, V.; Tremblay, M. G.; Moss, T. *Oncotarget* **2015**, *6*, 27519-27536.

(298) Small molecule BMH-compounds that inhibit RNA polymerase I and cause nucleolar stress. Peltonen, K.; Colis, L.; Liu, H.; Jaamaa, S.; Zhang, Z.; Af Hallstrom, T.; Moore, H. M.; Sirajuddin, P.; Laiho, M. *Mol. Cancer Ther.* **2014**, *13*, 2537-2546.

(299) Design, synthesis, and structure-activity relationships of pyridoquinazolinecarboxamides as RNA polymerase I inhibitors. Colis, L.; Ernst, G.; Sanders, S.; Liu, H.; Sirajuddin, P.;

Peltonen, K.; DePasquale, M.; Barrow, J. C.; Laiho, M. *J. Med. Chem.* **2014**, *57*, 4950-4961.

(300) A targeting modality for destruction of RNA polymerase I that possesses anticancer activity. Peltonen, K.; Colis, L.; Liu, H.; Trivedi, R.; Moubarek, M. S.; Moore, H. M.; Bai, B.; Rudek, M. A.; Bieberich, C. J.; Laiho, M. *Cancer Cell* **2014**, *25*, 77-90.

(301) DNA intercalator BMH-21 inhibits RNA polymerase I independent of DNA damage response. Colis, L.; Peltonen, K.; Sirajuddin, P.; Liu, H.; Sanders, S.; Ernst, G.; Barrow, J. C.; Laiho, M. *Oncotarget* **2014**, *5*, 4361-4369.

(302) Mechanism of ribonuclease cytotoxicity. Kim, J.-S.; Soucek, J.; Matousek, J.; Raines, R. T. *J. Biol. Chem.* **1995**, *270*, 31097-31102.

(303) Cellular uptake of ribonuclease A relies on anionic glycans. Chao, T.-Y.; Lavis, L. D.; Raines, R. T. *Biochemistry* **2010**, *49*, 10666–10673.

(304) Human cancer antigen globo H is a cell-surface ligand for human ribonuclease 1. Eller, C. H.; Chao, T. Y.; Singarapu, K. K.; Ouerfelli, O.; Yang, G.; Markley, J. L.; Danishefsky, S. J.; Raines, R. T. *ACS Cent. Sci.* **2015**, *1*, 181-190.

(305) Bovine brain ribonuclease is the functional homolog of human ribonuclease 1. Eller, C. H.; Lomax, J. E.; Raines, R. T. *J. Biol. Chem.* **2014**, *289*, 25996-26006.

(306) Cancer chemotherapy—ribonucleases to the rescue. Leland, P. A.; Raines, R. T. *Chem. Biol.* **2001**, *8*, 405-413.

(307) Design of cytotoxic ribonucleases by cationization to enhance intracellular protein delivery. Futami, J.; Yamada, H. *Curr. Pharm. Biotechnol.* **2008**, *9*, 180-184.

(308) Potentiation of ribonuclease cytotoxicity by a poly(amidoamine) dendrimer. Ellis, G. A.; Hornung, M. L.; Raines, R. T. *Bioorg. Med. Chem. Lett.* **2011**, *21*, 2756-2758.

(309) Efficacy of ribonuclease QBI-139 in combination with standard of care therapies. Strong, L. E.; Kink, J. A.; Pensinger, D; Mei, B.; Shahan, M.; Raines, R. T. *Cancer Res.* **2012**, *72*.

(310) First in human phase I clinical trial of QBI-139, a human ribonuclease variant, in solid tumors. Strong, L. E.; Kink, J. A.; Mei, B.; Shahan, M. N.; Raines, R. T. *J. Clin. Oncol.* **2012,** *30*.

(311) Tandemization endows bovine pancreatic ribonuclease with cytotoxic activity. Leich, F.; Koditz, J.; Ulbrich-Hofman, R.; Arnold, U. *J. Mol. Biol.* **2006**, *358*, 1305-1313.

(312) Endocytotic internalization as a crucial factor for the cytotoxicity of ribonucleases. Leich, F.; Stohr, N.; Rietz, A.; Ulbrich-Hofmann, R.; Arnold, U. *J. Biol. Chem.* **2007**, *282*, 27640-27646.

(313) Crystal structure of RNase A tandem enzymes and their interaction with the cytosolic ribonuclease inhibitor. Arnold, U.; Leich, F.; Neumann, P.; Lilie, H.; Ulbrich-Hofmann, R. *FEBS J.* **2011**, *278*, 331-340.

(314) At the center of eukaryotic life. Moss, T.; Stefanovsky, V. Y. *Cell* **2002**, *109*, 545-548.

(315) Delivery of therapeutic proteins. Pisal, D. S.; Kosloski, M. P.; Balu-Iyer, S. V. *J. Pharm. Sci.* **2010**, *99*, 2557-2575.

(316) Emerging roles of tRNA in adaptive translation, signalling dynamics and disease. Kirchner, S.; Ignatova, Z. *Nat. Rev. Genet.* **2015**, *16*, 98-112.

(317) Controlling translation via modulation of tRNA levels. Wilusz, J. E. *Wiley Interdiscip. Rev. RNA* **2015**, *6*, 453-470.

(318) tRNA-derived G-quadruplex protects motor neurons. Yang, X. L. *Proc. Natl. Acad. Sci. USA* **2014**, *111*, 18108-18109.

(319) Aberrant methylation of tRNAs links cellular stress to neuro-developmental disorders. Blanco, S.; Dietmann, S.; Flores, J. V.; Hussain, S.; Kutter, C.; Humphreys, P.; Lukk, M.; Lombard, P.; Treps, L.; Popis, M.; Kellner, S.; Holter, S. M.; Garrett, L.; Wurst, W.; Becker, L.; Klopstock, T.; Fuchs, H.; Gailus-Durner, V.; Hrabe de Angelis, M.; Karadottir, R. T.; Helm, M.; Ule, J.; Gleeson, J. G.; Odom, D. T.; Frye, M. *EMBO J.* **2014**, *33*, 2020-2039.

(320) Emerging roles of tRNA-derived fragments in viral infections: The case of respiratory syncytial virus. Ivanov, P. *Mol. Ther.* **2015**, *23*, 1557-1558.

(321) HSPC117 is the essential subunit of a human tRNA splicing ligase complex. Popow, J.; Englert, M.; Weitzer, S.; Schleiffer, A.; Mierzwa, B.; Mechtler, K.; Trowitzsch, S.; Will, C. L.; Luhrmann, R.; Soll, D.; Martinez, J. *Science* **2011**, *331*, 760-764.

(322) tRNA ligase catalyzes the GTP-dependent ligation of RNA with 3′-phosphate and 5′-hydroxyl termini. Desai, K. K.; Raines, R. T. *Biochemistry* **2012**, *51*, 1333-1335.

(323) The sequential 2′,3′-cyclic phosphodiesterase and 3′-phosphate/5′-OH ligation steps of the RtcB RNA splicing pathway are GTP-dependent. Chakravarty, A. K.; Shuman, S. *Nucleic Acids Res.* **2012**, *40*, 8558-8567.

(324) Archaeal 3′-phosphate RNA splicing ligase characterization identifies the missing component in tRNA maturation. Englert, M.; Sheppard, K.; Aslanian, A.; Yates, J. R., 3rd; Soll, D. *Proc. Natl. Acad. Sci. USA* **2011**, *108*, 1290-1295.

(325) Making ends meet: A role of RNA ligase RtcB in unfolded protein response. Filipowicz, W. *EMBO J.* **2014**, *33*, 2887-2889.

(326) RtcB-1 mediates neuroprotection via XBP-1 mRNA splicing in the unfolded protein response pathway. Ray, A.; Zhang, S.; Rentas, C.; Caldwell, K. A.; Caldwell, G. A. *J. Neurosci.* **2014**, *34*, 16076-16085.

(327) IRE1α/XBP1-mediated branch of the unfolded protein response regulates osteoclastogenesis. Tohmonda, T.; Yoda, M.; Iwawaki, T.; Matsumoto, M.; Nakamura, M.; Mikoshiba, K.; Toyama, Y.; Horiuchi, K. *J. Clin. Invest.* **2015**, *125*, 3269-3279.

(328) A synthetic biology approach identifies the mammalian UPR RNA ligase RtcB. Lu, Y.; Liang, F. X.; Wang, X. *Mol. Cell* **2014**, *55*, 758-770.

(329) The mammalian tRNA ligase complex mediates splicing of XBP1 mRNA and controls antibody secretion in plasma cells. Jurkin, J.; Henkel, T.; Nielsen, A. F.; Minnich, M.; Popow, J.; Kaufmann, T.; Heindl, K.; Hoffmann, T.; Busslinger, M.; Martinez, J. *EMBO J.* **2014**, *33*, 2922-2936.

(330) Biogenesis and function of tRNA fragments during sperm maturation and fertilization in mammals. Sharma, U.; Conine, C. C.; Shea, J. M.; Boskovic, A.; Derr, A. G.; Bing, X. Y.; Belleannee, C.; Kucukural, A.; Serra, R. W.; Sun, F.; Song, L.; Carone, B. R.; Ricci, E. P.; Li, X. Z.; Fauquier, L.; Moore, M. J.; Sullivan, R.; Mello, C. C.; Garber, M.; Rando, O. J. *Science* **2016**, *351*, 391-396.

(331) Regulated portals of entry into the cell. Conner, S. D.; Schmid, S. L. *Nature* **2003**, *422*, 37-44.

(332) Mechanisms of endocytosis. Doherty, G. J.; McMahon, H. T. *Annu. Rev. Biochem.* **2009**, *78*, 857-902.

(333) Molecular mechanism and physiological functions of clathrin-mediated endocytosis. McMahon, H. T.; Boucrot, E. *Nat. Rev. Mol. Cell Biol.* **2011**, *12*, 517-533.

(334) Molecular mechanisms of clathrin-independent endocytosis. Hansen, C. G.; Nichols, B. J. *J. Cell Sci.* **2009**, *122*, 1713-1721.

(335) Mechanisms of pathogen entry through the endosomal compartments. Gruenberg, J.; van der Goot, F. G. *Nat. Rev. Mol. Cell Biol.* **2006**, *7*, 495-504.

(336) Defining macropinocytosis. Kerr, M. C.; Teasdale, R. D. *Traffic* **2009**, *10*, 364-371.

(337) Derailed endocytosis: An emerging feature of cancer. Mosesson, Y.; Mills, G. B.; Yarden, Y. *Nat. Rev. Cancer* **2008**, *8*, 835–850.

(338) Hallmarks of cancer: The next generation. Hanahan, D.; Weinberg, R. A. *Cell* **2011**, *144*, 646–674.

(339) Ribonucleases as novel chemotherapeutics: The ranpirnase example. Lee, J. E.; Raines, R. T. *BioDrugs* **2008**, *22*, 53-58.

(340) Aspects of the cytotoxic action of ribonucleases. Arnold, U. *Curr. Pharm. Biotechnol.* **2008**, *9*, 161-168.

(341) Fang, E. F.; Ng, T. B. *Biochim. Biophys. Acta* **2011**, *1815*, 65-74.

(342) Rational design and evalution of mammalian ribonuclease cytotoxins. Lomax, J. E.; Eller, C. H.; Raines, R. T. *Methods Enzymol.* **2012**, *502*, 273-290.

(343) *Exocytosis and endocytosis*; Ivanov, A. I., Ed.; Humana Press: Totowa, NJ, **2007**.

(344) The interaction of soluble horseradish peroxidase with mouse peritoneal macrophages *in vitro*. Steinman, R. M.; Cohn, Z. A. *J. Cell Biol.* **1972**, *55*, 186–204.

(345) Cell-penetrating peptides—a reevaluation of the mechanism of cellular uptake. Richard, J. P.; Melikov, K.; Vives, E.; Ramos, C.; Verbeure, B.; Gait, M. J.; Chernomordik, L. V.; Lebleu, B. *J. Biol. Chem.* **2003**, *278*, 585-590.

(346) A non-exchangeable fluorescent phospholipid analog as a membrane traffic marker of the endocytic pathway. Kok, J. W.; Beest, M.; Scherphof, G.; Hoekstra, D. *Eur. J. Cell. Biol.* **1990**, *53*, 173–184.

(347) Monitoring secretory membrane with FML-43 fluorescence. Cochilla, A. J.; Angleson, J. K.; Betz, W. J. *Annu. Rev. Neurosci.* **1999**, *22*, 1–10.

(348) Fluorescent lipid probes: Some properties and applications. Maier, O.; Oberle, V.; Hoekstra, D. *Chem. Phys. Lipids* **2002**, *116*, 3–18.

(349) Streamlined synaptic vesicle cycle in cone photoreceptor terminals. Rea, R.; Li, J.; Dharia, A.; Levitan, E. S.; Sterling, P.; Kramer, R. H. *Neuron* **2004**, *41*, 755–766.

(350) Studying lipids involved in the endosomal pathway. Bissig, C.; Johnson, S.; Gruenberg, J. *Methods Cell Biol.* **2012**, *108*, 19-46.

(351) Trimethyl lock: A trigger for molecular release in chemistry, biology, and pharmacology. Levine, M. N.; Raines, R. T. *Chem. Sci.* **2012**, *3*, 2412-2420.

(352) Latent fluorophore based on the trimethyl lock. Chandran, S. S.; Dickson, K. A.; Raines, R. T. *J. Am. Chem. Soc.* **2005**, *127*, 1652–1653.

(353) Fluorogenic label for biomolecular imaging. Lavis, L. D.; Chao, T.-Y.; Raines, R. T. *ACS Chem. Biol.* **2006**, *1*, 252–260.

(354) Latent blue and red fluorophores based on the trimethyl lock. Lavis, L. D.; Chao, T.-Y.; Raines, R. T. *ChemBioChem* **2006**, *7*, 1151–1154.

(355) Trimethyl lock: A stable chromogenic substrate for esterases. Levine, M. N.; Lavis, L. D.; Raines, R. T. *Molecules* **2008**, *13*, 204–211.

(356) Cytotoxic ribonucleases: The dichotomy of coulombic forces. Johnson, R. J.; Chao, T.-Y.; Lavis, L. D.; Raines, R. T. *Biochemistry* **2007**, *46*, 10308-10316.

(357) Synthesis of fluorogenic polymers for visualizing cellular internalization. Mangold, S. L.; Carpenter, R. T.; Kiessling, L. L. *Org. Lett.* **2008**, *10*, 2997–3000.

(358) Onconase cytotoxicity relies on the distribution of its positive charge. Turcotte, R. F.; Lavis, L. D.; Raines, R. T. *FEBS J.* **2009**, *276*, 4270–4281.

(359) Mechanism of ribonuclease a endocytosis: Analogies to cell-penetrating peptides. Chao, T.-Y.; Raines, R. T. *Biochemistry* **2011**, *50*, 8374-8382.

(360) Selective esterase–ester pair for targeting small molecules with cellular specificity. Tian, L.; Yang, Y.; Wysocki, L. W.; Arnold, A. C.; Hu, A.; Ravichandran, B.; Sternson, S. M.; Looger, L. L.; Lavis, L. D. *Proc. Natl. Acad. Sci. USA* **2012**, *109*, 4756-4761.

(361) *Lipid analysis: Isolation, separation, identification and lipidomic analysis*. Christie, W. W.; Han, X.; 4th ed.; Woodhead Publishing Limited: Cambridge, UK, **2010**.

(362) Temperature effect on endocytosis and exocytosis by rabbit alveolar macrophages. Tomoda, H.; Kishimoto, Y.; Lee, Y. C. *J. Biol. Chem.* **1989**, *264*, 15445-15450.

(363) Quantification of low density lipoprotein and transferrin endocytic sorting HEp2 cells using confocal microscopy. Ghosh, R. N.; Gelman, D. L.; Maxfield, F. R. *J. Cell Sci.* **1994**, *107*, 2177-2189.

(364) Novel fluorescent acidic organelle-selective dyes and mitochondrion-selective dyes that are well retained during cell fixation and permeabilization. Zhang, Y.-Z.; Diwu, Z.; Mao, F.; Leung, W.; Haugland, R. P. *Mol. Biol. Cell* **1994**, *5 (Suppl.)*, 113a.

(365) Membrane flow during pinocytosis. A stereologic analysis. Steinman, R. M.; Brodie, S. E.; Cohn, Z. A. *J. Cell Biol.* **1976**, *68*, 665-687.

(366) Synthesis of a new long-wavelength latent fluorimetric indicator for analytes determination in the DT-Diaphorase coupling dehydrogenase assay system. Huang, S.-T.; Peng, Y.-X.; Wang, K.-L. *Biosens. Bioelectron.* **2008**, *23*, 1793–1798.

(367) Pathways of clathrin-independent endocytosis. Mayor, S.; Pagano, R. E. *Nat. Rev. Mol. Cell Biol.* **2007**, *8*, 603–612.

(368) Endocytosis of nanomedicines. Sahay, G.; Alakhova, D. Y.; Kabanov, V. A. *J. Control. Rel.* **2010**, *145*, 182-195.

(369) Enhancing cell therapies form the outside in: Cell surface engineering using synthetic nanomaterials. Stephan, M. T.; Irvine, D. J. *Nano Today* **2011**, *6*, 309-325.

(370) Synthetic cell surface receptors for delivery of therapeutics and probes. Hymel, D.; Peterson, B. R. *Adv. Drug Deliv. Rev.* **2012**, *64*, 797-810.

(371) Crystal structure of porcine ribonuclease inhibitor, a protein with leucine-rich repeats. Kobe, B.; Deisenhofer, J. *Nature* **1993**, *366*, 751-756.

(372) Oxidation of sulfhydryl groups of ribonuclease inhibitor in epithelial cells is sufficient for its intracellular degradation. Blazquez, M.; Fominaya, J. M.; Hofsteenge, J. *J. Biol. Chem.* **1996**, *271*, 18638-18642.

(373) Variants of ribonuclease inhibitor that resist oxidation. Kim, B. M.; Schultz, L. W.; Raines, R. T. *Protein Sci.* **1999**, *8*, 430-434.

(374) Inhibition of the human pancreatic ribonuclease by the human ribonuclease inhibitor protein. Johnson, R. J.; McCoy, J. G.; Bingman, C. A.; Phillips, G. N.; Raines, R. T. *J. Mol. Biol.* **2007**, *368*, 434–449.

(375) Disruption of shape-complementarity markers to create cytotoxic variants of ribonuclease A. Rutkoski, T. J.; Kurten, E. L.; Mitchell, J. C.; Raines, R. T. *J. Mol. Biol.* **2005**, *354*, 41–54.

(376) Knockdown of ribonuclease inhibitor expression with siRNA in non-invasive bladder cancer cell line BIU-87 promotes growth and metastasis potentials. Chen, J.; Ou-Yang, X.; Gao, J.; Zhu, J.; He, X.; Rong, J. *Mol. Cell Biochem.* **2011**, *349*, 83-95.

(377) Down-regulating ribonuclease inhibitor enhances metastasis of bladder cancer cells through regulating epithelial-mesenchymal transition and ILK signaling pathway. Xiong, D.; Liou, Y.; Shu, J.; Li, D.; Zhang, L.; Chen, J. *Exp. Mol. Pathol.* **2014**, *96*, 411-421.

(378) Inactivation of ribonuclease inhibitor by thiol-disulfide exchange. Fominaya, J. M.; Hofsteenge, J. *J. Biol. Chem.* **1992**, *267*, 24655-24660.

(379) Cysteine-mediated redox signaling: Chemistry, biology, and tools for discovery. Paulsen, C. E.; Carroll, K. S. *Chem. Rev.* **2013**, *113*, 4633-4679.

(380) Systematic modulation of Michael-type reactivity of thiols through the use of charged amino acids. Lutolf, M. P.; Tirelli, N.; Cerritelli, S.; Cavalli, L.; Hubbell, J. A. *Bioconjug. Chem.* **2001**, *12*, 1051-1056.

(381) Reactivity of biologically important thiol compounds with superoxide and hydrogen peroxide. Winterbourn, C. C.; Metodiewa, D. *Free Radic. Biol. Med.* **1999**, *27*, 322-328.

(382) PhosphoSitePlus, 2014: Mutations, PTMs and recalibrations. Hornbeck, P. V.; Zhang, B.; Murray, B.; Kornhauser, J. M.; Latham, V.; Skrzypek, E. *Nucleic Acids Res.* **2015**, *43*, D512-520.

(383) Ribonuclease A variants with potent cytotoxic activity. Leland, P. A.; Schultz, L. W.; Kim, B. M.; Raines, R. T. *Proc. Natl. Acad. Sci. USA* **1998**, *95*, 10407-10412.

(384) Endowing human pancreatic ribonuclease with toxicity for cancer cells. Leland, P. A.; Staniszewski, K. E.; Kim, B. M.; Raines, R. T. *J. Biol. Chem.* **2001**, *276*, 43095-43102.

(385) Cytotoxic ribonucleases: The dichotomy of coulombic forces. Johnson, R. J.; Chao, T. Y.; Lavis, L. D.; Raines, R. T. *Biochemistry* **2007**, *46*, 10308-10316.

(386) Glycans in cancer and inflammation—potential for therapeutics and diagnostics. Dube, D. H.; Bertozzi, C. R. *Nat. Rev. Drug Discov.* **2005**, *4*, 477-488.

(387) Cellular uptake of ribonuclease a relies on anionic glycans. Chao, T. Y.; Lavis, L. D.; Raines, R. T. *Biochemistry* **2010**, *49*, 10666-10673.

(388) Secretory ribonucleases are internalized by a dynamin-independent endocytic pathway. Haigis, M. C.; Raines, R. T. *J. Cell Sci.* **2003**, *116*, 313–324.

(389) Structure and function of glycosphingolipids and sphingolipids: Recollections and future trends. Hakomori, S. I. *Biochim. Biophys. Acta* **2008**, *1780*, 325-346.

(390) A vital role for glycosphingolipid synthesis during development and differentiation. Yamashita, T.; Wada, R.; Sasaki, T.; Deng, C.; Bierfreund, U.; Sandhoff, K.; Proia, R. L. *Proc. Natl. Acad. Sci. USA* **1999**, *96*, 9142-9147.

(391) Switching of the core structures of glycosphingolipids from globo- and lacto- to ganglio-series upon human embryonic stem cell differentiation. Liang, Y. J.; Kuo, H. H.; Lin, C. H.; Chen, Y. Y.; Yang, B. C.; Cheng, Y. Y.; Yu, A. L.; Khoo, K. H.; Yu, J. *Proc. Natl. Acad. Sci. USA* **2010**, *107*, 22564-22569.

(392) Selection of tumor antigens as targets for immune attack using immunohistochemistry: I. Focus on gangliosides. Zhang, S.; Cordon-Cardo, C.; Zhang, H. S.; Reuter, V. E.; Adluri, S.; Hamilton, W. B.; Lloyd, K. O.; Livingston, P. O. *Int. J. Cancer* **1997**, *73*, 42-49.

(393) Dynamic light scattering based microelectrophoresis: Main prospects and limitations. Uskokovic, V. *J. Dispers. Sci. Technol.* **2012**, *33*, 1762-1786.

(394) Fluorogenic label to quantify the cytosolic delivery of macromolecules. Chao, T. Y.; Raines, R. T. *Mol. Biosyst.* **2013**, *9*, 339-342.

(395) Nanoluc complementation reporter optimized for accurate measurement of protein interactions in cells. Dixon, A. S.; Schwinn, M. K.; Hall, M. P.; Zimmerman, K.; Otto, P.; Lubben, T. H.; Butler, B. L.; Binkowski, B. F.; Machleidt, T.; Kirkland, T. A.; Wood, M. G.; Eggers, C. T.; Encell, L. P.; Wood, K. V. *ACS Chem. Biol.* **2016**, *11*, 400-408.

(396) Continuous cultures of fused cells secreting antibody of predefined specificity. Kohler, G.; Milstein, C. *Nature* **1975**, *256*, 495-497.

(397) Phage display of a catalytic antibody to optimize affinity for transition-state analog binding. Baca, M.; Scanlan, T. S.; Stephenson, R. C.; Wells, J. A. *Proc. Natl. Acad. Sci. USA* **1997**, *94*, 10063-10068.

(398) Antibody humanization using monovalent phage display. Baca, M.; Presta, L. G.; O'Connor, S. J.; Wells, J. A. *J. Biol. Chem.* **1997**, *272*, 10678-10684.

(399) Two-state selection of conformation-specific antibodies. Gao, J.; Sidhu, S. S.; Wells, J. A. *Proc. Natl. Acad. Sci. USA* **2009**, *106*, 3071-3076.

(400) Beyond natural antibodies: The power of *in vitro* display technologies. Bradbury, A. R.; Sidhu, S.; Dubel, S.; McCafferty, J. *Nat. Biotechnol.* **2011**, *29*, 245-254.

(401) Scalable high throughput selection from phage-displayed synthetic antibody libraries. Miersch, S.; Li, Z.; Hanna, R.; McLaughlin, M. E.; Hornsby, M.; Matsuguchi, T.; Paduch, M.; Saaf, A.; Wells, J.; Koide, S.; Kossiakoff, A.; Sidhu, S. S. *J. Vis. Exp.* **2015**, *95*, 51492-51497.

(402) Global, *in vivo*, and site-specific phosphorylation dynamics in signaling networks. Olsen, J. V.; Blagoev, B.; Gnad, F.; Macek, B.; Kumar, C.; Mortensen, P.; Mann, M. *Cell* **2006**, *127*, 635-648.

(403) Structural changes in glycogen phosphorylase induced by phosphorylation. Sprang, S. R.; Acharya, K. R.; Goldsmith, E. J.; Stuart, D. I.; Varvill, K.; Fletterick, R. J.; Madsen, N. B.; Johnson, L. N. *Nature* **1988**, *336*, 215-221.

(404) An allosteric mechanism for activation of the kinase domain of epidermal growth factor receptor. Zhang, X.; Gureasko, J.; Shen, K.; Cole, P. A.; Kuriyan, J. *Cell* **2006**, *125*, 1137-1149.

(405) Requirements for Cdk7 in the assembly of Cdk1/cyclin B and activation of Cdk2 revealed by chemical genetics in human cells. Larochelle, S.; Merrick, K. A.; Terret, M. E.; Wohlbold, L.; Barboza, N. M.; Zhang, C.; Shokat, K. M.; Jallepalli, P. V.; Fisher, R. P. *Mol. Cell* **2007**, *25*, 839-850.

(406) Protein kinases—the major drug targets of the twenty-first century? Cohen, P. *Nat. Rev. Drug Discov.* **2002**, *1*, 309-315.

(407) The mutational landscape of phosphorylation signaling in cancer. Reimand, J.; Wagih, O.; Bader, G. D. *Sci. Rep.* **2013**, *3*, 2651.

(408) Protein phosphorylation in neurodegeneration: Friend or foe? Tenreiro, S.; Eckermann, K.; Outeiro, T. F. *Front. Mol. Neurosci.* **2014**, *7*, 42.

(409) Inactivation of isocitrate dehydrogenase by phosphorylation is mediated by the negative charge of the phosphate. Thorsness, P. E.; Koshland, D. E., Jr. *J. Biol. Chem.* **1987**, *262*, 10422-10425.

(410) A mechanism for cell-cycle regulation of MAP kinase signaling in a yeast differentiation pathway. Strickfaden, S. C.; Winters, M. J.; Ben-Ari, G.; Lamson, R. E.; Tyers, M.; Pryciak, P. M. *Cell* **2007**, *128*, 519-531.

(411) Requirements for phosphorylation of MAP kinase during meiosis in xenopus oocytes. Posada, J.; Cooper, J. A. *Science* **1992**, *255*, 212-215.

(412) Chemoselective Staudinger-phosphite reaction of azides for the phosphorylation of proteins. Serwa, R.; Wilkening, I.; Del Signore, G.; Muhlberg, M.; Claussnitzer, I.; Weise, C.; Gerrits, M.; Hackenberger, C. P. *Angew. Chem. Int. Ed. Engl.* **2009**, *48*, 8234-8239.

(413) Synthetic phosphorylation of p38α recapitulates protein kinase activity. Chooi, K. P.; Galan, S. R.; Raj, R.; McCullagh, J.; Mohammed, S.; Jones, L. H.; Davis, B. G. *J. Am. Chem. Soc.* **2014**, *136*, 1698-1701.

(414) Site-specifically phosphorylated lysine peptides. Bertran-Vicente, J.; Serwa, R. A.; Schumann, M.; Schmieder, P.; Krause, E.; Hackenberger, C. P. *J. Am. Chem. Soc.* **2014**, *136*, 13622-13628.

(415) Direct access to site-specifically phosphorylated-lysine peptides from a solid-support. Bertran-Vicente, J.; Schumann, M.; Schmieder, P.; Krause, E.; Hackenberger, C. P. *Org. Biomol. Chem.* **2015**, *13*, 6839-6843.

(416) New water-soluble phosphines as reductants of peptide and protein disulfide bonds: Reactivity and membrane permeability. Cline, D. J.; Redding, S. E.; Brohawn, S. G.; Psathas, J. N.; Schneider, J. P.; Thorpe, C. *Biochemistry* **2004**, *43*, 15195-15203.